Studies on carbon dioxide capture using polymer based carbon adsorbents

Thesis
Submitted in partial fulfillment for the award of degree
of

Doctor of Philosophy

By

DEEPAK TIWARI
(Registration No.: 901401017)

Under the guidance of

Prof. Haripada Bhunia
Professor
Department of Chemical Engineering,
Thapar Institute of Engineering &
Technology (Deemed to be University), Patiala

Prof. Pramod K. Bajpai
Ex-Distinguished Professor
Department of Chemical Engineering,
Thapar Institute of Engineering &
Technology (Deemed to be University), Patiala

Department of Chemical Engineering
Thapar Institute of Engineering & Technology (Deemed to be University)
Patiala – 147004, Punjab (India)
www.thapar.edu

February 2018

Dedicated

To

My Parents

Dr. Radhey Shyam Tiwari & Smt. Manju Tiwari

My Brothers and Sisters

Dr. Rahul Tiwari, Mr. Vishnukant Mishra, Mrs. Priyanka Chandrayan and Mrs. Deepika Dubey

And

My wife and son

Dr. Neha Singh Tiwari and Vivaan Tiwari

Certificate

This is to certify that the thesis entitled **"Studies on carbon dioxide capture using polymer based carbon adsorbents"** being submitted by Mr. Deepak Tiwari to Department of Chemical Engineering, Thapar Institute of Engineering & Technology (Deemed to be University), Patiala for the award of degree of **Doctor of Philosophy**, is a record of bonafide research work carried out by him under our guidance and supervision and has fulfilled the requirements for the submission of this thesis, which to our knowledge has reached the requisite standard.

The results embodied in the thesis have not been submitted in part or full to any other University or Institute for the award of any degree or diploma.

25-02-2018

(Haripada Bhunia)
Professor
Department of Chemical Engineering,
Thapar Institute of Engineering &
Technology (Deemed to be University),
Patiala

25-02-2018

(Pramod K. Bajpai)
Ex-Distinguished Professor
Department of Chemical Engineering,
Thapar Institute of Engineering &
Technology (Deemed to be University),
Patiala

Acknowledgements

I would like to thank most sincerely my supervisors **Prof. Haripada Bhunia and Prof. Pramod K. Bajpai**, Department of Chemical Engineering, Thapar Institute of Engineering & Technology (Deemed to be University), for providing me such a valuable research opportunity and for their countless guidance, knowledge and motivation during the course of my research. I learnt a lot from them over the course of this Ph.D work. Their goal oriented style of work, passion towards research, work ethic, has been very inspiring for me. Their daily practice of following up on recent scientific literature is something that I also tried to adopt and greatly benefitted. I really appreciate their unconditional support and encouragement towards doing high-calibre research. It's been a great honour to work under their guidance.

I am extremely thankful to **Prof. Prakash Gopalan**, Director, Thapar Institute of Engineering & Technology (Deemed to be University), **Prof. O. P. Pandey**, Dean of Research & Sponsored Projects, Thapar Institute of Engineering & Technology (Deemed to be University) and **Dr. Raj K. Gupta**, Head, Department of Chemical Engineering, Thapar Institute of Engineering & Technology (Deemed to be University) for extending the opportunity to undertake this doctoral research.

I would like to profoundly thank to my doctoral committee members **Dr. Sudhir K. Singh** and **Dr. Vijaya Kumar Bulasara** of Chemical Engineering and **Prof. Bonamali Pal**, School of Chemistry & Biochemistry, Thapar Institute of Engineering & Technology (Deemed to be University) for their immense help and guiding me towards the right direction. My heartful thank to the staff members of Department of Chemical Engineering, Thapar Institute of Engineering & Technology (Deemed to be University) for their valuable contribution, spiritual and moral support.

I would like especially to thank **Dr. Chitrakshi Goel**, Post-Doctoral Researcher, Ghent University, Ghent, Belgium who patiently and in a very dedicated way offered undivided attention and advice. I would also like to thank **Dr. Gaurav Madhu**, Associate Professor and Joint Director, Indian Institute of Packaging, Mumbai for helping and motivation.

My endless thanks goes to **Mr. Dev Kumar Mandal, Mrs. Meenakshi Sheoran Nandal, Ms. Metali Sarkar, Mrs. Balpreet Kaur, Mr. Jasminder Singh, Ms. Simarjot Kaur** for their valuable contribution, spiritual and moral support at various stages of my work.

My deepest gratitude goes to my beloved parents, **Dr. R. S. Tiwari, Smt. Manju Tiwari**, my father in law, **Mr. Ramesh Singh** and my mother in law, **Mrs. Ragnee Singh** my sisters, **Mrs. Priyanka Chandrayan, Mrs. Deepika Dubey** and my brothers, **Dr. Rahul Kumar Tiwari** and my cousin brother **Mr. Vishnukant Mishra**, my sister in law, **Dr. Urvashi Ojha Tiwari** and **Mrs. Neetu Singh** my brother in law, **Mr. Anucool Singh** who have always supported me through highs and lows of life. They have touched my life in many ways. My last word is reserved for my love, **Dr. Neha Singh Tiwari**, for her true companionship.

I would like to gratefully acknowledge the financial support from **Department of Science & Technology (DST)**, Government of India throughout the course of this work.

Finally I wish to thank the "**ALMIGHTY**" God for his sufficiency.

25/2/18

Deepak Tiwari

Abstract

Carbon dioxide (CO_2), a major greenhouse gas, is one of the greatest challenges of the twenty-first century. Its increase in the atmosphere is mainly due to fossil-fuel power sector and energy-intensive industries. Consequences like global warming and climate change concerns initiated global efforts to reduce CO_2 concentration. Among the various mitigation pathways, CO_2 capture and storage (CCS) technology is attracting higher interest which can lower down the release of CO_2 into the atmosphere. Pre-combustion, post-combustion, and oxy-fuel combustion are the CCS technologies among which post combustion is considered as economic and green technologies. The available post-combustion technologies for CO_2 capture are absorption, adsorption, cryogenic distillation, and membrane separation. Mature technology like absorption has been used most but it is having disadvantages like high regeneration cost, equipment corrosion, and amine oxidative degradation. Adsorption is believed to be economically and least interfering ways due to its easy application as it fulfills the objective of very small modification to power plants, less energy penalty and low equipment cost. Therefore, for post-combustion CO_2 capture, there is a great need for the development of adsorbent materials with high adsorption capacity, selectivity and fast kinetics coupled with good thermal and mechanical stability.

Carbon based adsorbents are found to be attractive and have been extensively used for CO_2 adsorption due to its high surface area, lesser amount of energy for regeneration, good thermal/mechanical stability and hydrophobicity. It was seen that many researchers were trying to develop adsorbent either by direct carbonization or by physical/chemical activation. Also, they tried to evaluate their uptake capacity mainly under static condition at room temperature. But, the disadvantage of their studies is both the synthesis and performance evaluation. It was reported that direct carbonized adsorbent synthesis was time consuming and requires high amount of energy. Moreover, CO_2 adsorption under static condition provides higher value but it is not applicable for flue gas applications. Thus, objectives of our work are to overcome this gap, in which nanocasting technique, direct carbonization followed by activation using appropriate activation conditions and carbon sources having higher nitrogen and oxygen contents is carried out to improve the texture, surface properties and CO_2/N_2 selectivity of carbon adsorbents. Also, adsorption study under dynamic fixed bed conditions at different CO_2

concentrations (5-12.5%) and temperatures (30-100 °C), which is more important than static conditions, adsorption kinetics, binary system adsorption equilibria and thermodynamics have been carried.

Three different types of nanostructured carbons were developed by nanocasting technique for capture of CO_2 under simulated flue gas conditions. Three polymeric materials namely melamine-formaldehyde, urea-formaldehyde and epoxy resins were synthesized and were used as polymeric precursors for nanocasting technique along with mesoporous zeolite as hard template. Also, using direct carbonization followed by a standard chemical activation with KOH at appropriate activation conditions were used. Developed adsorbents were characterized using various sophisticated techniques namely N_2 sorption isotherms, XRD (X-ray diffraction), TEM (transmission electron microscopy), SEM (scanning electron microscopy), TGA (thermogravimetric analysis), CHNS (elemental analysis), FTIR (Fourier transform infrared spectroscopy), TPD (temperature programmed desorption), XPS (X-ray photoelectron spectroscopy), and Raman spectroscopy. Dynamic adsorption-desorption experiments were conducted in the fixed-bed system to evaluate their CO_2 adsorption capacities, selectivity and regenerability under simulated flue gas conditions. CO_2 adsorption was studied at several adsorption temperatures (30 to 100 °C) under varying CO_2 concentrations (5% to 12.5% by volume). Three kinetic models i.e., pseudo-first order, pseudo second order and fractional order kinetic models were used to fit CO_2 adsorption kinetics on the prepared adsorbents. The equilibrium adsorption data fitted with three isotherm model i.e., Langmuir, Freundlich and Temkin isothermal models Thermodynamic functions such as molar Gibbs free energy change, entropy change, and enthalpy change were evaluated numerically. Finally, energy duty for desorption of adsorbed CO_2 and energy penalty for the whole process system was also estimated.

Fig. 1 shows schematic of the overall thesis work.

Nitrogen enriched carbon adsorbents were successfully prepared using precursor melamine-formaldehyde resin and mesoporous zeolite (MCM-41) as template through nanocasting technique. Different characterization techniques were used for the thorough characterization of the prepared adsorbents. Using physical activation with CO_2 and high nitrogen content carbon precursor resulted in a development of nanostructured carbon denoted as MFZ-700. This sample possesses a surface area of 193 $m^2\ g^{-1}$, pore volume of 0.32 $cm^3\ g^{-1}$ and nitrogen content of 22.27%. Dynamic CO_2 uptake capacity of 0.64 mmol g^{-1} for the sample

(MFZ-700) at 30 °C under 12.5% CO_2 flow was obtained. Complete regenerability for the adsorbents over four adsorption-desorption cycles was obtained. Furthermore, fractional order kinetic models provided best description over all adsorption temperatures and CO_2 concentrations. Heterogeneity of the adsorbent surface was confirmed from Temkin isotherms fit and isosteric heat of adsorption values. The isosteric heat of adsorption is found to be 15.05 kJ mol^{-1}, which indicates physiosorption process and also supports easy regenerability of the adsorbent. Thermodynamic parameters ΔH^0 and ΔS^0 are estimated to be -5.7 kJ mol^{-1} and 0.033 kJ mol^{-1} K^{-1}. The energy penalty estimated for the whole process is 2.15 MJ per kg CO_2.

Oxygen enriched carbon adsorbents were successfully synthesized for the first time from template zeolite and epoxy resin as precursor using a nanocasting technique. Carbonization and CO_2 activation were performed at various temperatures (500 to 800 °C) to prepare different carbon structure adsorbents. Several characterization techniques were used to characterize for the textural properties, oxygen content and surface functional groups of the adsorbents. The carbon adsorbents show high oxygen content (53.98 %), highest surface area (S_{BET} = 686 m^2 g^{-1}) and pore volume (0.60 cm^3 g^{-1}). The materials were evaluated using fixed-bed adsorption and the highest CO_2 uptake of 0.65 mmol g^{-1} was observed due to highly basic nature of the surface. Regeneration studies of adsorbent indicated easy regenerability and stable operation over four adsorptions-desorption cycles. Kinetic models for CO_2 adsorption at various CO_2 concentrations and temperatures were studied. The fractional order provided best fitting for the adsorption behavior with an error of less than 5%. The experimental data for CO_2 adsorption were analyzed using different isotherm models and found that the Freundlich isotherm model presented perfect fit among all isotherm models considered indicating adsorbent surface to be heterogeneous. The isosteric heat of adsorption is 9.09 kJ mol^{-1}, indicating physiosorption process. The values of ΔG^0 and ΔH^0 have confirmed the adsorption process to be spontaneous and exothermic in nature.

Urea-formaldehyde resin (high nitrogen) as precursor and mesoporous zeolite (MCM-41) as template, using nanocasting technique results in development of nanostructured cabon having high surface area (337 m^2 g^{-1}), mesopores (0.644 cm^3 g^{-1}), and micropores (0.123 cm^3 g^{-1}). The CO_2 capture capacity depends more on the nitrogen functionalities in addition to textural properties and nitrogen content as UFZ-700 shows highest CO_2 uptake of 0.84 mmol g^{-1}. Furthermore, it was found that adsorbent can be easily regenerated, which was also seen by the lower value of isosteric heat of adsorption. Four adsorption-desorption cycles show

established materials' excellent stability as an adsorbent. Different kinetic models were fitted for the adsorption data and on the basis of correlation coefficient (R^2), fractional order provided best fit with the experimental data. Heterogeneous adsorbent surface was confirmed from best fit of equilibrium adsorption data with Freundlich isotherm. Exothermic, feasible and spontaneous nature was confirmed from thermodynamic values.

High surface area nitrogen enriched carbon adsorbents were prepared from a low cost and widely available urea-formaldehyde resin using a standard chemical activation with KOH. Maximum surface area and total pore volume of 4547 $m^2 g^{-1}$ and 4.50 $cm^3 g^{-1}$ respectively were found by controlling the activation conditions. Nitrogen content of this sample was 5.62%. Maximum CO_2 uptake of 1.40 mmol g^{-1} for UFA-3-700 at 30 °C under 12.5% CO_2 flow was obtained. Complete regenerability of the adsorbents over multiple adsorption-desorption cycles was obtained. Fractional order kinetic model provided best description over all adsorption temperatures and CO_2 concentrations. Heterogeneity of the adsorbent surface was confirmed from Temkin adsorption isotherm model fit and isosteric heat of adsorption values. Spontaneous, feasible and exothermic nature was confirmed from negative values of $\Delta G°$ and $\Delta H°$. Overall, very high surface area of carbon adsorbent makes this adsorbent a new promising carbon material for CO_2 capture from power plant flue gas and for other relevant applications.

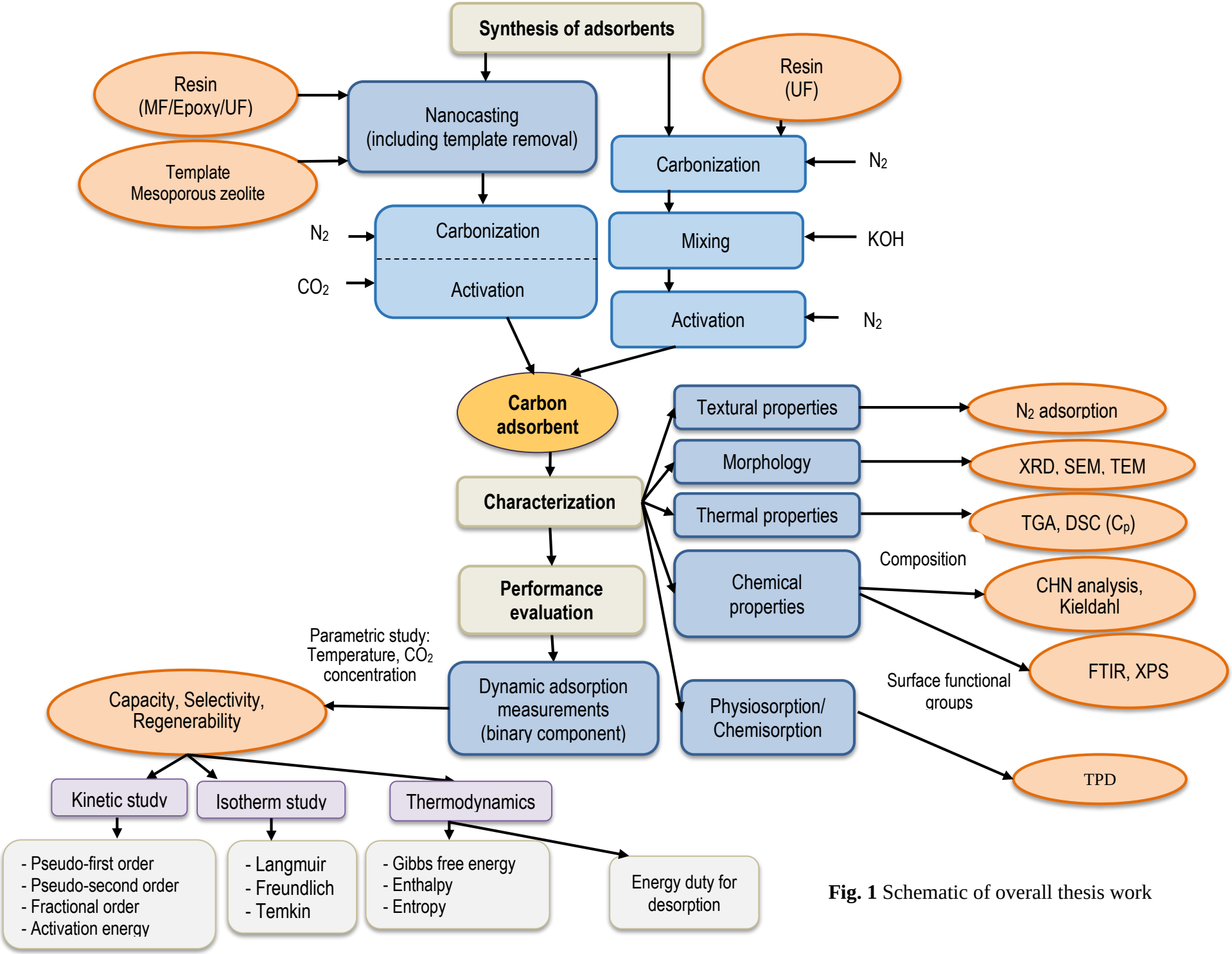

Fig. 1 Schematic of overall thesis work

TABLE OF CONTENTS

List of Figures

List of Tables

List of Symbols

b	Heat of adsorption, J mol^{-1}
C	Effluent CO_2 concentration, volume%
C_o	CO_2 inlet concentrations, volume%
C_p	Specific heat capacity of the adsorbent, J g^{-1} K^{-1}
d_{002}	Interlayer d-spacing of (002) diffraction plane, nm
E_a	Activation energy, J mol^{-1}
Error (%)	Error function
k_1	Pseudo-first order rate constant, min^{-1}
k_2	Pseudo-second order rate constant, g $mmol^{-1}$ min^{-1}
k_n	Fractional order rate constant
m	Fractional order model constant related to diffusion resistance
M	Mass of the adsorbent, g
n	Fractional order model constant related to driving force
N	Total number of experimental points
q_e	Dynamic adsorption capacity at equilibrium, mmol g^{-1}
$q_{e,i}$	Equilibrium adsorption capacity of component *i* in the mixture, mmol g^{-1}
$q_{t,exp}$	Amount of CO_2 adsorbed at a given time *t* determined experimentally, mmol g^{-1}
$q_{t,pred}$	Amount of CO_2 adsorbed at a given time *t* predicted, mmol g^{-1}
q_i	Adsorbed amount of component *i* in mixture, mmol g^{-1}
q_m	Maximum monolayer adsorption capacity, mmol g^{-1}
q_t	CO_2 adsorption capacity at time t, mmol g^{-1}
q_T	Total adsorbed amount in mixture, mmol g^{-1}
Q	Gas flow rate, ml min^{-1}

Q_{st}	Isosteric heat of adsorption, kJ mol^{-1}
Q_{th}	Thermal energy, J mol^{-1}
R	Universal gas constant, kJ mol^{-1} K^{-1}
R^2	Regression coefficient
S_{BET}	BET surface area, m^2 g^{-1}
S_{CO_2}	Selectivity of CO_2 over N_2
t	Time, min
t_b	Breakthrough time, min
T	Temperature, K
V_{meso}	Mesopore volume, cm^3 g^{-1}
V_{micro}	Micropore volume, cm^3 g^{-1}
V_P	Total pore volume obtained at a relative pressure of 0.99, cm^3 g^{-1}

Greek Letters

θ	Bragg's angle
µm	Micrometer

List of Abbreviations

A%	Relative area contribution
B. E.	Binding energy
BET	Brunauer–Emmett–Teller
BJH	Barrett–Joyner–Halenda
DEA	Diethanol amine
DSC	Differential scanning calorimetry
ED	Ethylenediamine
FWHM	Full width at half maximum
GHG	Greenhouse gase
Gt CO_2eq	Gigatonnes CO_2-equivalents
HFC	Hydrofluorocarbons
IPA	Isopropanol amine
MDEA	Methyldiethanol amine
MEA	Monoethanol amine
PEI	Polyethyleneimine
PFC	Perfluorocarbons
ppm	Parts per million
PPy	Polypyrrole
PSA	Pressure swing adsorption
PSD	Pore size distribution
SEM	Scanning electron microscopy
SSE	Sum of the squared relative error
TEM	Transmission electron microscopy
TEPA	Tetraethylene penta amine
TG	Thermogravimetry

TPD	Temperature programmed desorption
TSA	Temperature swing adsorption
wt.%	weight%
XPS	X-ray photoelectron spectroscopy
XRD	X-ray diffraction

Chapter 1 – Introduction

1.1 Climate change and CO_2 emission

The increase in the concentration of anthropogenic greenhouse gas (GHG) is considered to be the major reason for global climate change. Carbon dioxide (CO_2), methane (CH_4), nitrous oxide (N_2O), ozone (O_3), perfluorocarbons (PFCs), hydrofluorocarbons (HFCs) and sulphur hexafluoride (SF_6) are the major greenhouse gases [1, 2] among which CO_2 is the main greenhouse gas effecting the global climate change. The increase in the concentration of CO_2 is due to energy, transport, industry sectors (such as steels mills and refineries) that produce GHGs by the burning of fossil fuels like coal, oil, etc [3, 4].

According to the Intergovernmental Panel on Climate Change (IPCC), carbon dioxide concentration in the atmosphere has globally grown by more than 100 ppm (44%) in the last 250 years: from 275–285 ppm in the pre-industrial age to around 407.96 ppm in 2017 and it may reach up to 570 ppm by 2100. In 2010, about 38±3.8 $GtCO_2eq$ (~76%) CO_2 emissions from burning of fossil fuels was found which further increased in the year 2010-2011 and 2011-2012 at a rate of 3% and 1-2% respectively. Strong dependence on fossil fuels for energy requirements has resulted in increase in average global temperature causing glaciers retreat, rise in sea level and increase of melting of surface ice [5, 6]. It seems that the arctic ice got thinned by nearly 40% in recent decades. During the period of 1901-2010, global sea level has risen by 0.19 m. Marine life gets effected by the increase in the CO_2 levels in ocean which increases the acidity due to pH drop by 0.1 [7-9]. In recent times, frequency of the weather pattern gets increased like large storms, heat waves, droughts, heavy rainfall and wild fires. By the end of 21st century, this increasing rate of CO_2 levels will cause rise of average global temperature by 2-6 °C, therefore CO_2 concentration stabilization to a level of 450 ppm is considered [10, 11]. Fig. 1.1 shows global greenhouse gas emissions during in the year between 1980 and 2017.

Latest CO_2 reading
February 13, 2018

408.00 ppm

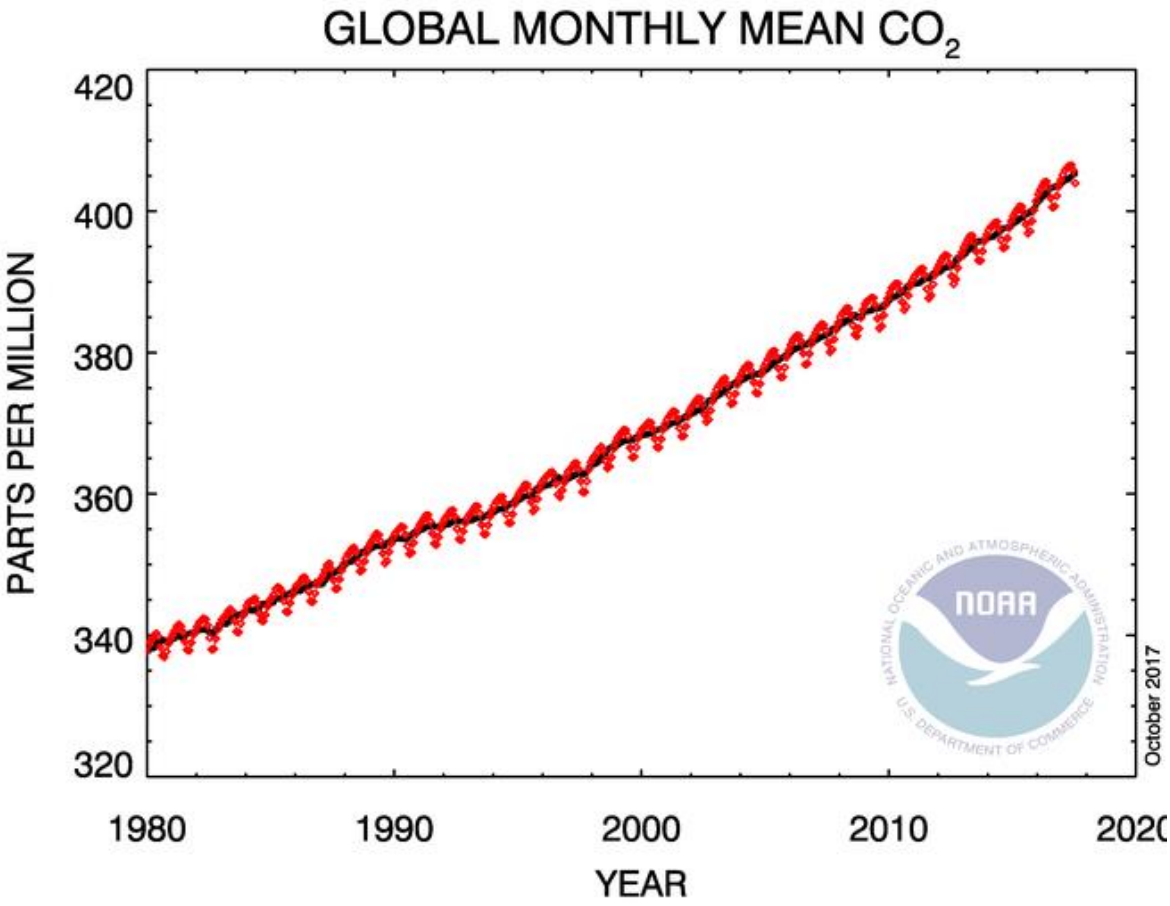

Fig. 1.1 Global greenhouse gas emissions during 1980-2017 [3]

1.2 Mitigation pathways

There are various approaches by which CO_2 concentrations can be reduced. Approaches are:

i. reduction in energy demand by improving the efficiency of energy conversion devices,
ii. using renewable energy sources and increased usage of low carbon fuels including natural gas, hydrogen or nuclear power,
iii. applying geo-engineering approaches, e.g. afforestation and reforestation.
iv. carbon dioxide capture and sequestration (CCS).

Among the mentioned approaches, CCS is considered to be a key technology which can drastically reduce the increasing CO_2 concentrations and allowing fossil fuels usage for meeting the energy requirements [12, 13]. The other approaches having great potential but they are still under development and are not yet commercially viable to meet the present energy demands.

1.3 Carbon dioxide capture and sequestration

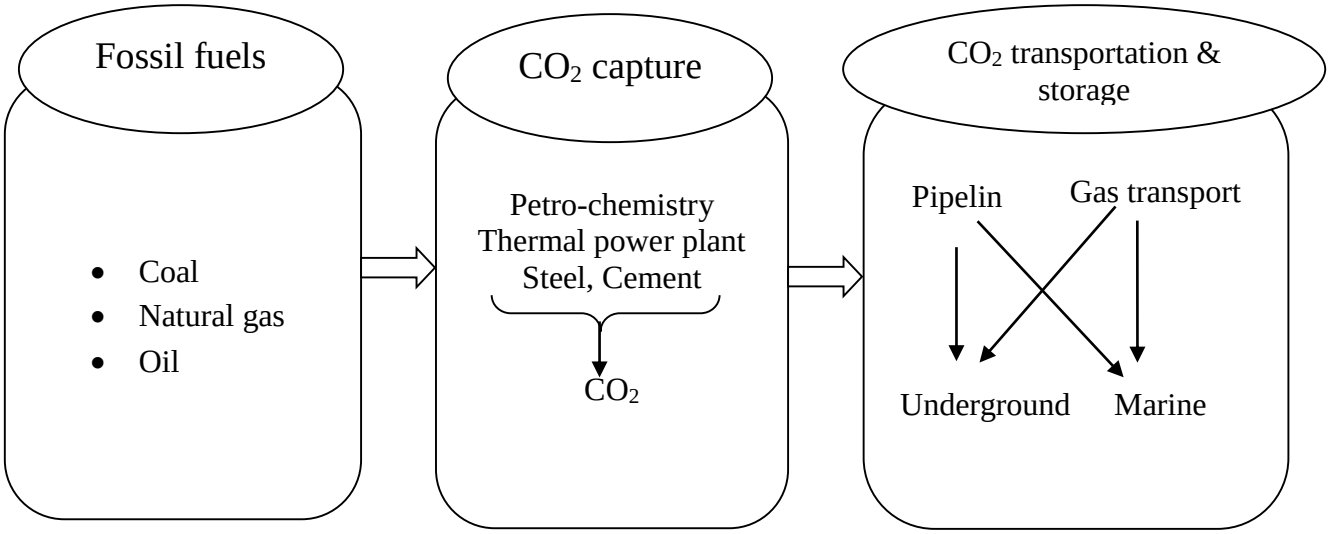

Fig. 1.2 Concept and summary of CO_2 and storage (CCS) [14]

Fig. 1.2 shows overall CCS technology which is generally capturing CO_2 from energy sources without discharging into atmosphere and sequestration/storage. There are several important factors which need to be considered related to cost involved for application of CCS on fossil fuels. Factors are capture plants scale, fuel cost, distance between capture location and storage site, characteristic of power plants technology, etc. Transportation of compressed CO_2 to a storage site via. pipeline are marginal portion of overall cost [7, 15]. CO_2 storage sites include geological formation like oil and gas fields which is estimated to sequester around 1120–3400 $GtCO_2$. Sequestration requires high pressure and concentrated CO_2 stream considering the economics involved in its transportation and injection into storage site. Therefore, cost effective and efficient CO_2 capture technology developed holds the highest priority in the field of CCS.

1.3.1 CO_2 capture technologies

There are three main CO_2 capture approaches namely, post-combustion, pre-combustion and oxyfuel combustion.

1.3.1.1 Pre-combustion capture

In the pre-combustion CO_2 capture process, CO_2 is captured prior to fossil fuel combustion. This is done by either partial oxidation/gasification of fuel (coal or natural gas) conducted in a gasifier under low oxygen level to produce synthesis gas which considers CO and H_2 as shown in Fig. 1.3. This is free from other pollutants gas. Further syngas under water-shift reaction with steam need to be developed to produce CO_2 and H_2. This process has several dis-advantages like conversion of fuel is expensive and process is complex. This process is used in mainly integrated gasification combined cycle (IGCC) plant using fuel like coal but with disadvantage of efficiency loss of 7-8%. Also, in fertilizer industry and hydrogen generation, this process is used.

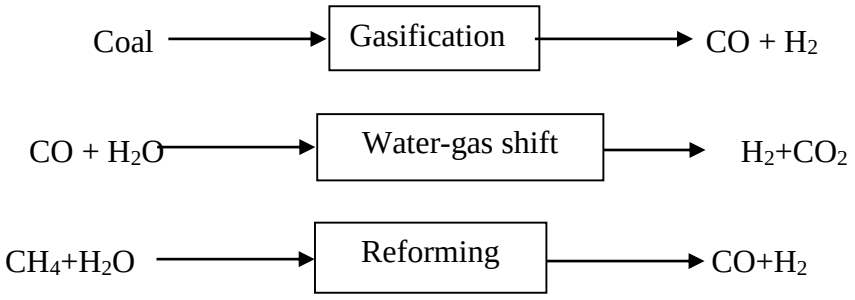

Fig. 1.3 Schematic diagram of pre-combustion CO_2 capture process

1.3.1.2 Oxyfuel-combustion capture

This combustion capture technology, instead of air, uses pure oxygen (95% purity) for fossil fuel combustion and this is in trial phase. As oxygen is used for combustion, major composition of flue gas is CO_2, water, particulates and SO_2. Particulates and SO_2 are removed by conventional electrostatic precipitator and flue gas desulphurization methods, respectively. Remaining gas is of high concentration CO_2 which can be compressed, transported and stored as shown in Fig. 1.4. The disadvantage of this process is that it consumes huge amount of oxygen coming from energy intensive air separation unit which results in energy penalty of

over 7% in comparison to without CCS. Corrosion problem occurs due to high concentration of SO_2 in flue gases [16-18].

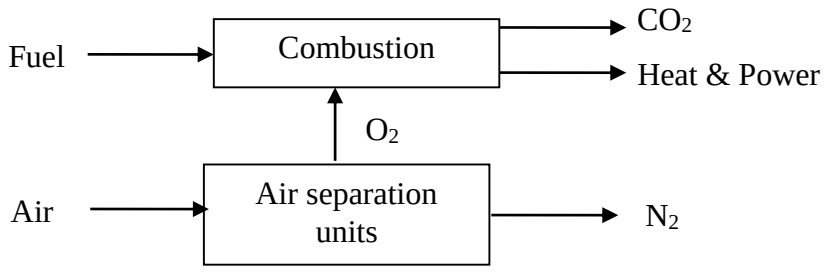

Fig. 1.4 Schematic diagram of oxyfuel-combustion CO_2 capture process

1.3.1.3 Post-combustion capture

This type of capture technology is the most preferable one because it gets retrofitted to existing power plants without changing the configuration of the plant. It is flexible because its maintenance does not stop power plant operation and it can be controlled. It is the separation of CO_2 from mainly N_2 in flue gas derived from combustion of fossil fuels such as coal, natural gas, or oil in air. CO_2 is captured from flue gas after combustion at low pressure (atmospheric pressure) and low CO_2 content (3-20%). At small scale, this technology with CO_2 recovery rate of 800t/day proved to be the best among this technology. The challenge for this technology is energy penalty and cost of CO_2 capture unit for reaching CO_2 concentration of above 95.5% needed for transportation and storage [19-21].

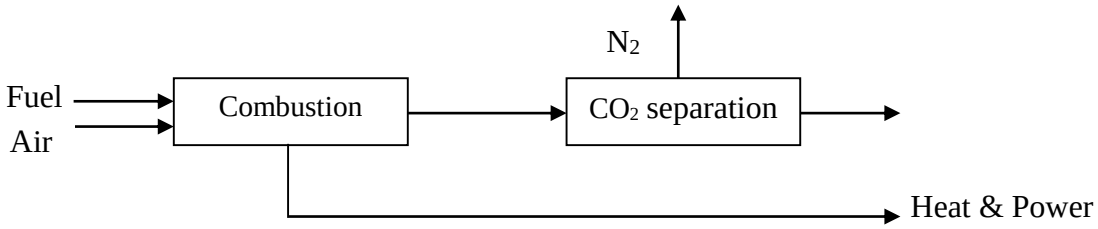

Fig. 1.5 Schematic diagram of post-combustion CO_2 capture process

Post-combustion carbon capture technologies are; (a) absorption [22] (b) membrane [23, 24] (c) cryogenic [25] (d) microalgal bio-fixation [26] and (e) adsorption. Fig. 1.6 shows complete technology option.

1.3.1.3.1 Absorption

This process is the most matured and established technology in petroleum and chemical industries for CO_2 separation. In this process, CO_2 is absorbed from flue gas into an absorbent soultion i.e., amines like monoethanol amine (MEA), diethanol amine (DEA), methyldiethanol amine (MDEA) etc., ammonia solution, rectisol (chilled methanol) by chemical action, leaving the remaining gas stream to pass through absorption column freely [27-29]. Fig. 1.7 shows absorption carbon capture process.

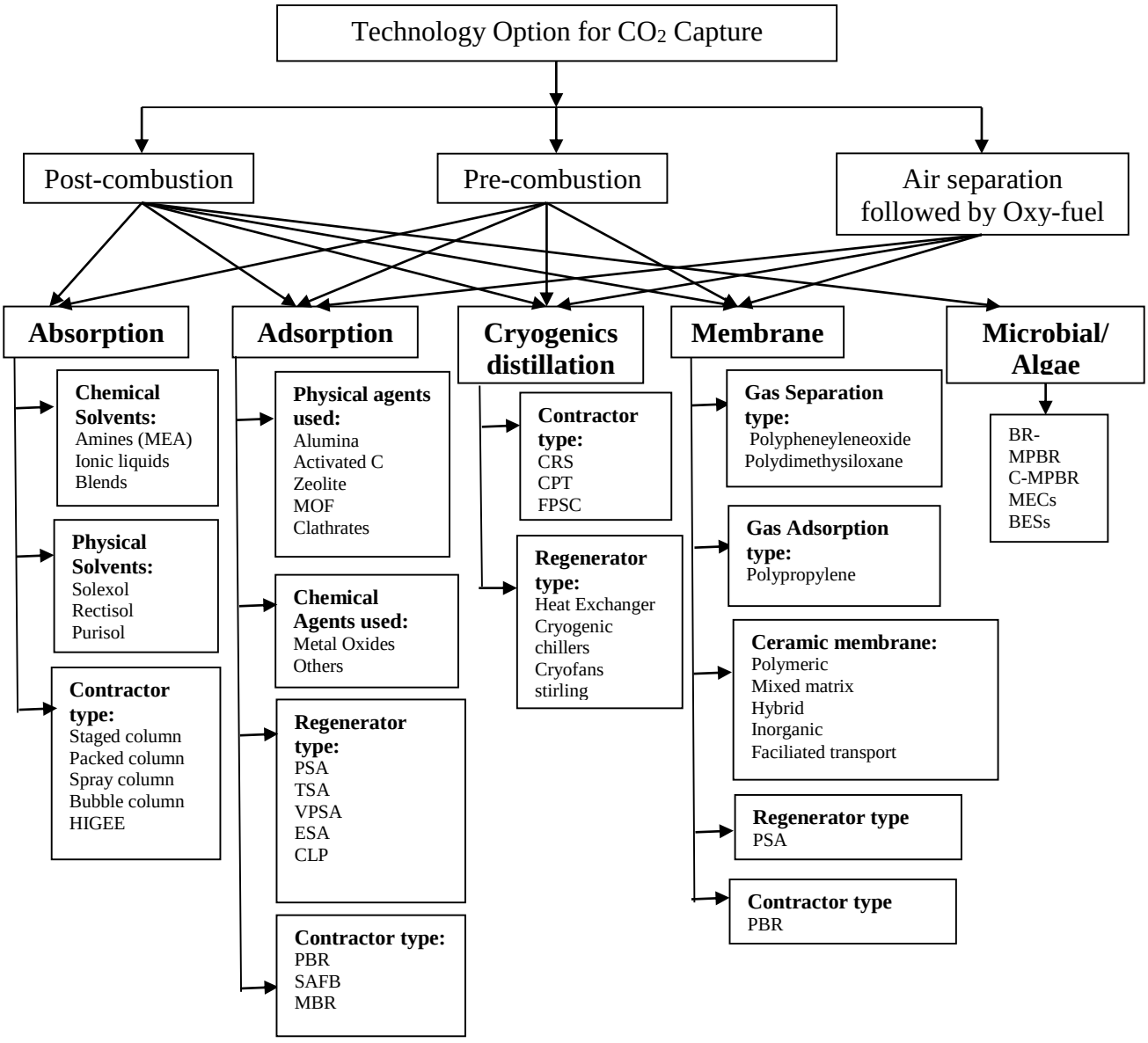

Fig. 1.6 Technology options for CO_2 separation and capture

Veawab *et al.* [30] and Aaron *et al.* [31] in their studies for CO_2 separation found MEA to be the most efficient for CO_2 absorption of about 90%. At present, capacity of $1tCO_2/h$ pilot plant has been tested successfully for coal fired power plant which is using 30% MEA solution. Other sorbents like piperazine and anion-functionalized ionic liquid [32] have attracted attention because piperzine react much faster than MEA but having problem of larger volatility than MEA.

This technology suffers from problem like amine degradation resulting in solvent loss, equipment loss, generation of volatile degradation compounds and high energy requirement for regeneration which impede its implementation [32, 33].

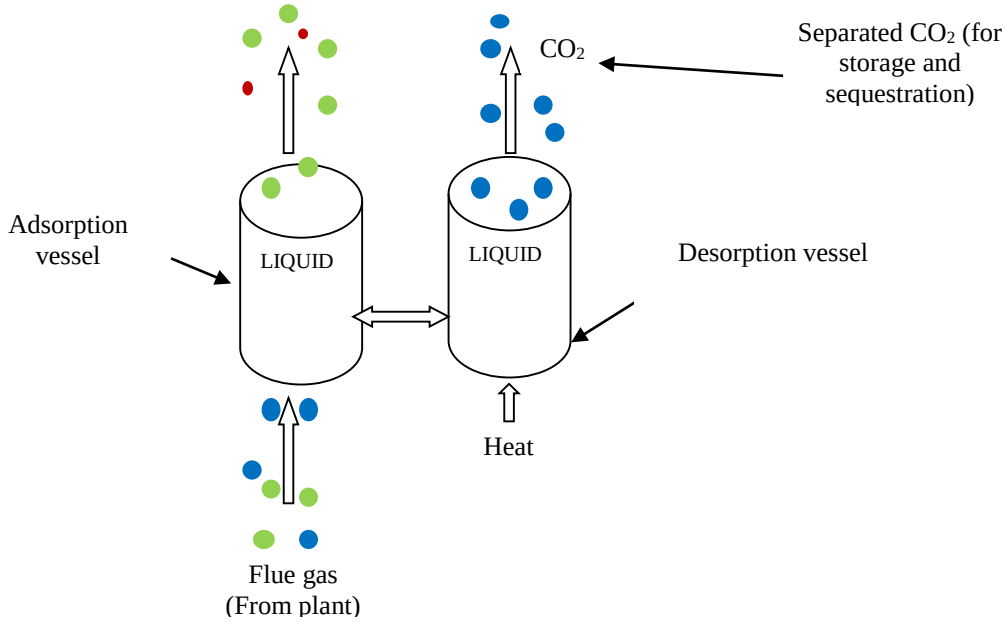

Fig. 1.7 Schematics of absorption carbon capture process using amine [34]

1.3.1.3.2 Membrane separation

In this process, membrane like polymer/ceramic made membrane is used to allow only CO_2 to pass through and not allowing the other flue gas components (Fig.1.8). Membrane, which is the essential part of this process, made up of polymer and ceramic materials in which a thin selective layer is bonded to thick low-cost non-selective layer, which provides mechanical support to the membrane [35]. The major hurdle of this process is low CO_2

concentration and pressure. This process is used to separate O_2 from N_2 and CO_2 from natural gas.

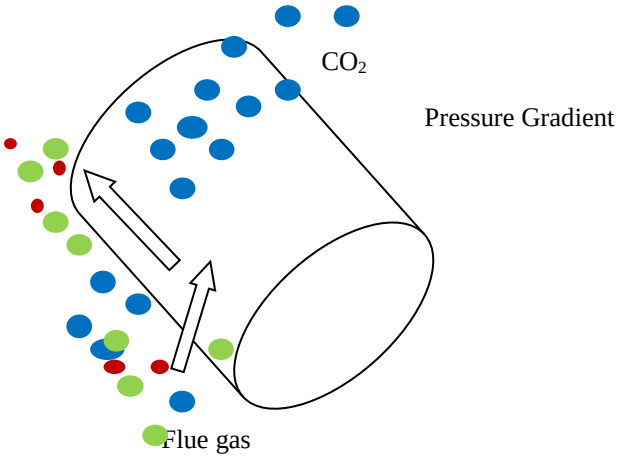

Fig. 1.8 Schematic of membrane carbon capture process

1.3.1.3.3 Cryogenic distillation

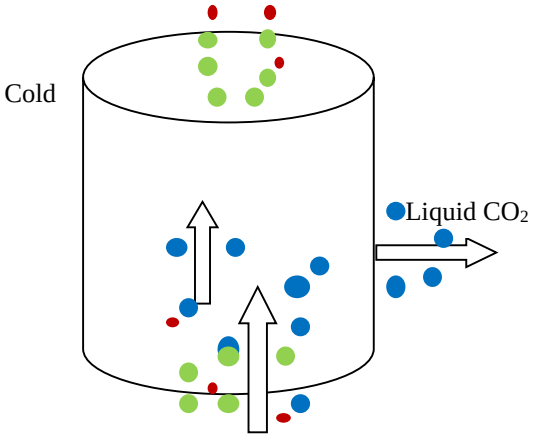

Fig. 1.9 Schematic of cryogenic carbon capture process

This process is carried out at high pressure and low temperature and is similar to other conventional distillation process. The major difference is that it is used to separate gaseous mixture on the basis of their boiling point while other processes separate the liquid. In this process CO_2 separation is done by cooling flue gas containing CO_2 to desublimation temperature (100 to 135 °C). After this, the solidified CO_2 is separated from light gas and

compressed to 100-200 atmospheric pressure. In this process upto 90-95% CO_2 is recovered but as it is carried out at low temperature and high pressure, it is energy intensive. Also, this process is applicable for only high CO_2 concentration which makes its application unsuitable for practical applications [31, 36].

1.3.1.3.4 Micro-Algal bio fixation

This technique uses photosynthetic organisms (microalgae) for capture of anthropogenic CO_2. Among the microalgae, aquatic microalgae considered to be having greater potential due to their higher carbon fixation rates than land plants. Culturing of microalgae is quite expensive but process produces high value compounds that can be used for revenue generation [37]

1.3.1.3.5 Adsorption

Adsorption using solid adsorbents has received much attention because of reducing energy penalty. Also, some characteristics like high adsorption capacity, selectivity and fast kinetics coupled with good thermal and mechanical stability provide its use in near term[38]. Potential adsorbent such as zeolites [39-41], activated carbons [42, 43], metal-organic frameworks [44, 45], amine supported mesoporous materials [46, 47], etc. have been studied. It was found that conventional adsorbents suffer from disadvantage of low selectivity towards CO_2 and large pressure and/or temperature gradient between adsorption and desorption steps. Therefore, there is a need to develop an effective and selective adsorbent for CO_2 capture which make adsorption the most promising technology.

1.4 Thesis motivation and objectives

It was seen that researchers tried to improve uptake capacity and selectivity of conventional adsorbents through amine modification or high thermal treatments with various chemical agents, but they faced problems like poor stability and blocking of adsorbent pores. Therefore, carbon based adsorbents are found to be attractive among them due to its high surface area, lesser energy requirement for regeneration, good thermal/mechanical stability and hydrophobicity [48]. It was seen that many researchers were trying to develop carbon adsorbent either by direct carbonization or by physical/chemical activation of starting materials. Also, they tried to evaluate their uptake capacity mainly under static condition at room temperature. But, the disadvantage of their studies is both the synthesis and performance evaluation. It was

reported that direct carbonized adsorbent synthesis was time consuming and requires high amount of energy. Moreover, evaluation of adsorbent carried under static condition gives higher value of uptake capacity and it will not provide the real picture for flue gas applications. To overcome this gap, this study has been conducted in which textural properties was improved by nanocasting technique and CO_2 adsorption under dynamic conditions was performed at different CO_2 concentrations (5-12.5%) and temperatures (30-100 °C), which is more practical than static conditions. Also, chemical activation of selected carbon adsorbents have been performed and adsorption study have been conducted for the same.

The overall objective of the research is to develop effective sorption process for the continuous removal of CO_2 from point source. The specific objectives are:

- Synthesis of carbon adsorbents with specific pore structures and surface areas using nanocasting and without nanocasting from various polymers.
- Chemical activation of selected carbon adsorbents.
- Characterization of synthesized adsorbents for their relevant properties.
- Study the adsorption performance of adsorbent using a fixed bed adsorption at different flow rates, temperatures, pressures and feed concentrations of CO_2.
- To fit the equilibrium and kinetic models for the experimental data.

1.5 Thesis overview

This thesis has been divided into **eight chapters**. Three different types of nanostructured carbons by nanocasting technique and one high surface area nitrogen enriched carbon were developed by direct carbonization followed by chemical activation for CO_2 capture. Textural, surface and chemical properties was studied by thorough characterization of the prepared carbons. Dynamic adsorption-desorption experiments were conducted in the fixed-bed system to evaluate their CO_2 adsorption capacities, selectivity and regeneration under simulated flue gas conditions. Adsorption of CO_2 on these adsorbents was also evaluated from kinetics, isotherm and thermodynamic point of view. Energy required for CO_2 desorption was also calculated.

The schematic of the overall thesis work is shown in Fig. 1.

Chapter one (Introduction) presents the current environmental issues and the brief description of CO_2 capture. It covers the various greenhouse gases especially CO_2 and its

impact on global climate. Approaches for mitigating these issues have also been addressed in this chapter and provides the problem statement and the objectives of this research.

Chapter two (literature review) discusses different types of adsorbents and their adsorption performances were compared. More emphasis has been given to carbon based adsorbents as the current work focuses on them.

Chapter three (Materials and methods) shows the outline of **experimental** works in this research. This chapter is divided into three parts. The materials, chemicals and experimental methods used for the characterization and performance evaluation used for carrying out the adsorption-desorption experiments are listed in the first and second part. The experimental setup for fixed-bed adsorption study is also presented in this chapter. In the third part, various adsorption kinetic, isotherm models and thermodynamic parameters are discussed.

Chapter four discusses the synthesis of carbon adsorbents from melamine-formaldehyde resin via nanocasting technique followed by thorough characterization. CO_2 adsorption performance of the prepared carbons has been evaluated and the results are related to their physico-chemical properties. The optimized sample of this series was further studied under simulated flue gas conditions at varying adsorption temperatures. This chapter also includes the complete kinetic, isothermal and thermodynamic study of CO_2 adsorption on the optimized sample along with energy calculation required for desorption.

Chapter five covers the development and characterization of nanostructured carbons from epoxy resin and mesoporous zeolite as polymeric precursor and hard template respectively. CO_2 adsorption-desorption studies on these carbons were carried out under dynamic conditions and the optimized sample was investigated comprehensively. Kinetic models and isotherms were fitted to the experimental data and thermodynamic parameters were also calculated. Finally, energy penalty for the whole process system was estimated.

Chapter six covers the development and characterization of nanostructured carbons from urea-formaldehyde resin and mesoporous zeolite as polymeric precursor and hard template respectively. CO_2 adsorption-desorption studies on these carbons were carried out under dynamic conditions and the optimized sample was investigated comprehensively. Kinetic models and isotherms were fitted to the experimental data and thermodynamic

parameters were also calculated. Energy penalty for the whole process system was also estimated.

Chapter 7 covers the development and characterization of high surface area adsorbents from UF and activation with KOH. CO_2 adsorption-desorption studies on these carbons were carried out under dynamic conditions and the optimized sample was investigated comprehensively. Kinetic models and isotherms were fitted to the experimental data and thermodynamic parameters were also calculated. Energy duty required for desorption of adsorbed CO_2 was calculated.

Finally, chapter eight (Conclusions and recommendations) summarizes the data reported and also gives some recommendations for future research.

At the end, the references cited in this thesis have been listed

Chapter 2 – Literature Review

2.1 Adsorption technology

In this technology, the adsorbate (CO_2) molecules are adsorbed onto a surface of solid sorbent. The process can be classified as physical adsorption (physiosorption) and chemical adsorption (chemisorption) depending on the interaction between the adsorbent and adsorbate molecules. Physical adsorption involves weak Van der Waal forces while chemisorption involves chemical bond between adsorbent and adsorbate molecules.

In this technology, CO_2 adsorption is carried out by using several approaches like (i) isothermal regeneration means, like pressure swing adsorption (PSA), including vacuum (VSA) or (ii) non-isothermal regeneration means, like temperature swing adsorption (TSA) [49-52]. In case of PSA, CO_2 adsorption is carried out at higher pressure while depressurization is done by swing to low pressure (usually atmospheric pressure). In TSA, desorption is done by raising the temperature. TSA requires large amount of time than PSA but it provides higher purity of CO_2 i.e more than 95% and 80% of recovery can be achieved [53, 54].

2.2 Types of adsorbents

Several available adsorbents for CO_2 capture are zeolites, silica, metal organic frameworks, activated alumina, carbon based adsorbents, carbon nanotubes (CNTs), activated carbon fibers, and graphene [55, 56]. For effective capture of CO_2 by adsorption process, strengths and limitations of each adsorbent like low energy requirement complete regenerability and high adsorption capacity should be considered. It is very difficult by a single technology to fulfill all these criteria by NETL and DOE. Eventually, adsorbents that can work effectively within the practical CO_2 capture process will be the winners.

2.2.1 Silica based adsorbents

Mesoporous silica materials due to their high surface area, tunable porous structure, provide faster diffusion of gas received much attention for CO_2 capture application. Larger presence of hydroxyl groups on the surface facilitates grafting of amine groups by which the adsorption capacity gets enhanced.

First study was carried out by Xu *et al.* [57] on CO_2 adsorption (determined by thermogravimetric analysis) using amine-impregnated mesoporous silica. Using wet impregnation method, they impregnated polyethyleneimine (PEI) at different loadings on MCM-41 silica which was termed as "molecular basket" [58-61]. With 75 wt.% PEI loading at 75 °C under 10% CO_2 in N_2 atmosphere, CO_2 uptake of ~2.1 mmol g^{-1} was achieved [57]. With increase in temperature from 25 °C to 75 °C, adsorption capacity gets increased [58, 60, 61]. They compared two other two methods (two-step impregnation and mechanical mixing method); one-step wet impregnation method was better [61]. Effect of moisture on adsorption capacity of PEI-impregnated MCM-41 was also studied [59]. With 10% moisture and 13% CO_2, CO_2 adsorption capacity increased to 2.84 mmol g^{-1} as comparison to simulated dry flue gas having 15% CO_2 which shows CO_2 adsorption of 2.01 mmol g^{-1}. No further rise in CO_2 uptake was observed for further rise in moisture content in the feed stream.

Franchi *et al.* [62] worked on pore-expanded MCM-41 (PE-MCM-41) in which diethanolamine (DEA) impregnation was carried out. CO_2 adsorption was studied thermogravimetrically and 2.93 mmol g^{-1} capacity at 5% CO_2 atmosphere and 25 °C was observed. Here, moisture had no effect on CO_2 uptake of DEA-loaded PE-MCM-41.

In another study by Belmabkhout *et al.* [63] on MCM-41 type mesoporous silicas in which CO_2 capture at different temperatures from 60 °C to 120 °C was evaluated. At 1 bar pressure and at 100 °C, CO_2 adsorption capacity of 0.66 mmol g^{-1} was obtained while at 45 bar and 25 °C, CO_2 adsorption capacity of 14.7 mmol g^{-1} was obtained. Using MCM-41-100 and hydrothermal treatment, prepared pore-expanded mesoporous silica (PE-MCM-41) grafted with a triamine, CO_2 adsorption was carried out thermogravimetrically at four different temperatures and at very low pressure up to 1 bar. TRI-PE-MCM-41 at 25 °C and 1 bar exhibit CO_2 adsorption capacity of 2.8 mmol g^{-1} and with moisture, the adsorption capacity increased because of partial formation of bicarbonate [64, 65].

Chen *et al.* [66] impregnated PEI and tetraethylene penta amine (TEPA) on monolithic silica and observed that for 5% CO_2 feed stream, 65% PEI loaded monolith silica at 75 °C, maximum gravimetric adsorption capacity was 3.75 mmol g^{-1} which was better than PEI modified KIT-6 [67] under same conditions. On the other hand, TEPA modified monolith silica at 75 °C under 100% CO_2 flow showed CO_2 adsorption capacity of 5.91 mmol g^{-1}. The disadvantage of using TEPA is that it showed decrease in uptake capacity after 5 runs of adsorption–desorption cycle.

Sanz-Pe ´rez *et al.* [115] using SBA-15-TEPA using a simulated gas mixture, found that after 10 adsorption–desorption cycles, the CO_2 adsorption capacity of SBA-15-TEPA was 86% of the initial value. The adsorption capacity under 100% CO_2 at 318 K was 2.57 mmol g^{-1}. Under 15% CO_2 concentration at 318 K and 1 bar, CO_2 adsorption capacity of 3.68 mmol g^{-1} is oobtained in a humid stream. They concluded that presence of 5% moisture greatly affects the CO_2 adsorption capacity, the capacity gets increased

Mello *et al.* [68] on amine-modified MCM-41 mesoporous silica showed that at 0.1 bar pressure, CO_2 uptake of MCM-41-NH_2 was 3.08 wt.%, which is much higher than that of 0.53 wt.% for MCM-41. This could be because of higher affinity of CO_2 (Lewis acid) towards basic amine sites at lower pressure. On the other hand, at 2.1 bar pressure, the CO_2 uptake was almost similar to MCM-41-NH_2 and MCM-41 of 1.15 and 1 mmol g^{-1}, respectively

2.2.2 Zeolites based adsorbents

Zeolites are highly ordered crystalline microporous aluminosilicates frameworks materials with large internal specific surface areas and uniform pore size of 0.5-1.2 nm, forming networks of interconnecting channels for adsorbing gas molecules [38, 69, 70]. They are generally used at high pressures (> 2 bar) and their adsorption capacity is reported to reduce drastically in the presence of moisture in gas stream. This is because of hydrophilic nature in which polar water molecules get adsorbed on zeolite surface and block the access for CO_2 by which CO_2 capacity get reduced. This is the main reason for very high temperature (>300 °C) requirement for regeneration of zeolites and therefore large energy are required for regeneration [71-73].

Bertsch *et al.* [74-76] using zeolite X and Y confirmed that physiosorption was the dominating process for these zeolites. A very small adsorption of 0.15 mmol g^{-1} was found. In this study, the effects of aluminum content on CO_2 adsorption properties of zeolites are shown.

Barthomeuf *et al.* [77] showed the strength of basic site on different zeolites X, Y, mordenite (MOR), and ZSM-5 (MFI). They showed that with the increase of aluminium content, basic strength of zeolites increased due to lower electronegativity of aluminium. In other study, same authors showed different types of exchangeable cations. They found that basicity increases with decrease in electronegativity and base strength of Cs-exchanged zeolite X is highest among all. It was also suggested that porous characteristics are also having effect on CO_2 adsorption capacities on commercially available zeolites and synthesized zeolites.

Cavenati *et al.* [78] synthesized zeolite 13X and showed CO_2 uptake of 6.5 mmol g^{-1} at 25 °C and 10 bar. On the other hand, synthesized zeolite 5A by Saha *et al.* [79] at 25 °C and 1 bar and 10 bar pressure showed CO_2 uptake of ~4.7 mmol g^{-1} and 5.06 mmol g^{-1} respectively. In another study on commercial zeolites 13X and 4A by Siriwardane *et al.* [80] at 25 °C and 1 bar showed static equilibrium CO_2 adsorption capacity of 3.64 mmol g^{-1} and 3.07 mmol g^{-1}, respectively.

Dominguez worked on three different natural zeolites erionite (ERI), mordenite (MOR), and clinoptilolite (HEU). At 290 K and 0.1 bar, adsorption capacities were found in the range of 1.6 to 2.7 mmol g^{-1} [81].

Harlick *et al.* [82] carried out pure component adsorption study on different synthetic zeolite, including 13X, NaY, HiSiv-1000, HY-5, ZSM-5-30 (MFI), and HiSiv-3000. They found that at 22 °C and 1 bar, adsorption capacities of these zeolites varied from 1.2 mmol g^{-1} (HY-5) to 4.5 mmol g^{-1} (13X). It is seen that CO_2 adsorption capacities are greatly influenced by H_2O which is present in flue gas. H_2O over CO_2 competes for adsorption sites on zeolites [82].

Bertsch showed effect of preadsorbed H_2O at low CO_2 partial pressures. He found that its presence accelerates the CO_2 adsorption on NaX zeolite. Within a few minutes, it attained equilibrium while more than 60 h was taken by dehydrated zeolite [74]. This is due to decrease in activation energy for CO_2 diffusion, owing to the occupation of high-energy sites by H_2O molecules.

Ruthven showed effect of H_2O on adsorption capacities on various zeolites such as NaLSX, LiLSX, and CaX [73]. He found that the adsorption capacity reduced strongly with the presence of H_2O. With the increase in H_2O concentration from 0.8 to 16.1 wt%., at 0.06 bar and 50 °C, CO_2 uptake on CaX zeolites decreased from 2.5 to 0.1 mmol g^{-1}.

Siriwardane *et al.* [83] carried out adsorption/desorption study on zeolite 13X at 22 °C and 17 bar under 15% CO_2 concentrations. Under humid conditions, they found that after carrying out 2 adsorption/desorption cycles, adsorption capacity decreased from 6 to 4 mmol g^{-1}.

Similarly, Tezel reported that the CO_2 adsorption capacity of zeolite 13X could be completely recovered with negligible changes in the isotherms by regenerating the adsorbents at 200 °C for 12 h [82].

Some research groups modified the adsorption capacity of zeolitic adsorbents by exchanging the cations with various alkali or alkaline earth metal species and also by using different amines like MEA, ethylenediamine (ED) and isopropanol amine (IPA). For example, LeVan *et al.* [84] in a study on zeolites NaX and NaY by ion exchange with other alkali metal cations, observed that CO_2 adsorption, with the increase of ionic radii get increased in the order of Cs+ < Rb+ < K+ < Na+ < Li+ Adsorption capacity at 25 °C and 1 bar pressure, of 5.6 and 5.2 mmol g^{-1} was observed by exchanging Li+ with X and Y respectively. In ther case, adsorption capacity of 3.1 and 2.6 mmol g^{-1} was obtained for Cs+.

Jadhav *et al.* [85] using monoethanol amine (MEA) via impregnation method worked on zeolite 13X. They observed that after modification the CO_2 adsorption capacity reduced at 30 °C and 50 °C but the trend of CO_2 adsorption at 75 °C and 120 °C was different. For unmodified zeolite, it was 0.28 and 0.14 mmol g^{-1} but changed to 0.35 and 0.49 mmol g^{-1}. This is because of reduction in surface area and pore volume and due to chemical interactions between amine groups on zeolite and CO_2 molecules. Chatti *et al.* [86] using different amines like MEA, ethylenediamine (ED) and isopropanol amine (IPA) modified the CO_2 adsorption capacity of zeolite 13X. Dynamic CO_2 adsorption capacity of IPA modified zeolite under 15% CO_2 (remaining He) flow was 0.52 mmol g^{-1} > MEA modified zeolite (0.45 mmol g^{-1}) > bare zeolite (0.36 mmol g^{-1}). Under 100% CO_2 at 75 °C, equilibrium adsorption capacity of MEA modified zeolite and bare zeolite was 1.1 and 0.85 mmol g^{-1} respectively.

2.2.3 Carbon based adsorbents

Carbon based adsorbents have been considered as potential CO_2 adsorbents because of advantages like complete regenerability, preparation from low cost sources, high surface area, etc [6, 87, 88]. Different carbon based adsorbents are activated carbons, carbon molecular sieves [89-91] and carbon nanotubes (CNT) [92]. Different activated carbons are synthesized using biomass sources, coal, industrial byproducts, wood and have been evaluated for CO_2 adsorption [93, 94].

2.2.3.1 Commercial activated carbons

. For high pressure CO_2 capture application, carbon based materials such as activated carbon, charcoal and coal have been used [26,48] because of low cost, their insensitivity to moisture and high surface areas [49].

Na *et al.* [95] in his study carried out on commercial activated carbon, using pressure swing adsorption, evaluated CO_2 adsorption capacity of the adsorbents at 1 bar at different temperatures of 15 °C and 55 °C. The obtained equilibrium adsorption capacity was 3.2 and 1.6 mmol g^{-1} respectively at 1 bar under pure CO_2 flow.

Himeno *et al.* [96] using MAXSORB activated carbon showed static equilibrium CO_2 adsorption capacity of 25.7 mmol g^{-1} at 30 bar and 25 °C.

2.2.3.2 Carbon adsorbents from renewable resources

In the recent time, porous carbons have been produced by pyrolysis of different carbon containing resins, fly ash, or biomass [26]. Due to large number of availability of raw materials, tailoring of these materials in terms of pore size distribution, pore structure, active surface structure, and other factors like adsorption properties can be done [56].

Using raw materials, these materials can be prepared by using two steps: carbonization and activation. Carbonization was carried out by heating and pyrolysis of precursors in an inert atmosphere to produce carbonaceous material (char) [94]. During this process, precursor releases non-carbon elements such as hydrogen, oxygen, and nitrogen. This develops the materials having a rigid carbon skeleton known as chars having poor surface properties [97]. To improve the surface areas, porosity and active sites, activation was performed using physical or chemical treatment [94]. Physical activation is carried out at higher temperatures around 600 to 900 °C by the partial gasification of chars with steam, CO_2, air, or a combination of these [97]. Chemical activation is performed at lower temperature by using chemicals such as KOH, $ZnCl_2$, NaOH, H_3PO_4 etc. [98]. In chemical activation, the yield of carbon is much higher with well-developed porosity and surface areas [98, 99]. Wang *et al.* [100] using waste celtuce leaves developed porous carbons by carbonization followed by chemical activation with potassium hydroxide (KOH). The obtained material shows surface area of 3404 m^2 g^{-1} and equilibrium CO_2 uptake of 4.36 mmol g^{-1} at 1 bar pressure and 25 °C

Adsorbents obtained using fly ash via. impregnation of organic bases like polyethyleneimine (PEI) aided by polyethylene glycol, tetraethylene-pentaamineacrylonitrile (TEPAN) and diethanolamine (DEA). The obtained materials exhibited CO_2 uptake in the range of 0.91–1.3 mmol g^{-1} with pure CO_2 flow at 75 °C [101]. In another study carried out on fly ash derived carbons, obtained by impregnation of different kind of amines (MEA, DEA, and MDEA) to improve the textural properties, were evaluated the CO_2 adsorption performance at different temperatures. CO_2 uptake of 1.56 mmol g^{-1} was observed for MEA impregnated carbon at 30 °C which was higher than parent activated fly ash carbon (0.95 mmol g^{-1}). It was also observed that due to impregnation, specific surface area of the carbons decreased because of blocking of the pores [102].

Plaza *et al.* [103] in his study using biomass residue (olive stones) by CO_2 activation and treatment with ammonia (NH_3) developed activated carbons. The obtained carbon activated by CO_2 at 25 °C and 100 °C under 100% CO_2 atmosphere showed CO_2 uptake of 2.4 mmol g^{-1} and 0.7 mmol g^{-1} respectively. On the other hand, at same condition but NH_3 treated carbons showed CO_2 capacities of 1.9 mmol g^{-1} and 0.6 mmol g^{-1}, respectively.

In another study on almond shell based activated carbons, obtained from CO_2 activation under 15% CO_2 in N_2 exhibited CO_2 uptake of 1.2 mmol g^{-1} and 2.6 mmol g^{-1} under 100% CO_2 atmosphere at 25 °C while aminated almond shells based carbons, (with 4.5% nitrogen), at 25 °C under 15% and 100% CO_2 flow exhibited CO_2 uptake of 1.1 and 2.2 mmol g^{-1} [104].

Wang *et al.* [200] successfully developed a high surface area 700 m^2/g and N content of 10% novel imine-linked polymer (ILP) and further developed N-doped porous carbons by direct pyrolysis of ILP at 600-800 °C, having specific surface area and narrow micropore size distributions of 366 m^2/g. The CO_2 adsorption capacity of porous ILP and N-doped porous carbons at 25 °C were 1.05 and 1.95 mmol g^{-1}, respectively. This study also confirms the effect of narrower micropore sizes adsorbents on CO_2 adsorption capacity.

Nitrogen enriched carbons were prepared by Thote *et al.* [105] using soybean via. chemical activation by zinc chloride and physical activation with CO_2. The obtained material exhibited dynamic CO_2 uptake (0.51 mmol g^{-1}) in comparison to commercial carbon (0.36 mmol g^{-1}) at 75 °C under 15.4% CO_2 concentration. The higher uptake capacity is due to presence of nitrogen functionality in the carbon matrix. The specific surface area of the prepared carbon was similar to that of commercial activated carbon. The disadvantage of this

adsorbent is that it was not able to regenerate at 75 °C, showing zero adsorption in the next cycle.

Olivares-Martin *et al.* [106] developed carbon adsorbents from waste carpet materials using carbonization and activation with KOH. The obtained material at 30 °C under 100% CO_2 flow shows CO_2 uptake of 3.13 mmol g^{-1}. With the rise of adsorption temperature upto 100 °C, the capacity reduced to 0.7 mmol g^{-1}. Under 15% CO_2 concentration, CO_2 uptake of 0.89 mmol g^{-1} and 0.16 mmol g^{-1} at 25 °C and 100 °C was attained. This study shows the effect of activation conditions and type of precursor used.

In another work, Sevilla *et al.* [107] developed porous carbons from polysaccharides (starch and cellulose) and biomass (sawdust) using hydrothermal carbonization and chemical activation with KOH. The obtained material (at 25 °C and 50 °C, 1 bar pressure) showed static CO_2 uptake of 4.8 mmol g^{-1} and 3.6 mmol g^{-1} respectively.

2.2.3.3 Carbon adsorbents from synthetic polymers

Synthetic polymers have also gained popularity in present studies as polymeric precursor apart from conventional activated carbons and biomass derived carbons. Since the developed porous carbons contain refined pore structures, improved chemical properties and better surface chemistry.

Sol-gel process, chemical vapor deposition, nanocasting and direct carbonization of precursor are different methods developed for the synthesis of porous carbons. Nanocasting techniques can be employed for synthesizing carbons since it improves textural properties and develops a controlled pore structure which cannot be easily synthesized from conventional activation technique. Moreover, conventional technique has disadvantages to that of nanocasting techniques since its synthesis process is complex and requires expensive reagents [108, 109]. This section deals with synthesis process of porous carbons into two part (a) template free synthesis i.e. by carbonization and/or activation of carbon-containing polymer, and (b) templating method i.e. by nanocasting technique.

2.2.3.3.1 Template free synthesis

Drage *et al.*[110] produced nitrogen enriched carbons from urea-formaldehyde (UF) and melamine–formaldehyde (MF) resins polymerized in the presence of K_2CO_3 as a chemical

activation agent followed by thermal activation over a range of temperatures. Adsorbents from UF and MF at 25 °C under pure CO_2 showed CO_2 uptake of 1.86 and 1.03 mmol g^{-1}, respectively.

Hao *et al.* [111] synthesized nitrogen doped carbons by carbonization of resorcinol and formaldehyde using L-lysine as catalyst. CO_2 uptake of these carbons, determined volumetrically, at 25 °C and 1 bar under pure CO_2 showed uptake of 3.13 and 0.62 mmol g^{-1} respectively.

Sevilla *et al.* [112] using polypyrrole (PPy) and chemical activation developed nitrogen-doped carbons. The CO_2 uptake capacity of the adsorbent activated (KOH/PPy = 2) at 600 °C showed high static CO_2 uptake of 6.2 mmol g^{-1} at 0 °C. But the capacity decreased to 3.9 mmol g^{-1} and 2.1 mmol g^{-1} respectively at 25 °C and 50 °C. On the other hand, by activation carried out (KOH/PPy = 4), equilibrium CO_2 capacity up to 2.1–2.6 mmol g^{-1} was obtained at 25 °C and 1 bar. Higher amount of nitrogen functional groups (pyridonic-N and pyridinic-N) and microporosity in mildly activated carbons than severely activated carbons caused higher CO_2 uptake.

Meng *et al.* [113] developed nitrogen containing nanoporous carbon using polypyrrole and chemical activation with sodium hydroxide. Nitrogen content upto 7 wt%, high surface area of 2169 m^2 g^{-1} and narrow microporosity was obtained. Static CO_2 uptake at (25 °C, 1 bar) was 4 mmol g^{-1}.

High nitrogen content carbons synthesized by Liu *et al.* [114] using urea-formaldehyde and chemical activation with KOH showed static CO_2 uptake of 3.21 mmol g^{-1} at 25 ˚C. This study shows that in addition to microporosity, heteroatoms also to be considered as important factor in CO_2 adsorption performance. In another work, same authors using precursors urea and furfural and carbonization followed by chemical activation with KOH developed N-doped carbons which equilibrium CO_2 uptake of 4.6 mmol g^{-1} at 25 °C and 1 bar. This study concluded that both nitrogen content and microporosity play a major role in CO_2 adsorption capacity [115].

Balsamo *et al.* [116] using coal tar pitch, furfural and carbonization followed by steam activation developed activated carbon (F50) which shows dynamic CO_2 adsorption capacity (using breakthrough column study) at 30 °C under 15% CO_2 of 0.61 mmol g^{-1}. Both

microporous structure and oxygen functionalities play major role. CO_2 uptake shows decrease in uptake (0.30 mmol g^{-1} to 0.15 mmol g^{-1}) with temperature rise from 50 °C to 75 °C.

Tseng *et al.* [117] using melamine modified phenol-formaldehyde resin and steam activation developed highly porous carbons. The obtained material, at 0 °C and 1 bar showed CO_2 uptake of 6.71 mmol g^{-1} and with temperature rise from 25 °C to 50 °C decreased from 2.2 to 0.4 mmol g^{-1}.

2.2.3.3.2 Carbons from nanocasting technique

Carbon material prepared by nanocasting technique is effective because it can overcome the challenges of conventional synthesis process, improves textural properties, and possible to control pore structure characteristics. In this technique, precursor is introduced to the template pores, carbonized and lastly template is removed [108, 118]. In this technique, synthesis takes place in confined nanospace, provided by the template pores resulting in development of nanostructured carbon. Depending upon the pore characteristics of template, porous structure of the template can be tailored. For synthesis of carbon material like high nitrogen and oxygen content (urea-formaldehyde resin, melamine-formaldehyde resin, acrylonitrile, acetonitrile) is important as they incorporate nitrogen and oxygen functionalities resulting in enhancement of basic nature of carbons which is beneficial for interaction between carbon surface and acidic CO_2 molecules.

Xu *et al.* [119] developed mesoporous carbons using sucrose as precursor and nano-$CaCO_3$ as hard template. The effect of template to precursor ratio on the textural properties of the prepared materials was studied in this study.

High nitrogen content carbon adsorbents prepared by Pevida *et al.*[120] from melamine-formaldehyde resin at 25 °C under 15% and 100% CO_2 flow, respectively showed CO_2 uptake of 1.41 and 2.25 mmol g^{-1}. This study shows the effect of both textural parameters and surface chemistry on the CO_2 capture performance of the adsorbents. Carbonization carried out at above 600 °C, cause decrease in basic nature of the adsorbent. It was seen that carbonization carried out at 700 °C, shows best textural properties but the capacity obtained at this temperature was lower as compared to others.

Sevilla *et al.* [121] using carbon source (furfural alcohol) and two hard templates mesostructured silica (hexagonally ordered SBA-15 and cubic ordered KIT-6) developed

mesoporous carbons. These carbons show static CO_2 capacity of 3.2 mmol g^{-1} and 2.0 mmol g^{-1} respectively at 25 °C and 50 °C and 1 bar. Nanocasting technique followed by chemical activation with KOH was used for the synthesis of adsorbents.

Zhao *et al.* [122] using two different precursors (i) p-diaminobenzene, and (ii) combination of p-diaminobenzene and furfural alcohol and IBN-9 mesoporous silica template developed nitrogen-doped carbons. Nanocasting technique and chemical activation with KOH at 600 °C were carried out for the development of the material. Improved textural properties of both the prepared carbons with maximum micropore area of 890 m^2 g^{-1} and equilibrium CO_2 uptake of 4.5 mmol g^{-1} at 25 °C and 1 bar was obtained.

Carbon nitride spheres were synthesized by Li *et al.* [123] using nanocasting technique and precursors (ethylenediamine and carbon tetrachloride) and hard template (spherical mesoporous cellular silica foams). The obtained material shows high nitrogen content of 17.8 wt% and highly mesoporous structure with specific surface area of 550 m^2 g^{-1}. The CO_2 uptake at 25 °C and 75 °C under pure CO_2 flow was 2.9 mmol g^{-1} and 0.97 mmol g^{-1} respectively.

2.2.3.4 Carbon nanotubes

Carbon nanotubes can be used for CO_2 capture due to their distinct pore structure, which allows them to achieve an ample series of surface functional groups when treated thermally or chemically [130, 131]. They comprise of single-walled carbon nanotubes (SWCNTs) and multi-walled carbon nanotubes (MWCNTs) modified with amine solutions. CO_2 was adsorbed on purified SWCNTs with temperature ranging from 0 to 200 °C.

Cinke *et al.* [92] developed purified SWCNTs in the temperature range of 0-200 °C, which exhibited high surface area and total pore volume of 1587 m^2 g^{-1} and 1.55 cm^3 g^{-1}. Higher adsorption capacity (~4.1 mmol g^{-1}) as compared to activated carbon (~2.2 mmol g^{-1}) at 35 °C and 1 bar was obtained.

Lu *et al*. [124] developed multi-walled carbon nanotubes (MWCNTs) impregnated with 3-aminopropyltriethoxysilane (APTS), which at 25 °C under 10% and 50% CO_2 flow, showed dynamic CO_2 adsorption capacity of 0.93 and 2.2 mmol g^{-1} respectively. Su *et al.* [125] also developed MWCNTs impregnated with APTS which under 15% and 50% CO_2 flow at 25 °C reported CO_2 adsorption capacity of 2.25 and 3.0 mmol g^{-1} respectively. Ye *et al.* [126], using

impregnation of 30 wt% TEPA onto commercially available MWCNTs, under 2% CO_2 flow exhibited CO_2 adsorption capacity of 2.97 and 3.56 mmol g^{-1} at 25 °C and 40 °C, respectively.

It can be concluded from the literature that the development of adsorbents by direct carbonization, and physical/chemical activation have been studied. Less attention has been paid to the preparation of carbon materials based on nanocasting technique which enhances the textural property of the material. Theoretically, evaluation performed under static condition at 0 ˚C or 30 ˚C, shows higher CO_2 uptake values but from CCS point, performance evaluation should be carried out at high temperature under dynamic condition. Therefore, there is a need to develop material using nanocasting technique. Also, there is a need to work on physical activation and direct carbonization followed by chemical activation and to evaluate these materials under flue gas conditions, i.e. low CO_2 partial pressure and high temperatures, by dynamic methods, to predict the applicability of these materials in real situation.

Chapter 3 – Experimental Methods, Kinetics and adsorption equilibrium isotherms

3.1 Materials

Template (mesoporous zeolite, MCM-41) used in this study was purchased from M/s Tianjin Chemist Scientific Ltd., China. It is having surface area and pore diameter of 800 m^2 g^{-1} and 3 nm. It was used as hard template to obtain porous carbon materials by nanocasting technique.

Melamine, and urea as precursors and other chemicals like sulfuric acid, potassium carbonate, methanol, di-sodium tetra borate (borax), sodium hydroxide pellets, formaldehyde solution (37% w/v), acetone (100% pure), and potassium hydroxide (KOH) were supplied by M/s S.D. Fine Chemicals Ltd., India.

Epoxy-resin, Lapox L-12 DGEBA (Di Glycidyl Ether of Bisphenol-A) with a density of 1.1-1.2 g cm^{-3} and viscosity of 9000-12000 mPa.s. used as precursor was procured from M/s Atul Chemicals Ltd., Gujarat, India.

Helium gas (99.995%), carbon dioxide gas (99.999%) and nitrogen gas (99.995%) used in this study were procured from M/s. Sigma Gases and Services, India.

3.2 Characterization methods

3.2.1 Surface area and pore size distribution

Nitrogen adsorption-desorption isotherms at -196 °C were obtained using a Micromeritics ASAP 2010 sorption analyzer. Prior to measurements, the samples were degassed at 220 °C under vacuum for 6 h to remove physically adsorbed gases from the adsorbent surface. The specific surface area (S_{BET}) was calculated by using the Brunauer-Emmet-Teller (BET) method. The total pore volume (V_{total}) was estimated from the amount of N_2 adsorbed in the relative pressure range of p/p_o = 0.99. Meso- and micro- pore size distributions were derived from the adsorption branch using Barrett-Joyner-Halenda (BJH) model.

3.2.2 X-ray diffraction (XRD)

The powder X-ray diffraction (XRD) patterns of samples were obtained on a PANalytical X'Pert PRO diffractometer using Cu–K_α radiation. It was taken in low angle 2θ range of 0-10° and wide angle 2θ range of 10-80° with current and tube voltage of 40 mA and 45 kV.

3.2.3 Transmission electron microscopy (TEM)

TEM was performed on the JEOL (JEM-2100) transmission electron microscope under a working voltage of 200 kV. Before analysis, samples were prepared by placing a drop of the dispersion of carbon adsorbent in toluene on carbon-coated copper grid.

3.2.4 Scanning electron microscopy (SEM)

The surface morphology of sorbent was analyzed by scanning electron microscope (JEOL JSM – 6510 LV) at an accelerating voltage of 20 kV. Before the analysis, sample was coated with gold of 50 µm thickness with the help of automatic sputter coater (Polaron) to prevent sample charging problems.

3.2.5 Thermal analysis

3.2.5.1 Thermogravimetric analysis (TGA)

Thermal stability measurements of samples was performed on TA Q500, USA thermogravimetric analzer. For the analysis, about 20 mg of the sample was placed in a platinum pan and was heated from room temperature to 900 ˚C at a heating rate of 10 ºC min^{-1} under N_2 flow (50 ml min^{-1}).

3.2.5.2 Differential scanning calorimetry (DSC)

Specific heat capacity of the samples was determined using differential scanning calorimeter (NETZSCH DSC 200F3, Netzsch-Geratebau GmbH, Germany). To determine this about 10 mg of sample was heated to 300 °C at the rate of 10 ºC min^{-1} under N_2 atmosphere.

3.2.6 Elemental (CHNS) analysis

Elemental analysis was carried out using Thermo Scientific Flash 2000 organic elemental analyzer. N content was determined using Kjeldahl method also. Oxygen content was determined by difference [105].

3.2.7 Fourier transform infrared (FTIR) spectroscopy

Surface functional groups of the adsorbents were characterized by Fourier transform infrared (FT-IR) spectrometer (Spectrum 100 FTIR Spectrometer, Perkin Elmer, USA). Samples were scanned over the spectral range of 4000-650 cm^{-1} at a resolution of 4 cm^{-1}.

3.2.8 X-ray photoelectron spectroscopy (XPS)

XPS measurements were carried out to identify nitrogen, carbon and oxygen moieties on carbon adsorbents. This was carried on Kratos axis ultra DLD system using a monochromatic Al-kα source operated at anode potential of 15 kV. The survey spectra were recorded with a pass energy of 50 eV while the high resolution spectra with a pass energy of 20 eV and emission current of 10 mA. Pressure in the analysis chamber was maintained at 2×10^{-9} torr. Data processing was performed using the XPS peak 4.1 software and the core level spectra were fitted with mixed Gaussian-Lorentzian convoluted function (80/20) and Shirley function was used for background subtraction.

3.2.9 Temperature programmed desorption (TPD)

TPD analysis was carried on Micromeritics Autochem II 2920 chemisorption analyzer equipped with TCD. Prior to analysis, pretreatment was performed under helium (He) flow at 200 °C. Next, adsorption was done by reducing temperature to 30 °C for 30 min and switching over the gas from He to CO_2 atmosphere. Desorption was carried after adsorption by increasing the temperature to 300 °C and by switching over of gas from CO_2 to He.

3.2.10 Raman spectroscopy

Raman spectra of the samples, before and after CO_2 adsorption, were obtained using a confocal Raman microscope (WITec alpha 300R, Germany) with $\lambda = 532$ nm laser excitation to evaluate any structural changes occurring in the adsorbent due to adsorption of CO_2. It was

also used to examine the presence and position of D-(disordered) and G-(graphitic) peak and their intensity ratio.

3.3 Performance evaluation of adsorbents

3.3.1 Fixed-bed adsorption study setup

Dynamic CO_2 adsorption-desorption measurements were performed in an adsorption column built with stainless steel having height of 30 cm and an inner diameter of 0.939 cm shown in Fig. 3.1. The system is operated under atmospheric pressure. Temperature resistant glass wool was used on the both ends of the column to minimize the adsorbent loss. CO_2 and N_2 are mixed in a gas mixing section, prior to adsorption column. K-type thermocouple was placed in middle of bed to measure bed temperature along the column. Gas mixing section consists of mass flow controllers, pre-mixer and non-return valves. The feed gas of pure CO_2 and N_2 is regulated by using mass flow controllers (Bronkhorst, Netherlands). Gas mixture (simulated flue gas) is passed through the adsorption bed. It can be also bypassed directly to the gas chromatograph, to measure the inlet concentration of the gas mixture entering the adsorption column. The CO_2 and N_2 concentration is analyzed periodically using (GC 7890A, Agilent Technologies, US) gas chromatograph equipped with a thermal conductivity detector. Helium was used as carrier gas and GC was operated at injection temperature of 180 °C, oven temperature of 60 °C and detector temperature of 200 °C.

Fused silica capillary column of 30 m length having inner diameter of 0.32 mm and 20 μm film thickness of polystyrene divinylbenzene (HP Plot Q, Agilent Technologies, USA) is used for the analysis.

3.3.2 Dynamic CO_2 adsorption/desorption measurements

Prior to the adsorption/desorption analysis, the sample was kept in an oven at 200 °C overnight to ensure complete removal of moisture. For the adsorption study, approximately 2 g of adsorbent was preconditioned in flowing N_2 (50 ml min^{-1}) by elevating the temperature from room temperature to 200 ºC at 10 ºC min^{-1} and held at this temperature for 2 h. This was performed to remove the moisture and pre-adsorbed gases. Afterwards, the temperature was brought down to a desired adsorption temperature (30, 50, 75 and 100 °C). Next, a mixture of N_2 and CO_2 volumetric concentrations ranging from 5% to 12.5% was passed at a flow rate of 80 ml min^{-1} to perform the adsorption study. After adsorption, the gas was switched to pure N_2

flow and the temperature was raised to 200 °C for the desorption process. Desorption was performed for 2 h and repeated four times to investigate the recyclability of the adsorbents.

The CO_2 uptake of the synthesized adsorbent, expressed as q_t (mmol g^{-1}), was calculated using Eq. (3.1),

$$q_t = \frac{1}{m}\int_0^t Q\left(C_O - C\right)dt \tag{3.1}$$

where m (g) is mass of adsorbent located in column, Q (ml min^{-1}) is gas flow rate, C_0 and C are CO_2 inlet and effluent concentrations in (vol. %) and t (min) is the time.

3.3.2 Equilibrium sorption measurements

Pure component adsorption measurements on nanostructured carbon adsorbent were performed using a Micrometrics ASAP 2010 volumetric analyzer. The analysis on the prepared adsorbent was performed at 30, 50, 75 and 100 °C in the pressure range of 0 to 1 atm. High purity CO_2 and N_2 gases were used for the analysis. Before performing the analysis, sample was outgassed for 12 h at 200 °C under vacuum.

3.4 Kinetic study

Adsorption kinetics which gives important information for predicting adsorption rates such as diffusion control and mass transfer which can be very useful for adsorber design and modeling of adsorption operation was studied by fitting the experimental data with a series of popular models like, pseudo–first order, pseudo-second order, and fractional-order kinetic models.

3.4.1 Pseudo-first order model

Lagergren's pseudo-first order adsorption model [127] is used to describe the kinetic of adsorption process on the basis of adsorption capacity. It is based on the assumption that adsorption rate is proportional to number of vacant adsorption sites in the adsorbent and it can be given as:

$$\frac{dq_t}{dt} = k_1(q_e - q_t) \tag{3.2}$$

where, k_1 is the pseudo-first order adsorption rate constant (min^{-1}). Integrating eq. (3.2) with boundary conditions: $q_t|_{t=0}=0$ *and* $q_t|_{t=t}=q_t$ yields

$$\log\frac{q_e}{q_e-q_t}=\frac{k_1}{2.303}t$$

which can be rearranged to:

$$q_t=q_e\left(1-\exp\left(-k_1t\right)\right) \tag{3.3}$$

where, q_e and q_t are the adsorption capacities (in mmol g^{-1}) at various times *t* and at equilibrium, respectively.

3.4.2 Pseudo-second-order model

Pseudo-second order model is based on the assumption that adsorption rate is proportional to square of the number of vacant adsorption sites in the adsorbent. It was given by Ho *et al.* [128] and is expressed as:

$$\frac{dq_t}{dt}=k_2(q_e-q_t)^2 \tag{3.4}$$

where, k_2(g $mmol^{-1}$ min^{-1}) is the pseudo–second-order rate constant. Integrating eq. (3.4) with initial conditions: $q_t|_{t=0}=0$ *and* $q_t|_{t=t}=q_t$, yields

$$q_t=\frac{k_2q_e^2t}{1+k_2q_et} \tag{3.5}$$

3.4.3 Fractional – order model [129]

Fractional order kinetic model is based on the assumption that adsorption rate is proportional to n^{th} power of driving force and m^{th} power of the adsorption time [130, 131] and is expressed as:

$$\frac{dq_t}{dt}=k_n(q_e-q_t)^nt^{m-1} \tag{3.6}$$

k_n, m and n are the constants for the fractional-order kinetic model. Integrating eq-(3.6) yields

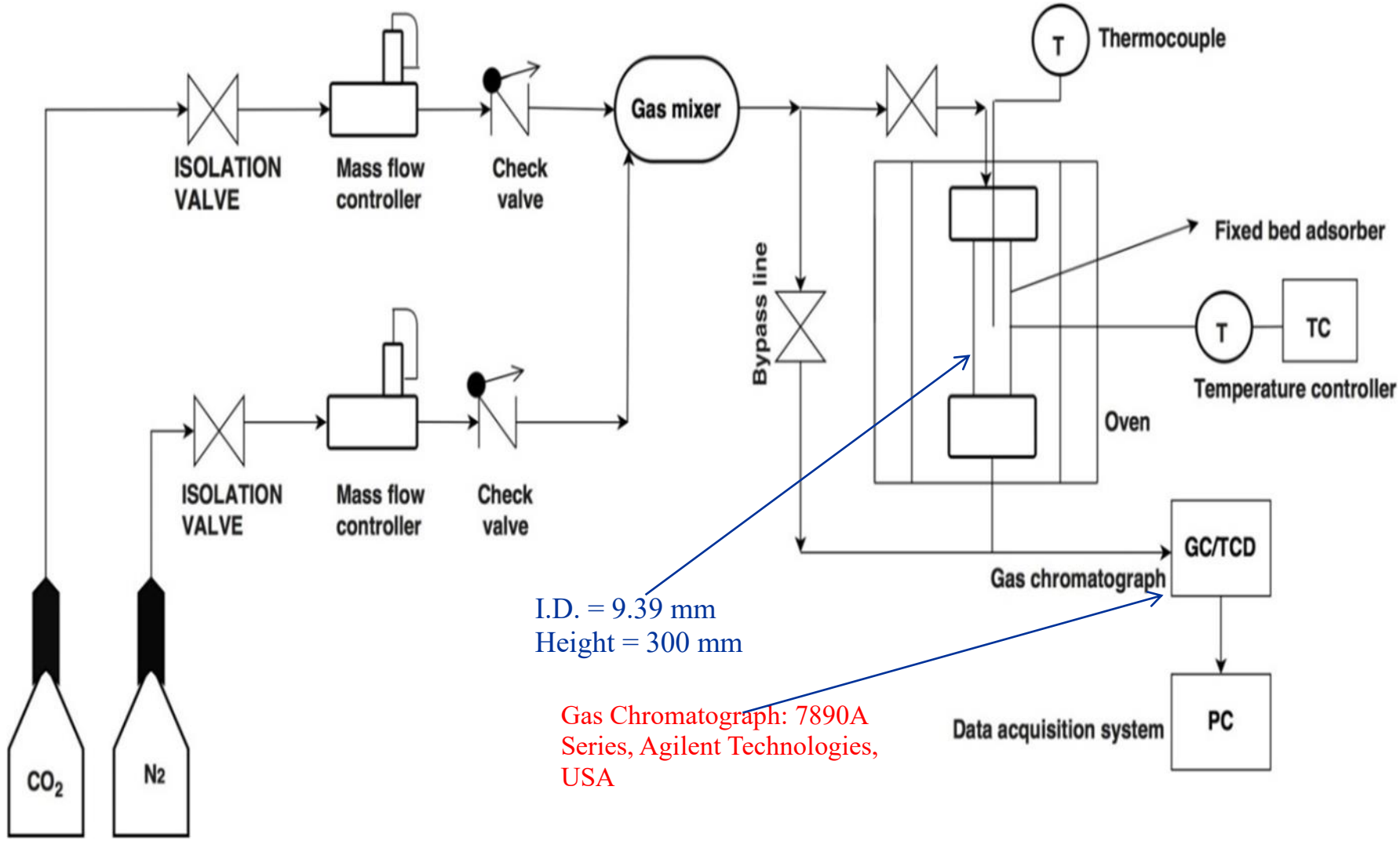

Fig. 3.1 Schematic diagram of the experimental setup

Adsorption study setup: Fabricated by Chemito Technologies Pvt. Ltd., India

$$q_t = q_e - \frac{1}{[((n-1)k_n/m)t^m + (1/q_e^{n-1})]^{1/n-1}} \quad (3.7)$$

Here, n reflects effect of driving force and m refers to diffusion resistance [132].

3.4.4 Error calculation

The correctness of the models was assessed by the coefficient of determination (R^2) and error (%).

$$Error(\%) = \frac{\sqrt{\sum[(q_{t,\exp} - q_{t,pred})/q_{t,\exp}]^2}}{N-1} \times 100 \quad (3.8)$$

where, $q_{t(exp)}$ and $q_{t(pred)}$ are the experimental and predicted CO_2 loading, respectively, and N is the number of measurements.

3.4.5 Activation energy

Arrhenius equation was used to determine the rate constant (k) for adsorption at different temperatures:

$$k = A\exp(-E_a/RT) \quad (3.9)$$

where A and E_a (J mol^{-1}) are pre-exponential factor and activation energy of Arrhenius equation. Here, slope of arrhenius plot was used to obtain activation energy for CO_2 adsorption.

3.5 Adsorption equilibrium isotherms

Adsorption isotherm describes adsorption mechanism on adsorbent surface and indicates relationship between adsorption capacity at equilibrium and equilibrium concentration at constant temperature. Several equilibrium isotherm equations, namely, Langmuir, Freundlich and Temkin have been evaluated to represent the experimental sorption isotherm data.

3.5.1 Langmuir isotherm model

Langmuir isotherm model [133], assumes monolayer coverage of adsorbate over the homogenous adsorbent surface. In this after equilibrium, no adsorption takes place further. This model is applicable to homogenous sorption where the adsorption of each molecule has equal sorption activation energy. It can be expressed as:

$$q_e = \frac{q_m K_L P}{1 + K_L P} \tag{3.10}$$

where q_m (mmol g^{-1}): maximum adsorption capacity and q_e: amount adsorbed at equilibrium, P (atm): CO_2 partial pressure and K_L (atm^{-1}): Langmuir constant.

3.5.2 Freundlich isotherm model

Freundlich isotherm model [134] is an empirical equation and predicts sorption of sorbate molecules on a heterogeneous surfaces without considering saturation of sorbate binding sites. It is expressed as:

$$q_e = K_F P^{1/n} \tag{3.11}$$

where, K_F is Freundlich constants, indicates adsorption capacity and n is Freundlich coefficients indicates adsorption intensity. Its value lie in the range of 1 to 10.

3.5.3 Temkin isotherm model

Temkin isotherm model [135] assumes that heat of adsorption of molecules in the layer decreases linearly rather than logarithmic with coverage of molecules due to interactions between the adsorbent and the adsorbate.

$$q_e = B \ln(K_T P) \tag{3.12}$$

where, K_T (atm^{-1}) and $B = RT/b$ with b (J mol^{-1}) are Temkin constants with R (8.314 J mol^{-1} K^{-1}) and T (K) is the temperature. Here, constant b = heat of adsorption.

3.6 Selectivity

Selectivity, which is one of the main characteristic properties of adsorbent, can also be calculated for CO_2 over N_2 (S_{CO_2}) and is compared with the experimental data obtained from breakthrough curve.

$$S_{CO_2} = \frac{x_{CO_2} / x_{N_2}}{y_{CO_2} / y_{N_2}} \tag{3.13}$$

Where

x_{CO_2} and x_{N_2} = mole fractions of CO_2 and N_2 in the adsorbed phase respectively and

y_{CO_2} and y_{N_2} = molar ratios of CO_2 and N_2 in the gas phase respectively.

3.7 Thermodynamics study

3.7.1 Thermodynamic parameters

The Gibbs free energy shows spontaneous adsorption process where a high negative value reflects energetically favorable adsorption. The standard Gibbs free energy ΔG^0 (J mol^{-1}) can be expressed as:

$$\Delta G^{\circ} = -RT \ln(K_{eq}) \tag{3.14}$$

where ΔG^0 and K_{eq} are free energy change and equilibrium constant respectively [132].

Thermodynamic parameters such as change in enthalpy and entropy were estimated using van't Hoff equation [132].

$$\ln(K_{eq}) = -\frac{\Delta H^{\circ}}{R}\frac{1}{T} + \frac{\Delta S^{\circ}}{R} \tag{3.15}$$

where ΔH^0 (standard molar adsorption enthalpy) and ΔS^0(standard entropy change) are calculated from the slope and intercept of van't Hoff plot, respectively [132].

3.7.2 Energy duty for desorption

The thermal energy (Q_{th}) needed for regeneration of adsorbent can be obtained from following equation (3.16),

$$Q_{th} = Q_{st} + sensible\ \ heat \tag{3.16}$$

where sensible heat is amount of heat required for raising the temperature of adsorbent to desorption temperature.

$$Sensible\ \ heat = \frac{C_p \Delta T}{adsorption\ \ capacity} \tag{3.17}$$

where C_P (J g^{-1} K^{-1}) = heat capacity.

Isosteric heat of adsorption represents differential change between activation energy for adsorption and desorption. It is used to measure the strength of binding forces between adsorbate molecules and adsorbent surface. In this Q_{st} is calculated by plotting ln *P* against 1/*T*, at constant amount of adsorbed gas. Quantification of *Qst* is very important for kinetic studies of adsorption process because the heat released upon adsorption is partially adsorbed on sorbents which causes a rise in adsorbent temperature and thus influences the rate of adsorption. The governing equation is given below.

$$Q_{st} = -R\left[\frac{\partial \ln P}{\partial\left(\frac{1}{T}\right)}\right]_{q_e} \tag{3.18}$$

where Q_{st}(kJ mol^{-1}) at a given q_e is calculated from Clausius-Clapeyron equation [136].

3.8 Software used

Here, fitting of various kinetic and adsorption isotherm models with the experimental data was done using Origin Pro 8 software.

Chapter 4 - Melamine based Nitrogen Enriched Nanostructured Carbons for Carbon Dioxide Capture

4.1 Preparation of adsorbent

4.1.1 Templated resin synthesis

Melamine (46.6 g) was dissolved in methanol solution (200 ml of 5 wt. %), stirred and heated to about 70 °C. 200 ml, 37%w/v of formaldehyde solution was slowly added to the above mixture for 3 h to form hexamethylomelamine. K_2CO_3 was added until pH of 8-9 was achieved. To carry out advanced polymerization, temperature of reaction mixture was increased to 75 °C and continuous stirring was done for 2 h. Di-sodium tetra borate 0.4 g and N/10 sodium hydroxide solution were added to maintain pH of 7-8. Next, sulfuric acid (6 ml of 48% v/v) and zeolite (15g) were added and stirred till homogenous solution was achieved followed by cooling to room temperature.

4.1.2 Carbonization of templated resin

After curing for 2 h at 60 °C, carbonization/physical activation was performed in a quartz tube furnace by heating the samples @ heating rate of 10 °C min^{-1} and flow rate of 60 ml min^{-1} of N_2. Here the temperature was raised to the different carbonization temperatures and then held isothermally for 2 h. Carbonization was performed under nitrogen atmosphere for 1 h and physical activation under CO_2 atmosphere for 1 h. After physical activation, gas was switched from CO_2 to N_2 during cooling to room temperature to avoid excess gasification.

4.1.3 Removal of template

Template removal was done by dissolution in 40 wt. % NaOH solution for 48 h followed by washing several times with distilled water. The samples (denoted as MFZ-*x*) were dried at 100 °C, where *x* stands for carbonization/activation temperature (500-800 °C). The block diagram for adsorbent preparation is shown in Fig. 4.1.

4.1.4 Carbonization of melamine-formaldehyde resin

Also, a reference sample was prepared by direct carbonization for comparison and labeled as MF-700.

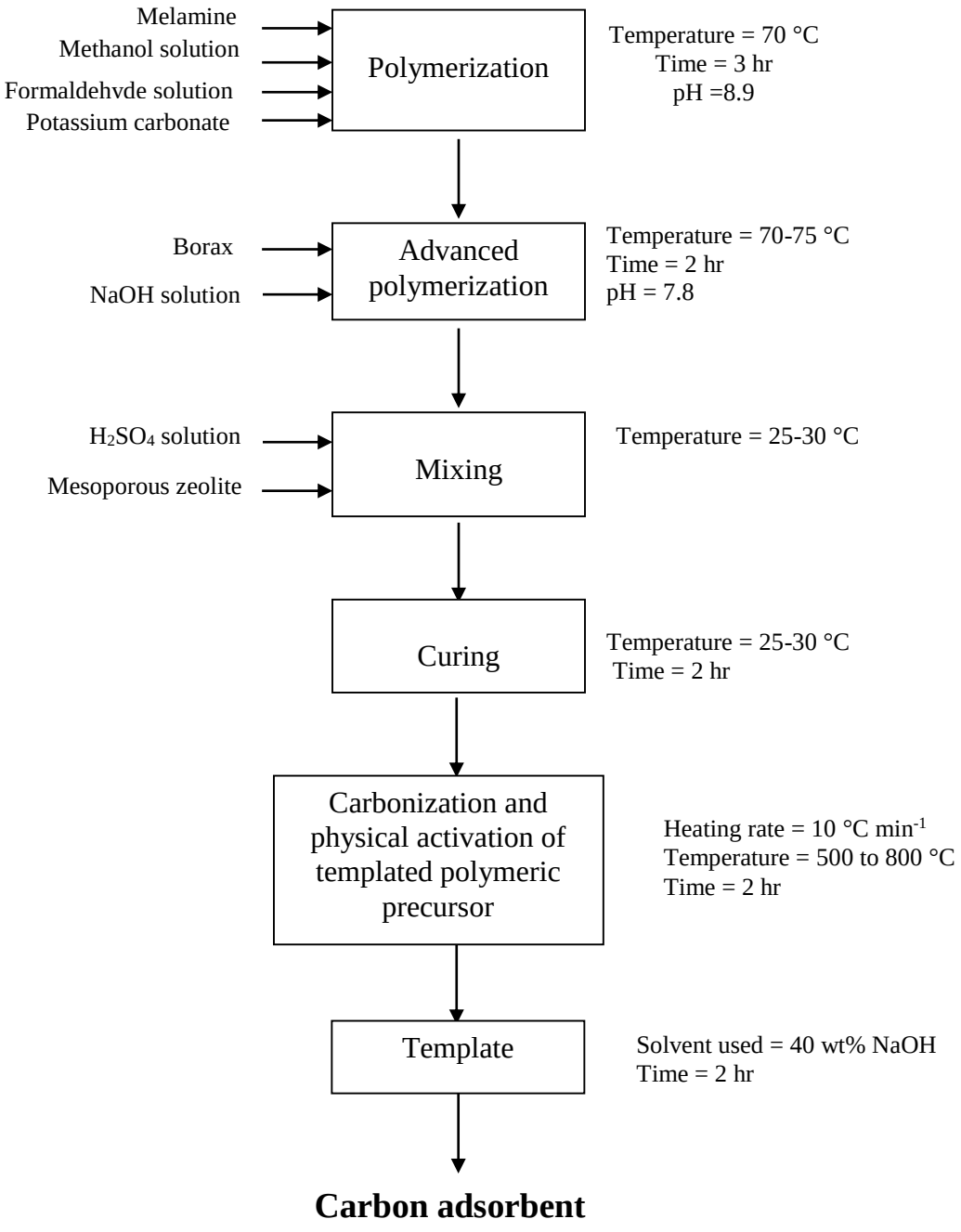

Fig. 4.1 Preparation of nitrogen-enriched carbon adsorbent by nanocasting technique – block diagram

4.2 Characterization of adsorbent

4.2.1 Surface area and pore size distribution

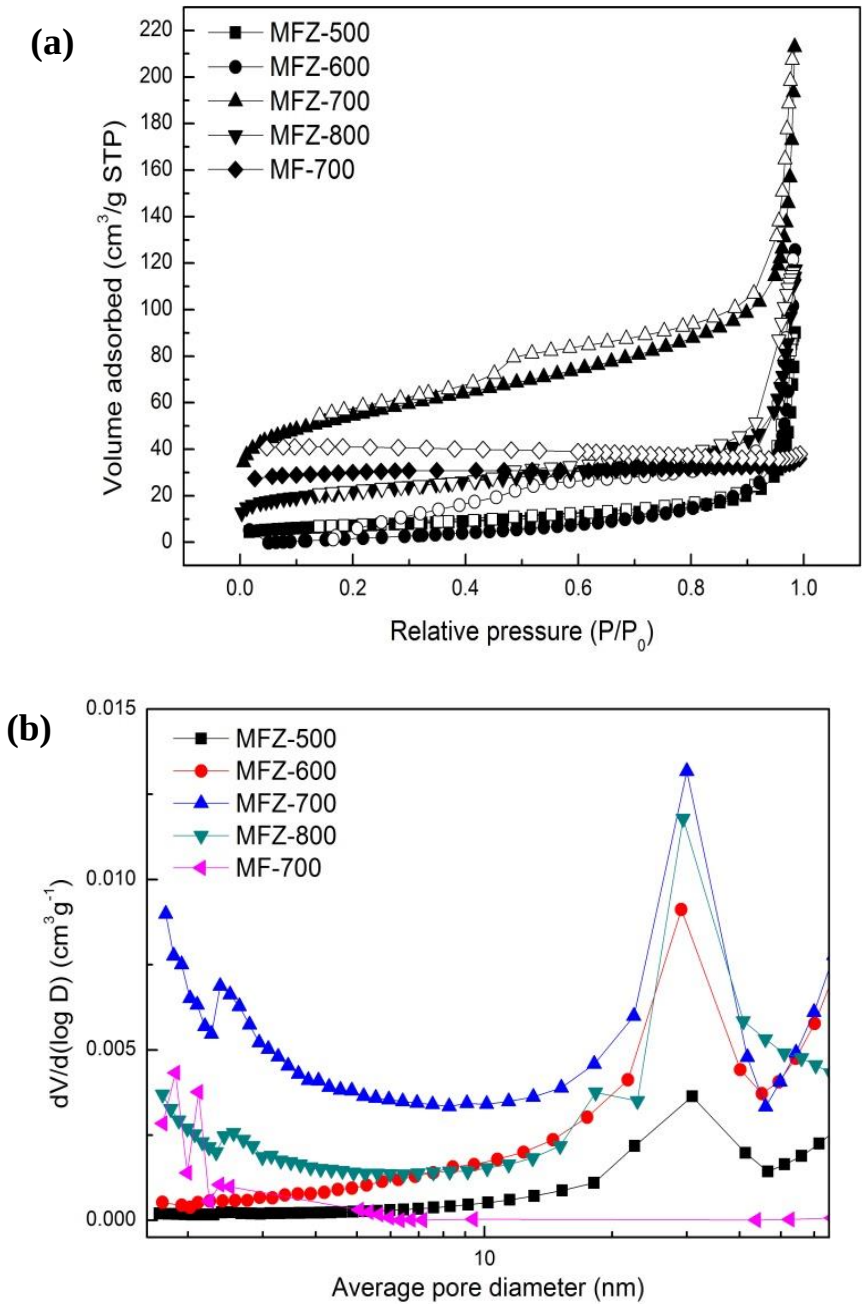

Fig. 4.2(a) N_2 sorption isotherms, and (b) BJH pore size distribution of carbon adsorbents

Fig. 4.2(a) shows the isotherms of the adsorbents. The sample carbonized at 500 and 600 °C show poorest porosity confirmed from lower volume of N_2 adsorbed while nitrogen sorption is higher for sample carbonized at 700 °C showing well developed porosity. Samples, except MFZ-700 and MFZ-800 show the presence of mesopores which is confirmed from Type IV isotherm. MFZ-700 and MFZ-800 show both micro and mesopores as they exhibit both Type I and Type IV isotherms. Here, microposity and mesoporosity is due to CO_2 activation and dissolution of zeolite template. The samples indicate H4 hysteresis loop in the pressure range of 0.45-1 [132]. This indicates capilliary condensation phenomena, characteristic of mesoporous materials [137]. Fig. 4.2(b) shows pore size distribution of the adsorbents which lie in the range of 20-40 nm signifying mesopore distribution.

Table 4.1 Textural properties of MF based carbons

Materials	Surface area ($m^2\ g^{-1}$)	Total pore volume ($cm^3\ g^{-1}$)	Micropore volume ($cm^3\ g^{-1}$)	Mesopore volume ($cm^3\ g^{-1}$)
MFZ-500	25	0.13	-	0.129
MFZ-600	45	0.19	-	0.19
MFZ-700	193	0.32	0.026	0.29
MFZ-800	77	0.18	0.010	0.17
MF-700	50	0.045	0.014	0.031

Table 4.1 shows the textural properties of the prepared carbon adsorbents. Activation performed at lower temperature is responsible for the generation of meso and macropores while higher temperature generates micro and meso pores [137]. Surface area increased with increase in carbonization/activation temperature and the highest value was observed at 700 °C (193 $m^2\ g^{-1}$). Pore volume and porosity also increased with activation temperature up to 700 °C but reduced beyond this temperature. Increase in temperature generates mesoporosity in the sample. For sample 800 °C, decrease in textural properties are observed. This is due to extensive gasification which causes collapse of pore structures and widening of pores. MFZ-700 also shows smaller micropore volume of 0.026 $m^3\ g^{-1}$. MFZ-500 and MFZ-600 show low BET surface area, total pore volume and mesopore volume show the inadequacy of this temperature in improving textural properties. The reference sample MF700 (without nanocasting) showed the non-porous structure.

4.2.2 XRD analysis

Fig. 4.3(a) shows XRD diffraction peak at 2θ = 1.99° which corresponds to (110) diffraction plane, signifying hexagonal mesostructure [22]. Peak shifting from 2θ = 0.98° to 1.41° shows effect of nanocasting technique. In wide angle XRD diffraction patterns (Fig. 4.3(b)), peak at 2θ = 26° corresponds to (002) diffraction planes of hexagonal graphite carbon [22]. Samples show low crystallinity as interlayer spacing of 0.345 to 0.358 nm is higher than that of ideal graphite (d_{002} = 0.335 nm) [23]. This is further confirmed by broadening of peak, suggesting the sample is nanostructured. With the rise in carbonization and activation temperature, the intensity of (002) diffraction plane is decreased, indicating that higher temperatures destroy layer structures and hence textural properties get affected. A weak diffraction peak at 2θ = 44° corresponds to (101) diffraction plane of the graphite carbon suggesting disordered stacking of micrographites in the material [24].

(a)

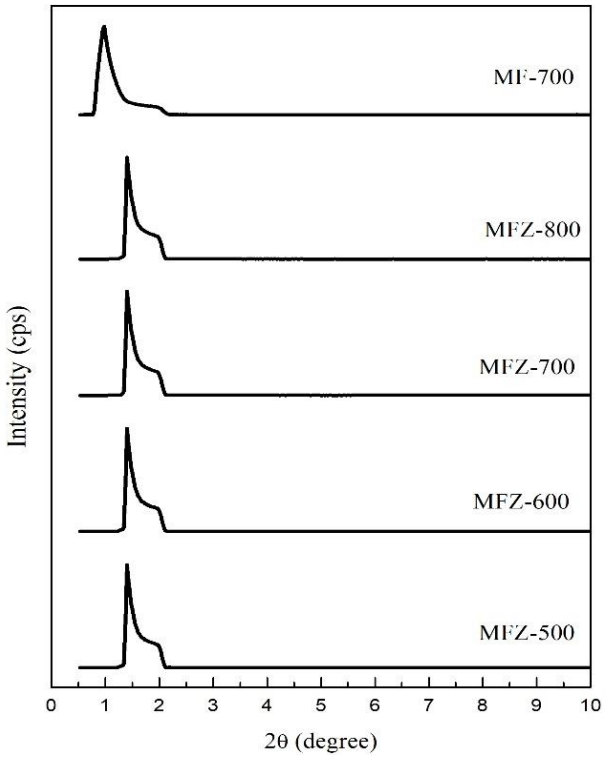

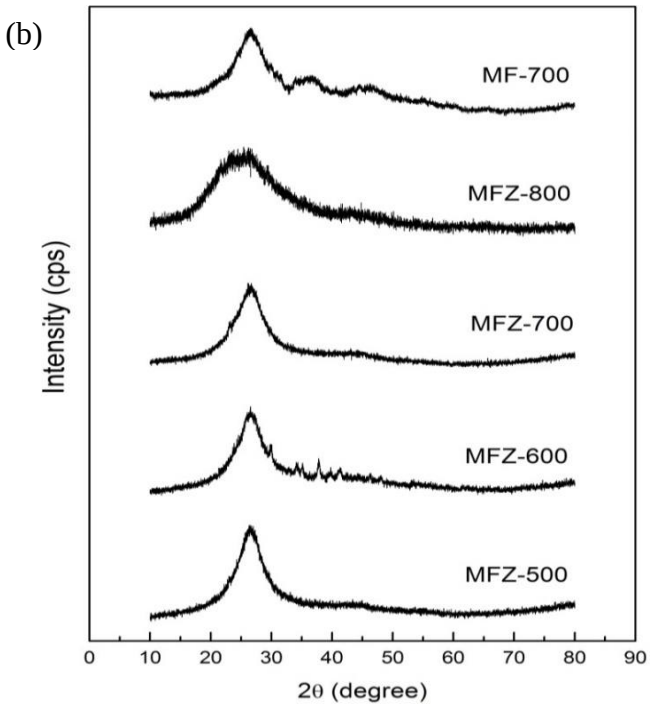

Fig. 4.3 XRD patterns of carbon adsorbent (a) low angle, and (b) wide angle

4.2.3 TEM analysis

Fig. 4.4 depicts TEM images of carbon samples. Samples prepared by nanocasting show development of nanostructured carbon materials in the size range of 30-50 nm. Sample MF-700 {(Fig. 4.4(e)} shows very big particles of the sample which does not lie in the mesopore range. This indicates the advantage of template in developing carbon adsorbents.

4.2.4 SEM analysis

Fig. 4.5 depicts the surface morphology of the carbon samples. With an increase in temperature, nanocasting samples show formation of a large number of irregular and heterogenous pores on the adsorbent surface with well-developed porosity at 700 °C which helps in diffusion of gas from bulk to adsorbent surface. But, with rise of carbonization temperature upto 800 °C {Fig. 4.5(d)} shows compact surface due to collapse of pore structure and sintering of material. Fig. 4.5(e) sample MF-700 (directly carbonized) shows non-porous structure. This confirms the importance of nanocasting technique in development of adsorbent from completely non-porous to porous.

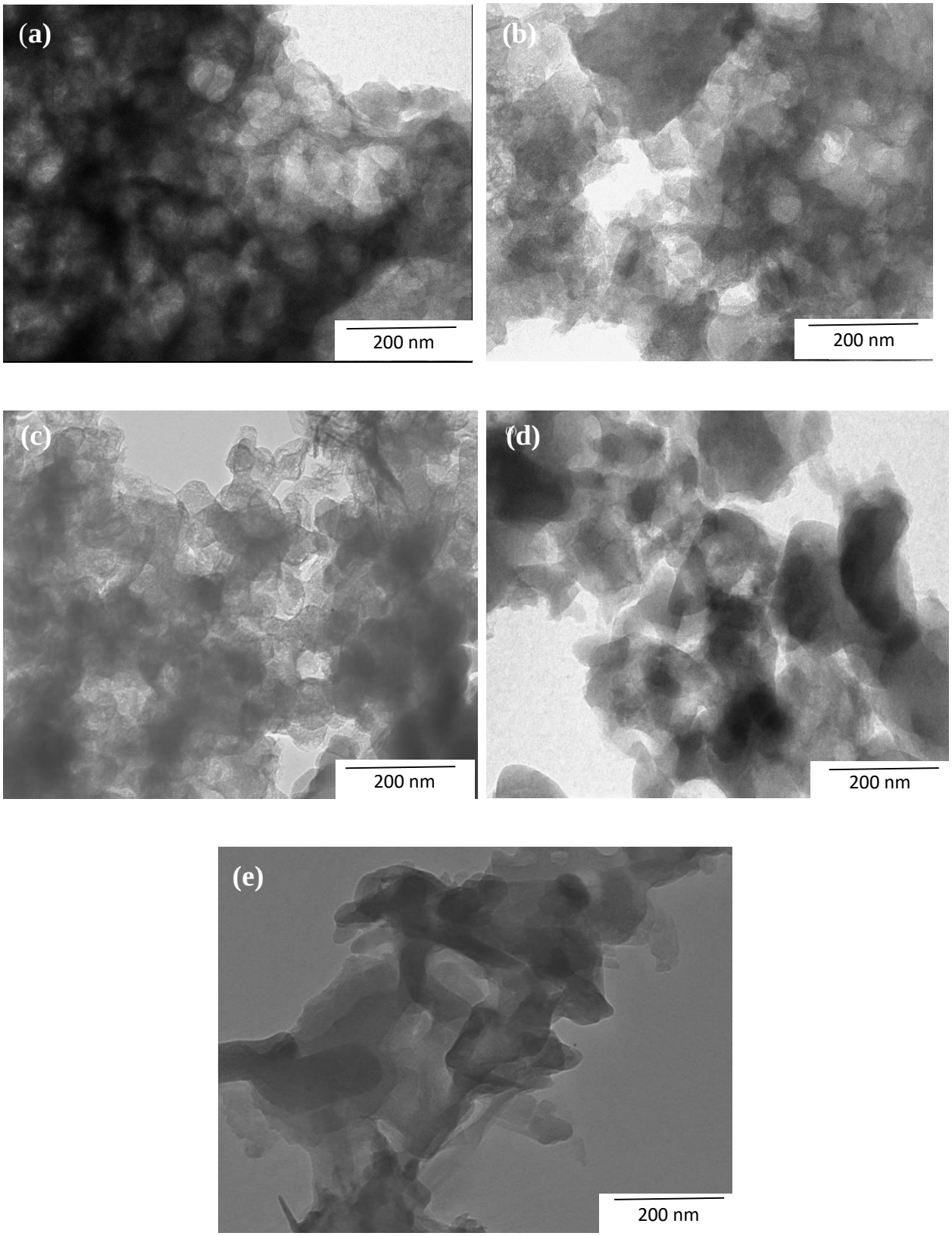

Fig. 4.4 TEM images of (a) MFZ-500, (b) MFZ-600, (c) MFZ-700, (d) MFZ-800, and (e) MF-700

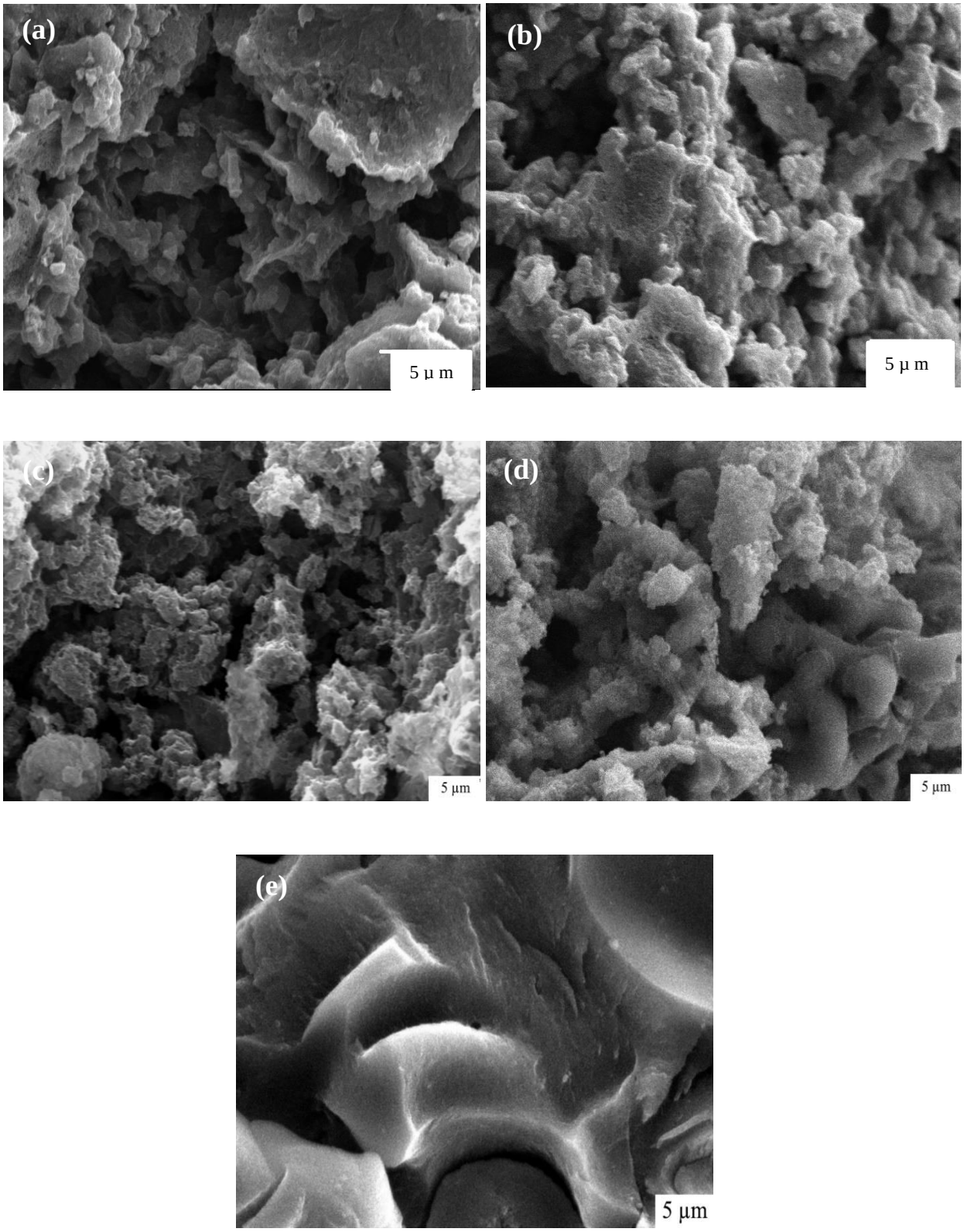

Fig. 4.5 SEM images of (a) MFZ-500, (b) MFZ-600, (c) MFZ-700, (d) MFZ-800, and (e) MF-700

4.2.5 TG analysis

Fig. 4.6 shows the thermogravimetric analysis (TGA) of the samples performed in N_2 atmosphere. TGA curves show weight loss profile with respect to temperature. These curves show two regions of weight loss, out of which first of around 9% at 100 °C signifies the removal of moisture. MFZ-700 shows highest mass loss in the first region. Stability pattern follows the order as: MFZ-500 and MFZ-600 are stable up to 400 °C, MFZ 700 and MFZ-800 are stable up to 450 °C and 500 °C, respectively signifying that with increase in carbonization-activation temperature, thermal stability increases. After this temperature, decrease in weight loss is observed. Sample MF-700 shows maximum weight loss while for others the order is: MFZ-500>MFZ-600>MFZ-700>MFZ-800.

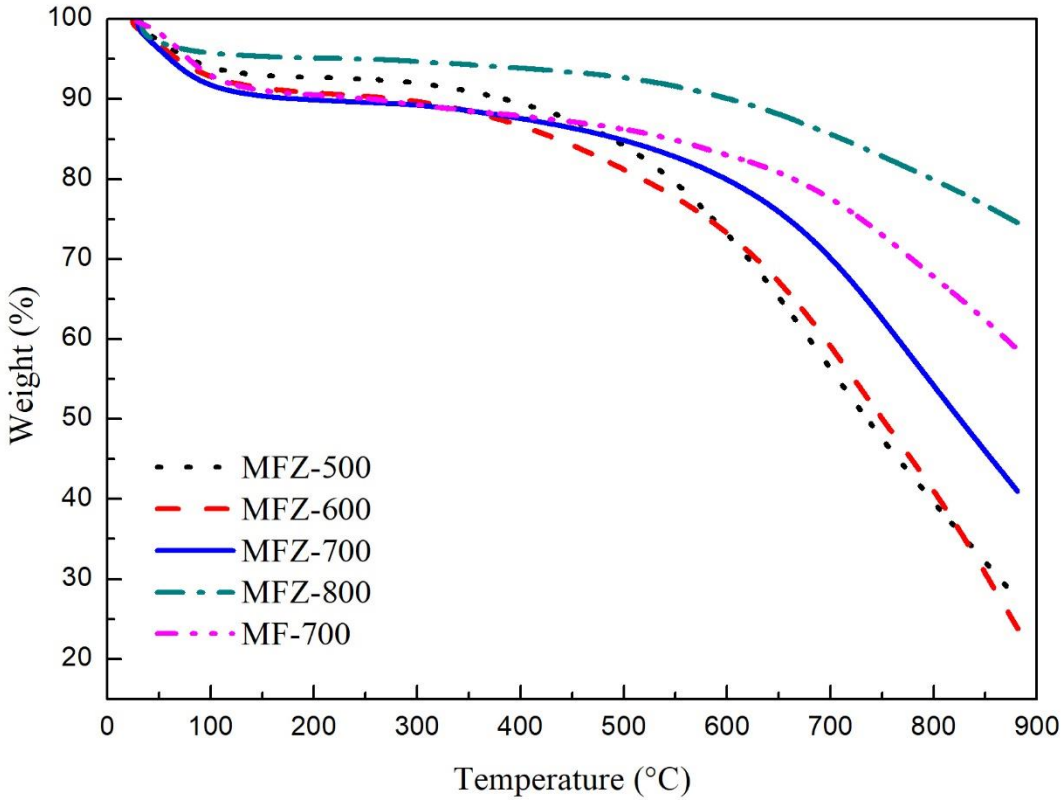

Fig. 4.6 Thermogravimetric profile of nitrogen enriched mesoporous carbon adsorbents

4.2.6 Elemental analysis

Table 4.2 shows the elemental analysis of the samples. With rise of carbonization temperature, nitrogen decreased from 31.35 to 5.09 wt. %, respectively, suggesting nitrogen in the material gets oxidized. Kjeldahl nitrogen also shows similar trend. Carbon content shows slight increase from 45 % to 48% because of CO_2 activation [138]. Drastic decrease in nitrogen and carbon contents, with rise in carbonization temperature upto 800 °C, is observed. A rise in activation temperature decreases the hydrogen content from 2.13% to 0.55%. Oxygen content was found to increase with the increase of temperature due to surface oxidation of carbon on CO_2 activation. Similar kind of observations were observed by Goel *et al.* [137] also. As compared to MFZ-700, MF-700 shows lesser carbon and higher oxygen content, showing that template affects the composition of samples.

Table 4.2 Elemental analysis of carbons

Sample	Kjeldahl nitrogen (%)	Composition (wt. %)			
		C	N	H	O[a]
MFZ-500	26.8	45.76	31.35	2.13	20.76
MFZ-600	24.4	43.27	28.41	1.78	28.41
MFZ-700	19.4	48.03	22.27	1.29	27.95
MFZ-800	5.46	20.64	5.09	0.55	73.72
MF-700	23.12	43.24	23.63	1.23	31.9

[a]*Calculated by difference*

4.2.7 FTIR analysis

Fig. 4.7 shows FTIR spectra of the adsorbents showing small peak of C-H bond in aliphatic -CH_2-NH-CH_2- at 3000 cm^{-1}. The peak at 2300 cm^{-1} is due to C-N functional group. The peak at 1056 cm^{-1} is assigned to stretching vibration of C-O bond in alcohol, ester or ether group [139]. Intensity of peak at 1600-1750 cm^{-1} corresponds to stretching vibration of C=O bond is getting reduced. This may be due to activation of samples under CO_2 atmosphere. Based on the FTIR and

elemental analysis, the presence of nitrogen functional groups on the surface of carbon adsorbent is confirmed. This functional group helps in providing Lewis base sites for adsorption of CO_2.

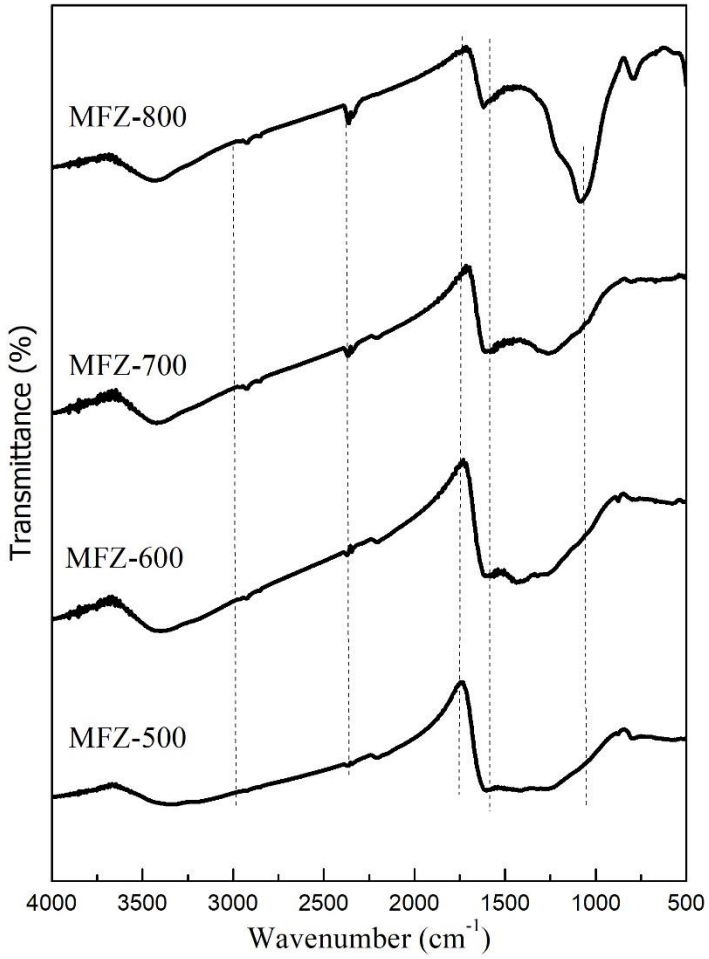

Fig. 4.7 FTIR spectra of the adsorbents

4.2.8 XPS analysis

Fig. 4.8 shows C1s spectra, which can be deconvoluted into five peaks. Here, sp^2 and sp^3 carbon atom (C1) assigned at 284.8eV, C-O bond of phenol & alcohol or ether and/or C=N bond (C2) at 285.6eV, carbonyl or quinone groups and/or C-N linkage (C3) at 286.5eV, carboxyl or ester linkage (C4) at 287.6eV and shake up satellite peaks because of π-π* transitions in aromatic rings (C5) at 289.7eV [140]**.** For MFZ-700, area% of C1 increased from 8.58% to 27.98%, showing highest graphitization character at higher temperature, On further increase in temperature,

it slightly decreased. Major contribution is shown by C2 for all the samples. Table 4.3 shows variation in C1, C2, and C3 area%, suggesting cleavage of C-O, C-N and C=O structures and formation of more stabilized structure.

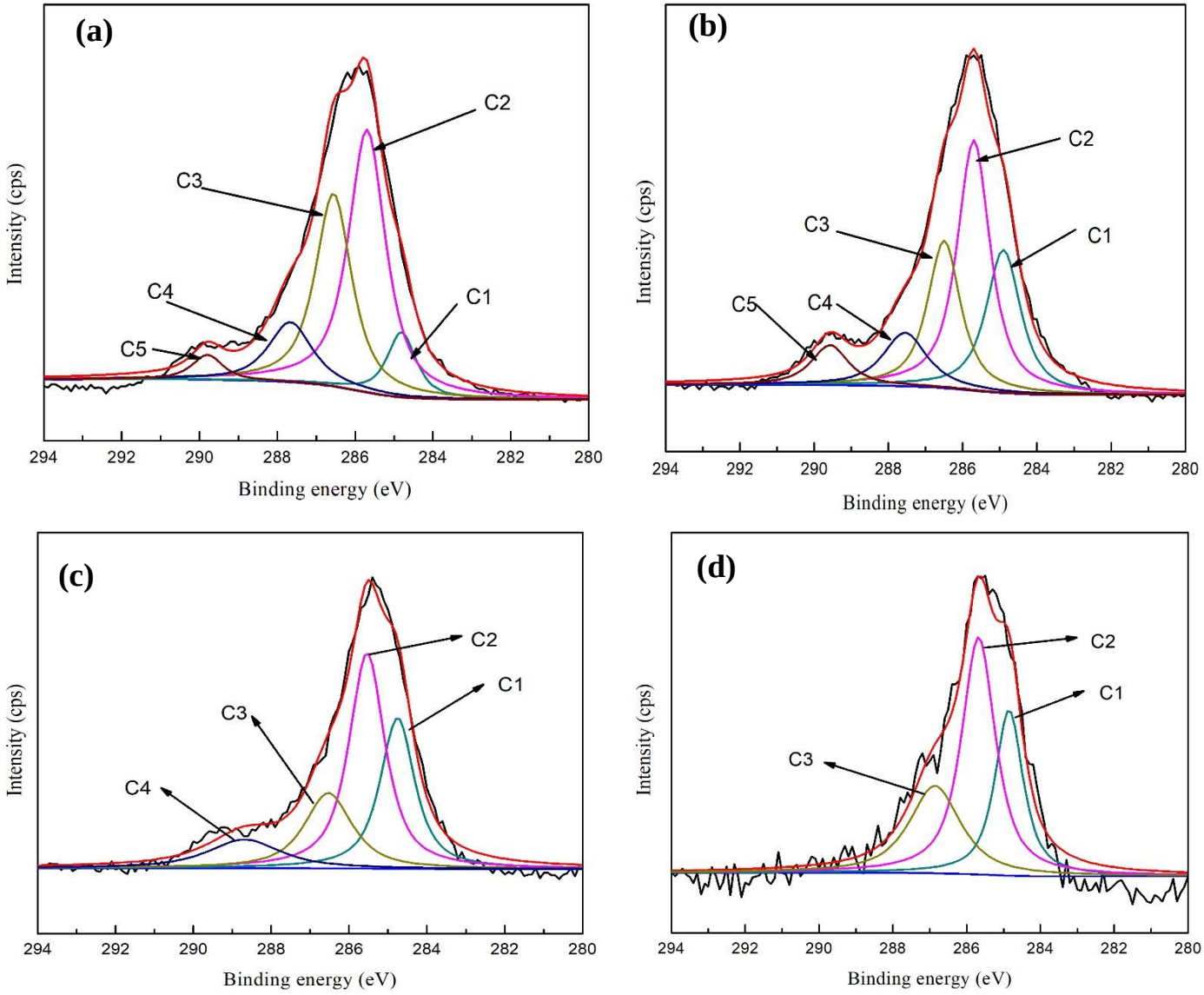

Fig. 4.8 C1s spectra of (a) MFZ-500, (b) MFZ-600, (c) MFZ-700, (d) MFZ-800

Table 4.3 Deconvolution data of C1s core level spectra of MF based carbons

Sample		C1	C2	C3	C4	C5
MFZ-500	BE	284.81	285.69	286.56	287.67	289.80
	FWHM	0.88	1.13	1.11	1.33	0.93
	A%	8.58	44.27	31.81	11.87	3.45
MFZ-600	BE	284.90	285.70	286.50	287.55	289.57
	FWHM	1.11	1.05	1.047	1.39	1.19
	A%	22.745	37.63	22.13	10.68	6.821
MFZ-700	BE	284.75	285.54	286.53	288.69	-
	FWHM	1.051	1.096	1.448	2.21	-
	A%	27.98	41.62	19.21	11.18	-
MFZ-800	BE	284.85	285.68	286.86	-	-
	FWHM	0.91	1.09	1.65	-	-
	A%	27.30	46.71	25.99	-	-

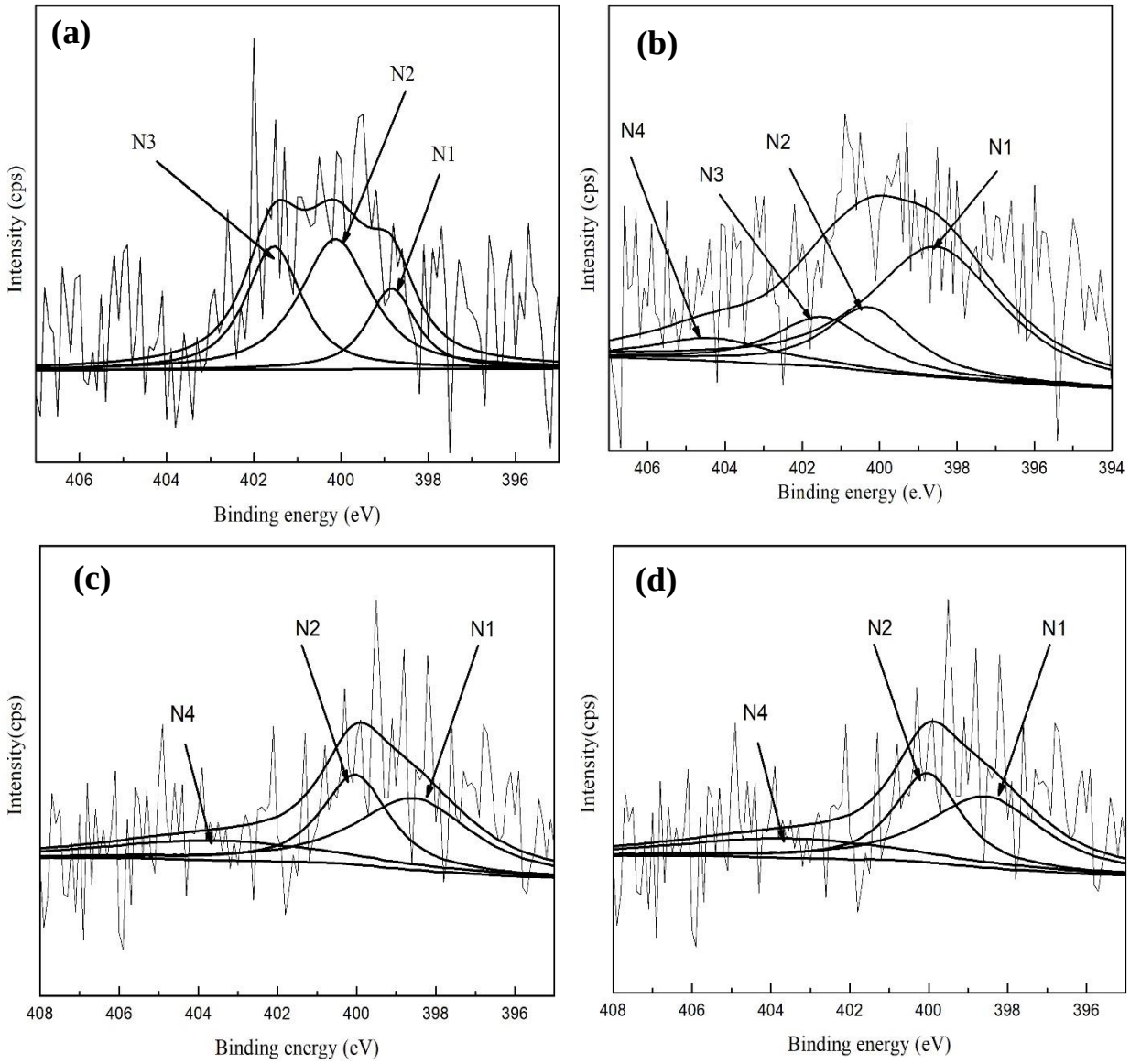

Fig. 4.9 N1s spectra of (a) MFZ-500, (b) MFZ-600, (c) MFZ-700, (d) MFZ-800

Fig 4.9 shows XPS N1s spectra of the carbons prepared at different temperatures which can be deconvoluted into four different peaks having the binding energy of ~ 398.8, 400.2, 401.5 and 404.3 eV corresponding to pyridinic nitrogen (N1), pyrrolic and/or pyridonic nitrogen (N2), quaternary nitrogen (N3) and pyridinic nitrogen oxide (N4) [27]. Table 4.4 presents binding energy (B.E), full width half maximum (FWHM) and relative area contribution (A%) of deconvoluted peaks of a carbon samples. For carbonization at 500 °C, the major contribution is ascribed to pyrrolic and/or pyridonic nitrogen (46.09%) showing nitrogen moieties exist in this form. But for further carbonization up to 800 °C, major contribution is ascribed to pyridinic nitrogen. For 600 °C, area % of N1 increased while N2 and N3 decreased. This shows the transformation of (N2) and (N3) to (N1). Upon carbonization at 700 °C, the contribution of (N3) is negligible showing complete conversion into pyrrolic and pyridonic nitrogen and pyridinic nitrogen oxide. This also signifies that the sample prepared at this temperature exhibits high Lewis basicity as compared to other samples [16]. But at 800 °C, there is a slight increase in the contribution of all nitrogen except pyridinic nitrogen oxide due to complete conversion of (N4) into (N1), (N2) or (N3). Since the major contribution is from (N1), and (N2), which have electron donating capability as reported in literature that Lewis basicity favors CO_2 capture [28].

Table 4.4 Deconvolution data of N1s core level spectra of MF based carbons

Sample		N1	N2	N3	N4
MFZ-500	BE	398.84	400.13	401.54	-
	FWHM	1.32	1.94	1.53	-
	A%	19.45	46.09	34.44	-
MFZ-600	BE	398.54	400.27	401.29	404.35
	FWHM	4.07	2.63	2.98	3.73
	A%	56.99	18.01	15.82	9.15
MFZ-700	BE	398.55	400.03	-	403.49
	FWHM	3.44	2.03	-	6.633
	A%	44.10	32.56	-	23.32
MFZ-800	BE	398.77	400.21	401.57	-
	FWHM	2.31	3.16	2.79	-
	A%	55.34	34.02	10.63	-

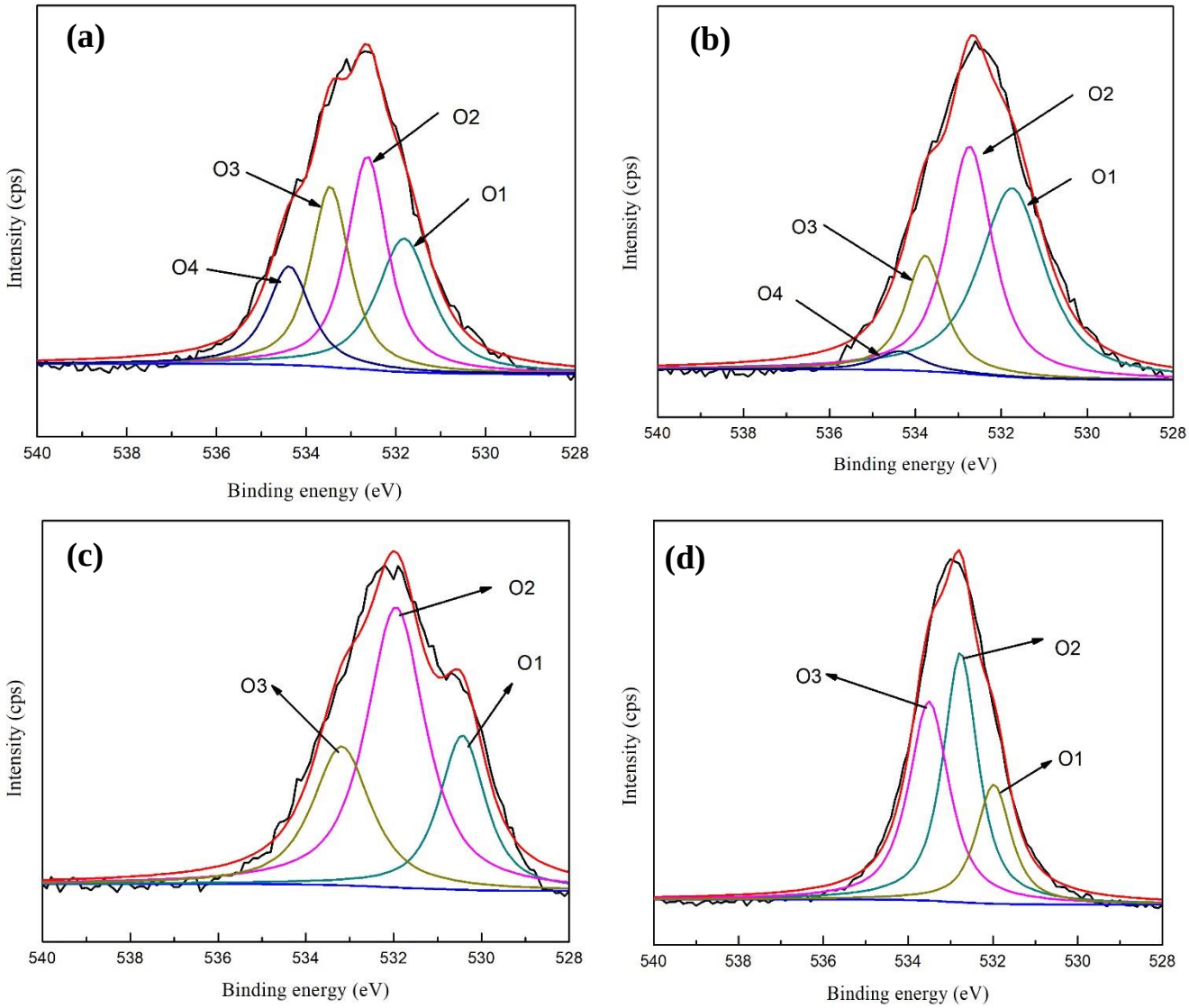

Fig. 4.10 O1s spectra of (a) MFZ-500, (b) MFZ-600, (c) MFZ-700, and (d) MFZ-800.

Fig 4.10 shows O1s spectra having four peaks. Here, ketone (O1) assigned at 531.8 eV [141], ether & alcohol (O2) at 532.6eV, carboxyl group (O3) at 533.4eV and oxygen in water at 534.3eV (O4) [132]. Table 4.5 shows that for MFZ-500, O2 contributes maximum. MFZ-600 has maximum contribution of O1. Here, mainly O3 and O4 are converted to O1 and O2. In MFZ-700, O2 contributes maximum at the expense of O1, O3 and O4. MFZ-800 shows decrease in O1 contribution from 22.41% to 4.47. Also, O3 gets increased and O2 gets decreased in small amount. O1 and O4 are converted to O3 for MFZ-800. As reported in literature, O1 and O2 are responsible for acidic and O3 for basic nature [132], therefore, MFZ-700 exhibits highly basic character.

Table 4.5 Deconvolution data of O1s core level spectra of MF based carbons

Sample		O1	O2	O3	O4
MFZ-500	BE	531.814	532.64	533.46	534.38
	FWHM	1.459	1.079	1.036	1.13
	A%	26.89	31.79	25.86	15.44
MFZ-600	BE	531.75	532.73	533.77	534.38
	FWHM	1.825	1.27	1.063	1.25
	A%	44.105	37.07	15.78	3.04
MFZ-700	BE	530.43	531.94	533.19	-
	FWHM	1.243	1.593	1.57	-
	A%	22.41	52.03	25.56	-
MFZ-800	BE	531.98	532.763	533.51	-
	FWHM	0.97	0.973	1.13	-
	A%	4.473	49.60	45.92	-

4.3 CO_2 adsorption performance

4.3.1 Effect of carbonization temperature

Fig. 4.11 shows breakthrough curves and the equilibrium uptake capacity of all the adsorbents at 30 °C under 12.5% CO_2 flow. With increase in carbonization/activation temperature from 500 to 700 °C, a shift in breakthrough curves towards higher time was observed showing an increase in CO_2 uptake capacity, but with a further rise in carbonization temperature, breakthrough curves shifted towards lower times showing a decrease in CO_2 uptake capacity. Here t_b i.e. breakthrough time (when the adsorption zone reaches the last part of the bed, and the bed becomes

ineffective) for MFZ-700 was 1.68 min. Steepest and broadest breakthrough curve was shown by MFZ-500 and MFZ-700. MFZ-700 shows highest CO_2 uptake of 0.64 mmol g^{-1} due to better textural properties and highest basic nature due to higher amount of N1 and N2 and negligible amount of N3 which was confirmed from XPS. CO_2 uptake decreased for MFZ-800 (0.39 mmol g^{-1}) due to acidic nature because of quaternary nitrogen as confirmed from XPS and also due to deterioration in textural properties. Above observations show that CO_2 uptake depends not only on nitrogen content but it depends also on the nitrogen functionalities.

CO_2 uptake follows order of: MFZ-700> MFZ-800>MFZ-600>MFZ-500>MF-700. The MF-700 exhibits least adsorption capacity due to poorest textural property and nonporous nature as confirmed from N_2 adsorption/desorption and SEM. Since the adsorption capacity of sample MFZ-700 has been the highest, further studies were conducted with MFZ-700.

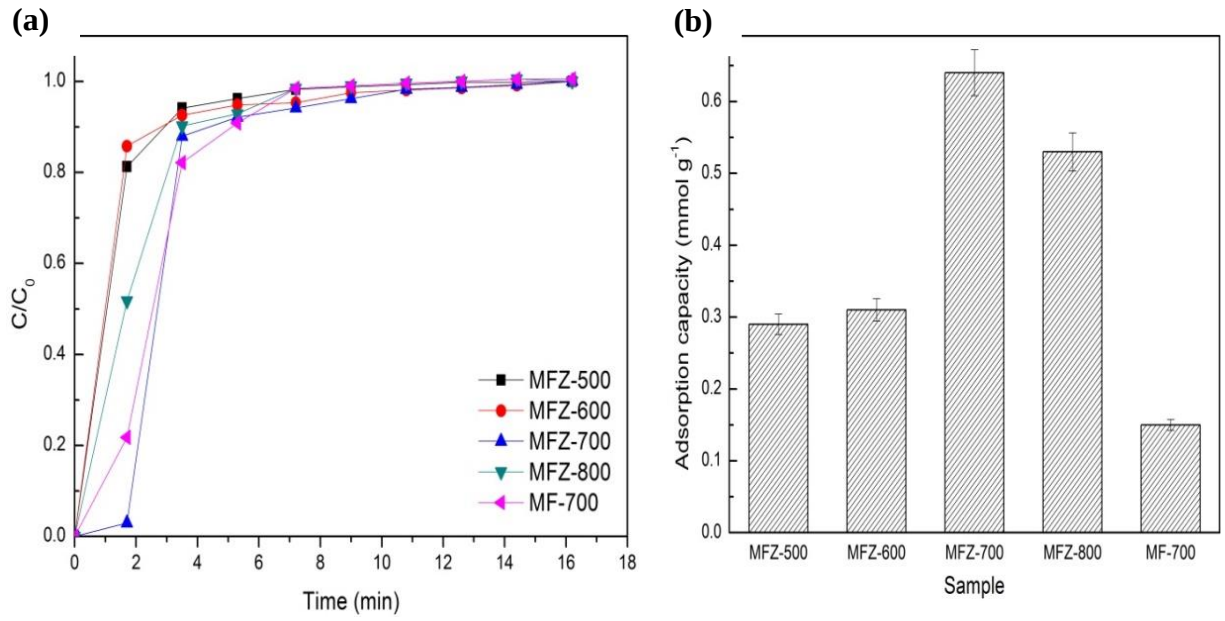

Fig. 4.11(a) CO_2 breakthrough curves, and (b) CO_2 uptake capacity of adsorbents at 12.5% CO_2 and 30 °C

4.3.2 Effect of adsorption temperature and CO_2 feed concentration

Fig. 4.12 shows breakthrough curves of MFZ-700 showing the effect of adsorption temperature (30, 50, 75, 100 °C) and CO_2 concentration (5%, 7.5%, 10% and 12.5%) on adsorption capacity of adsorbent. At first, in the initial phase, no CO_2 was observed in the effluent due to complete adsorption of CO_2 by the surface and pore sites. After 3.33 min, the bed became saturated and the effluent concentration was equal to the inlet concentration. Here the C/C_o gradually reaches 1 when the adsorbent gets saturated where C and C_o are the effluent and influent CO_2 concentrations. It was seen that, for 5% CO_2 concentration, t_b decreased from 3.5 min to 1.2 min as temperature increased from 30 to 100 °C showing breakthrough curve shifting towards lower time with increase in temperature. The adsorption capacity for this fixed concentration and different temperatures varies from 0.38 to 0.12 mmol g^{-1} as shown in Table 4.6. On the other hand, for 12.5% CO_2 concentration with increase in temperature, t_b decreased from 1.66 min to 1.16 min depicting that the equilibrium is attained faster for higher adsorbate concentration. The decrease in adsorption capacity with increase in temperature is because the rate of desorption is higher at higher temperature due to higher kinetic energy. Therefore, adsorbed CO_2 gets unstable due to increase of surface energy and molecular diffusion and saturation is achieved much faster. This also shows the exothermic nature of the process. Pevida *et al.* [15] also observed similar behavior.

The effect of CO_2 concentration at 5% CO_2 and 12.5% CO_2 at 30 °C shows that t_b gets accelerated with increase in CO_2 concentration causing bed saturation faster. The t_b value for a 5% CO_2 and at 30 °C is 3.20 min while for 12.5% at the same temperature is 1.40 min. This shift in t_b value is because with the increase in CO_2 concentration, increase in CO_2 mass transfer rate occurs outside the boundary layer and inside pores of the carbon adsorbents which affect saturation and breakthrough time

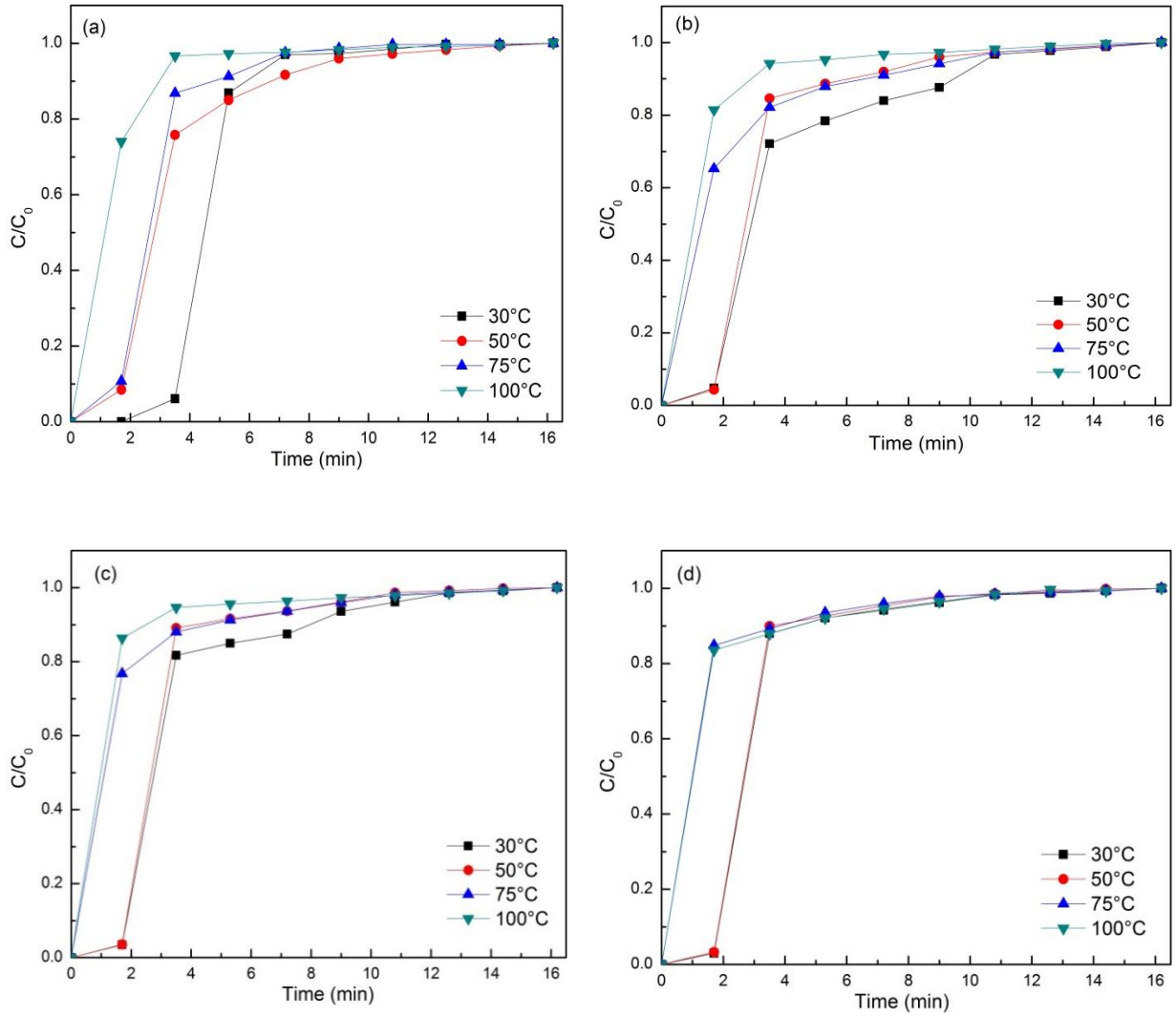

Fig. 4.12 Breakthrough curves of (a) 5%, (b) 7.5%, (c) 10% and (d) 12.5 % CO_2 in feed gas at different adsorption temperatures

Table 4.6 CO_2 uptake of MFZ-700 at different temperatures and CO_2 concentrations

CO_2 concentration (%)	Adsorption capacity (mmol g^{-1}) at temperatures			
	30 °C	50 °C	75 °C	100 °C
5	0.38	0.28	0.23	0.12
7.5	0.49	0.35	0.29	0.19
10	0.59	0.41	0.35	0.24
12.5	0.64	0.49	0.39	0.29

The adsorbents prepared from coal tar pitch and furfuralcohol by Balsamo *et al*. [30] showed CO_2 uptake of 0.61 mmol g^{-1} at 30 °C but the uptake capacity at 50 °C and 75 °C was 0.30 and 0.15 mmol g^{-1} respectively which was lower than the present study even at high temperature. Carbon adsorbents prepared from KOH activation of carpet material by Olivares *et al*. [142] showed CO_2 uptake of 0.16 mmol g^{-1} at 15% CO_2 concentration and 100 °C, which was much lower than the present study at higher temperature. In the present study at 12.5% CO_2 concentration at 100 °C, the adsorption capacity is 0.29 mmol g^{-1}. Carbon adsorbents prepared by Arhellius *et al*. [143] from carbazole, acridine and urea and chemical activation with KOH exhibited CO_2 uptake of 0.27 mmol g^{-1} at 100 °C which was similar to this study. The above results show that the adsorbents developed from nanocasting technique showed higher CO_2 uptake capacity even at higher temperature and lower CO_2 concentration as compared to the reported values. Therefore, we can say that nanocasting technique is more effective than other methods which is able to develop high capacity adsorbents with controlled textural properties

4.3.3 CO_2 selectivity

Fig. 4.4 shows the breakthrough curves for CO_2 and N_2 for MFZ-700 at two different temperatures with 12.5% CO_2 concentrations (rest N_2). Very small adsorption capacity for N_2 is seen as it detected instantly at the outlet of the column. For around 2 min, no CO_2 was observed showing higher attraction of adsorbent towards CO_2. Due to higher concentration of N_2 than CO_2 in the feed gas, it dominates i.e. occupy more sites in starting but with time N_2 is replaced by CO_2 because of high selectivity of adsorbents towards CO_2 [132]. The above results are similar to those reported by Goel *et al*. [138].

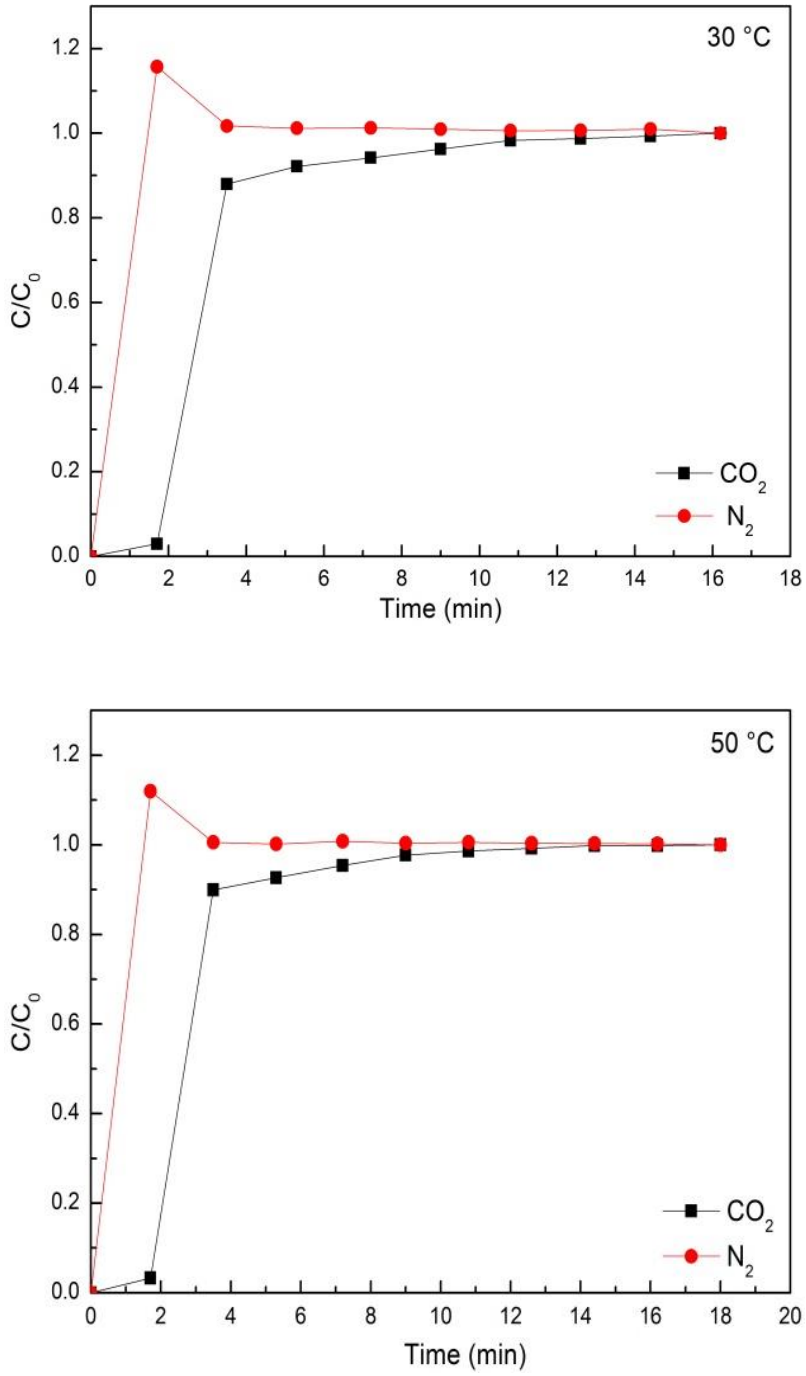

Fig. 4.13 Breakthrough curves of CO_2 and N_2 for 12.5% CO_2 rest N_2 on MFZ-700 at 30 °C and 50 °C

4.3.4 Cyclic adsorption-desorption study

Fig. 4.14(a) shows multiple adsorption-desorption cycles and the CO_2 adsorption capacity at 12.5% CO_2 concentration at different temperatures. A sudden fall in the C/C_0 values was observed showing all the CO_2 previously adsorbed is quickly desorbed from the adsorbent surface. Complete regeneration was achieved for all the materials and no difference in their adsorption capacities was observed with the number of cycles suggesting the reusability of the carbon adsorbent. Fig. 4.14(b) shows that adsorption capacity is constant over different cycles, showing complete regeneration. This shows no loss in the performance of adsorbent during its repeated application. Carbon adsorbents reported by Thote *et al*. [105] from soyabean by chemical activation with $ZnCl_2$ exhibited CO_2 uptake of 0.93 mmol g^{-1} at 30 °C but the adsorbent could not be regenerated in 2^{nd} cycle showing very poor adsorption capacity. This confirms that the synthesized adsorbent in the present study is effective and has stable uptake capacity over four cycles.

4.3.5 TPD study

Fig. 4.15 shows TPD profile of MFZ-700 adsorbent. A broad peak at 100-170 °C was observed with maximum at 130 °C and then the CO_2 signal got smaller with a tail extending beyond 200 °C. This suggests multiple type of adsorption sites with different binding strengths in this adsorbent. The peak at 130 °C may be due to the removal of physically adsorbed CO_2 molecules from the adsorbent surface and tail to higher temperatures shows smaller contribution of chemisorption behavior. Similar kind of observation was also seen by Goel *et al.* [144], Chen *et al*. [145] and Mane *et al.* [146]. Overall, it can be concluded that the adsorbent shows predominantly physiosorption behavior.

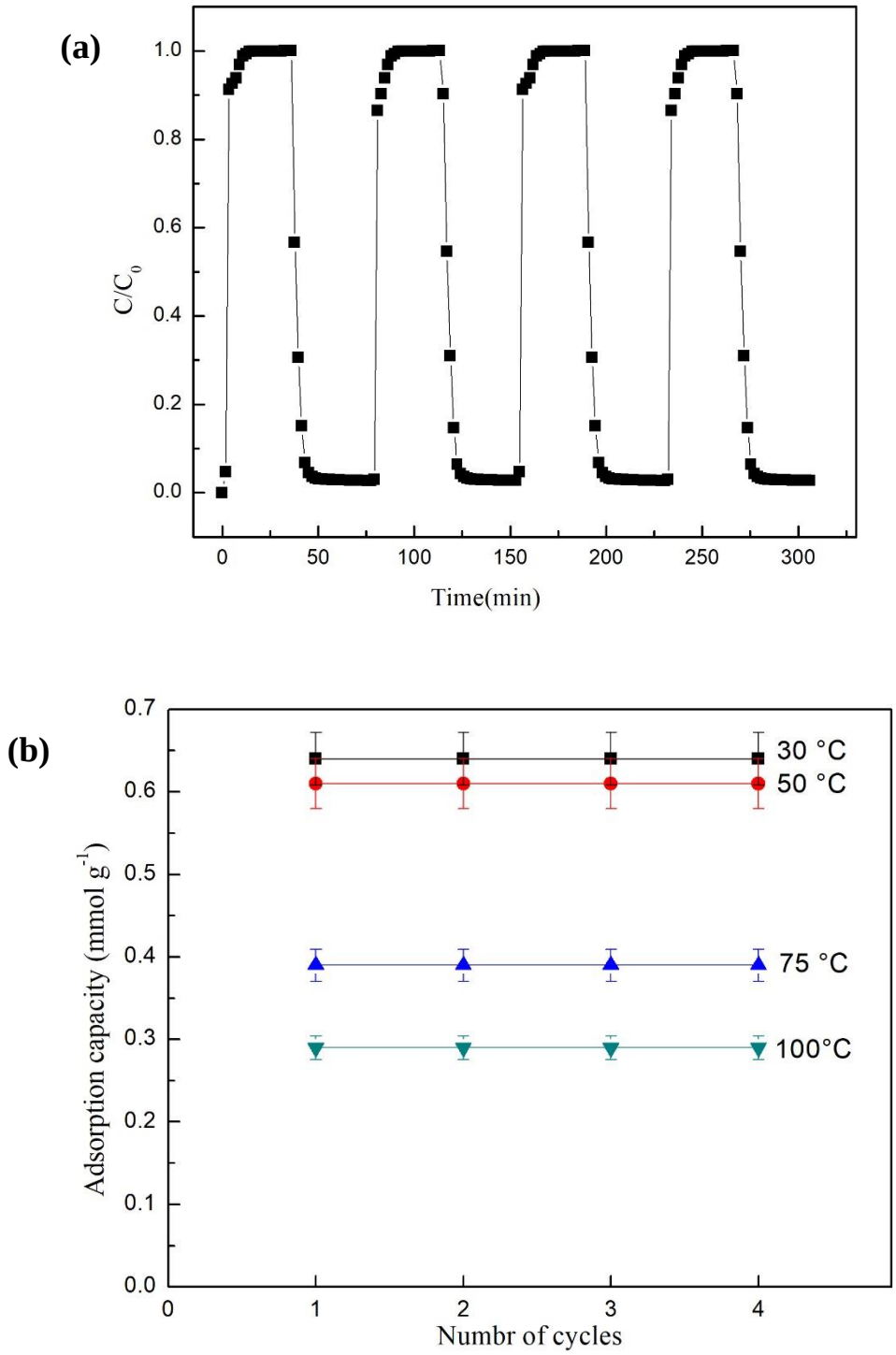

Fig. 4.14(a) Multiple adsorption-desorption curves for MFZ-700 at 30 °C and 12.5% CO_2 in the feed gas, (b) multiple cycle CO_2 uptake capacity at different temperatures with 12.5% CO_2

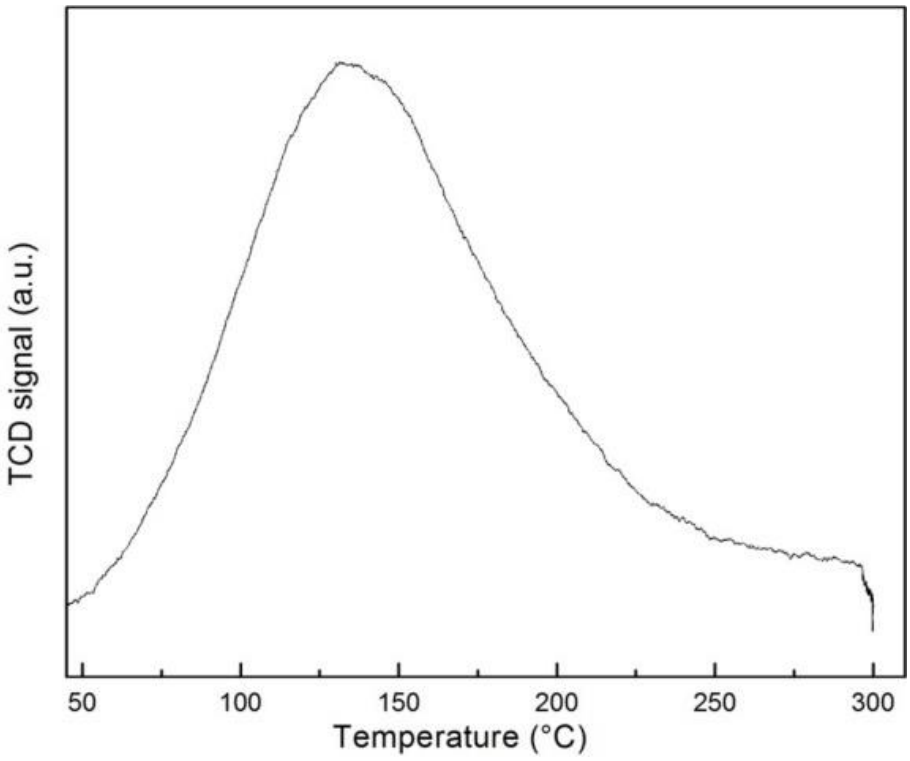

Fig. 4.15 Temperature programmed desorption of CO_2 from MFZ-700

4.4 Equilibrium sorption measurements

Fig. 4.16 shows pure component adsorption-desorption isotherms of MFZ-700 at different temperatures and pressures. Fig. 4.16(a) shows the volumetric adsorption capacity for CO_2 on MFZ-700. It is found that increase of pressure caused an increase in adsorption capacity while the opposite trend is seen for temperature: adsorption capacity decreased with increase in temperature from 1.34 to 0.6 mmol g^{-1}. MFZ-700 shows very low N_2 adsorption capacity (0.10 mmol g^{-1} at 30 °C and 0.03 mmol g^{-1} at 100 °C) (Fig. 4.16(b)). The adsorbent has a higher selectivity towards CO_2. Also, adsorption-desorption isotherms of CO_2 and N_2 show hysteresis at all adsorption temperatures, suggesting that small amount of energy is required for reuse of adsorbent. Adsorbent prepared by Lakhi *et al*. [147] from carbon-nitride by polymerization of ethylenediamine and carbon-tetrachloride in pores of FDU-12 mesoporores silica exhibited CO_2 uptake of 1.4 mmol g^{-1} at 25 °C. This uptake capacity was similar to our study. Carbon adsorbents prepared by Hao *et*

al. [111] from direct pyrolysis of resorcinol, formaldehyde and lysine as a catalyst exhibited CO_2 uptake of 3.13 mmol g^{-1} at 30 °C and 0.62 mmol g^{-1} at 120 °C in a study in static system for RFL-500. The uptake capacity for this study was almost similar with the reported literature at high temperature. In fact, the static capacity of the adsorbent is always higher than the dynamic capacity but dynamic capacity is more relevant for CO_2 capture from flue gas point application.

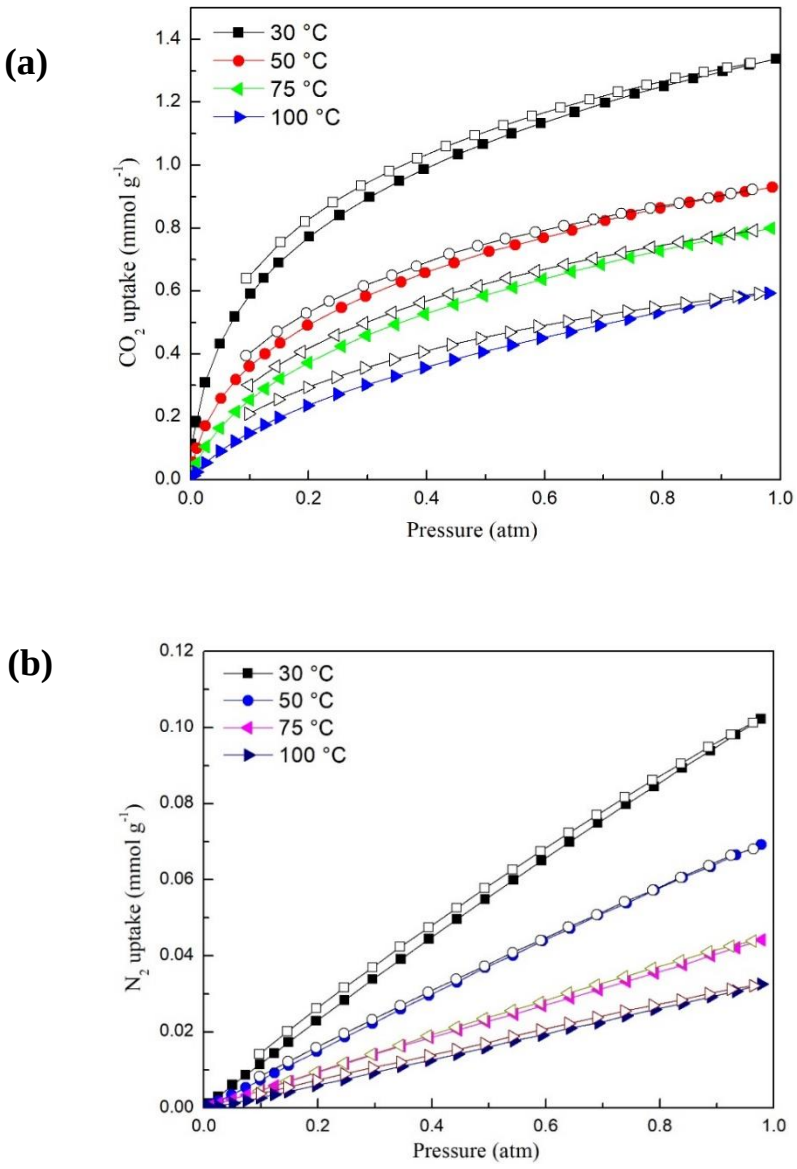

Fig. 4.16 Adsorption-desorption of (a) pure CO_2, and (b) pure N_2 from MFZ-700 at different adsorption temperatures (closed symbols for adsorption and open symbols for desorption)

4.5 Kinetic study

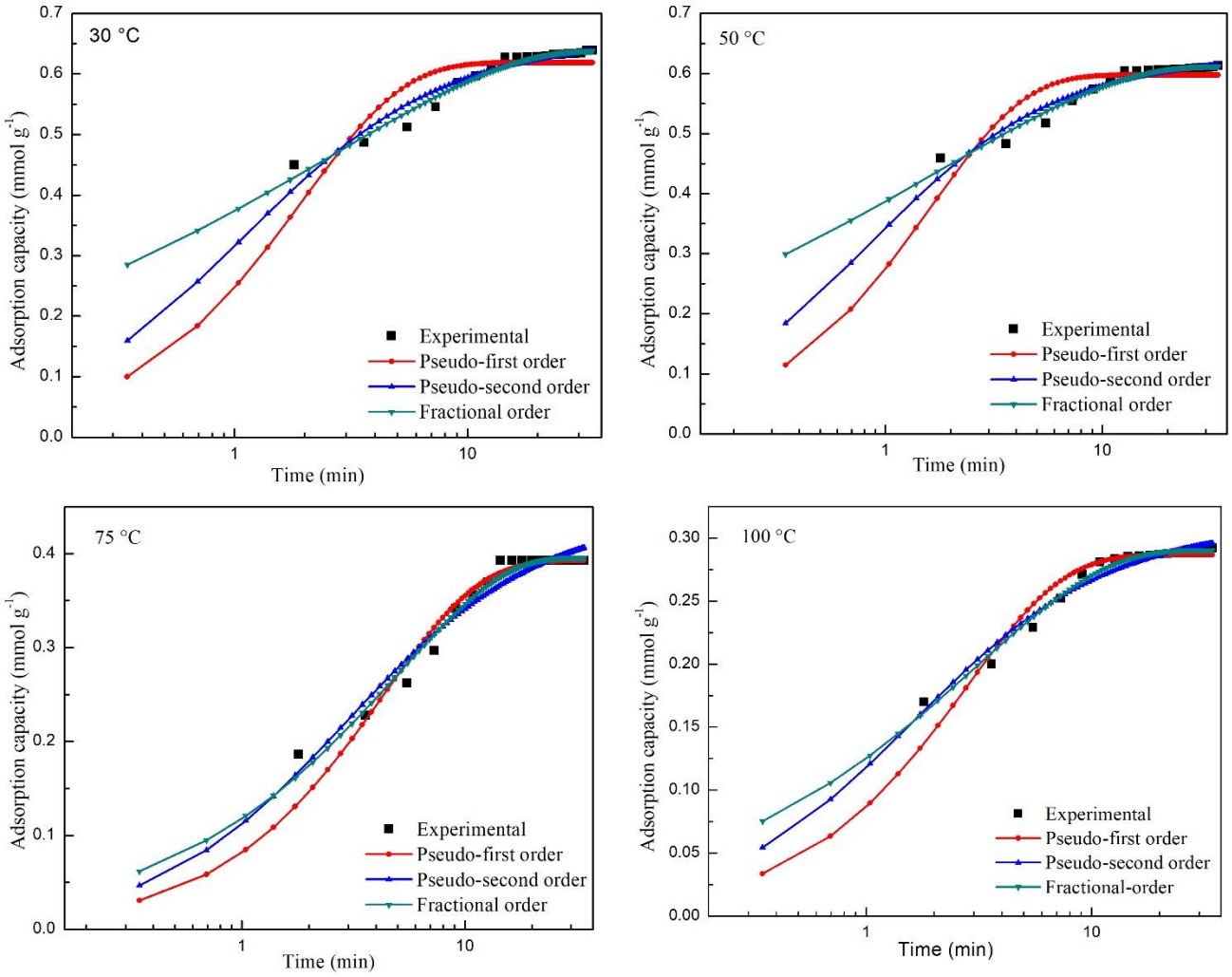

Fig. 4.17 Experimental and model predicted CO_2 uptake kinetics at 12.5% CO_2 and different temperatures

Fig. 4.17 shows experimental and model predicted CO_2 uptake of the adsorbent as a function of time. It was found that 90% of adsorption occurred within few minutes of contact with CO_2. After this, it gets slower until equilibrium is attained. This is because of decrease in unoccupied active sites and increase in diffusion resistance. Table 4.7 shows kinetic parameters, errors and correlation coefficients (R^2) obtained from equation (3.3-3.7). Pseudo-first and second-order

shown in Fig. 4.17 show higher values of error% suggesting that these models are not following experimental CO_2 uptake for carbon adsorbent.

Based on the R^2 value of 0.99 and maximum error of 3.68% on fitting the fractional order model, it can be said that this model describes the adsorption process quite well. This is further confirmed by experimental and predicted q_e values. Pseudo-second order model is found to show the higher values of the equilibrium adsorption capacity at 75 °C and 100 °C (Table 4.7). Exothermic nature and faster adsorption at higher temperature is confirmed from decrease in rate constant k_n and increase in n and m values with rise in adsorption temperature [132].

Table 4.7 Kinetic parameters of CO_2 adsorption on carbons at different temperatures and 12.5% CO_2

Model	Parameters	Temperature (°C)			
		30	50	75	100
Pseudo-first-order	k_1 (min^{-1})	0.50	0.61	0.23	0.36
	q_e (mmol g^{-1})	0.62	0.59	0.39	0.28
	R^2	0.95	0.96	0.97	0.97
	Error %	15.10	22.92	23.37	8.12
Pseudo-second-order	k_2 (g $mmol^{-1}$ min^{-1})	1.40	1.90	0.77	1.98
	q_e (mmol g^{-1})	0.65	0.62	0.44	0.31
	R^2	0.98	0.991	0.98	0.98
	Error %	22.22	2.28	4.52	3.69
Fractional-order	k_n ($mmol^{1-m}$ g^{m-1} min^{-1})	0.22	0.19	0.17	0.16
	q_e (mmol g^{-1})	0.64	0.61	0.39	0.29
	n	0.55	0.61	0.72	0.74
	m	0.32	0.33	0.67	0.56
	R^2	0.99	0.995	0.99	0.99
	Error %	1.19	1.65	3.68	1.48

Table 4.8 shows activation energies E_a, and pre-exponential factors A, at different concentrations, calculated from the slope and intercept of Arrhenius plot. The negative value of E_a, is due to decrease in the kinetic rate constant with rise in temperature.

Table 4.8 Arrhenius parameters for CO_2 adsorption on MFZ-700

CO_2 concentration (Vol. %)	A	E_a (kJ mol^{-1})	R^2
5	0.0341	-4.8	0.97
7.5	0.031	-3.1	0.88
10	0.0307	-3.3	0.91
12.5	0.0320	-3.8	0.99

4.6 Isotherm study

Table 4.9 shows the parameters estimated from different models at different temperatures, obtained from the non-linear fitting of equilibrium data of MFZ-700 at 30 ˚C. Based on the coefficient of determination (R^2), the best result of the equilibrium data fit well with the Temkin isotherm at different adsorption temperatures. This shows that the adsorbent surface is heterogeneous [55]. The maximum value of b (17.22 kJ mol^{-1}) shows physical adsorption process. Also, the decrease in Langmuir (K_L) and Freundlich (K_F) constants with increase in temperature indicates physiosorption behavior. This is also confirmed from the similar values of q_m and also decrease in value with rise of temperature. The value of q_m is higher at 30 ˚C indicating the maximum adsorption taking place at this temperature. Value of n greater than 1 indicates a favorable condition for adsorption. Fig. 4.18 shows Temkin model fitting along with experimental data at different adsorption temperatures.

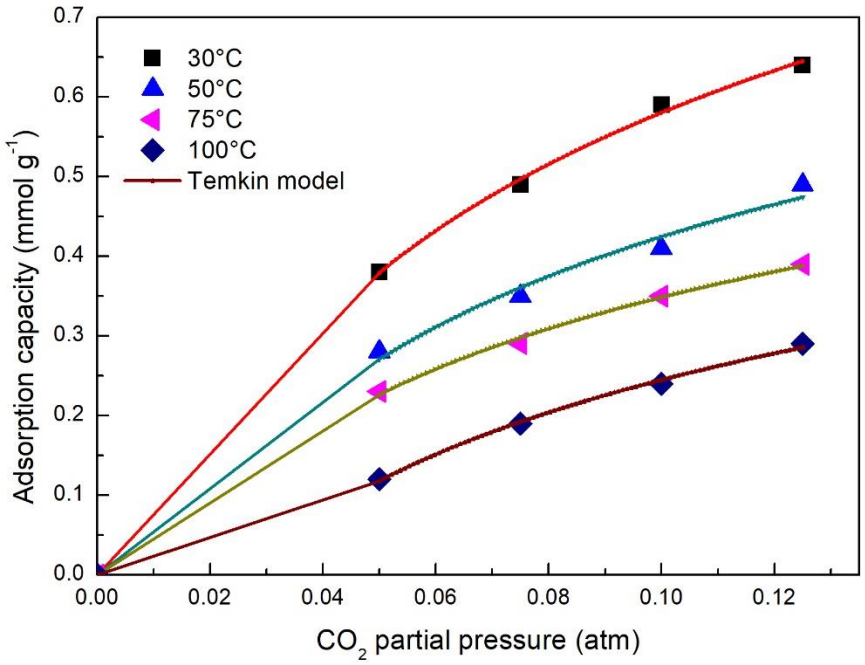

Fig. 4.18 Experimental and isotherm model predicted CO_2 uptake values at different temperatures

Table 4.9 Parameters of adsorption isotherm models

Parameters		Temperature (°C)			
		30	50	75	100
Langmuir isotherm	q_m (mmol g^{-1})	2.57	2.36	1.20	0.74
	K_L (atm $^{-1}$)	9.28	8.70	2.75	1.12
	R^2	0.97	0.98	0.99	0.98
Freundlich isotherm	K_F (mmol g^{-1} atm $^{-1/n}$)	3.29	2.11	1.97	1.13
	n	1.76	1.23	1.72	1.08
	R^2	0.983	0.98	0.99	0.99
Temkin isotherm	K_T (atm^{-1})	73.78	67.51	72.03	38.0
	b (kJ mol^{-1})	8.68	6.67	17.01	17.22
	R^2	0.993	0.98	0.992	0.99

4.7 Thermodynamic study

4.7.1 Thermodynamic parameters

Thermodynamic parameters at various temperatures are shown in Table 4.10. Standard enthalpy change (ΔH^0) and standard entropy change (ΔS^0) were estimated to be -5.7 kJ mol^{-1} and 0.033 kJ mol^{-1} K^{-1} showing exothermic nature. ΔG^0 value was found to be negative at all temperatures showing feasibility and spontaneity of adsorption process. The positive value of standard entropy change indicates adsorbents affinity towards CO_2 and at the adsorbate-adsorbent interface. It was reported in literature that ΔH^0 value <20 kJ mol^{-1} implies physiosorption behavior. Thus, a lower value of ΔH^0 (-5.7 kJ mol^{-1}) in this case indicates physiosorption behavior.

Table 4.10 Thermodynamic parameters of CO_2 adsorption on MFZ-700

T (˚C)	ΔG^0 (kJ mol^{-1})	ΔH^0 (kJ mol^{-1})	ΔS^0 (kJ mol^{-1} K^{-1})
30	-10.83	-5.7	0.033
50	-10.16		
75	-12.37		
100	-11.28		

Isosteric heat of adsorption (Q_{st}) calculated using Clausius-Clapeyron equation [136] (Fig. 4.19) at selected adsorbed amount of CO_2 shows that Q_{st} value lies in the range of 15.03 to 16.06 kJ mol^{-1} having a middle value of 15.055 kJ mol^{-1} showing high affinity of CO_2 molecules with adsorbent surface. With increase in surface coverage, first decrease and then increase in the value is observed, suggesting the heterogeneous adsorbent surface. The value of Q_{st} = 15.055 kJ mol^{-1} from this work is lower than the literature reported values (-20.3 kJ mol^{-1} for activated carbon) [148]. This shows that a lower amount of energy is needed for regeneration.

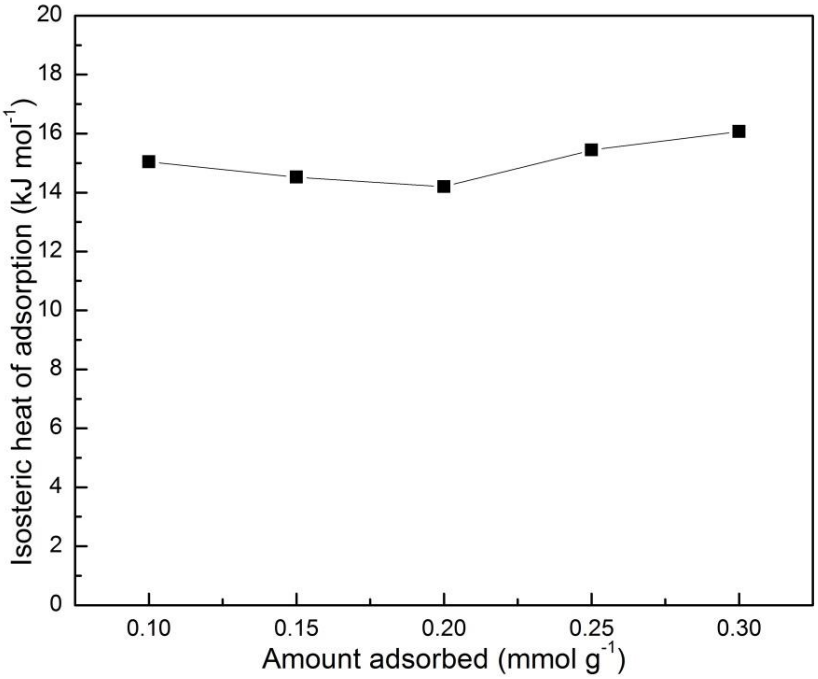

Fig. 4.19 Isosteric heat of adsorption of CO_2 versus adsorbed amount on MFZ-700

4.7.2 Energy duty for desorption of CO_2

Energy requirement for desorption of adsorbed CO_2 on MFZ-700 was calculated using Eq. (3.16). Thermal energy input for regeneration depends on both heat of desorption and sensible heat. Firstly, specific heat capacity of MFZ-700 carbon adsorbent was measured by DSC and then sensible heat required to raise the bed temperature for desorption was calculated.

Specific heat capacity (C_p) of the prepared carbon MFZ-700 = 1.2 J g^{-1} K^{-1}.

Adsorption conditions: 30 °C, 1 atm pressure, 12.5% CO_2 in N_2

Desorption conditions: 200 °C, purging with 100% N_2

Temperature difference, $\Delta T = (200 - 30)\ ℃ = 170\ ℃$

CO_2 adsorption capacity of MFZ-700 = 0.64 mmol CO_2/g adsorbent

= 0.64 × 10^{-3} mol CO_2/g adsorbent

= 0.028 kg CO_2/g adsorbent

Hence, sensible heat = $\frac{1.2 \times 170}{0.64 \times 10^{-3}}$ J per mole CO_2 = 318.75 kJ per mole CO_2

It is assumed that around 75% of the sensible heat required for heating the adsorbent can be recovered by direct or indirect heat exchanger [149].

Therefore, net sensible heat required in the process $= (25\% \text{ of } 318.75)$ kJ per mole CO_2

Sensible heat $=$ 79.68 kJ per mole CO_2

Isosteric heat of adsorption, $Q_{st} = 15.05$ kJ per mole CO_2

Thermal energy input $= (15.05 + 79.68)$ kJ per mole $CO_2 = 94.73$ kJ per mole CO_2

$= 2.15$ MJ per kg CO_2

Hence, desorption of 1 kg CO_2 requires energy equal to 2.15 MJ which is obtained from the burning of fossil fuels. For desorption of 0.64 mmol g^{-1} of CO_2 (0.028 kg kg^{-1}), energy required is 0.0603 MJ.

Assuming that bituminous coal is used as fossil fuel for energy production, amount of CO_2 generated is 0.0884 kg per MJ of energy [150].

Thus, CO_2 generated to produce 0.0603 MJ of energy for desorption = 0.00533 kg CO_2

It can be concluded (on 1 kg adsorbent basis) that energy duty for desorption of 0.028 kg CO_2 requires 0.0651 MJ of energy which leads to generation of 0.00533 kg CO_2 from combustion of fossil fuel (bituminous coal). This is energy penalty for CO_2 capture.

4.8 Conclusions

Nitrogen enriched carbon adsorbents were successfully developed through nanocasting technique using MF resin and mesoporous zeolite as precursor and template respectively. Carbonization followed by activation under CO_2 atmosphere results in development of nanostructured carbon adsorbents. Presence of nitrogen is confirmed from elemental analysis, FTIR and XPS. Highest dynamic CO_2 uptake capacity of 0.64 mmol g^{-1} at 30 °C and 12.5% CO_2 concentration on MFZ-700 is obtained. Decrease in CO_2 uptake capacity with increase in temperature confirms exothermic adsorption process. Adsorbents show complete regenerability, stability and better selectivity for CO_2. Fractional-order-model provided the best description of the process at various temperatures. CO_2 adsorption on the adsorbent surface fits well with Temkin isotherm, indicating heterogeneous nature. Exothermic and spontaneous nature is suggested from thermodynamic parameter values. Energy needed for regeneration, (calculated from the isosteric heat of adsorption and sensible heat) is equal to 2.15 MJ per kg CO_2, which is equivalent to 0.028 kg CO_2 (as energy penalty).

Chapter 5 – Epoxy based Oxygen Enriched Nanostructured Carbons for Carbon Dioxide Capture

5.1 Preparation of adsorbents

5.1.1 Templated epoxy resin preparation

Adsorbents were prepared by using epoxy resin (80 g) and 150 ml of pure acetone. Both resin and acetone were mixed in a beaker for 1 h followed by addition of 20 g of mesoporous zeolite (template). Next, heating at 120 ºC for 3 h for complete dryness was done to obtain templated resin.

5.1.2 Carbonization of templated epoxy resin

Carbonization (in nitrogen)-activation (in carbon dioxide) for 1 h each of templated resin was performed in tubular furnace loaded with ceramic boats at 500-800 ºC by heating at 10 ºC min^{-1}. After activation, sample was cooled under nitrogen atmosphere to room temperature.

5.1.3 Template removal

After cooling, sample was dipped in NaOH solution for 48 h followed by washing with copious amount of distilled water. Next after washing, sample was dried at 100 ºC and labeled as EZ-T where *T* denotes carbonization-activation temperature.

5.1.4 Carbonization of epoxy resin

A reference sample, for comparision, was prepared using direct carbonization of epoxy resin (without any template) at 700 ºC and labeled as E-T.

5.2 Characterization of adsorbents

5.2.1 Surface area and pore size distribution

Fig. 5.1(a) shows nitrogen adsorption-desorption isotherms of the adsorbents. Nitrogen adsorption-desorption isotherms show that E-700 is almost non-porous as nitrogen adsorption is negligible. For the sample EZ-500, adsorption of nitrogen was much lower which indicates the insufficiency of this temperature in development of porosity. Further increase in temperature, enhances the nitrogen adsorption (highest for sample EZ-700) which signifies the development of better porosity in the sample. For sample EZ-800, amount of nitrogen adsorption is lower as compared to EZ-600 and EZ-700 indicating collapse of pore structures. All samples, except (EZ-600 and EZ-700) show presence of mesopores as observed from Type IV isotherm. Presence of both micro and mesoporosity, observed in EZ-600 and EZ-700 is indicated by both Type I and Type IV isotherms. Here, the sample shows microporosity due to CO_2 activation while mesoporosity is due to removal of zeolite template. Isotherms indicate H3 hysteresis loops characteristic of mesoporous materials at a relative pressure range of 0.45-1.

Fig. 5.1(b) depicts pore size distributions (PSDs) of the synthesized adsorbents carbonized at different temperatures with nanocasting technique and direct carbonization. Here, instead of desorption branch of isotherm, adsorption branch was selected because PSDs obtained from desorption branch provide completely different results as compared to adsorption branch. This could be because of TSE (tensile strength effect). PSDs obtained from adsorption branch was not affected by TSE. The pore size of the adsorbents lie in the range of 2-6 nm which signifies mesopore distribution.

Table 5.1 shows the influence of carbonization-activation temperature and nanocasting on textural properties of the prepared carbon adsorbents. Surface area increased with increase in carbonization and activation temperature and the highest value was observed at 600 °C (686 $m^2 g^{-1}$). Pore volume and porosity also increased with activation temperature up to 600 °C but reduced beyond this temperature. Increase in temperature generates mesoporosity in the sample. For sample of 800 °C, decrease in all textural properties due to extensive gasification is observed. The reference sample E-700 showed the non-porous material. This indicates nanocasting effect in the development of sample from non-porous to porous structure.

(a)

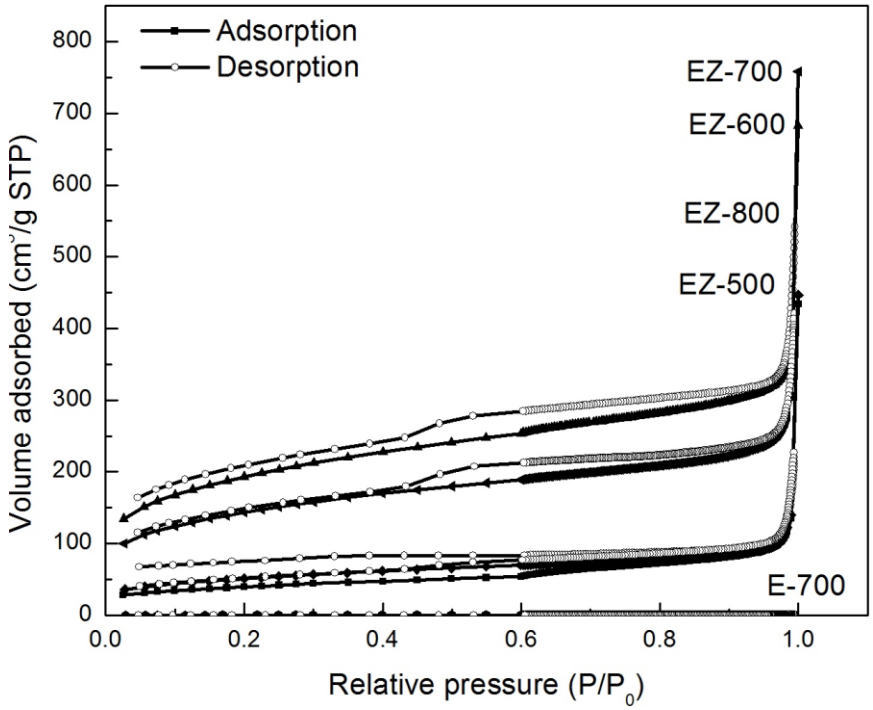

(b)

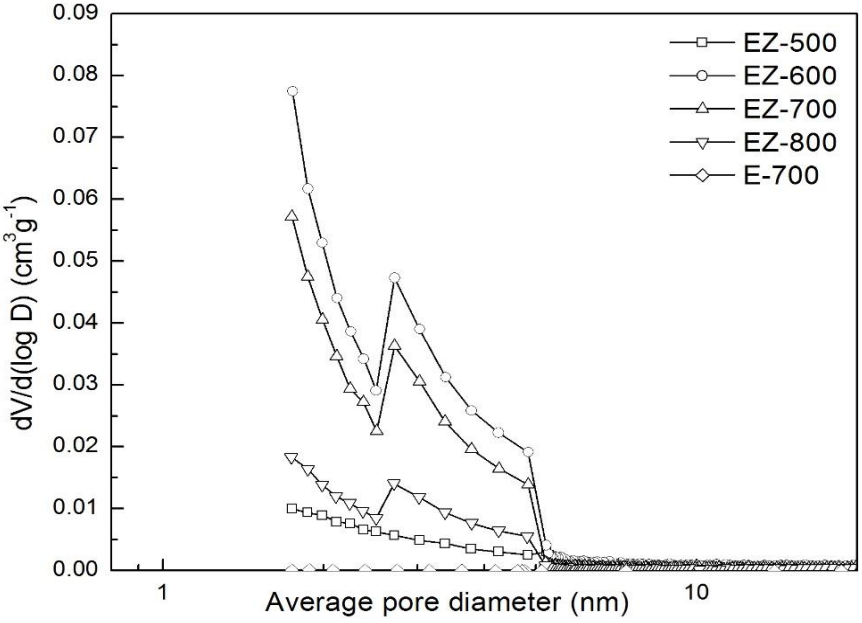

Fig. 5.1 (a) N_2 sorption isotherms, and (b) PSDs of samples

Table 5.1 Textural properties of carbon materials

Sample	N_2 adsorption at -196 °C			
	S_{BET} ($m^2\ g^{-1}$)	V_p ($cm^3\ g^{-1}$)	V_{meso} ($cm^3\ g^{-1}$)	V_{micro} ($cm^3\ g^{-1}$)
EZ-500	127	0.21	0.011	0.218
EZ-600	686	0.62	0.065	0.523
EZ-700	498	0.50	0.044	0.454
EZ-800	179	0.23	0.012	0.237
E-700	-	-	-	-

5.2.2 XRD analysis

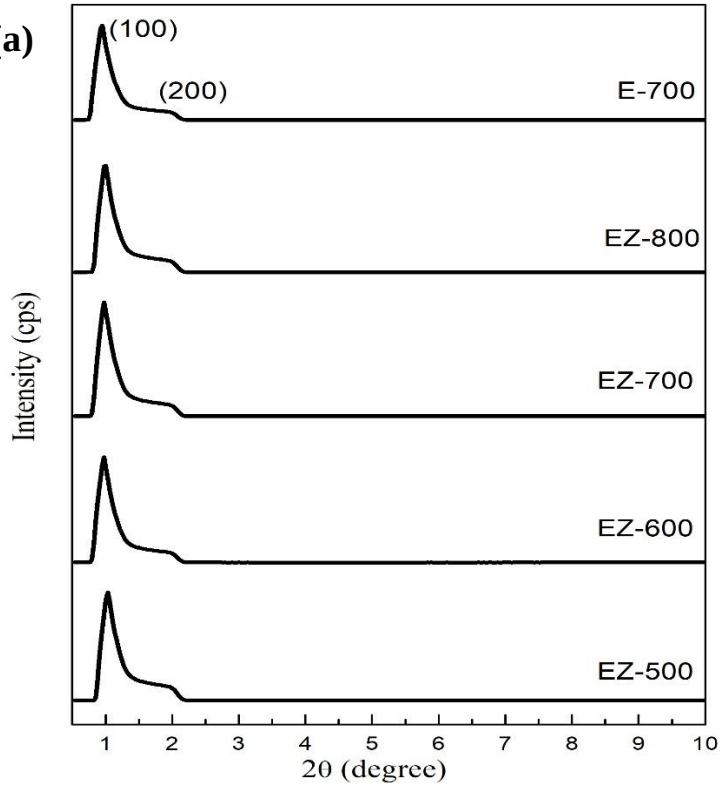

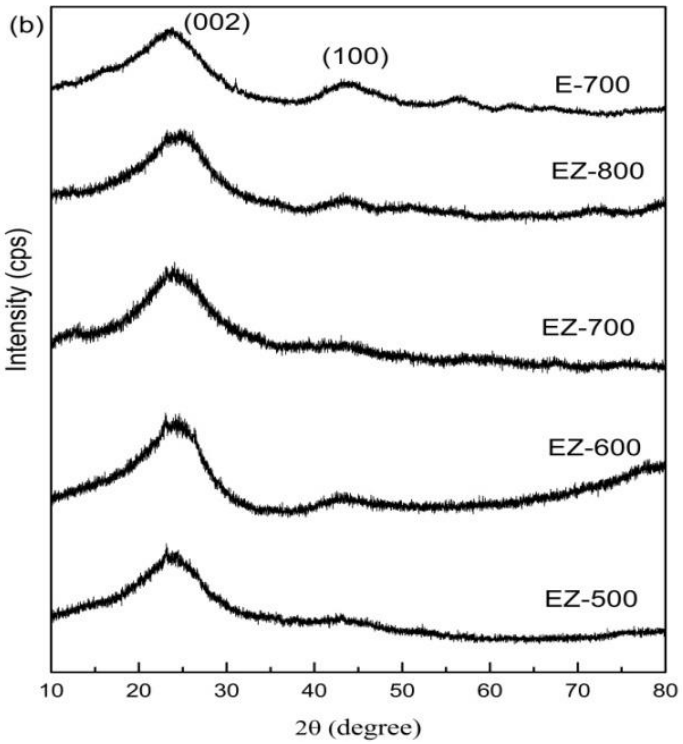

Fig. 5.2 XRD patterns of carbon samples (a) Low angle and (b) wide angle

Fig. 5.2a shows low angle XRD patterns exhibiting peaks at 2θ = 0.98˚ and 1.99˚ which correspond to (100), (200) diffraction planes, indicating hexagonal mesostructure [151]. Fig. 5.2b shows wide angle XRD patterns exhibiting peak around 24.11-25.31˚ correspond to (002) and other weak peak around 43.08-43.14˚ correspond to (100) diffraction from graphitic carbon [152]. Interlayer spacing is higher than ideal graphite (d_{002} = 0.335 nm), from 0.351 to 0.368 nm [153]. Development of nanostructured carbon and irregularity in layer structures was confirmed from broadening of peak and decrease in intensity of peak.

5.2.3 TEM analysis

Fig. 5.3(a-d) shows TEM images of samples at different carbonization-activation temperatures confirming the development of nanostructured materials within a range of 10-20 nm. Fig. 5.3(e) shows direct carbonized sample (E-700), which does not lie in nanomaterial range. This shows the role of template in the development of carbon samples.

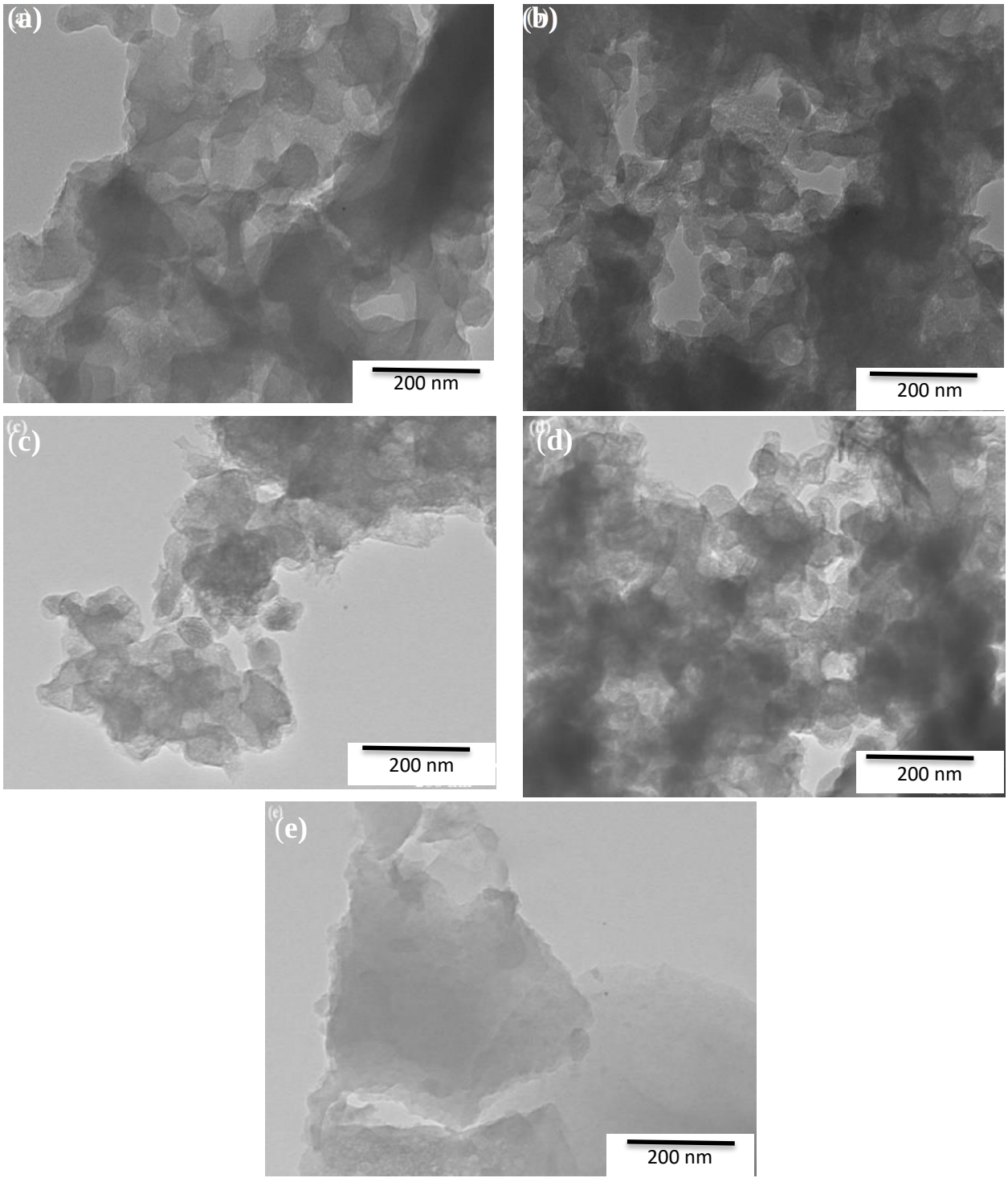

Fig. 5.3 TEM of (a) EZ-500, (b) EZ-600. (c) EZ-700, (d) EZ-800, (e) E-700

5.2.4 SEM analysis

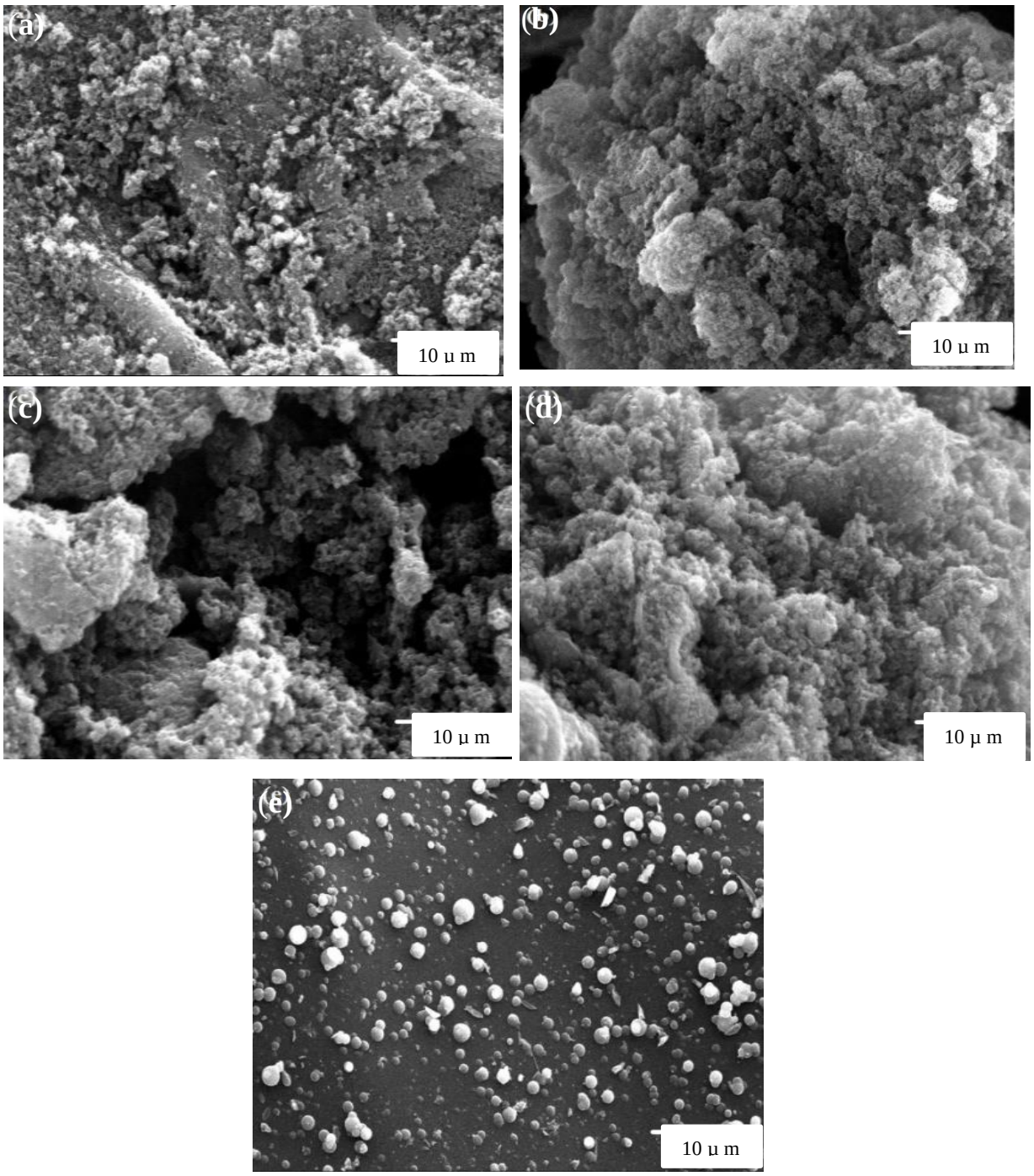

Fig. 5.4 SEM of (a) EZ-500, (b) EZ-600, (c) EZ-700, (d) EZ-800, (e) E-700

SEM images of samples prepared at different carbonization-activation temperatures are shown in Fig. 5.4(a-e). With increase in carbonization-activation temperatures upto 700 °C, samples showing improved porosity with maximum obtained for 700 °C. Higher porosity results in better diffusion of gas from bulk to the adsorbent surface for 700 °C. The sample of 800 °C shows more compact structure with negligible pores signifying the sintering at high temperature. On the other hand, direct carbonized sample E-700 (Fig. 5.4e) shows absence of porosity. This sample appears to be non-porous. The result is in good agreement with N_2 adsorption/desorption.

5.2.5 TG analysis

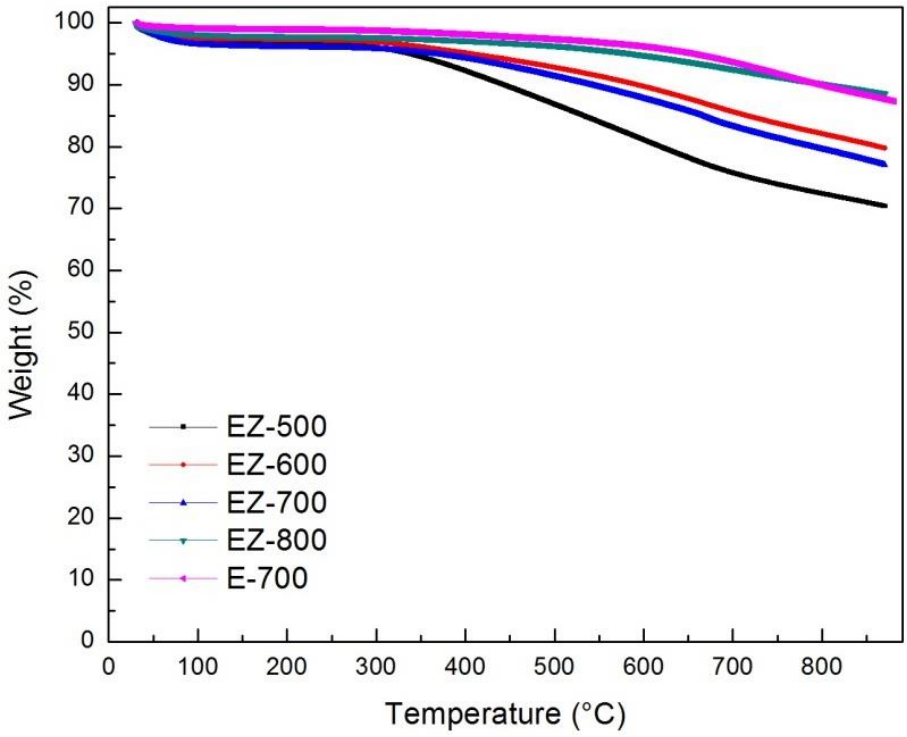

Fig. 5.5 TGA of prepared adsorbents

TGA curves of adsorbents in N_2 atmosphere are shown in Fig. 5.5. Slight decrease in weight% up to 100 °C is observed due to removal of moisture and adsorbed gases. After this, thermal stability decreases with increase in carbonization temperature. Sample of 800 °C shows thermal stability up to 350 °C. The sample of 500 °C is the least thermally stable, showing maximum

weight loss of 30%. EZ-600, EZ-700 and EZ-800 show maximum weight loss of 20%, 23% and 12%, respectively. The thermal stability of the E-700 shows loss of <1% up to 100 °C and also shows thermal stability similar to EZ-700.

5.2.6 Elemental analysis

Table 5.2 Chemical characteristics of carbon materials

Sample	Elemental analysis (wt. %)		
	C	H	O[a]
EZ-500	73.22	2.56	24.22
EZ-600	85.40	2.29	12.31
EZ-700	51.61	1.34	47.51
EZ-800	52.42	0.88	46.24
E-700	72.55	1.85	25.6

[a]*Calculated by difference*

Table 5.2 shows elemental analysis of the prepared adsorbents. It is observed that, oxygen content is highest for EZ-700 which is because of CO_2 activation causing decomposition of carbon containing groups. As expected due to activation, hydrogen content decreases linearly. On the other hand, due to breakage of C-O and C-H bonds, carbon content increases from 73.22 % to 85.40% upto 600 °C but further it decreases. As compared to EZ-700, E-700 shows lesser carbon and higher oxygen content, showing template affects the composition of samples.

5.2.7 FTIR analysis

Fig. 5.6 shows FTIR spectra of carbon adsorbents. Samples show peaks at 1056 cm^{-1}, 1250 cm^{-1}, 1777 cm^{-1} and 3000 cm^{-1} which are assigned to stretching vibration of alkoxy C-O bond, phenyl C-O bond, C=O bond of carboxyl groups [154] and C-H bond respectively. Peak intensity of 1560 cm^{-1} gets decreased for carbonization carried after 600 °C signifies loss of C=C bond (carbon content), at higher carbonization temperature. E-700 shows lower oxygen content as compared to other adsorbents which is confirmed from smaller peak of C-O bond. Elemental analysis also shows similar observations. This finding confirms the presence of oxygen functionalities onto the adsorbents.

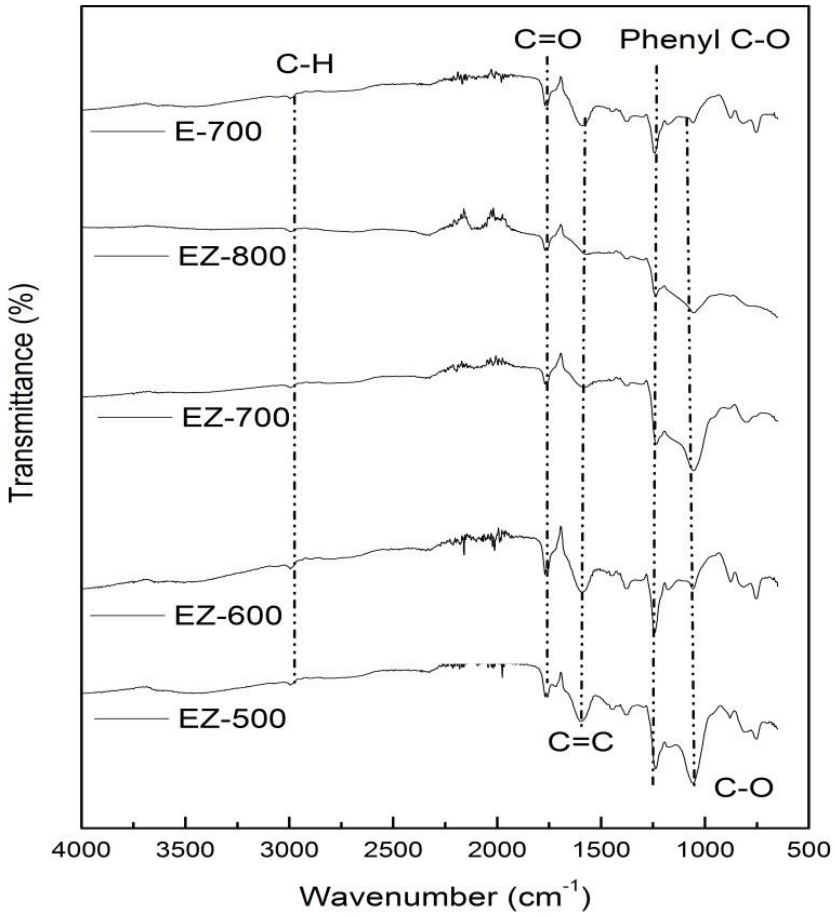

Fig. 5.6 FTIR spectra of carbon samples

5.2.8 XPS analysis

XPS study was performed to investigate the nature of oxygen moieties on the adsorbent surfaces. The results for EZ-700 and E-700 are shown in Fig 5.7 and Table 5.3. XPS O1s spectra of samples are deconvoluted into three different peaks. Ketone (O1) is assigned at binding energy of 531.81 eV [141], ether, alcohol (O2) at 532.92 eV and carboxyl group (O3) at 533.80 eV, respectively [132]. Table 5.3 presents binding energy (B.E), full width at half maximum (FWHM) and relative area contribution (A%). It is observed that O2 contributes maximum in the sample EZ-700, and O3 in E-700. It was reported in literature that ethers, ketones are responsible for surface basicity and carboxylic group is responsible for surface acidity [132]. As compared with EZ-700, E-700 contained higher amount of O3 and lower content of O2. This difference in these oxygen functionalities will affect the surface basicity of these carbons.

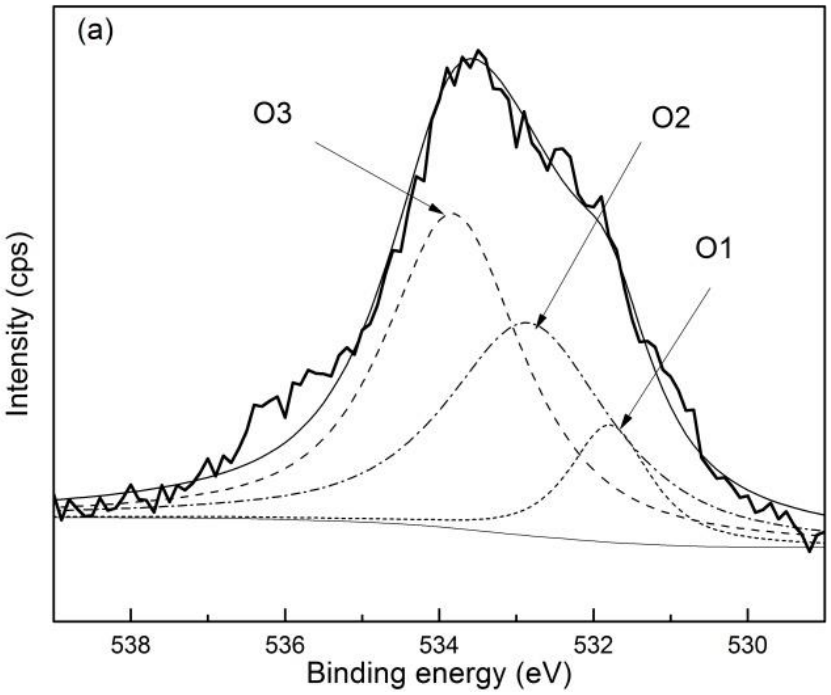

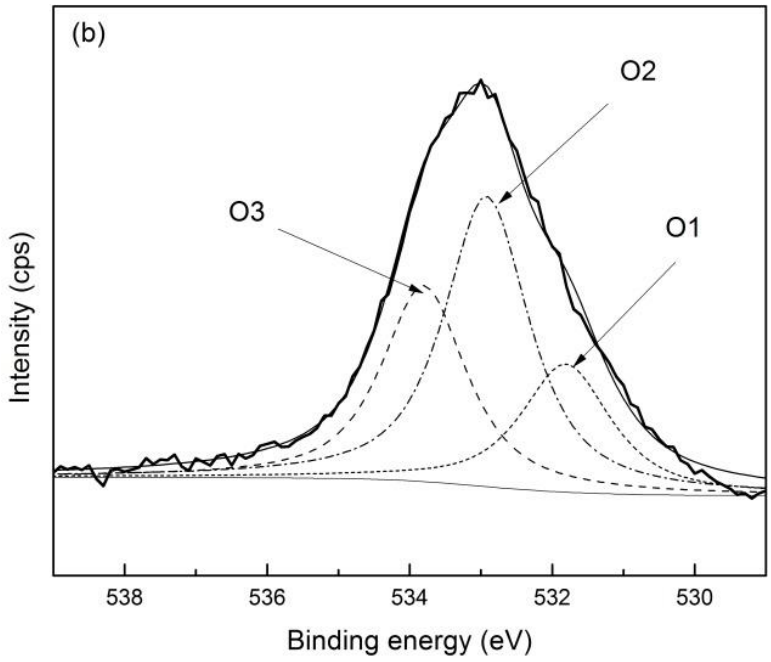

Fig. **5.7** X-ray photoelectron spectra of (a) E-700 and (b) EZ-700

Table 5.3 Binding energies, full width half maximum and relative area % of the O1s core level of XPS spectra

Sample		BE	FWHM	A%
EZ-700	O1	531.81	1.494	21.87
	O2	532.92	1.41	46.79
	O3	533.80	1.399	31.33
E-700	O1	531.79	1.25	10.93
	O2	532.85	2.51	39.70
	O3	533.82	2.11	49.35

5.3 CO_2 adsorption performance

5.3.1 Adsorption capacity with carbonization temperature

Fig. 5.8 shows breakthrough curves and CO_2 adsorption capacity of synthesized adsorbents at 30 °C under 12.5% CO_2 flow. Highest CO_2 uptake capacity was exhibited by sample EZ-700 (0.65 mmol g^{-1}) due to high basicity, which is confirmed from the XPS by the presence of ethers and ketones. But it was seen that by increasing the temperature from 500 to 600 °C, the absorbent EZ-600 exhibited highest surface area but showed the lesser adsorption capacity due to lower oxygen content. For 800 °C sample, adsorption capacity (0.32 mmol g^{-1}) decreased. This was due to a drastic decrease in all the textural and surface properties. E-700 shows lowest adsorption capacity (0.19 mmol g^{-1}) due to the acidic nature of the sample having higher amount of carboxylic group. This may also be due to poor textural properties and non-porous structure as confirmed from N_2 sorption and SEM analysis. Here, t_b and adsorption capacity follows order of EZ-700>EZ-600>EZ-800>EZ-500>E-700. As EZ-700 exhibited highest CO_2 uptake, it was selected for further detailed studies.

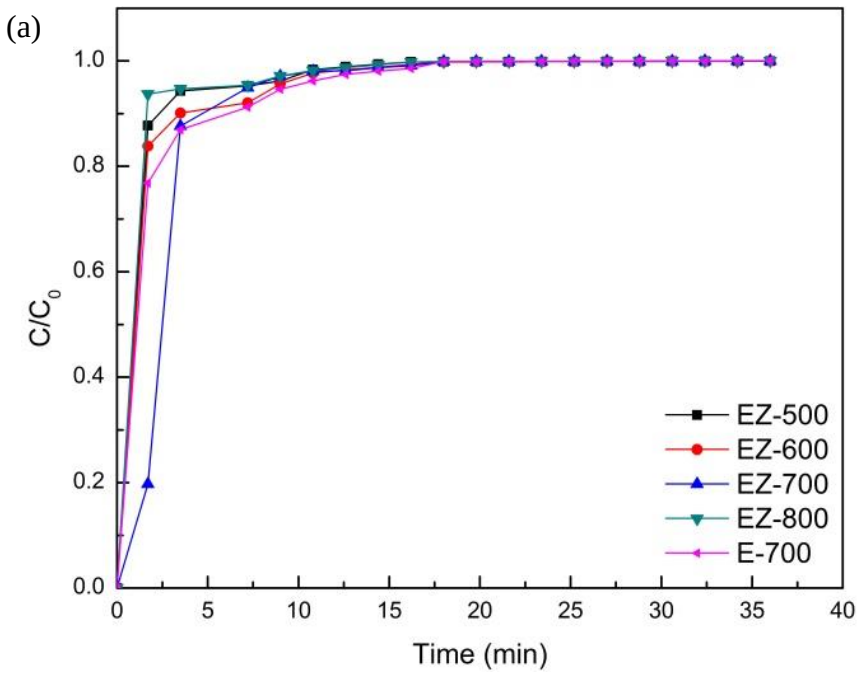

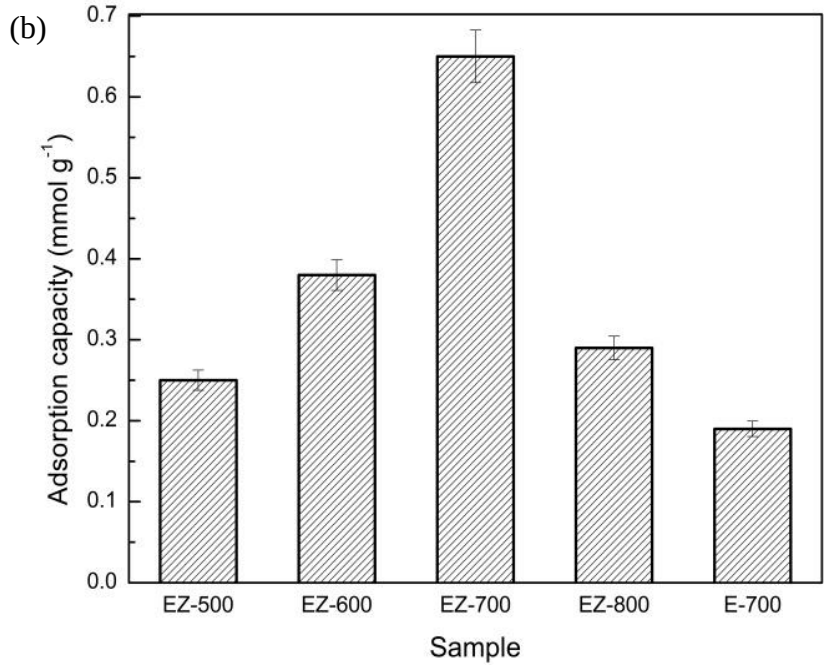

Fig. 5.8 (a) CO_2 breakthrough profiles (b) adsorption capacity of adsorbents at 12.5 % CO_2 and 30 °C

5.3.2 Adsorption capacity with adsorption temperature and CO_2 feed concentration

Fig. 5.9 and Table 5.4 show the effect of temperature and concentration on adsorption capacity of EZ-700. From Fig. 5.9(a), it is observed that at a fixed concentration and increase in adsorption temperature, t_b value decreases causing decrease in CO_2 uptake from 0.49 to 0.28 mmol g^{-1} signifying exothermic behavior. On the other hand, Fig. 5.9(b) for fixed temperature and increase in CO_2 concentrations (from 5 to 12.5%), adsorbent capacity increased but t_b value decreased. This is due to rise in mass transfer of CO_2 across the external boundary layer and within the adsorbent pores at higher concentrations.

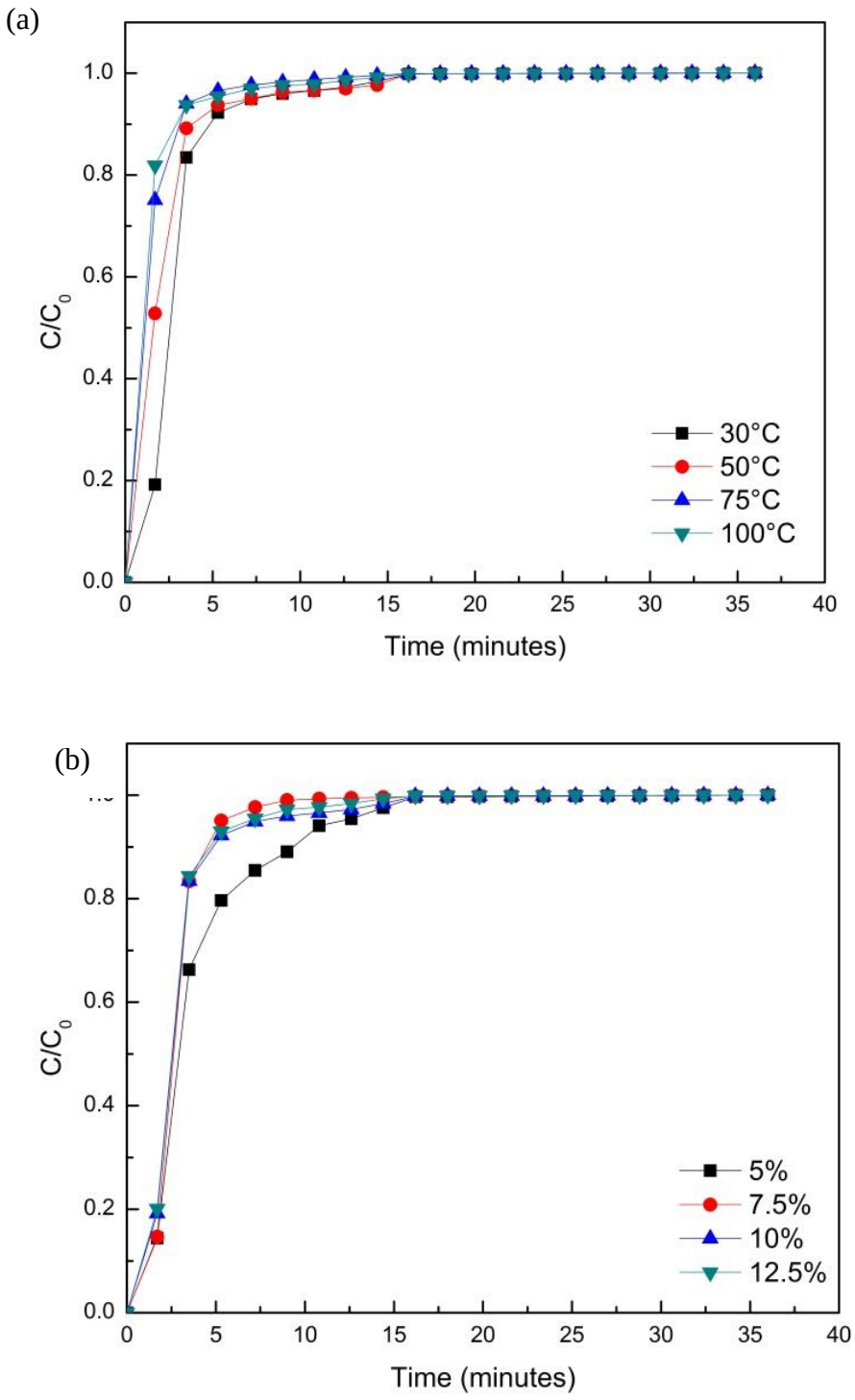

Fig. 5.9 (a) CO_2 breakthrough curves of 10% CO_2 at different temperatures (b) CO_2 adsorption capacity of adsorbents at different CO_2 feed concentrations and 30 °C

Table 5.4 CO_2 adsorption on EZ-700 at different temperatures and CO_2 concentrations

CO_2 concentration (%)	Temperature (°C)			
	30	50	75	100
5	0.30	0.21	0.19	0.16
7.5	0.39	0.30	0.27	0.22
10	0.49	0.41	0.33	0.28
12.5	0.65	0.49	0.39	0.32

Activated carbon prepared by Balsamo *et al.* [155] from furfural and coal tar pitch (by carbonization and steam activation) exhibited CO_2 uptake of 0.61 mmol g^{-1} at 15% CO_2 and 30 °C. CO_2 adsorption capacity reduced to 0.30 and 0.15 mmol g^{-1} at 50 °C and 75 °C, respectively. Our EZ-700 sample exhibited CO_2 uptake of 0.65, 0.49 and 0.39 mmol g^{-1} at 30 °C, 50 °C and 75 °C, respectively. Carbon adsorbents synthesized by Thote *et al.* [105] from soybean and $ZnCl_2$ activation exhibited CO_2 uptake of 0.93 mmol g^{-1} at 30 °C under 15.4% CO_2 flow, but the synthesized adsorbent was unable to regenerate in the next cycles showing zero adsorption capacity In this study, dynamic adsorption capacities of EZ-700 show higher values at same temperatures and lower CO_2 concentration (12.5%) with no deterioration in performance on its repeated use.

5.3.3 Selectivity and regenerability of adsorbents

5.3.3.1 CO_2 selectivity

Fig. 5.10 depicts breakthrough curves at 12.5% CO_2 concentration (rest N_2) of CO_2 and N_2 on EZ-700 at two different temperatures. Figure 5.10 shows lesser uptake of N_2 as compared to CO_2 as the N_2 is observed immediately in the outlet and CO_2 after 2 min. This was also confirmed by (C/C_0>1) for N_2 signifying it occupies more adsorption sites initially, but with time, these sites are swapped by CO_2 [132]. This indicates higher selectivity of adsorbent for CO_2.

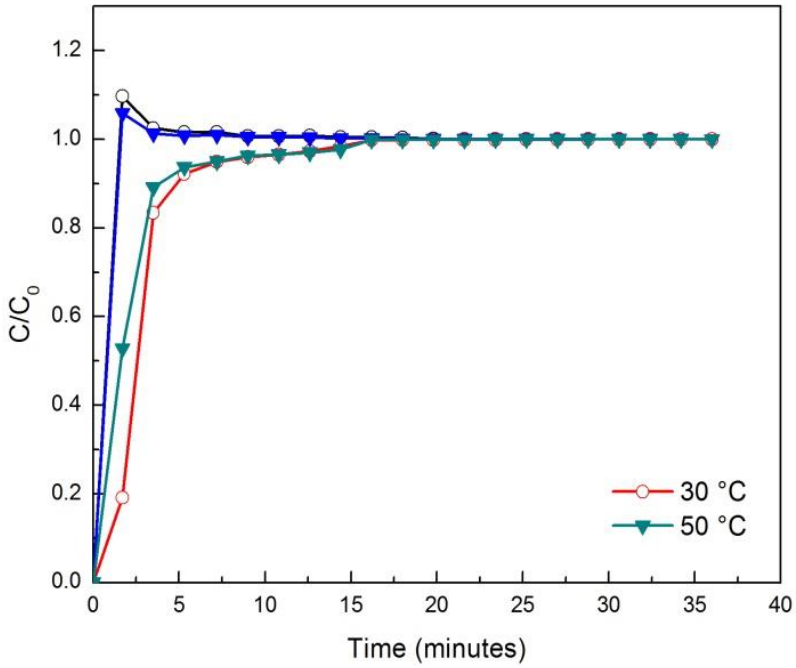

Fig. 5.10 Breakthrough curves of CO_2 (closed symbols) and N_2 (open symbols) at 12.5% CO_2 (rest N_2) on EZ-700 at 30 °C and 50 °C

5.3.3.2 Repeated adsorption-desorption on EZ-700

Multiple adsorption-desorption (at 200 °C) cycles under pure nitrogen at a flow rate of 50 ml min^{-1} was carried out to study the regenerability and stability of adsorbents. Fig. 5.11(a) shows adsorbent getting easily regenerated by raising the temperature which was confirmed from sudden decrease in C/C_0 value. Fig. 5.11 (b) shows that after performing four cycles, the adsorbent shows stable adsorption capacity. This indicates that the carbon adsorbent gets regenerated quickly without any loss in performance.

Fig. 5.12 shows TPD profile of EZ-700 adsorbent. A broad peak at 70-120 °C was observed with maximum at 90 °C and then the CO_2 signal got smaller with a tail extending beyond 200 °C. This suggests multiple type of adsorption sites with different binding strengths in this adsorbent. The peak at 90 °C may be due to the removal of physically adsorbed CO_2 molecules from the adsorbent surface and tail to higher temperatures shows smaller contribution of chemisorption behavior. Similar kind of observation was also seen by Goel *et al.* [144], Chen *et*

al. [145] and Mane *et al.* [146]. Overall, it can be concluded that the adsorbent shows predominantly physiosorption behavior.

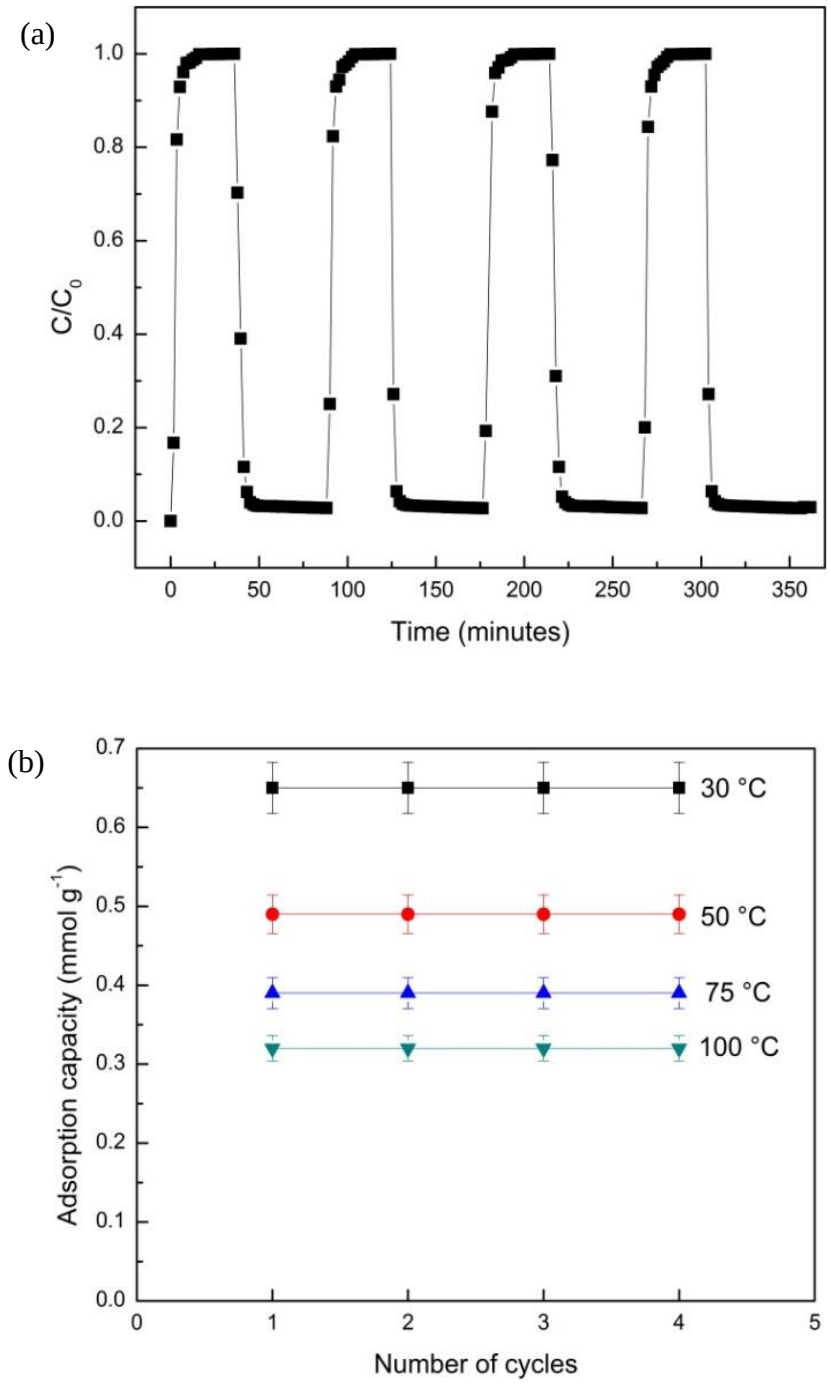

Fig. 5.11 (a) Repeated adsorption-desorption on EZ-700 at 30 °C (12.5% CO_2) (b) CO_2 adsorption-desorption cycles at different adsorption temperatures and 12.5% CO_2

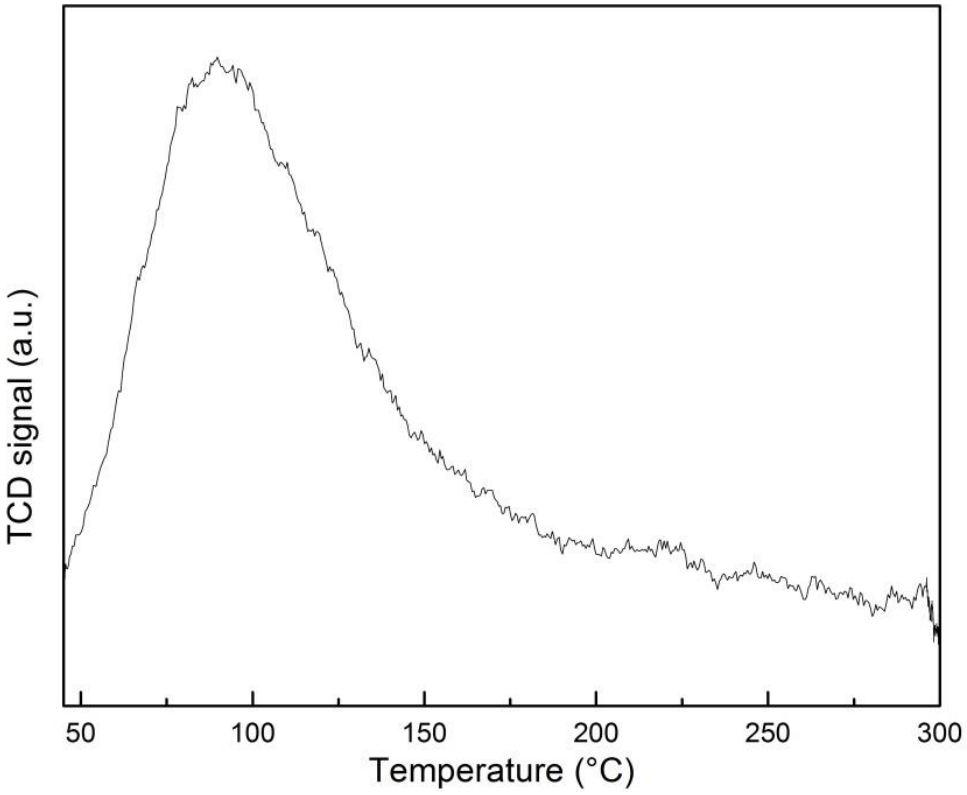

Fig. 5.12 Temperature programed desorption profile of CO_2 from EZ-700

5.4 Kinetic study

Fig. 5.13 shows experimental and model predicted adsorption capacities of the adsorbent as a function of time and at different temperatures with 12.5% CO_2. Table 5.5 shows the values of kinetic parameters, errors and correlation coefficients (R^2). It can be seen that most of the adsorption occurred within 4 minutes and then it slowed down until equilibrium. This could be due to decrease in unoccupied active sites and the increase in diffusion resistance. The pseudo first and second order models did not fit well in the initial and final parts with the experimental data. This was further confirmed by the higher values of error % and R^2. On the other hand, experimental data are well fitted with the fractional order model as confirmed by the high value of R^2 (0.99) and low value of error% (4.24%). Decrease in k_n (rate constant), with rise in adsorption temperature confirms the exothermic nature of adsorption [132]. With increase in temperature, n first decreased and then increased with maximum at 100 °C showing large driving force at this temperature.

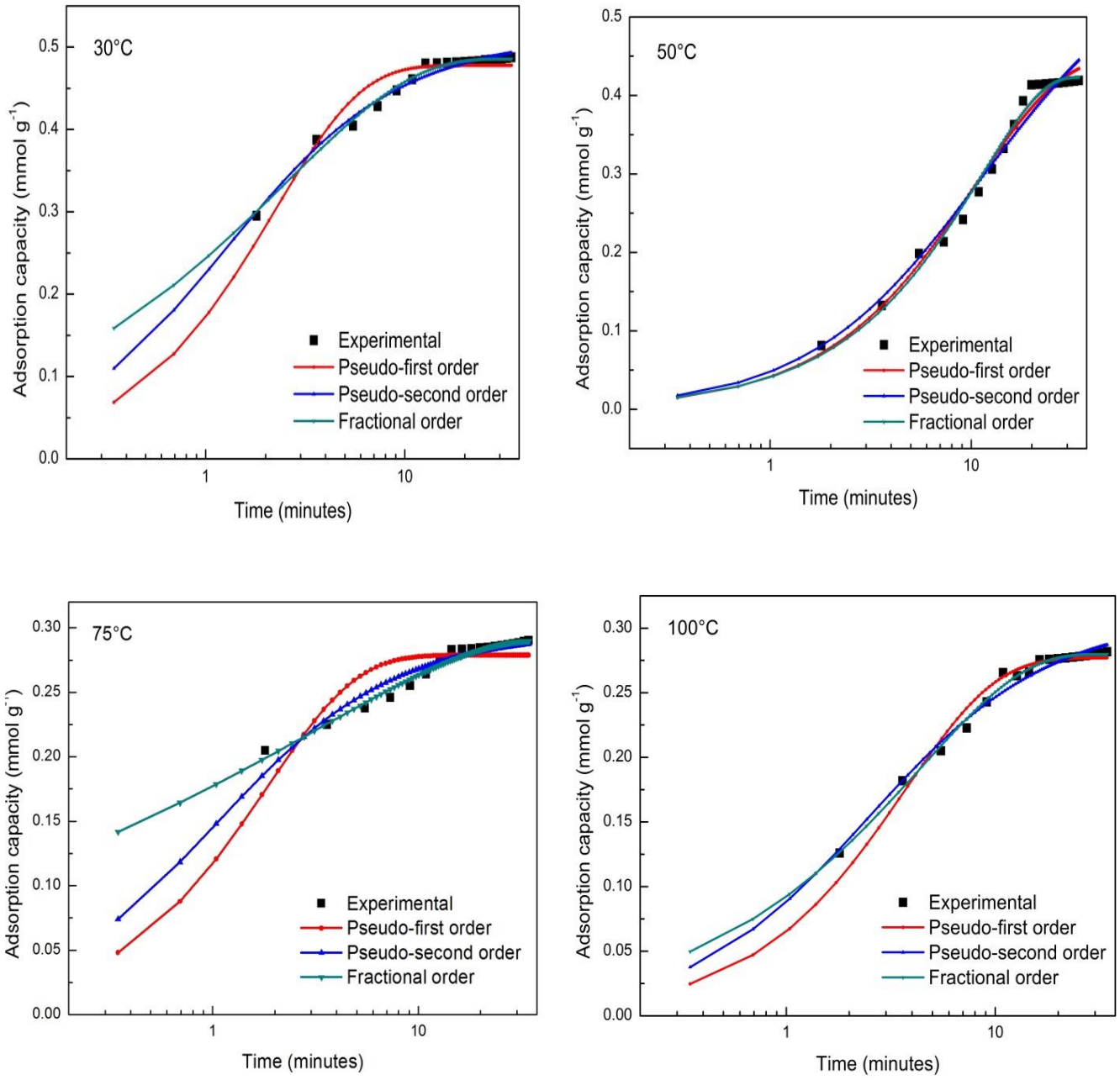

Fig. 5.13 Experimental and model predicted CO_2 uptake (EZ-700) at 12.5% CO_2 and different temperatures

Table 5.5 Kinetic parameters of CO_2 adsorption on prepared carbons at different temperatures and 10% CO_2

Kinetic model	Parameters	Temperature (°C)			
		30	50	75	100
Pseudo-first order	k_1 (min^{-1})	0.19	0.22	0.235	0.268
	q_e (mmol g^{-1})	0.477	0.45	0.321	0.27
	R^2	0.976	0.98	0.988	0.988
	Error %	22.67	5.05	4.93	4.35
Pseudo-second order	k_2 (g $mmol^{-1}$ min^{-1})	1.54	1.21	0.97	1.30
	q_e (mmol g^{-1})	0.51	0.59	0.32	0.30
	R^2	0.992	0.98	0.99	0.993
	Error %	22.40	5.31	2.70	2.19
Fractional order	k_n ($mmol^{1-m}$ g^{m-1} min^{-1})	0.256	0.20	0.18	0.15
	q_e (mmol g^{-1})	0.49	0.41	0.33	0.28
	n	0.72	0.65	0.71	0.77
	m	0.49	0.94	0.68	0.65
	R^2	0.993	0.99	0.996	0.997
	Error %	4.24	3.02	1.77	1.39

5.5 Isotherm study

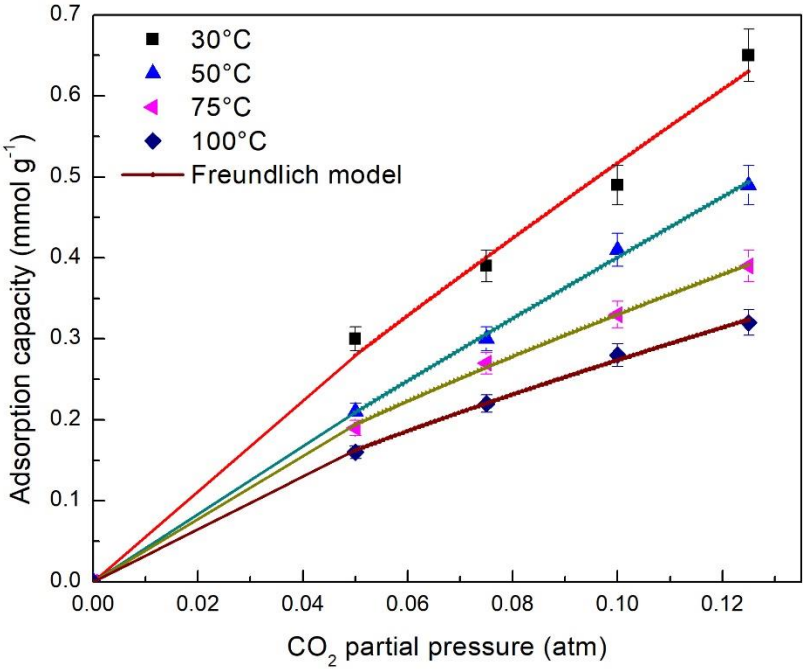

Fig. 5.14 Experimental and isotherm model predicted CO_2 uptake at different temperatures

The model predicted kinetic parameters were calculated and shown in Table 5.6. The Freundlich isotherm model is found to fit best with all the data as indicated by highest value of R^2 (0.998). This shows the heterogeneous nature of the adsorbent surface [156]. The experimental and model (Freundlich) predicted adsorption capacities at different temperatures are shown in Fig 5.14. The high value of n>1 shows the favorable adsorption process. Also, with an increase in temperature, decrease in Freundlich constant value (Table 5.6) indicates adsorption favoring at lower temperature (30 °C). Decrease in constant value with the increase in temperature also indicates physiosorption behavior.

Table 5.6 Adsorption isotherm data

Model	Parameters	Temperature (°C)			
		30	50	75	100
Langmuir	q_m (mmol g^{-1})	4.92	5.48	1.25	0.98
	K_L (atm $^{-1}$)	1.17	0.79	3.61	3.87
	R^2	0.96	0.99	0.992	0.993
Freundlich	K_F (mmol g^{-1} atm $^{-1/n}$)	3.99	3.46	1.92	1.55
	n	1.12	1.06	1.30	1.32
	R^2	0.963	0.998	0.996	0.997
Temkin	K_T (atm^{-1})	42.27	37.97	47.51	48.44
	b (kJ mol^{-1})	6.99	8.951	13.777	18.241
	R^2	0.89	0.97	0.99	0.99

5.6. Thermodynamic study

5.6.1 Thermodynamic parameters

Table 5.7 shows the thermodynamic constant values for CO_2 adsorption on EZ-700 at all adsorption temperatures. The negative value of ΔG^0 confirms spontaneity and feasibility of the adsorption process. The exothermic nature of the adsorption process is also confirmed by the negative value of ΔH^0 (-2.562 kJ mol^{-1}). It was reported in literature that ΔH^0 value <20 kJ mol^{-1} implies physiosorption process [137]. Therefore, lower value of ΔH^0 in the present study also implies physiosorption behavior.

Table 5.7 Thermodynamic parameters of CO_2 adsorption on EZ-700

Temperature (°C)	$\Delta G°$ (kJ mol^{-1})	$\Delta H°$ (kJ mol^{-1})	$\Delta S°$ (kJ mol^{-1} K^{-1})
30	-9.431	-2.562	0.033
50	-9.766		
75	-11.170		
100	-12.033		

Fig. 5.15 shows the isosteric heat of adsorption at different adsorbed amount of CO_2. This was calculated using Clausius-Clapeyron equation [136]. The value of Q_{st} lie in the range of 7.79 to 11.10 kJ mol^{-1} (average 9.09 kJ mol^{-1}) as compared to the heat of condensation of CO_2 (17 kJ mol^{-1}) signifying weak interaction between CO_2 molecules and adsorbent. This also signifies that lesser amount of energy is needed for regeneration. Also, the random change in the value of Q_{st} with increase in surface coverage indicates heterogeneity of the adsorbent surface [132].

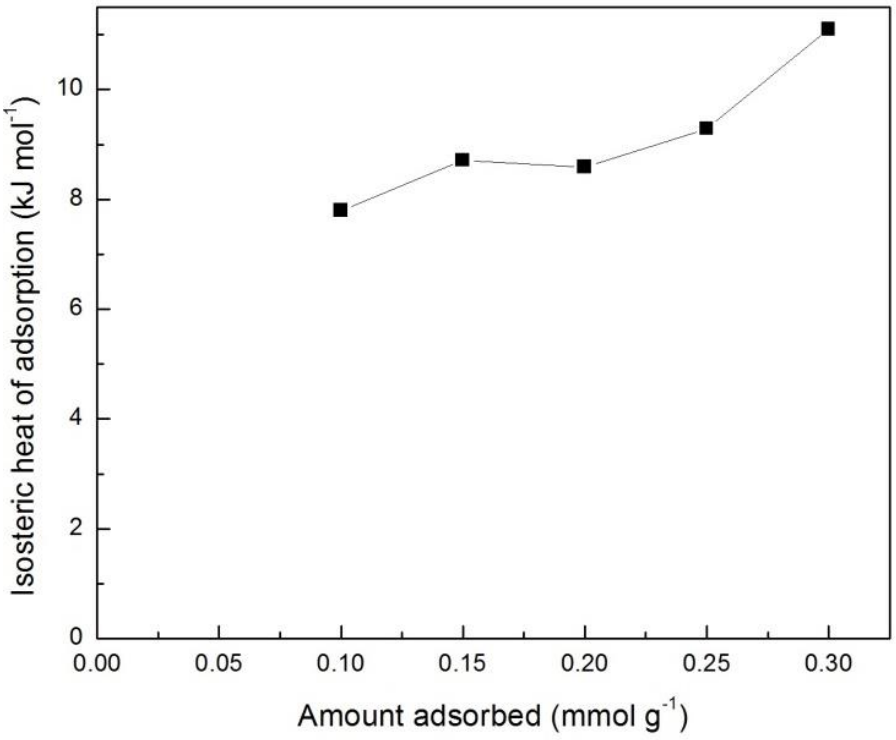

Fig. 5.15 Isosteric heat of CO_2 adsorption vs. adsorbed amount on EZ-700

5.6.2 Energy duty for desorption of CO_2

Specific heat capacity (C_p) of EZ-700 carbon, = 1.215 J g^{-1} K^{-1}

Adsorption conditions: 30 °C, 1 atm pressure, 12.5% CO_2 in N_2

Desorption conditions: 200 °C, purging with pure N_2

Temperature difference, $\Delta T = (200 - 30)\,℃ = 170\,℃$

CO_2 uptake of EZ700 $= 0.65$ mmol CO_2 per g adsorbent $= 0.0286$ kg CO_2 per kg adsorbent

$$\text{Therefore, sensible heat} = \frac{1.2 \times 170}{0.65 \times 10^{-3}} \text{ J per mole } CO_2 = 313.846 \text{ kJ per mole } CO_2$$

Net sensible heat required in this process = (25% of 313.846) kJ per mole CO_2 [149]), assuming 75 % heat recovery

Sensible heat = 78.46 kJ per mole CO_2

$$\text{Isosteric heat of adsorption, } Q_{st} = 9.09 \text{ kJ per mole } CO_2$$

Thermal energy input =(9.09 + 78.46) kJ per mole CO_2 = 87.55 kJ per mole CO_2

$$= 1.989 \text{ MJ per kg } CO_2$$

Therefore, for desorption of 0.65 mmol g^{-1} of CO_2 (0.0286 kg kg^{-1}), the energy required is 0.057 MJ.

Thus, CO_2 generated to produce 0.057 MJ of energy for desorption = 0.005038 kg CO_2)

5.7 Conclusions

Oxygen containing nanostructured carbons have been successfully developed from epoxy resin and zeolite as precursor and template using nanocasting technique. Carbonization-activation temperature influences the textural and surface properties. Presence of oxygen content is confirmed from elemental analysis and XPS. Nanocasting results in development of adsorbent with better textural and surface properties and highest CO_2 uptake of 0.65 mmol g^{-1} for EZ-700. Complete regenerability with stable adsorption capacity and physiosorption nature is exhibited by the synthesized adsorbent. Experimental values of CO_2 adsorption best fitted with fractional order kinetic model. Heterogenous nature of the adsorbent surface is confirmed from Freundlich isotherm and from random isosteric heat values at different adsorbed amounts. Thermodynamics suggest feasibility, spontaneity and the exothermic nature of the adsorption process.

Chapter 6 – Urea based Nitrogen Enriched Nanostructured Carbons for Carbon Dioxide Capture

6.1 Synthesis of adsorbent

6.1.1 Templated resin synthesis

Urea (224 g) was added to the solution of formaldehyde (600 ml, 37% w/v) followed by stirring for 30 minutes. Next, stirring was performed for 30 minutes, and pH was adjusted to 9 by adding 1 N NaOH. This was followed by heating to 80-85 ˚C for 2 h. Further, cooling was done to 55 ˚C followed by the addition of sulfuric acid to maintain the pH to 5-5.5. Further, the temperature was increased to 85-90 ˚C and maintained at this temperature for the next 1 h and then cooled. Next, template (57 g) and sulfuric acid were added to this solution and mixed until it became homogenous suspension. To ensure complete dryness, templated resin was kept in the oven for 3 h at 120 ºC. The total process block diagram is given in Fig. 6.1.

6.1.2 Carbonization of templated resin

Carbonization-activation of the templated resin was carried out in a tubular furnace under N_2 or CO_2 flow for 1 h each at 500-800 ºC at 10 ºC min^{-1} to generate a range of adsorbents. Gas flow of 60 ml min^{-1} was maintained throughout the experiment. After one hour, switching of gas from carbon dioxide to N_2 (60 ml min^{-1}) was performed. Here, CO_2 activation was done for gasification of carbon adsorbents and to improve their textural properties.

6.1.3 Template removal

The template was subsequently removed by dipping the sample in NaOH solution for 48 h followed by washing with copious amount of distilled water. After this, the sample was kept in the oven at 100 ºC for complete drying. The obtained samples were designated as UFZ-T, where T denotes the carbonization-activation temperature.

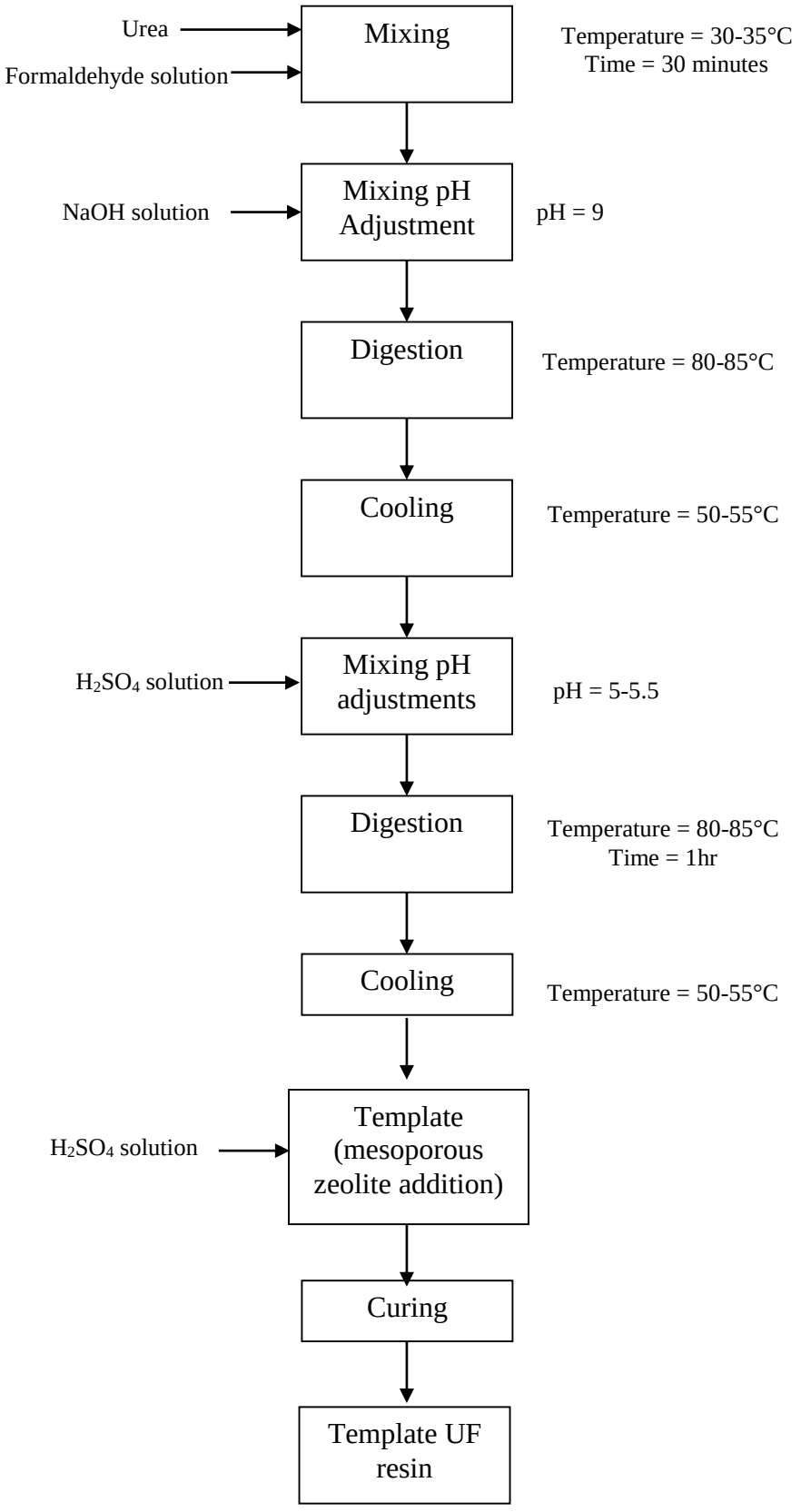

Fig. 6.1 Synthesis of templated UF resin – block diagram

6.1.4 Carbonization of urea-formaldehyde resin

For comparison, using direct carbonization of UF resin (without any template) at 700 ºC, a sample was prepared and labeled as UF-700.

6.2 Adsorbent characterization

6.2.1 Surface area and pore size distribution

N_2 adsorption-desorption isotherms and pore size distributions (from adsorption branch using BJH method) of prepared samples are displayed in Fig. 6.2(a & b). The samples exhibited Type IV isotherm with an H3 hysteresis loop. This shows the presence of mesopores which were generated due to dissolution of template. The hysteresis loop starts at 0.5-1 relative pressure range showing capillary condensation phenomena which is also a characteristics of mesoporous material [132]. It is seen that increase in temperature up to 700 ˚C, has increased mesopore volume and generated small amount of micropores while further increase up to 800 ˚C, causes decrease in mesopore volume and increase in micropore volume. This signifies collapse of mesopores at higher temperature due to extensive gasification of materials. Fig. 6.2(a) shows that nitrogen adsorption for sample UFZ-700 is highest whereas the sample UF-700, which is prepared at same carbonization temperature, shows almost negligible adsorption of nitrogen.

On the other hand, samples UFZ-500 and UFZ-600 show that this temperature level is not high enough for the development of porosity in the sample as confirmed from very low amount of nitrogen adsorption. This was further confirmed by textural parameter values from Table 6.1 which show S_{BET} = 18 m^2 g^{-1} for UFZ-500 and 53 m^2 g^{-1} for UFZ-600. However, further increase in carbonization and activation temperature shows increase in textural property with maximum at UFZ-800 (337 m^2 g^{-1}). The sample UFZ-700 shows mesoporosity with maximum 0.644 cm^3 g^{-1}. Also, the development of small amount of micropores is due to CO_2 activation. UF-700 shows negligible surface area and other parameter values. This shows effect of nanocasting technique in improving textural properties of adsorbent.

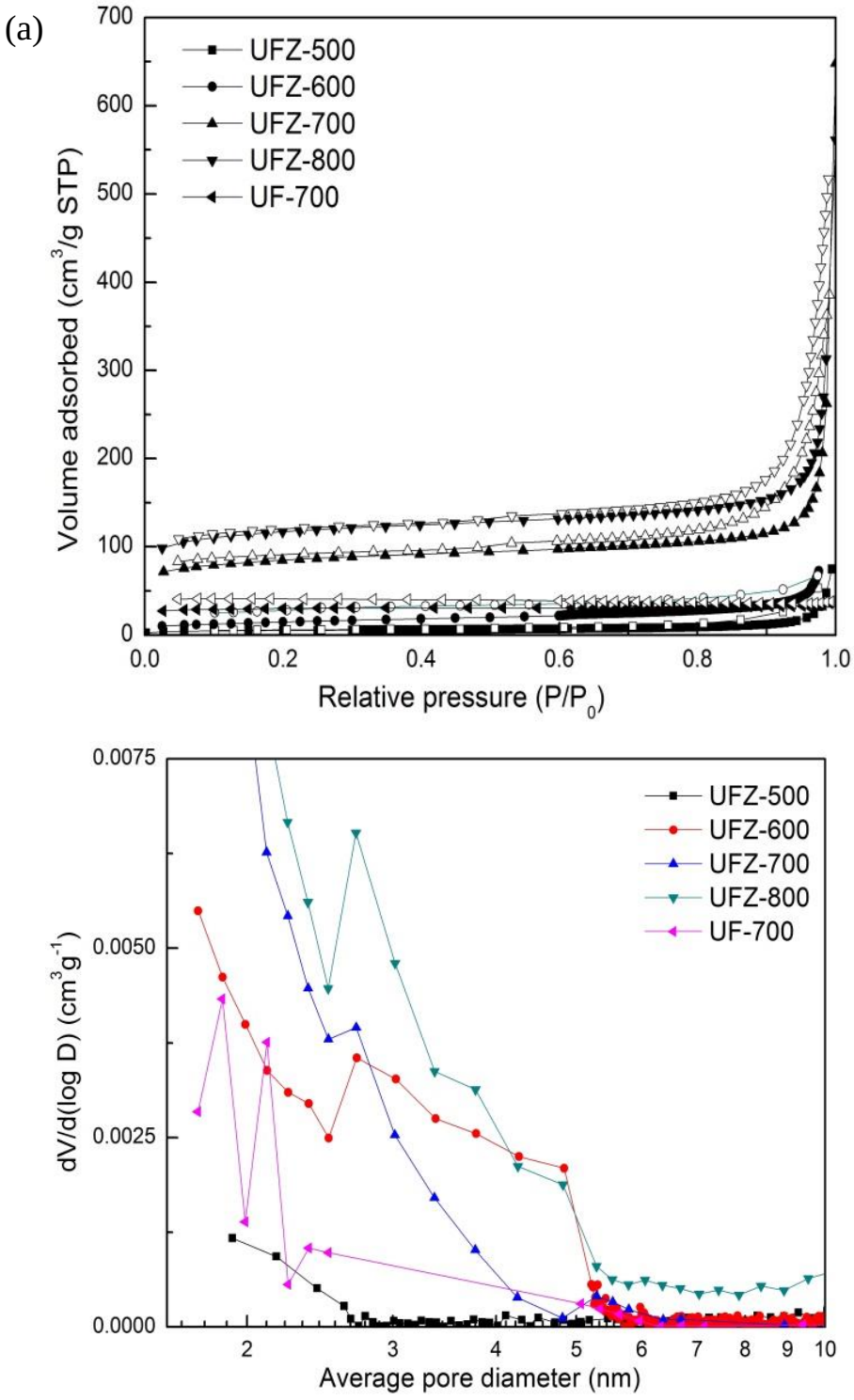

Fig. 6.2(a) N_2 adsorption-desorption isotherms at -196 ˚C for carbon adsorbents and (b) BJH pore size distribution of carbon adsorbent

Table 6.1 Structural parameters calculated from nitrogen sorption

Samples	S_{BET} (m^2 g^{-1})	V_P (cm^3 g^{-1})	V_{micro} (cm^3 g^{-1})	V_{meso} (cm^3 g^{-1})
UFZ-500	18	0.027	0.0027	0.0245
UFZ-600	53	0.103	0.000964	0.1021
UFZ-700	297	0.726	0.082	0.644
UFZ-800	337	0.72	0.123	0.596
UF-700	negligible	negligible	negligible	negligible

The pore size distributions (PSDs) derived from adsorption isotherm for samples using BJH method is shown in Fig. 6.2(b). Here, instead of desorption branch of the isotherm, adsorption branch was selected because (PSDs) derived from desorption isotherm provide entirely different results as compared to results obtained from adsorption branch. This is also because PSDs obtained from adsorption branch were not affected by TSE (tensile strength effect). The sample PSDs centered around 2 to 10 nm, signifying the presence of mesopores.

6.2.2 XRD analysis

Fig. 6.3(a) presents low angle XRD diffraction patterns of carbon adsorbents showing two peaks at $2\theta = 0.98^{\circ}$ and 1.99°, which correspond to (100) and (110) diffraction planes, respectively signifying 2*D* hexagonal mesostructure [137]. Wide angle XRD patterns (Fig. 6.3(b)) show two peaks. One broad peak at 26° corresponds to (002) diffraction plane of graphite carbon and other weak peaks at 44° corresponds to superposition of (100) and (110) reflection of graphite carbon [157]. Table 6.2 shows corresponding angle, and unit cell parameters values. Low crystallinity of the samples is seen. This is because interlayer spacing is greater for all the samples and lie in 0.365 to 0.384 nm range which is higher than that of ideal graphite (d_{002} = 0.335 nm)[158]. Decrease in (002) intensity, with rise of carbonization temperature upto 800 ˚C, indicates destruction of layer structure and textural properties. Also, peak broadening suggests development of nanostructured carbon materials and presence of amorphous carbon phase [159].

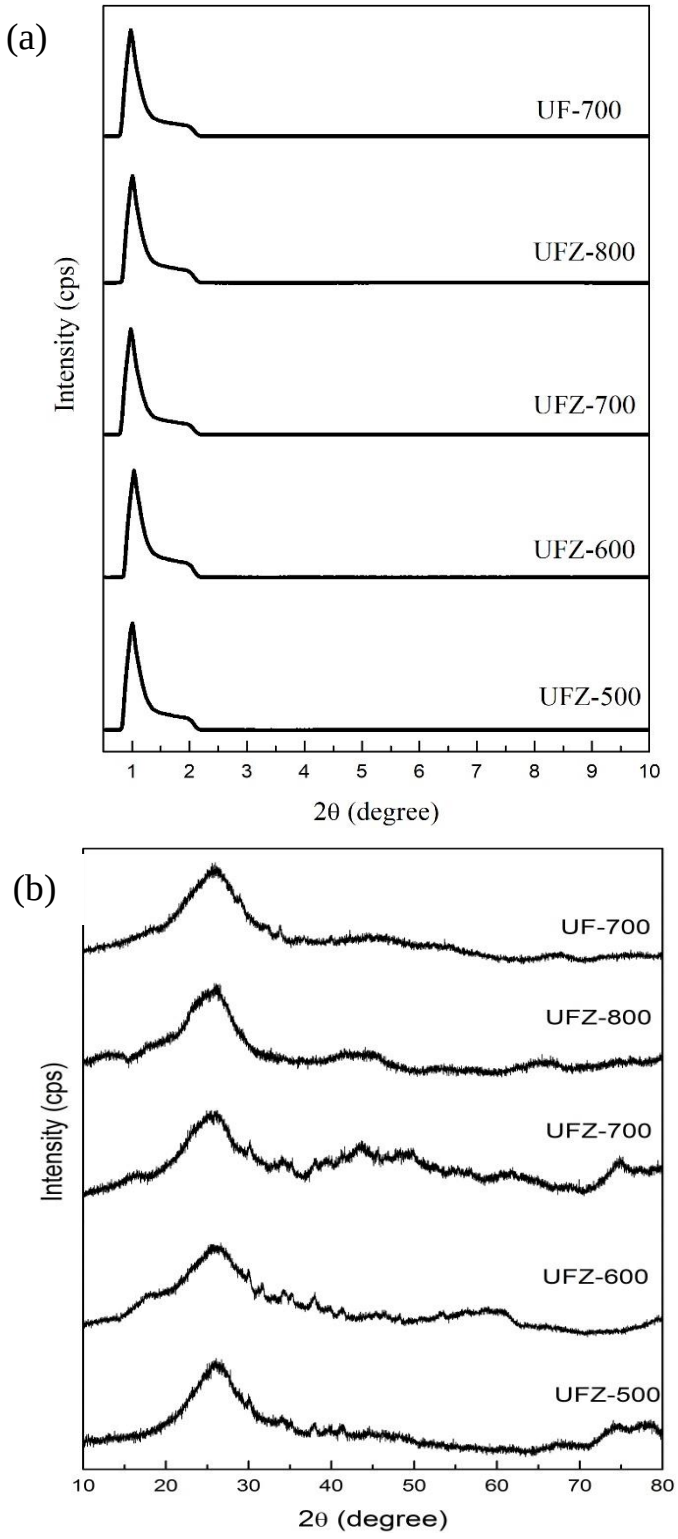

Fig. 6.3 XRD patterns of carbon samples (a) Low angle and (b) wide angle

Table 6.2 Structural parameters of carbon adsorbents

2θ	d_{002} (nm)	d_{101} (nm)	a_0 (nm)
24.3223 (UFZ-500)	0.365		0.516
25.731 (UFZ-600)	0.346		0.489
26.03 (UFZ-700), 44.99	0.342	0.201	0.483, 0.284
23.09 (UFZ-800), 45.56	0.384	0.198	0.543, 0.28
27.90 (UF-700)	0.139		0.196

6.2.3 TEM analysis

Fig. 3 presents TEM images of nanocasting sample showing development of nanostructured carbons with particle size of 10-20 nm. On the other hand, UF-700 shows very big particles. This shows the effect of template in development of nanostructured material.

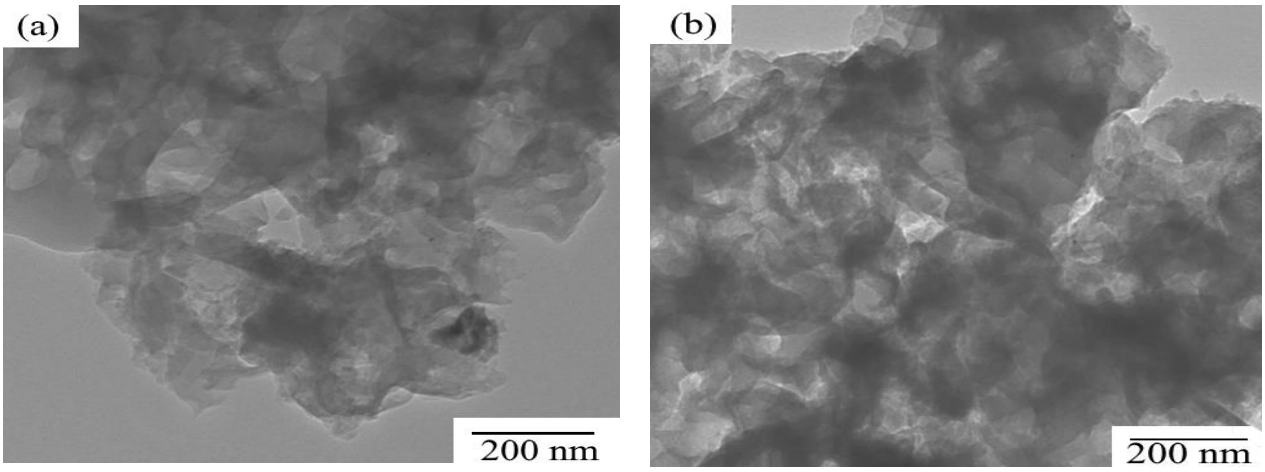

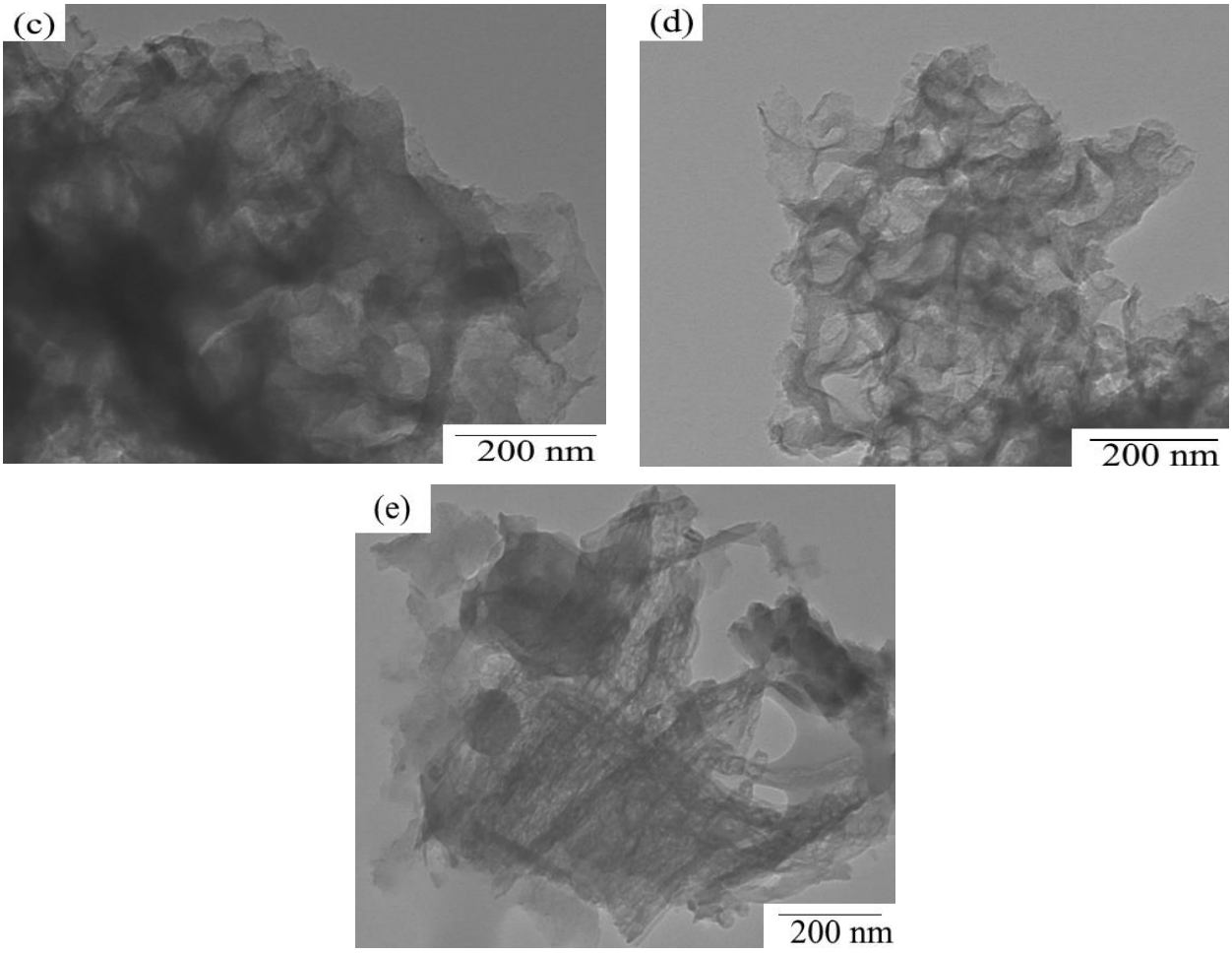

Fig. 6.4 TEM images (a) UFZ-500, (b) UFZ-600, (c) UFZ-700, (d) UFZ-800 and (e) UF-700

6.2.4 SEM analysis

Fig. 6.5 shows surface morphology of different samples. Sample prepared by nanocasting shows large pores between the particles. With increase in temperature from 500 to 700 °C, porosity get increased with maximum at 700 °C. UFZ-700 having irregular and heterogeneous type pores that can facilitate transport of CO_2 molecules towards the inner side of the adsorbent. Higher temperature of 800 °C results in sintering of material and decrease in porosity. On the other hand, UF-700 shows smooth surface with absence of pores. The results are in good agreement with N_2 adsorption/desorption. Similar kind of observations were also seen by Goel *et al*. [138] and Liu *et al*. [160].

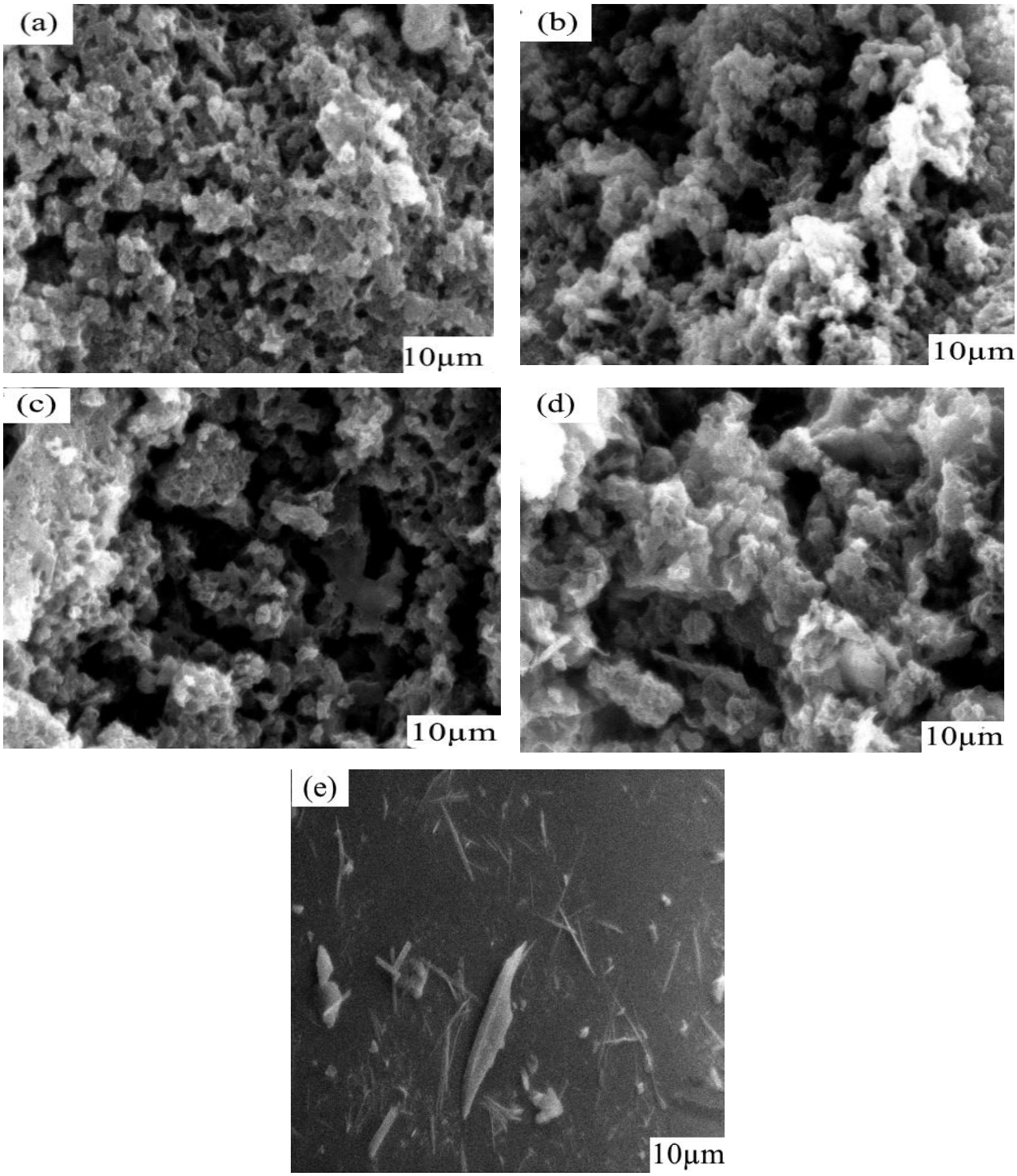

Fig. 6.5 SEM images (a) UFZ-500, (b) UFZ-600, (c) UFZ-700, (d) UFZ-800 and (e) UF-700

6.2.5 TG analysis

Fig. 6.6 shows TG curves of different adsorbents. TGA profile shows two main weight loss regions. First weight loss up to 100 °C due to moisture and other gases. The samples UFZ-500, UFZ-600, and UFZ-700 show weight loss of 3.78%, 5.39% and 5.32%, respectively. UFZ-800 (10.86%) show maximum weight loss, almost similar to UF-700 (10.88%). On the other hand, second region up to 400 °C, shows weight loss of UFZ-500 (51.43%), UFZ-600 (48.42%), UFZ-700 (36.26%), UFZ-800 (28.56%) and UF-700 (36.23%). Sample UF-700 shows similar behavior as that of UFZ-700.

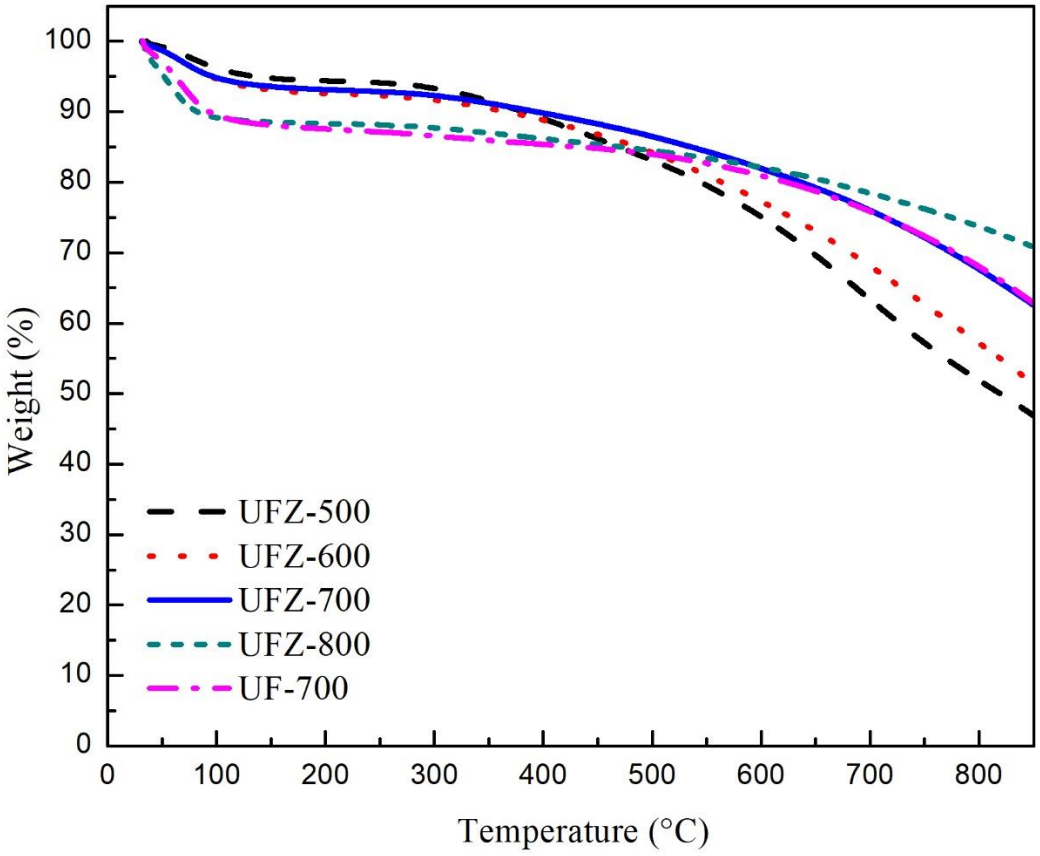

Fig. 6.6 Thermal stability test of adsorbents

6.2.6 Elemental analysis

Table 6.3 Elemental and Kjeldahl nitrogen analysis of carbon adsorbents.

Sample	Kjeldahl nitrogen (%)	Elemental analysis (wt. %)			
		C	N	H	O[a]
UFZ-500	24.5	58.56	25.58	2.66	13.2
UFZ-600	20.6	49.83	21.77	1.77	26.63
UFZ-700	15.7	48.60	17.18	1.73	32.49
UFZ-800	11.1	67.62	12.41	1.52	18.45
UF-700	17.3	59.30	18.03	1.61	21.06

[a]*Calculated by difference*

Elemental composition of the prepared adsorbents obtained from elemental analysis is shown in Table 6.3. It is observed that the increase in carbonization temperature (500-700 ˚C) causes a decrease in nitrogen content (from 25.58 to 17.18%) while oxygen content increases. This may be due to chemisorption of oxygen using heterogeneous reaction between the carbon surface and CO_2. However, there is decrease in content of carbon upto 700 ˚C due to activation with CO_2. The removal of nitrogen at higher temperature occurs due to oxidation. Similar kind of observation was seen by Goel *et al.* [137]. Kjeldahl nitrogen also shows similar pattern. On increase in temperature to 800 ˚C, carbon content increases due to breaking of C–O and C–H bonds. UFZ-500 shows approximately 25.58% nitrogen while UFZ-700 shows approximately 17.18% which shows nitrogen presence at higher temperature also. The sample UF-700 shows relatively lower contents of oxygen and nitrogen. This confirms that the template affects the composition of materials. Similar kind of observations was also observed by Tiwari *et al*.

6.2.7 FTIR analysis

Fig. 6.7 shows FTIR spectra of synthesized carbon adsorbents. Peak between 1236.66 cm^{-1} and 1249 cm^{-1} correspond to C-O stretching in alcohol, ester or ether groups and aromatic C-N stretching vibrations, respectively [161]. Peak at 1760 cm^{-1} ascribed to C=O stretching [139], small peak at 3000 cm^{-1} is due to stretching vibration of C-H bond of -CH_2-NH-CH_2- [97, 162]

and peak at 1625 cm^{-1} is assigned to amide group [163]. Absence of peak at 1760 cm^{-1} for UFZ-700 shows strong basic character as compared to others. Band at 3400 cm^{-1} and 2300 cm^{-1} is assigned to symmetric stretching vibration of N-H and CN bond in sample. Above observations confirmed presence of nitrogen functional groups, which provide Lewis base sites for adsorption of acidic CO_2.

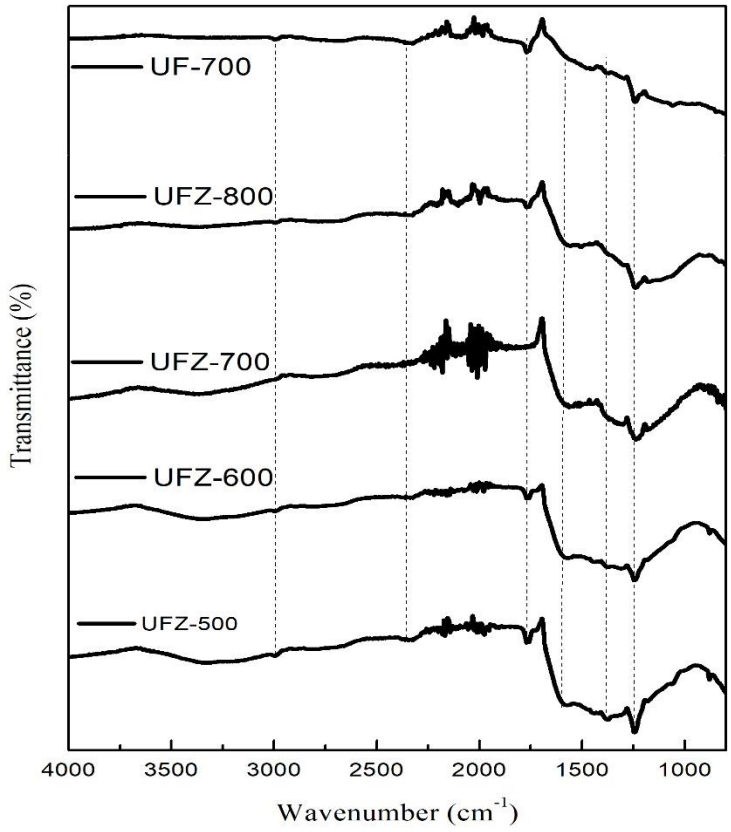

Fig. 6.7 FTIR spectrum of nitrogen enriched carbons

6.2.8 X-ray photoelectron spectroscopy

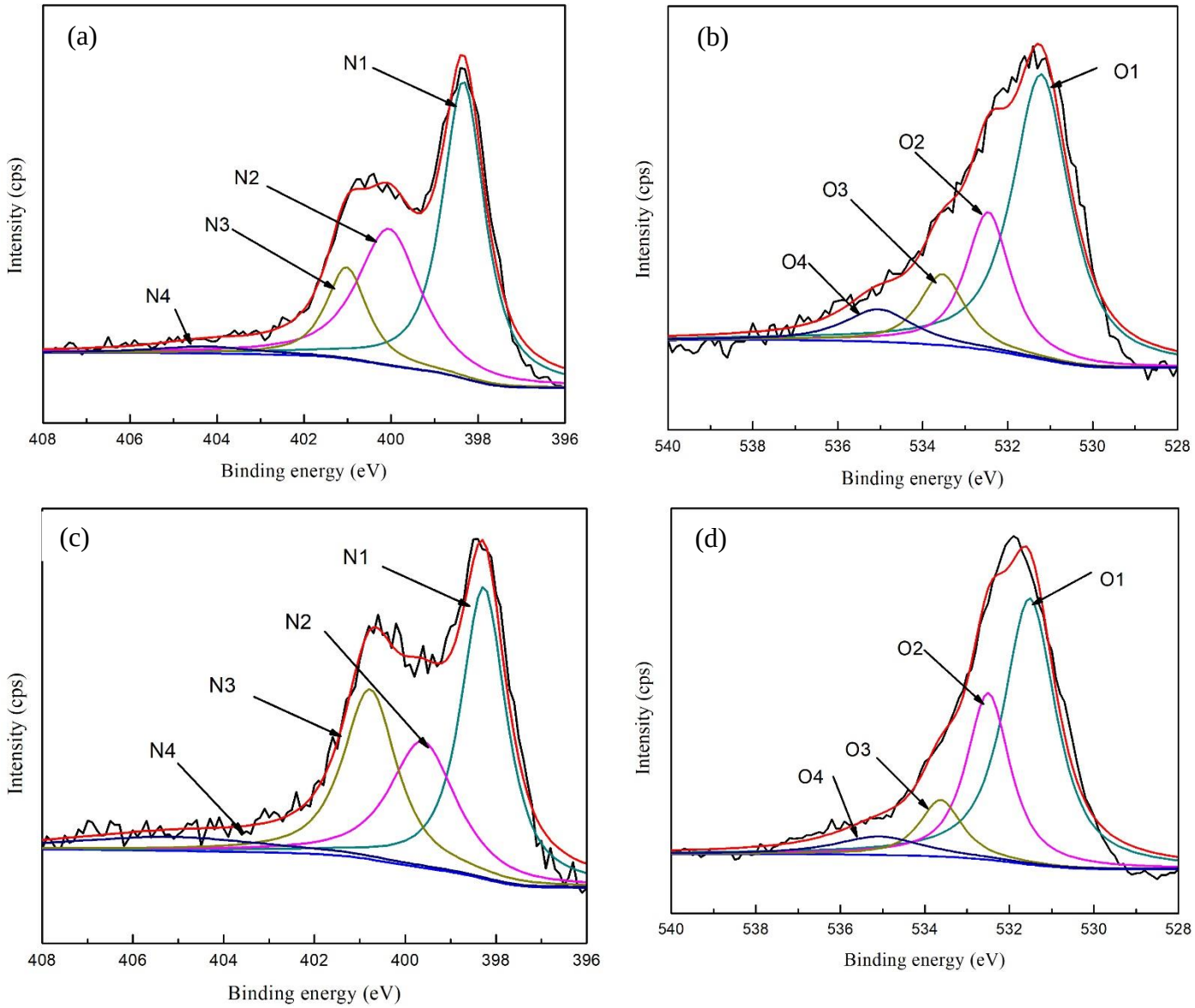

Fig. 6.8 XPS N1s spectra of (a) UFZ-700 and (b) UF-700; XPS O1s spectra of (c) UFZ-700 and (d) UF-700

Fig. 6.8 shows XPS spectra of UFZ-700 and UF-700. Fitting of N1s spectra [Fig. 6.8(a & b)] can be deconvoluted into four peaks. Table 6.4 shows the corresponding binding energy (B.E), relative area contribution (A %) and full width half maximum (FWHM) of the samples. Here, pyridinic-type nitrogen (N1) is assigned at 398.3 eV, pyrrolic and/ or pyridone-type nitrogen (N2) at 400.4 eV, quaternary nitrogen (N3) at 401.2 eV and last pyridine nitrogen oxide (N4) at 405.15 eV [164-167]. It can be seen from Table 6.4 that N1 and N2, reported to be responsible for basic nature, are having a higher area% for UFZ-700, while N3 and N4 are responsible for acidic nature [168] are higher for UF-700. Thus, UFZ-700 is more basic as compared to UF-700.

The O1s spectra of UFZ-700 and UF-700 shown in [Fig. 6.8(c & d)] can be deconvoluted into four peaks. The peaks O1(carbonyl, ketone or lactone groups) is assigned at 531.2 eV, O2(ether, alcohol) at 532.4 eV, O3(carboxyl group) at 533.5 eV and O4(oxygen in water) at 534.04 eV [132, 151]. It is observed that O1 & O2 are maximum in UFZ-700 and O3 & O4 are maximum in UF-700. It has been reported that O1 and O2 are responsible for basicity and O3 are responsible for acidity. Therefore, UFZ-700 is more basic in nature than UF-700.

Table 6.4 XPS data of UFZ-700 and UF-700 adsorbents

Atom	**Binding energy (eV)**		**Assignment(FWHM)**		**Area %**	
	UFZ-700	**UF-700**	**UFZ-700**	**UF-700**	**UFZ-700**	**UF-700**
N1	398.335	398.27	1.156	1.182	49.03	39.37
N2	400.48	399.617	1.722	1.736	33.58	25.08
N3	401.2	400.778	1.116	1.396	14.62	27.11
N4	404.263	405.151	2.752	5.290	2.74	8.42
O1	531.210	531.518	1.611	1.462	55.23	31.13
O2	532.460	532.500	1.246	1.215	28.77	21.96
O3	533.540	533.624	1.262	1.185	9.53	11.42
O4	535.040	535.080	1.930	2.468	6.45	8.01

6.2.9 Raman spectroscopy

Fig. 6.9 shows Raman spectra of carbon adsorbents before and after CO_2 adsorption. The spectra show two major peaks of D and G bands appearing in the range of 1300-1430 cm^{-1} and 1530-1582 cm^{-1}. These peaks are called Raman peaks for carbon materials [169]. The appearance of G-bands are due to in-plane bond-stretching motion of pair of sp^2 atom while on the other side D-band which seems to be more intense due to breathing mode of six-fold rings appears due to breakage of graphite layer into smaller units. The D-band intensity also indicates degree of disordered carbon. Its intensity is directly proportional to six fold aromatic ring. It also corresponds to sp^3 carbon atoms. Here, the Raman spectra also exhibit a band at 2685 cm^{-1} called as a G' band which is attributed to overtone of D band and typically this peak is for most graphitized material. As the peak is not much intense, it indicates multilayer graphene. Similar kind of observations were seen by Ferrari *et al.* [170].

On the other hand, the intensity ratio of D and G band i.e., I_D/I_G shows the structure of carbon and amount of disorganized carbon which have effect on both adsorption capacity and pore structure. It also represents degree of graphitic carbon materials and number of defect sites in carbon [171]. Haghseresht *et al.* [172] showed relationship between micropore volume, mesopore volumes, total BET surface area and other parameters. They showed that as the I_D/I_G ratio increases, adsorption capacity increases. They have also shown that if the quantity of disorganized carbon is higher, higher will be the amount of aromatic compounds in comparison with aliphatic carbon. As the disorganized carbon is higher, there is lesser space between the aromatic compounds.

Here, the I_D/I_G ratio of carbon adsorbents for UFZ-700 is 1.023 and for UF-700 is 1.004. As the intensity ratio of UFZ-700 is higher, it possesses most defective nature and reduced degree of graphitization. This shows higher porous nature and disordered structure of the UFZ-700 sample which is consistent with N_2 adsorption-desorption results. It is also seen that the intensity ratio of UF-700 is somewhat similar but the adsorption capacity is lower. This is due to the acidic nature of UF-700 as confirmed from XPS results.

From Fig. 6.9, the peak intensity reduction and shifting is seen. This shows the adsorption of CO_2 molecules in the adsorbent pores. Shifting of peak position towards lower frequencies is

due to the intermolecular interaction between CO_2 molecules and adsorbent, which alters the intermolecular potential of gas molecules due to displacement of vibrational modes [173]. This also indicates weaker interaction between CO_2 and adsorbent. On the other hand, decrease in the intensity of D-peak is due to the decrease in the amount of six-membered ring, which causes loss of aromaticity and disorderness. Here, the broader peak for UFZ-700 as compared to UF-700 also indicates large number of adsorption sites participating in gas binding. Similar kind of observation was also reported by Lazaro *et al.* [174] and Hansen *et al*. [175].

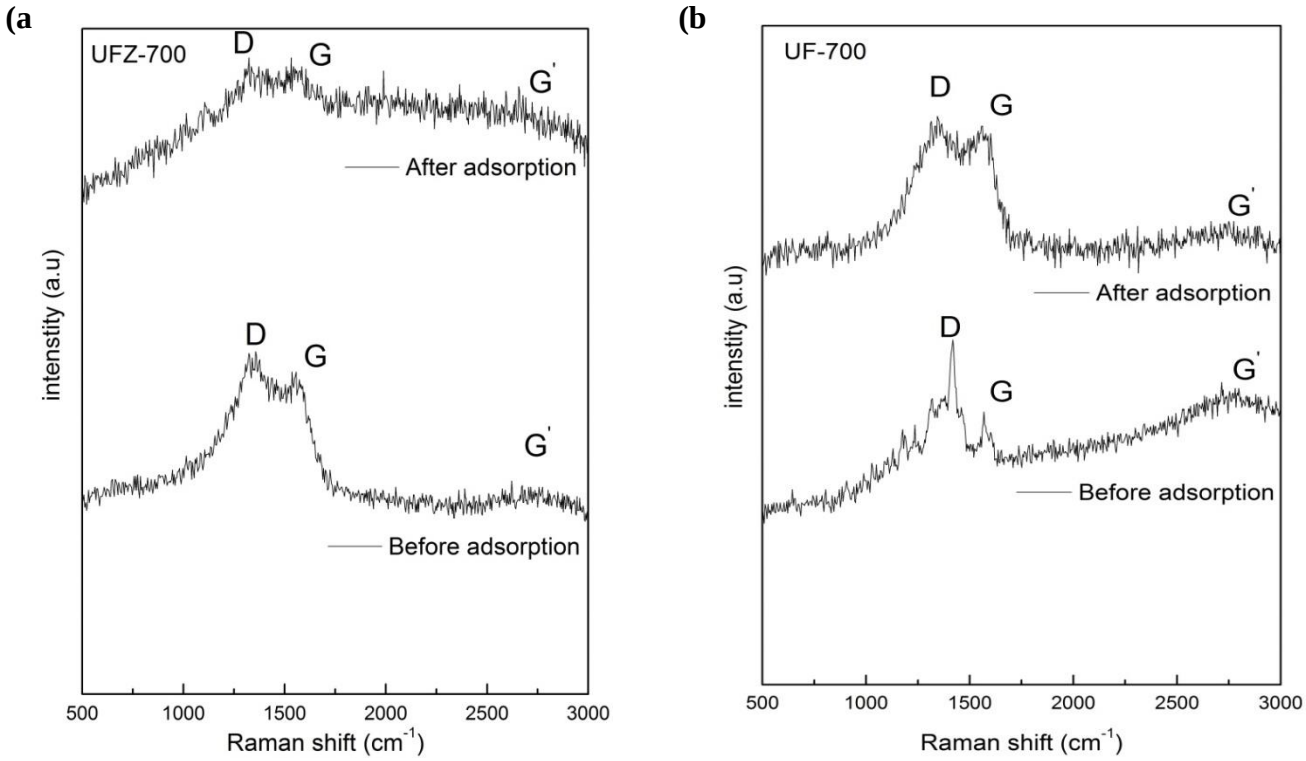

Fig. 6.9 Raman spectra of carbon adsorbents before and after CO_2 adsorption (a) UFZ-700 and (b) UF-700

6.3 CO_2 capture performance

6.3.1 Effect of carbonization temperature

Fig. 6.10 shows breakthrough curves and the equilibrium uptake capacities of the adsorbents at 30 °C under 12.5% CO_2 flow. As seen, no CO_2 was detected in the initial part (1 min) signifying that

the bed is not saturated but after 1 min, mass transfer reaches bed outlet and CO_2 appears in outlet for UFZ-600, UFZ-700, and UFZ-800. It is seen that UFZ-700 shows broadest breakthrough curve and highest adsorption capacity (0.84 mmol g^{-1}) due to the presence of N1, N2, O1, O2, and better textural properties as confirmed from XPS, SEM, TEM, N_2 sorption and Raman. The other samples (UFZ-500 and UF-700) show steepest curves. It is also observed that sample UFZ-800 is having better textural properties than UFZ-700 but shows lower uptake capacity. This was due to collapse in pore structure during gasification causing sintering at high temperature and also due to decrease in nitrogen content. UFZ-500 shows lowest uptake capacity as compared to others due to lowest surface area. On the other hand, UF-700 shows higher surface area as compared to UFZ-500 and UFZ-600 but shows lower capacity than UFZ-600 due to acidic and non-porous nature as confirmed from XPS, SEM and nitrogen adsorption. This shows that textural properties alone do not play an important role, nitrogen and oxygen functionalities also play an important role. The adsorption capacity and breakpoint time (t_b) follow order of UFZ700>UFZ-800>UF-700>UFZ-600>UFZ-500. Further studies were conducted with UFZ-700 for various parameters like CO_2 concentration and adsorption temperature.

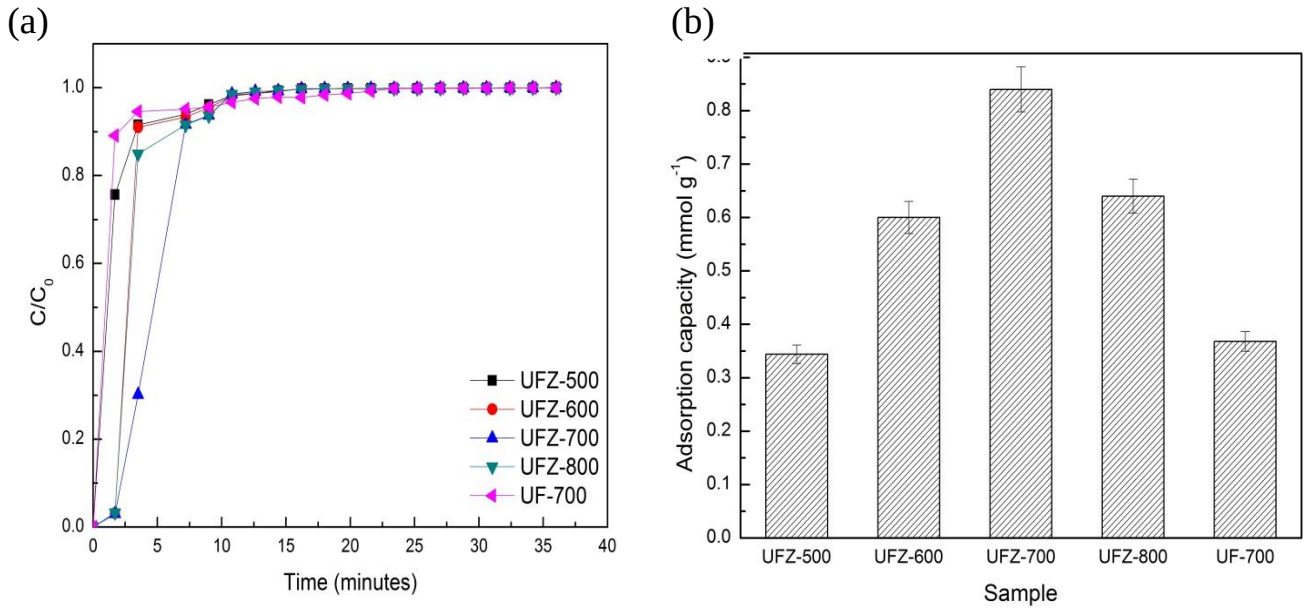

Fig. 6.10 (a) Breakthrough curves, and (b) equilibrium adsorption capacity of adsorbents at 30 °C and 12.5% CO_2

6.3.2 Effect of adsorption temperature and CO_2 feed concentration

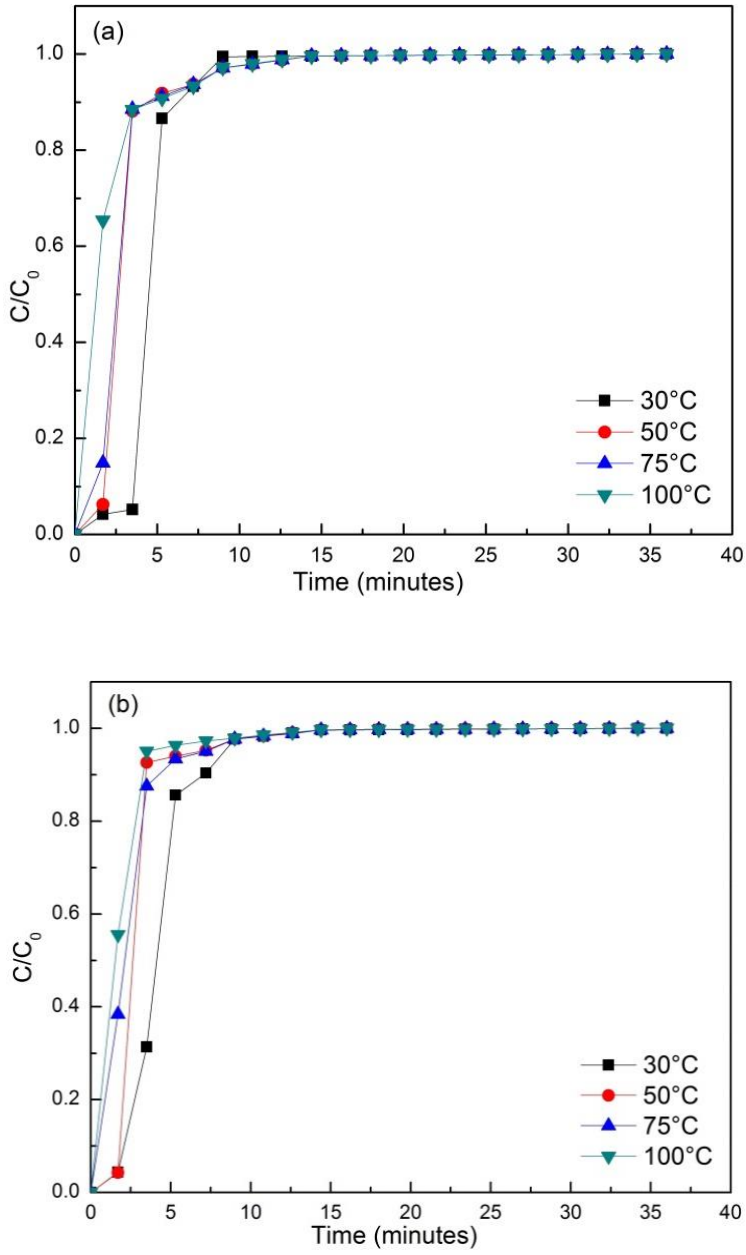

Fig. 6.11 Breakpoint time for (a) 7.5% and (b) 10% CO_2 at different temperatures for UFZ-700

Fig. 6.11 shows experimental breakthrough curves of UFZ-700 at fixed CO_2 concentration and different temperatures (30 °C, 50 °C, 75 °C and 100 °C). It can be seen that the adsorbent is saturated faster at higher temperature signifying faster rates at higher temperature. This was further

confirmed by shorter breakpoint times at higher adsorption temperature and longer breakpoint time at lower temperature. Decrease in CO_2 uptake at 10 % and at 30, 50, 75, 100 °C is 0.698, 0.481, 0.401, and 0.314 mmol g^{-1}, respectively signifying exothermic nature. Huang *et al*. [176] has also shown that increase in adsorption temperature accelerates internal energy of the adsorbent which causes release of CO_2 molecules from the surface.

Fig. 6.12 shows the effect of CO_2 feed concentration on the adsorption capacity of UFZ-700. At fixed temperature and 5% and 10% CO_2 concentrations, bed gets saturated faster at higher concentration. On increase in CO_2 concentration from 5% to 10%, breakpoint shifted from 3.46 to 1.73 minutes. Similar observations were seen by Goel *et al.* [151].

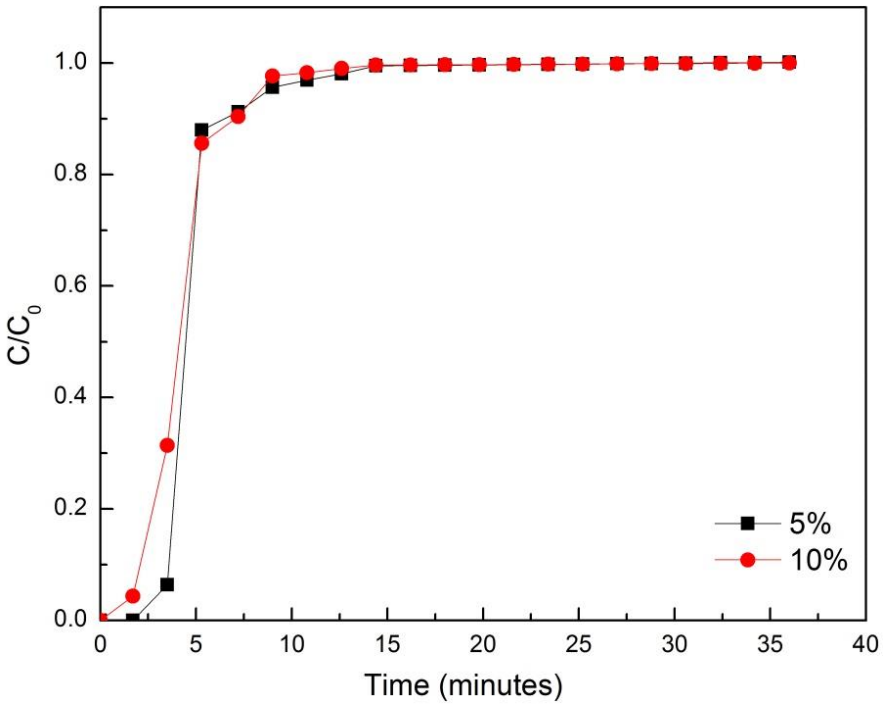

Fig. 6.12 Breakpoint time for (a) 5% and (b) 10%, CO_2 at 30 °C

Fig. 6.13 shows CO_2 uptake capacity of UFZ-700 at different temperatures and CO_2 concentrations. With increase of adsorption temperature, CO_2 uptake capacity decreases and with rise of concentration, CO_2 uptake increases. At 12.5% CO_2 concentration, CO_2 uptake reduced from 0.84 mmol g^{-1} to 0.373 mmol g^{-1} on increase in temperature from 30 to 100 °C while for 5% CO_2 concentration, CO_2 uptake reduced from 0.396 mmol g^{-1} at 30 °C to 0.197 mmol g^{-1} at 100 °C.

Table 6.5 Comparison of CO_2 adsorption capacity between reported literatures and present work of UFZ-700 at 30, 50, 75, 100 °C and at different CO_2 concentrations.

Sample	Experimental condition		CO_2 uptake	References
	CO_2 (vol.%)	Temperatures (°C)	(mmol g^{-1})	
UFZ-700	12.5(Dynamic)	30	0.84	Present work
UFZ-700	12.5(Dynamic)	50	0.591	Present work
UFZ-700	12.5(Dynamic)	75	0.464	Present work
UFZ-700	12.5(Dynamic)	100	0.373	Present work
AC	15%(Dynamic)	30, 50 and 80	0.61, 0.30, 0.15	[155]
AC	17%	55	0.25-0.8	[177]
FA2[a)]	100% (Dynamic)	30, 75	0.39, 0.23	[178]
RAC, R-MCM-41	100%	75	0.45	[179]
Carbon adsorbents	15.4 (Dynamic)	30, 75	0.93, 0.51	[105]
Carbon adsorbents	100 (Dynamic)	30	0.86	[110]
Carbon adsorbents	15 (Dynamic)	100	0.16	[142]
Carbon adsorbents	100 (Dynamic)	30, 100	1.09, 0.27	[143]
Carbon adsorbents	100 (Dynamic)	30	0.60	[143]

a) Steam activation of fly ashes

The adsorption capacities obtained in this research work at different temperatures and concentrations are also compared with the earlier reported values as shown in Table 6.5. Adsorbents prepared by Drage *et al*. [110] from melamine-formaldehyde resin by K_2CO_3 activation showed CO_2 uptake of 0.88 mmol g^{-1} at 30 °C which is comparable to the adsorption

capacity obtained in this study at 30 °C. However, at higher temperature adsorbents showed higher capacity under lower CO_2 concentration (12.5%). In other study, adsorbents prepared by Thote *et al*. [105] showed higher adsorption capacity at 15% CO_2 but the adsorbent was not able to regenerate completely in the second cycle. Therefore, it can be concluded that adsorbent synthesized by nanocasting technique in this study shows a higher capacity at high temperature (100 °C) at lower CO_2 concentration (12.5%) with quick regenerability and stability. This is not possible by the adsorbents synthesized by Balsamo *et al*. [155], Drage *et al*. [110], Martin *et al*. [142] and Arellinas *et al*. [143].

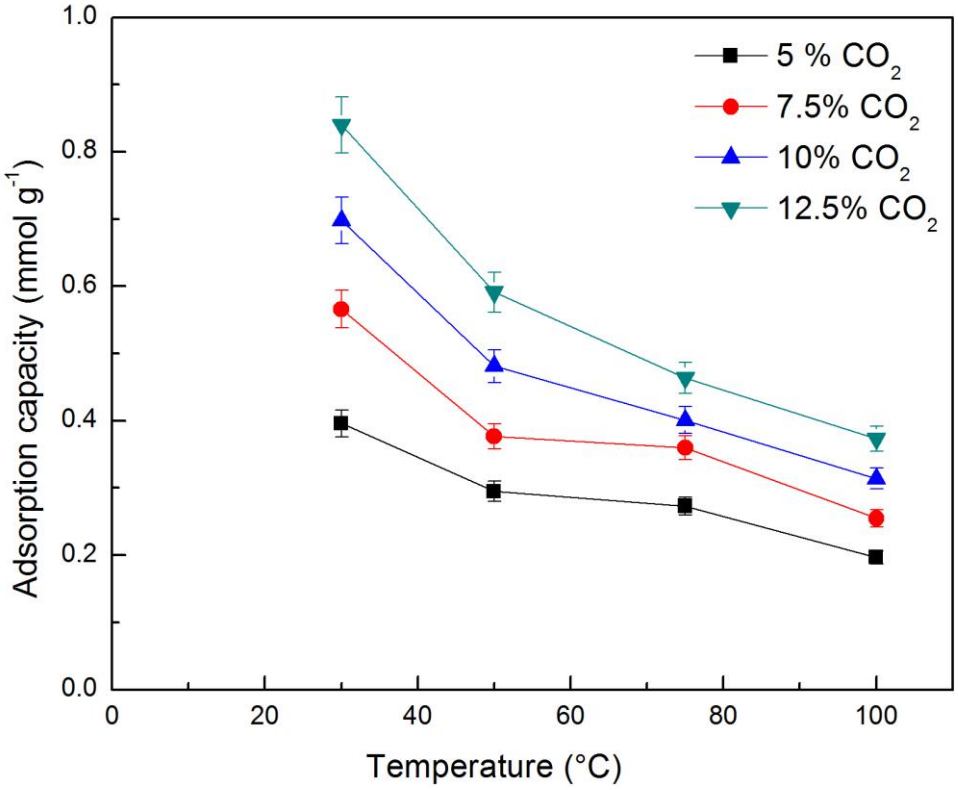

Fig. 6.13 CO_2 adsorption capacity of UFZ-700 at different temperatures under CO_2 concentrations

6.3.3 CO_2 selectivity

Fig. 6.14 shows the breakthrough curves at 12.5% CO_2 concentrations (rest N_2) of UFZ-700 for CO_2/N_2 selectivity. It can be seen that the N_2 adsorption capacity is very small as it detected instantly at the outlet of the column but CO_2 has taken around 3 min which shows higher affinity of adsorbent towards CO_2. As (C/C_0) is higher for N_2 as it occupies more sites in starting as it has higher concentration in feed gas, but as time progresses, N_2 sites are replaced by CO_2 showing higher selectivity towards CO_2 [132]. Similar observations were reported by Goel *et al*. [138].

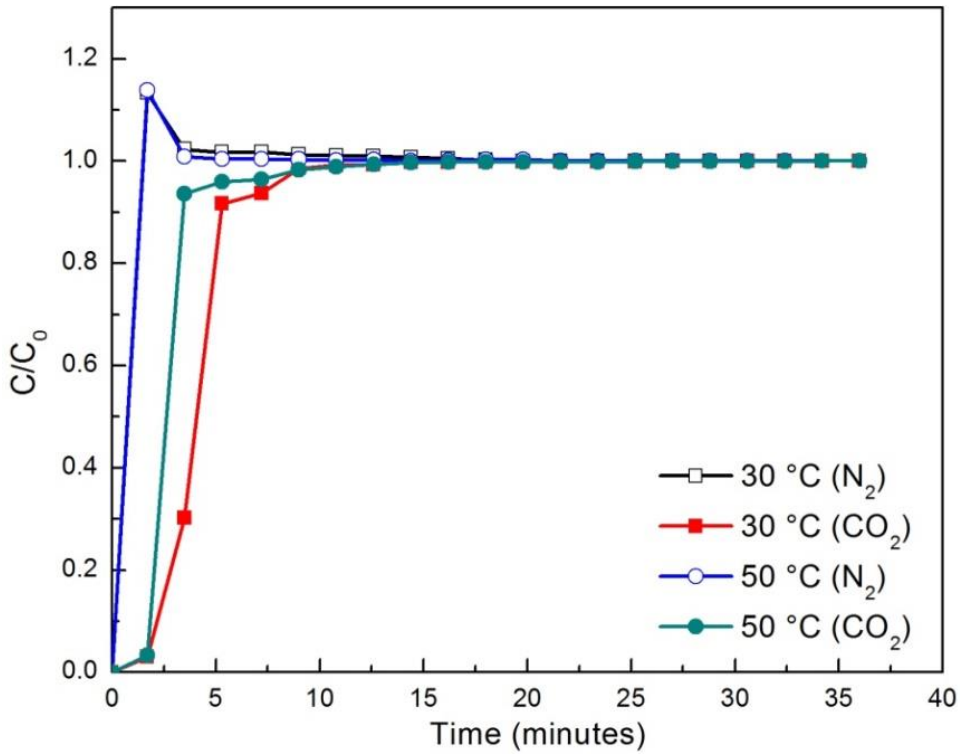

Fig. 6.14 CO_2/N_2 selectivity for 12.5% CO_2 (rest N_2) on UFZ-700

6.3.4 Cyclic adsorption/desorption study

The regeneration capability, which is one of the important parameters of the adsorbent, was also studied by increasing the temperature (to 200 °C) after adsorption. Four adsorption-desorption cycles were repeated to check its reusability for the long term use. The results of these experiments for UFZ-700 are presented in Fig. 6.15. Fig. 6.15(a), shows both fresh and regenerated breakthrough curves of adsorbent at 30 °C under 12.5% CO_2 showing similar curves, hence same

adsorption capacity. Fig. 6.15(b) shows sudden drop in CO_2 concentration to zero signifying that adsorbate gets quickly desorbed from the adsorbent surface. Fig. 6.15(c) shows complete regenerability over four continuous adsorption-desorption cycles signifying no loss in adsorption capacity. Carbon adsorbents prepared by Thote *et al.* [105] from soyabean by $ZnCl_2$ activation showed CO_2 adsorption of 0.93 mmol g^{-1} at 30 °C but not regenerated completely in second cycle. This shows that the adsorbent developed in this study is more effective as compared to others reported earlier.

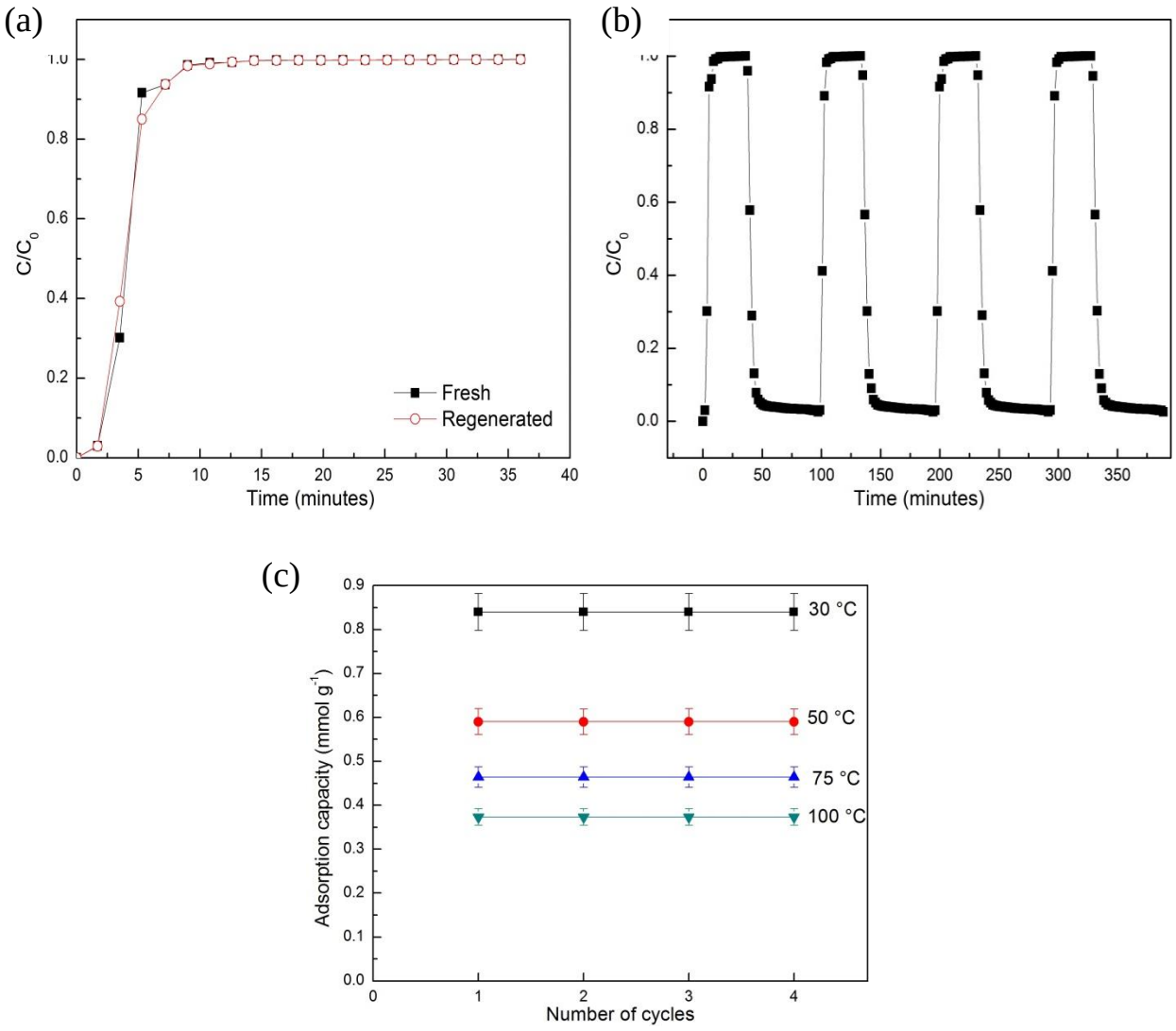

Fig. 6.15(a) Breakthrough curves of fresh and regenerated adsorbents (b) multiple cycles of adsorption-desorption of UFZ-700 (c) CO_2 uptake capacity at different temperatures and 12.5% CO_2

Fig. 6.16 shows TPD profile of UFZ-700 showing a broad peak in the range of 80-160 °C with maximum at 110 °C and then the CO_2 signal got smaller with a tail extending beyond 200 °C. This suggests multiple type of adsorption sites with different binding strengths in this adsorbent. The peak at 110 °C may be due to the removal of physically adsorbed CO_2 molecules from the adsorbent surface and tail to higher temperatures shows smaller contribution of chemisorption behavior. Overall, it can be concluded that the adsorbent shows predominantly physiosorption behavior [145].

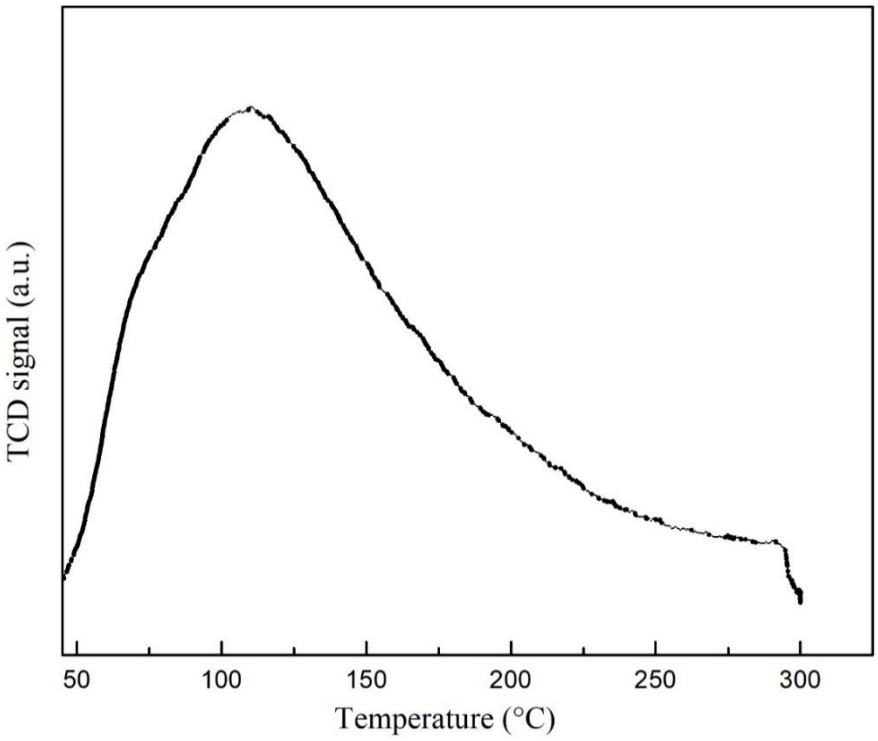

Fig. 6.16 TPD profile of UFZ-700

6.4 Kinetic study

Experimental and model predicted CO_2 adsorption on adsorbent as a function of time at different temperature under 12.5% CO_2 flow are shown in Fig. 6.17. The values of estimated kinetic parameters are shown in Table 6.6. The adsorption kinetics indicate two regions; first faster kinetic region and second slower for all samples until it reaches equilibrium. The first fast region is obtained in which before 10 minutes almost 90% of the adsorption takes place and the second

region in which the adsorption takes place slowly until it reaches equilibrium. This is due to decrease in the concentration gradient and decrease in unoccupied active sites.

It is found that the predicted data and the experimental data obtained from pseudo-first order and second order models are not fitting well and do not provide the proper description. The pseudo first order has overestimated initially for 30 °C and 50 °C while pseudo-second order not

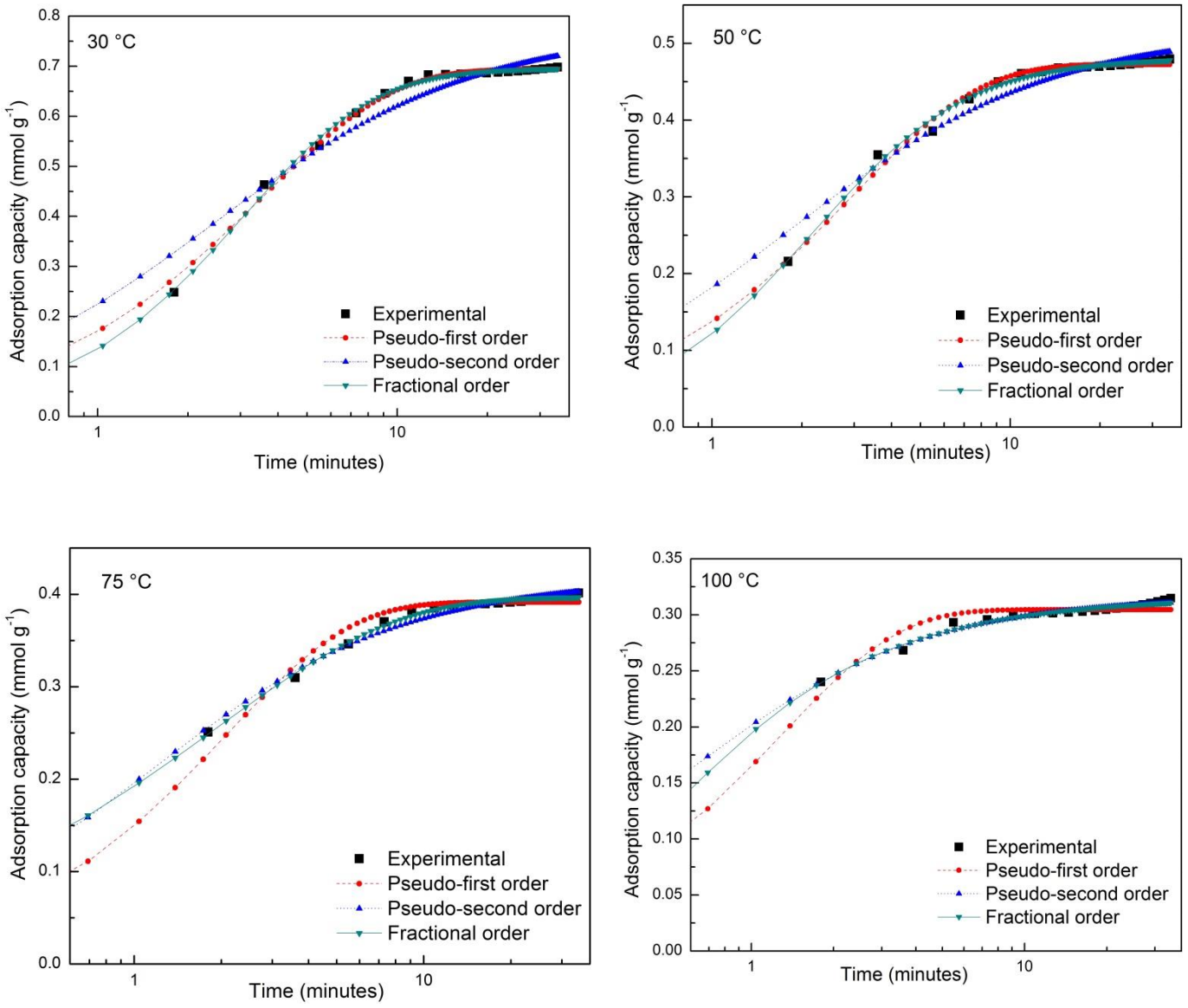

Fig. 6.17 Experimental and model predicted CO_2 uptake kinetics at 12.5% CO_2 and different temperatures

fitted in the entire range. This was further confirmed by poor error% and correlation coefficient value. On the other hand, fractional order fitted properly over entire range confirmed by lower error% and higher coefficient of determination (R^2) value (Table 6.6). This was also confirmed by predicted equilibrium adsorption capacity values which are in good agreement with experimental equilibrium adsorption capacity values. It was observed that increase in temperature causes decrease in the values of adsorption rate constant signifying exothermic nature. Also with rise of temperature, increase in both parameter values *n* and *m* of fractional-order-model is observed. Larger driving force at 30 °C, was confirmed by higher value of *n* at 30 °C. Similar kind of observation was seen by Liu *et al.* [180].

Table 6.6 Kinetic parameters of CO_2 uptake on UFZ-700

Model	Parameters	Temperature (°C**)**			
		30	50	75	100
Pseudo-first – order	k_1	0.28	0.34	0.48	0.77
	q_e	0.69	0.47	0.39	0.30
	R^2	0.98	0.986	0.98	0.989
	Error %	2.79	1.70	2.89	2.48
Pseudo-second –order	k_2	0.53	1.05	2.14	5.58
	q_e	0.77	0.51	0.41584	0.31
	R^2	0.97	0.98	0.996	0.998
	Error %	7.83	4.707	1.36	0.94
Fractional – order	k_n	0.82	0.43	0.39	0.33
	q_e	0.69	0.48	0.39	0.31
	n	1.75	1.35	1.07	1.03
	m	1.71	1.45	1.33	0.66
	R^2	0.998	0.997	0.998	0.998
	Error %	1.29	1.31	2.95	3.45

6.5 Isotherm study

Table 6.7 shows adsorption isotherm parameters at different temperatures which can be obtained from non-linear fitting of equilibrium data of CO_2 adsorption on UFZ-700. Here, both Langmuir and Freundlich isotherms closely fitted well with the experimental data but best fitting is obtained for Freundlich isotherm, which is also seen by the highest R^2 value. This shows that the adsorbent surface is heterogeneous in nature and multilayer CO_2 adsorption occurs [55]. As expected, physiosorption behavior is seen which is confirmed from decrease in K_F value with rise in temperature. Favorable adsorption condition is reflected by higher value of n >1 [181]. From the value obtained in Table 6.7 for q_m, we can say that the maximum adsorption has taken place at 30 °C. This was also further proved by the higher value of Freundlich constant K_F at 30 °C. The adsorption capacities at different temperatures (experimental as well as Freundlich model predicted) as function of partial pressure are shown in Fig. 6.18.

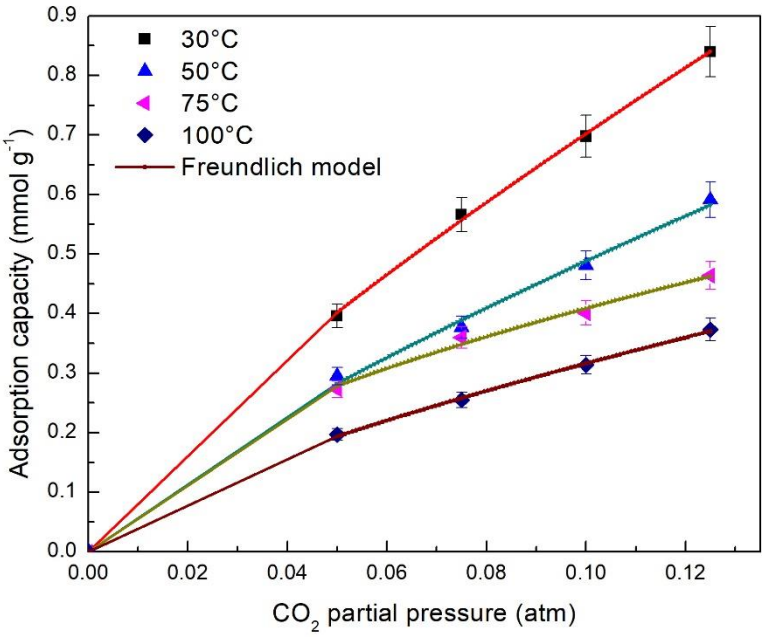

Fig. 6.18 Experimental and isotherm model predicted CO_2 uptake at different temperatures

Table 6.7 Adsorption isotherm data

Langmuir			
T (°C)	K_L (atm $^{-1}$)	q_m (mmol g^{-1})	R^2
30	2.82	3.20	0.998
50	2.94	2.15	0.978
75	9.79	0.83	0.983
100	4.82	0.97	0.99
Freundlich			
	K_F (mmol g^{-1} atm $^{-1/n}$)	n	R^2
30	4.48	1.24	0.998
50	3.01	1.26	0.986
75	1.46	1.80	0.982
100	1.61	1.41	0.997
Temkin			
	K_T (atm^{-1})	b (kJ mol^{-1})	R^2
30	44.87	5.29	0.987
50	47.61	8.44	0.941
75	77.68	14.39	0.984
100	54.20	16.94	0.971

6.6. Thermodynamic study

6.6.1 Thermodynamic parameters

Thermodynamic parameter values (calculated using equations 3.14 and 3.15) for CO_2 adsorption on UFZ-700 at different temperatures are shown in Table 6.8. As expected, exothermic nature was confirmed from negative value of $\Delta H°$. It has also been reported that the $\Delta H°$ value <20 kJ mol^{-1} implies for physiosorption. Therefore, lower value of $\Delta H°$ in the present work also implies physiosorption behavior. Also, spontaneous and feasible nature was confirmed from negative value of $\Delta G°$.

Table 6.8 Thermodynamic parameters of CO_2 adsorption on UFZ-700

Temperature (°C)	$\Delta G°$ (kJ mol^{-1})	$\Delta H°$ (kJ mol^{-1})	$\Delta S°$ (kJ $mol^{-1}K^{-1}$)
30	-9.58	-4.383	0.01
50	-10.374		
75	--12.593		
100	-12.382		

Fig. 6.19 shows Q_{st} values calculated from Clausius-Clapeyron equation for UFZ-700. Q_{st} value ranged from -8.83 to -11.53 kJ mol^{-1} with average -9.74115 kJ mol^{-1} is lower than reported Q_{st} for CO_2 adsorption on CNTs (-11.78 kJ mol^{-1}) [182], and activated carbon (-20.3 kJ mol^{-1})[148] signifying weak interaction between CO_2 molecules and the adsorbent i.e, weak vanderwaal force. This indicates that the lower energy is needed for regeneration. Also, random change in Q_{st} value with increase in surface coverage indicates heterogeneity of adsorbent surface.

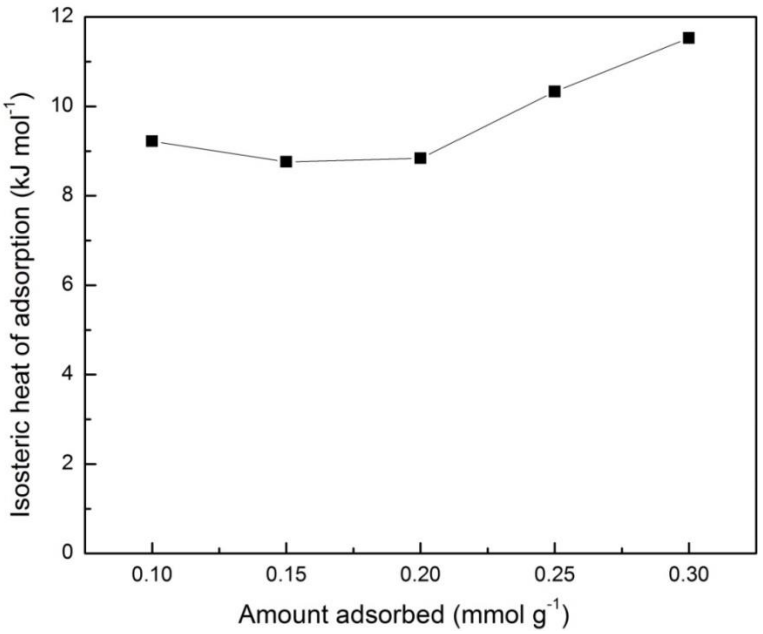

Fig. 6. 19 Isosteric heat of adsorption of CO_2 on UFZ-700

6.6.2 Energy duty for desorption of CO_2

C_p value for UFZ-700 = 1.215 J g^{-1} K^{-1}

$\Delta T = (200 - 30)\,℃ = 170\,℃$

UFZ-700 adsorption capacity (30 °C, 12.5% CO_2) = 0.84 mmol CO_2 per g adsorbent

= 0.84×10^{-3} mol CO_2 per g adsorbent = 0.03696 kg CO_2 per kg adsorbent

Hence, Sensible heat = $\frac{1.2 \times 170}{0.84 \times 10^{-3}}$ J per mole CO_2 = 242.85 kJ per mole CO_2

Net sensible heat needed for process = (25% of 242.85 kJ per mole CO_2), assuming 75% heat recovery

Sensible heat = 60.71 kJ per per mole CO_2 [149]

Isosteric heat of adsorption, Q_{st} = 9.74115 kJ per mole CO_2

Thermal energy input = (9.74 + 60.71 kJ per mole CO_2) = 70.45 kJ per mole CO_2

= 1.60 MJ per kg CO_2

Therefore, desorption of 0.84 mmol g^{-1} of CO_2 which is equal to 0.03696 kg CO_2 per kg adsorbent**,**
Energy required = 1.60 × 0.03696

= 0.059 MJ

Thus, CO_2 created to produce 0.059 MJ of energy for desorption = 0.0884 × 0.059 kg CO_2

= 5.21×10^{-3} kg CO_2

= 0.00521 kg CO_2

6.8 Conclusions

Mesoporous carbon adsorbents have been successfully prepared by nanocasting technique using low-cost urea-formaldehyde resin as precursor and mesoporous zeolite as template. The effect of nanocasting technique is seen by the characterization results. SEM results show better textural properties obtained for UFZ-700 as compared to UF-700. TEM results show that the obtained material is nanostructured as compared to the UF-700. Higher surface basicity for UFZ-700 is clearly seen by fitting of nitrogen and oxygen spectra from XPS. Adsorption capacity of UFZ-700 has been found to be highest (0.84 mmol g^{-1}) due to higher basicity and higher porosity. The adsorption capacity of adsorbent follows the order of: UFZ-700>UFZ-800>UF-700>UFZ-600>UFZ-500. In addition to N content and textural properties, surface functional groups play major role in CO_2 adsorption. Stability and quick regenerability is obtained over four adsorption-desorption cycles. Exothermic nature of adsorption is confirmed from the decrease in CO_2 adsorption capacity with increase in adsorption temperature. Experimental values of CO_2 adsorption is best fitted with fractional order kinetic model. Heterogeneity of the adsorbent surface is confirmed from the fitting of data with Freundlich isotherm models. Feasibility, spontaneity and exothermic nature of the adsorption process are confirmed from thermodynamic data.

Chapter 7 – Urea based Chemically Activated Nanostructured Carbons Adsorbents for Carbon Dioxide Capture

7.1 Preparation of activated carbon adsorbents

7.1.1 Synthesis of urea formaldehyde resin

About 224 g urea along with formaldehyde (600 ml, 37% w/v) solution were added in a 1000 ml three necked round bottom flask equipped with stirrer, condenser and a thermometer. Next, stirring was performed for 30 minutes, and pH was adjusted to 9 by adding 1 N NaOH. Then, the solution was heated to 80-85 ˚C for 2 h followed by cooling to 50-55 ˚C. Next, pH was adjusted to 5-5.5 by adding sulfuric acid. To carry out digestion, temperature of reaction mixture was increased to 85-90 ˚C and maintained for the next 1 h. Afterwards, the solution was cooled to 40-45 ˚C followed by the addition of sulfuric acid**.** The obtained sample was cured for 3 h at 120 ºC to ensure complete dryness. Fig. 7.1 presents the block diagram of preparation of UF resin.

7.1.2 Carbonization of urea formaldehyde resin

After this, carbonization of the samples was performed in a tubular furnace at 700 ºC in flowing N_2 atmosphere (flow rate = 60 ml min^{-1}). The holding time at this temperature was 2 h. The heating rate was 10 ºC min^{-1}. Then, the system was cooled to room temperature under the same N_2 flow. The obtained sample was designated as UF-700 and taken as a reference sample for this study. The block diagram of adsorbent preparation (UF-700) is shown in Fig. 7.2.

7.1.3 Chemical activation of urea formaldehyde resin at different KOH:UF ratio

For the activation process, potassium hydroxide (KOH) was used as activating agent. Here, the sample (UF-700) and KOH were thoroughly mixed at KOH/UF (mass ratio) of 1 to 4. Drying of the obtained mixed samples was done at 105 ºC for 12 h.

7.1.4 Carbonization of chemically activated adsorbents

Next, activation was performed by heating the dried material in a tubular furnace, at different activation temperatures of 500 ºC to 800 ºC under N_2 flow rate of 60 ml min^{-1}. The heating rate was 10 ºC min^{-1} and holding time was 2 h. After cooling to room temperature, it was washed with 1 M HCl and distilled water until the neutral pH was obtained. This was done to remove the chloride ions also. Finally, the activated samples were dried in oven at 120 ºC. Fig. 7.3 presents the block diagram of activation process. The obtained activated samples are listed in Table 7.1 with sample notation and preparation variables. The three parameters namely KOH:UF mass ratio, activation temperatures and activation times were also optimized for the preparation of carbon materials which have a major impact on the CO_2 adsorption capacity of the adsorbent.

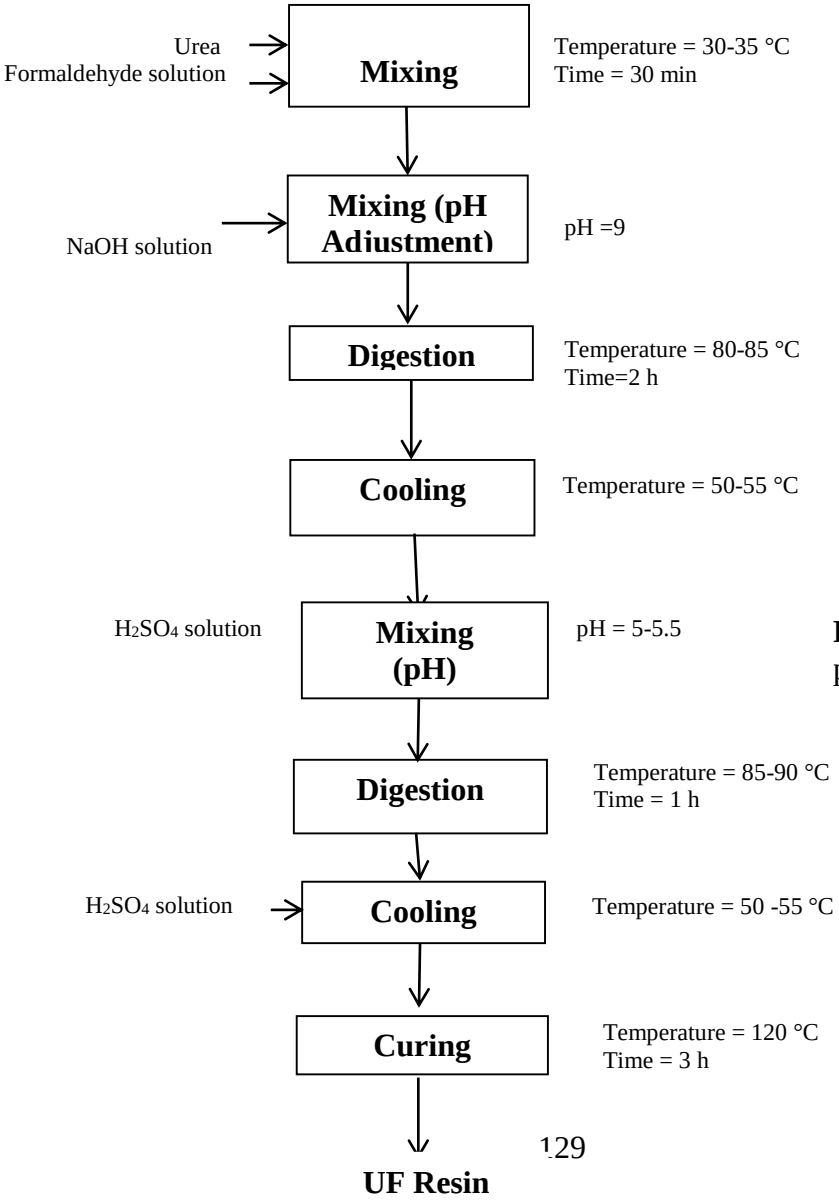

Fig. 7.1 Schematic representation of preparation method of UF resin

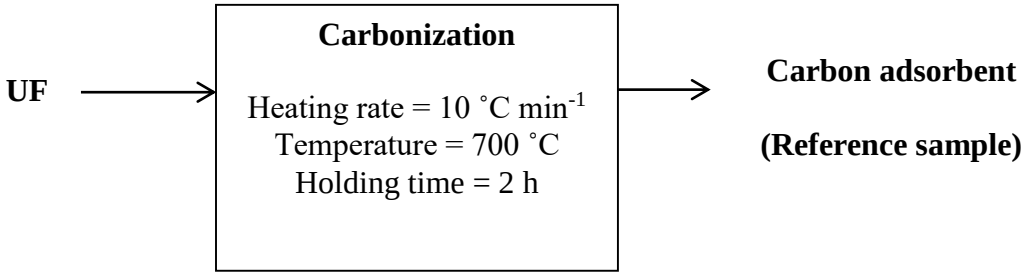

Fig. 7.2 Schematic representation of preparation of the carbon adsorbent by direct carbonization technique

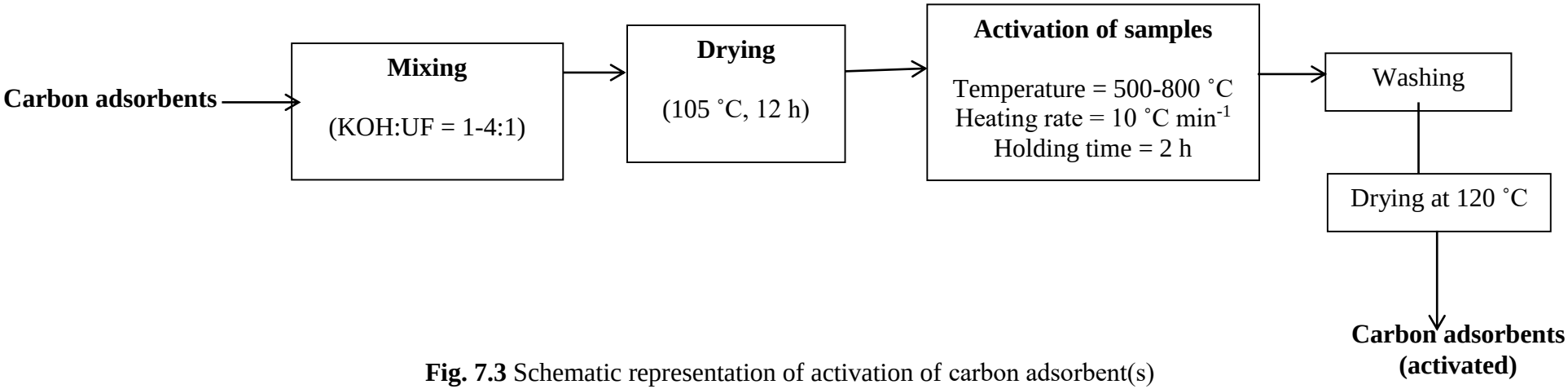

Fig. 7.3 Schematic representation of activation of carbon adsorbent(s)

Table 7.1

Samples prepared at various conditions

Samples notation	Carbonization temperature (ºC)	Activation temperature (ºC)	KOH:UF (mass ratio)
UF-700	700	-	-
UFA-1-700	700	700	1
UFA-2-700	700	700	2
UFA-3-700	700	700	3
UFA-4-700	700	700	4
UFA-3-500	700	500	3
UFA-3-600	700	600	3
UFA-3-800	700	800	3

7.2 Characterization of adsorbents

7.2.1 Surface area and pore size distribution

(a)

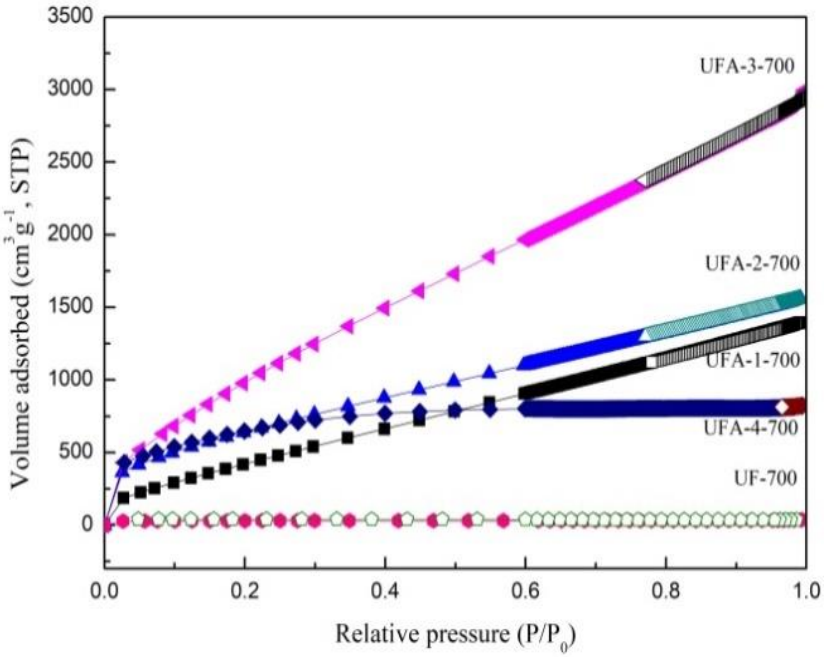

(b

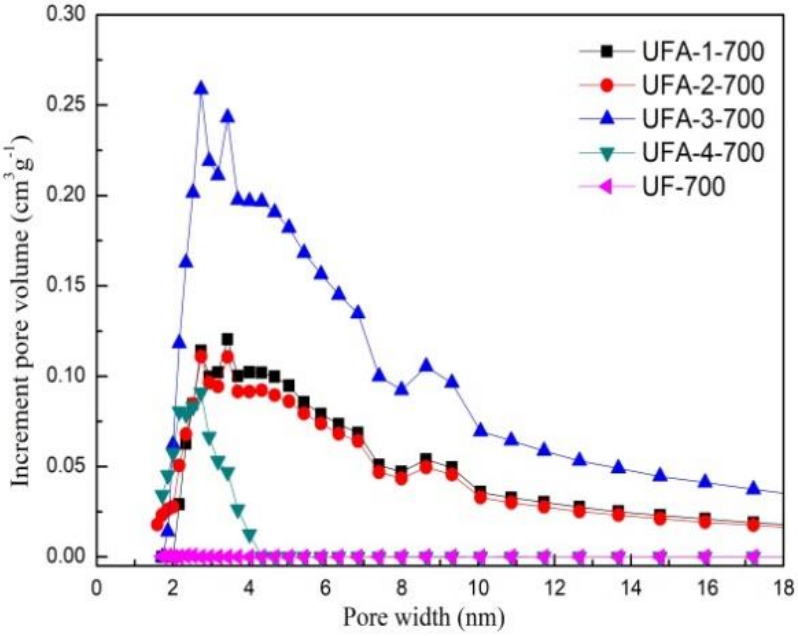

Fig. 7.4 (a) N_2 sorption isotherms and (b) PSD of adsorbents

Fig. 7.4(a) shows N_2 adsorption/desorption isotherms of UF-700 and activated samples. It is seen that the volume of N_2 adsorbed for the UF-700 is very small. This shows that the sample is almost non-porous. On the other hand, the sample prepared at same carbonization temperature but after KOH activation shows typical type 1 isotherm, as defined by IUPAC classification, showing the presence of abundant micropores. It was due to KOH which behaves as catalyst to accelerate the gasification reaction according to equations (7.2-7.4). At higher temperatures like 700 ˚C, it formed intermediates like K_2CO_3 and K_2O, which react with active carbon to construct abundant of micropores in the carbon framework [183]. This was seen for our activated samples. The volume of N_2 adsorbed for other samples was quite low as compared to UFA-3-700 which signifies that these samples have less pores as compared to UFA-3-700.

$$2KOH \rightarrow K_2O + H_2O \quad (7.1)$$

$$6KOH + 2C \rightarrow 2K + 3H_2 + 2K_2CO_3 \quad (7.2)$$

$$K_2CO_3 \rightarrow K_2O + CO_2 \quad (7.3)$$

$$K_2CO_3 + 2C \rightarrow 2K + CO \quad (7.4)$$

$$K_2O + C \rightarrow 2K + CO \quad (7.5)$$

The pore size distribution (PSDs), calculated using BJH method lie in the range of about 1.4 to 5 nm {Fig. 7.4(b)}, especially 1.4-3.5 nm which is good for small molecule adsorption.

Table 7.2 Textural properties calculated from nitrogen sorption

Materials	Surface area (m^2 g^{-1})	Total pore volume (cm^3 g^{-1})	Micro pore volume (cm^3 g^{-1})	Meso pore volume (cm^3 g^{-1})
UF-700	104	0.05	0.036	0.014
UFA-1-700	1984	2.137	0.045	2.092
UFA-2-700	2316	2.527	0.581	1.946
UFA-3-700	4547	4.50	0.260	4.24
UFA-4-700	2285	1.25	1.161	0.089

It is seen that BET surface area increased with increase in KOH content and is highest for UFA-3-700. BET surface area for UFA-3-700 is 4547 m^2 g^{-1}, which is one of the best surface areas reported till now for carbon based adsorbents (Table 7.2). The mesopore and micropore volume for this sample is 4.24 cm^3 g^{-1} and 0.26 cm^3 g^{-1}, respectively. Sample activated at KOH:UF mass ratio of 4 shows decrease in BET surface area and total pore volume probably due to some blockage of pores. When sample was activated by increasing KOH:UF ratio from 1 to 3, increase in surface area and total pore volume was observed. It was also seen that increase in KOH:UF ratio from 1 to 2, caused increase in microporosity and decrease in mesoporosity while further increase in KOH:UF ratio from 2 to 3 caused decrease in microporosity and increase in mesoporosity. It is noted that most of the pore volume is ascribed to mesopore volume. Meso-macropores may be generated or micropores are partially destroyed due to over activation. Thus, it signifies that activation process cannot only lead to high porosity but also effects the pore structure. Similar kind of observations were also seen by Liu et al. [160].

7.2.2 XRD analysis

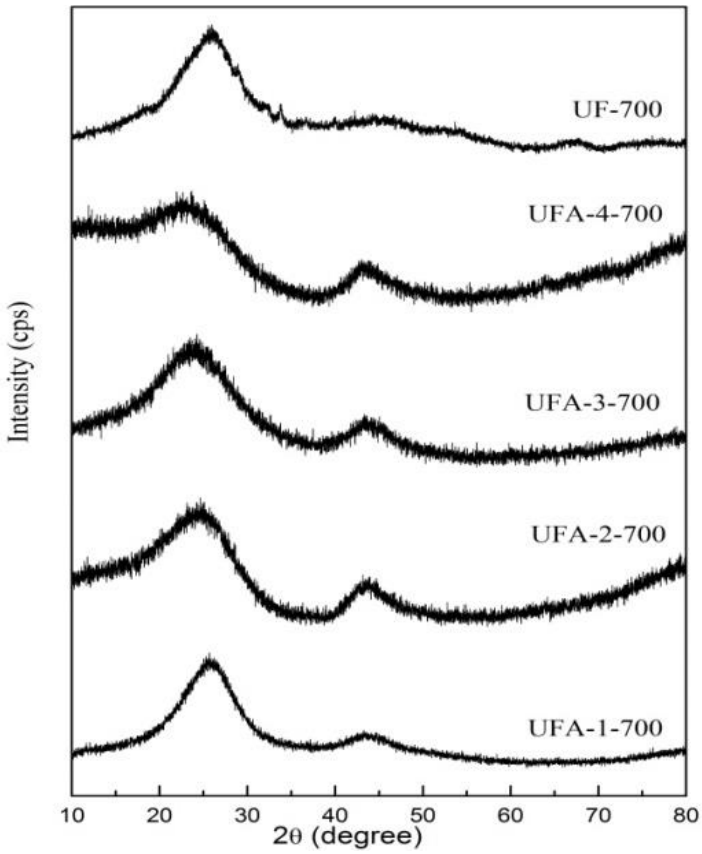

Fig. 7.5 Wide angle XRD patterns of adsorbents

Fig. 7.5 shows wide angle XRD diffraction patterns of carbon adsorbents showing peak at $2\theta = 26°$ which corresponds to (002) diffraction planes of hexagonal graphite carbon [137]. The *d*-spacing is found to be 3.437 indicating turbostactic ordering of the atoms in the graphene layers of the samples [160]. The weak peak at $2\theta = 45^{\circ}$ corresponds to (100) diffraction plane of graphite carbon [184]. Shifting of peak towards lower angle and decrease in intensities of peak was observed after KOH activation indicating increment in the *d*-spacing. Here, increase in the *d*-spacing indicates addition of nitrogen and oxygen. It was also observed that for UFA-4-700, intensities almost vanished, which signifies destructive interferences arising due to KOH addition.

7.2.3 TEM analysis

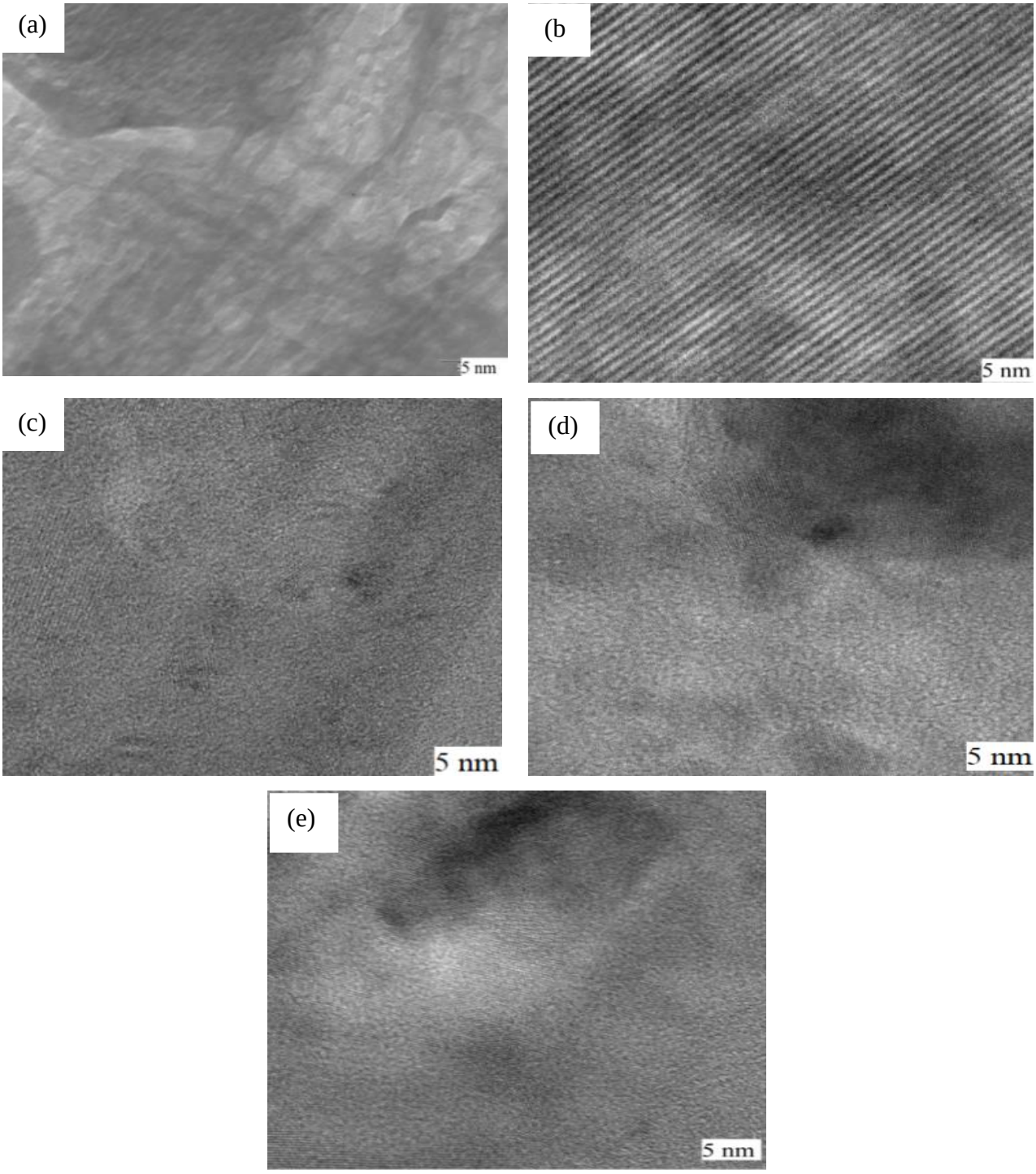

Fig. 7.6 Transmission electron micrographs of carbon adsorbents (a) UF-700, (b) UFA-1-700 (c) UFA-2-700, (d) UFA-3-700, and (e) UFA-4-700

Fig. 7.6 shows TEM images of the carbon adsorbents. From the images, non-porous and graphite like layer structures of UF-700 is seen which is stacked together layer by layer. However, samples after activation, graphite like layer structure is still maintained but shows randomly oriented uniform microporosity. Similar kind of observation was also seen by other researchers also [114]**.**

7.2.4 SEM analysis

Fig.7.7 depicts effect of KOH activation on SEM images of carbon adsorbents. Sample UF-700 shows almost absence of pores and graphite like layer structure while after activation with KOH, samples show large amount of pores due to removal of large volume of gases during the activation process according to stoichiometric redox reaction i.e. equations (7.3-7.5). Here, the pores help in better diffusion of gas from bulk to the adsorbent surface.

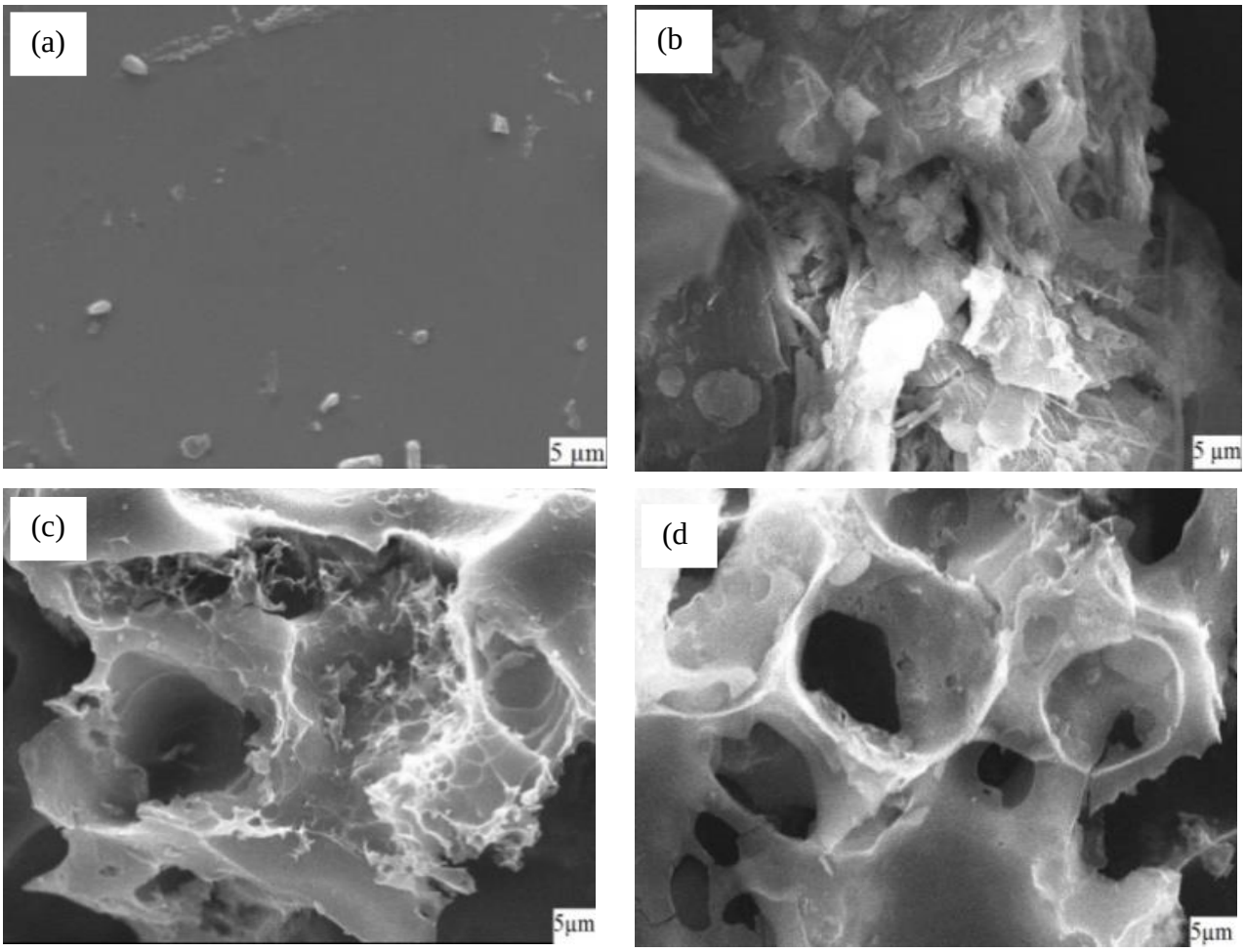

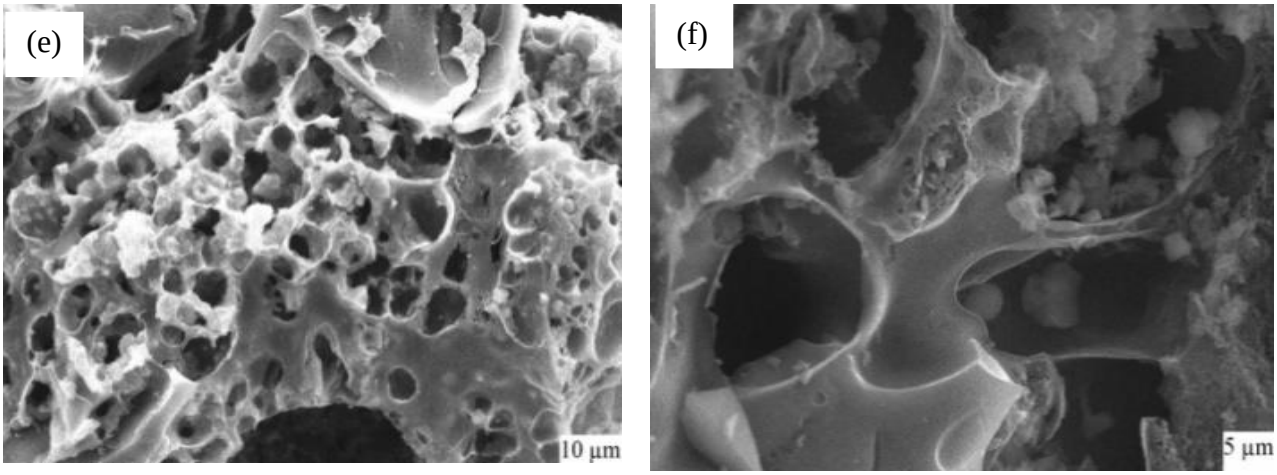

Fig. 7.7 SEM images of (a) UF-700, (b) UFA-1-700, (c) UFA-2-700, (d) UFA-3-700, (f) UFA-4-700 and (e) UFA-3-700 at lower magnification

7.2.5 TG analysis

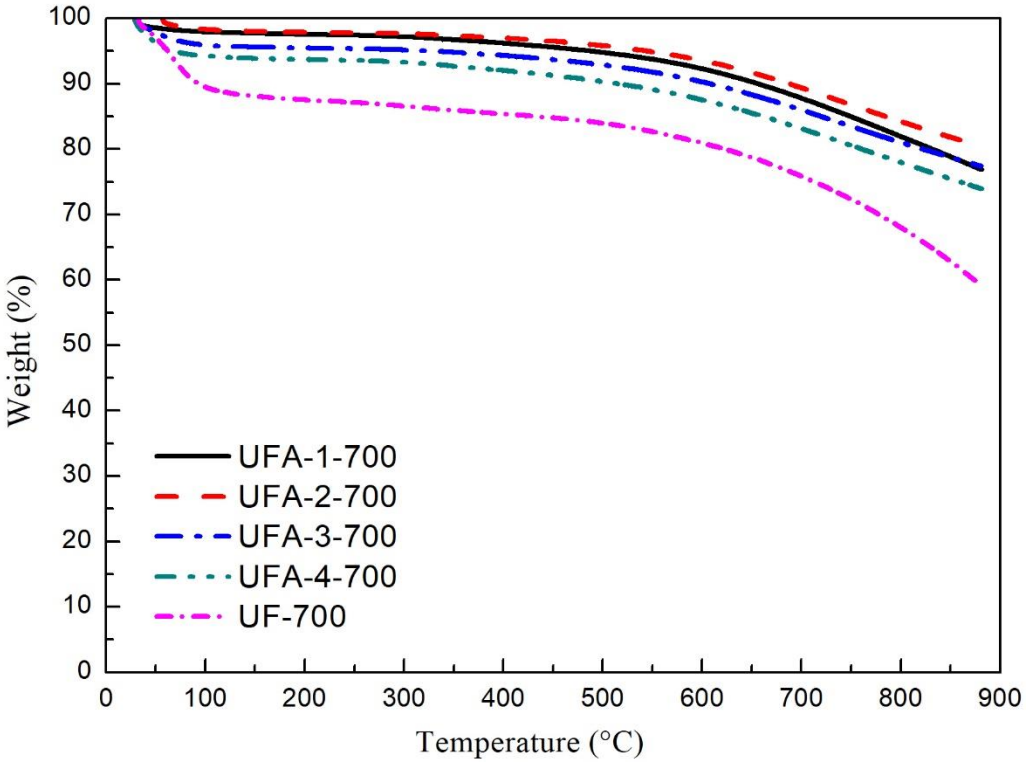

Fig. 7.8 Thermogravimetric profiles of the prepared adsorbents

Fig. 7.8 shows thermal stability behavior of carbon adsorbents. Two weight loss regions for all the samples is observed. First region upto 100 ˚C is due to removal of moisture and other gases. The second region shows weight loss of UFA-1-700 (23.13%), UFA-2-700 (22.49%),

UFA-3-700 (19.52%), UFA-4-700 (25.93%) and UF-700 (40.95%). It is seen that sample UF-700 is least stable and UFA-3-700 the most thermally stable.

7.2.6 Elemental analysis

Table 7.3 Elemental composition of carbon adsorbents

Sample	Elemental composition (weight %)				
	C	N	H	O[a]	TKN
UF-700	59.30	18.03	1.61	21.06	17.3
UFA-1-700	66.15	10.57	0.98	22.3	11.86
UFA-2-700	68.51	7.61	0.48	23.4	5.97
UFA-3-700	65.77	5.62	0.46	28.15	4.70
UFA-4-700	70.50	4.32	0.35	24.83	3.64

[a]*Calculated by difference*

Table 7.3 shows the elemental analysis and Kjeldahl nitrogen of the carbon adsorbents which confirms the presence of oxygen and nitrogen. Decrease in the content of nitrogen from 18.03 to 4.32% with increase in KOH:UF ratio suggests that the nitrogen is oxidized. The similar trend can be seen from Kjeldahl nitrogen also. Increase in oxygen content as compared to reference sample is seen which may be due to insertion of oxygen during the activation process. It is seen that carbon content shows increase upto KOH:UF mass ratio of 2 and then slight decrease for KOH:UF mass ratio of 3. This is because for UFA-3-700 proper activation is carried out which is seen from higher oxygen content and higher surface area resulting in higher adsorption capacity. This could be also due to cleavage of more C-C bonds than oxygen functional group.

7.2.7 FTIR analysis

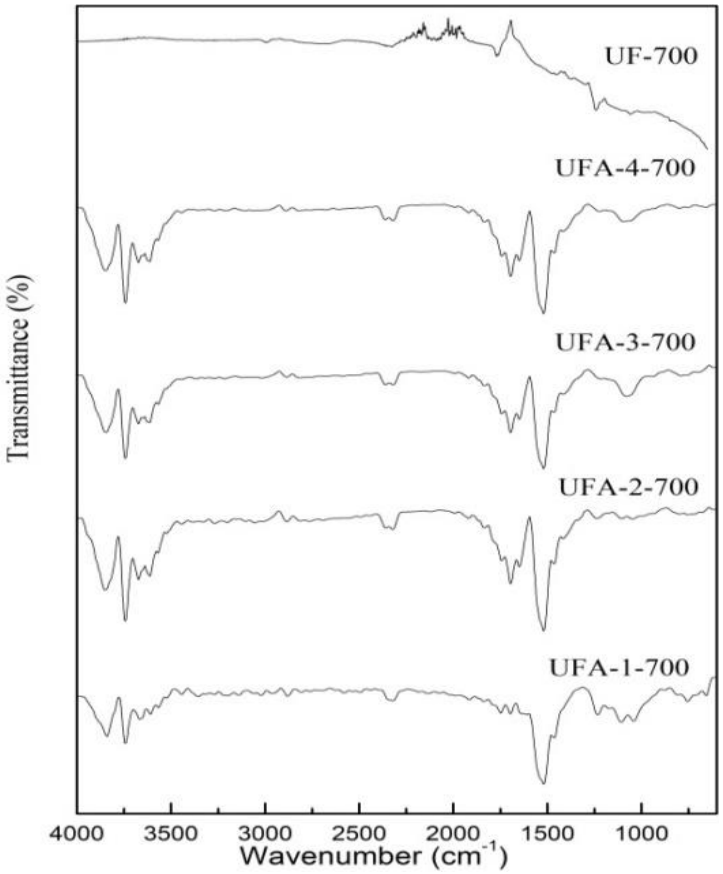

Fig. 7.9 FTIR spectra of UF-700 and activated samples of carbon adsorbents

The FTIR spectra of the carbonized sample and the activated samples are shown in Fig. 7.9. UF-700 shows broader and overlapping bands due to its complex structure [114]. Band at 1500 cm^{-1} and 1250 cm^{-1} is attributed to C=C stretching vibrations in graphitic structure and to C-N stretching vibrations. Band at 1079 cm^{-1} can be assigned to C-O stretch of C-OH which confirms the presence of oxygen [185]. After activation with KOH, intensities of these bands increase which shows that activation with KOH provides more oxygen into the matrix of samples. Elemental analysis shows similar results. Overall, FTIR analysis confirms the presence of C-N and C-O bonds.

7.2.8 X-ray photoelectron spectroscopy

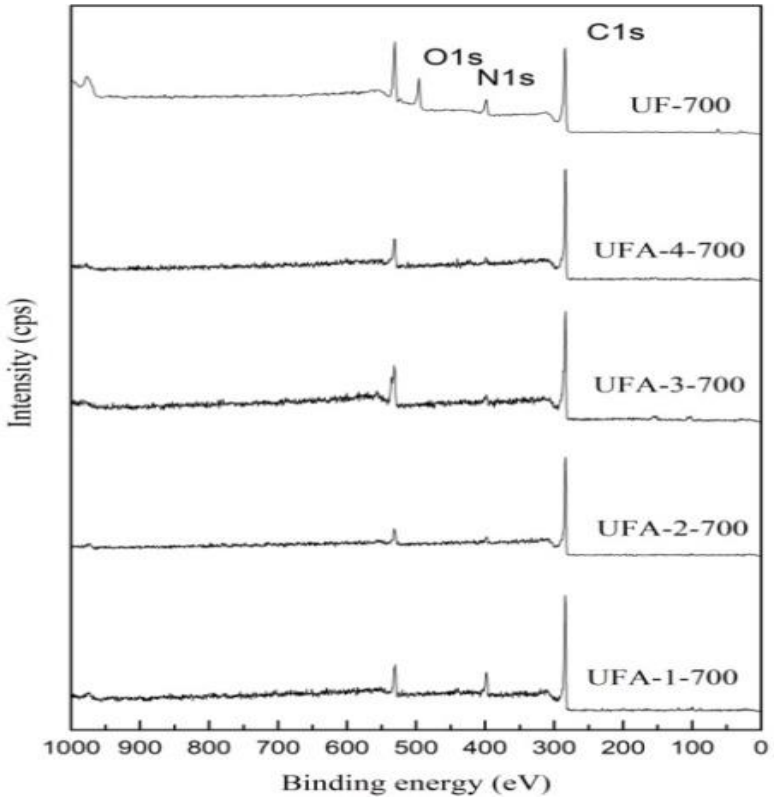

Fig. 7.10 XPS survey scan spectra of carbon adsorbents

Fig 7.10 shows survey scan spectra of the carbon adsorbents. Three distinct peaks at 285, 400, and 532 eV were observed attributing to carbon (C1s), nitrogen (N1s) and oxygen (O1s) respectively.

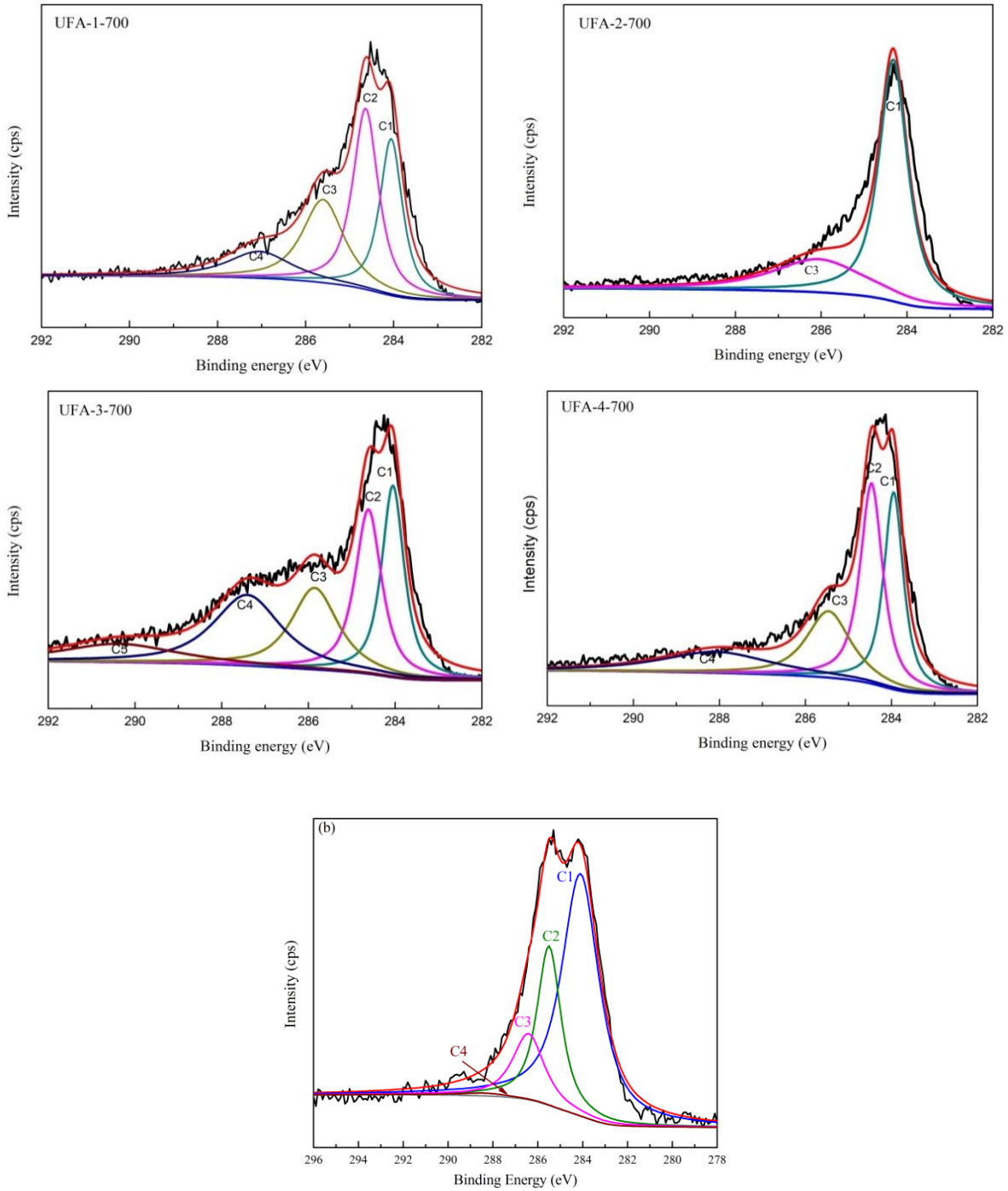

Fig. 7.11 Deconvoluted C1s XPS spectra of carbon adsorbents

Fig. 7.11 shows fitting of C1s spectra having deconvoluted five peaks with different B.E, FWHM, and A% of the carbonized and activated samples (Tables 7.4). Here, sp^2 and sp^3 carbon atom (C1) assigned at 284.39 eV, C-O bond of phenol & alcohol or ether and/or C=N bond (C2) at 285.8 eV, carbonyl or quinone groups and/or C-N linkage(C3) at 286.7 eV, carboxyl or ester linkages (C4) at 288.7 eV and shake up satellite peaks because of π-π* transitions in aromatic rings (C5) at 290.3 eV [140]. It is seen from table that with the increase

in KOH:UF ratio up to 2, A% of C1 peak increased from ca. 26.67% to 69.30% suggesting enhanced graphitization. Further rise in KOH:UF ratio up to 3, C1 gets transformed to C2, C4 and C5 suggesting formation of more stabilized structure.

Table 7.4 XPS data of C1s core level spectra of adsorbents

Sample		C1	C2	C3	C4	C5
UF-700	BE	284.38	285.89	286.71	288.74	-
	FWHM	0.55	0.67	1.19	3	-
	A %	25.08	32.56	26.41	15.94	-
UFA-1-700	BE	284.06	285.89	286.75	287.05	-
	FWHM	0.613	0.695	1.12	1.71	-
	A %	26.67	34.86	25.79	12.66	-
UFA-2-700	BE	284.32	-	286.05	-	-
	FWHM	0.79	-	2.57	-	-
	A %	69.30	-	30.69	-	-
UFA-3-700	BE	284.05	284.64	285.86	287.411	290.37
	FWHM	0.64	0.73	1.27	1.85	3.20
	A %	22.26	22.54	19.59	24.57	11.03
UFA-4-700	BE	283.95	284.47	285.46	-	288.08
	FWHM	0.54	0.65	1.21	-	3.03
	A %	28.28	33.38	19.57	-	11.03

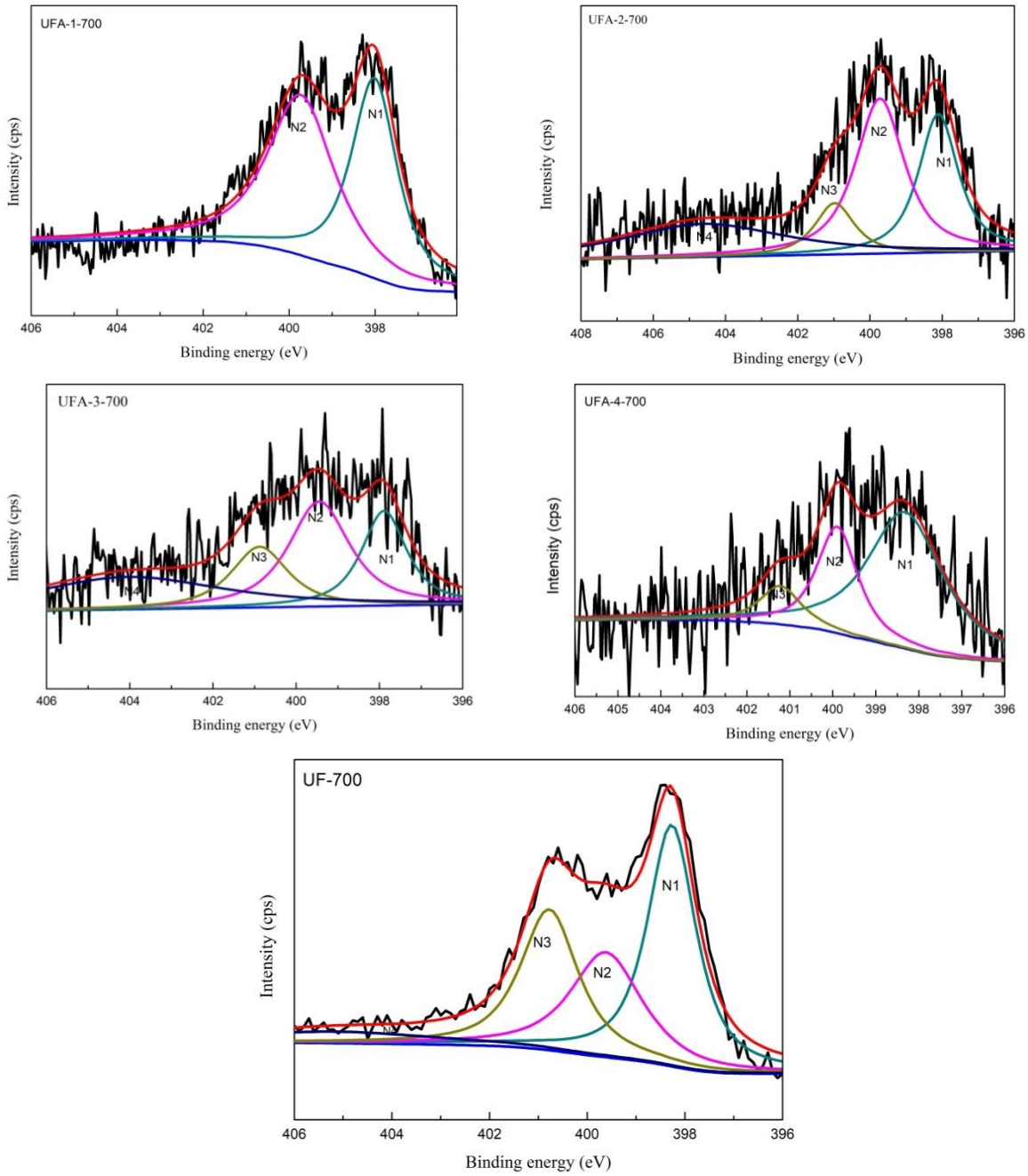

Fig. 7.12 Deconvoluted N1s XPS spectra of carbon adsorbents

Fig. 7.12 shows N1s spectra after deconvoluting into four peaks. Pyridinic-type nitrogen (N1) assigned at 398.3 eV, pyrrolic and/ or pyridone-type nitrogen (N2) at 400.4 eV, quaternary nitrogen (N3) at 401.2 eV and pyridine nitrogen oxide (N4) at 405.15 eV, respectively [164-167]. Table 7.5 shows that N1 & N2 are mainly obtained for UFA-3-700 and N3 & N4 for UF-700. This could be because N3 and N4 getting converted to N1 and N2 after activation. As reported, N1 contributes one electron to aromatic π-system and found in 6

membered ring structure (different B.E) while N2 contributes two p-electrons to π-system and found in 5 membered ring structure having same B.E. Therefore, they are having Lewis basic character and beneficial for capture of CO_2 (Lewis acid). Here, N3 is highly acidic [168], is higher for UF-700. Therefore, UFA-3-700 surface is highly basic in nature as compared to UF-700.

Table 7.5 XPS data of N1s core level spectra of adsorbents

Sample		N1	N2	N3	N4
UF-700	BE	398.27	399.62	400.77	405.15
	FWHM	1.18	1.73	1.39	5.29
	A %	20.81	25.09	27.11	30.98
UFA-1-700	BE	398.12	399.72	-	-
	FWHM	1.27	1.85	-	-
	A %	46.19	53.80	-	-
UFA-2-700	BE	398.10	399.725	400.98	404.62
	FWHM	1.30	1.62	1.30	5.47
	A %	26.62	36.94	9.8	26.60
UFA-3-700	BE	397.89	399.45	400.88	404.05
	FWHM	1.28	1.74	1.63	5.57
	A %	39.37	31.29	16.90	8.42
UFA-4-700	BE	398.31	399.89	401.22	-
	FWHM	2.098	1.137	1.163	-
	A %	63.35	26.76	9.8	-

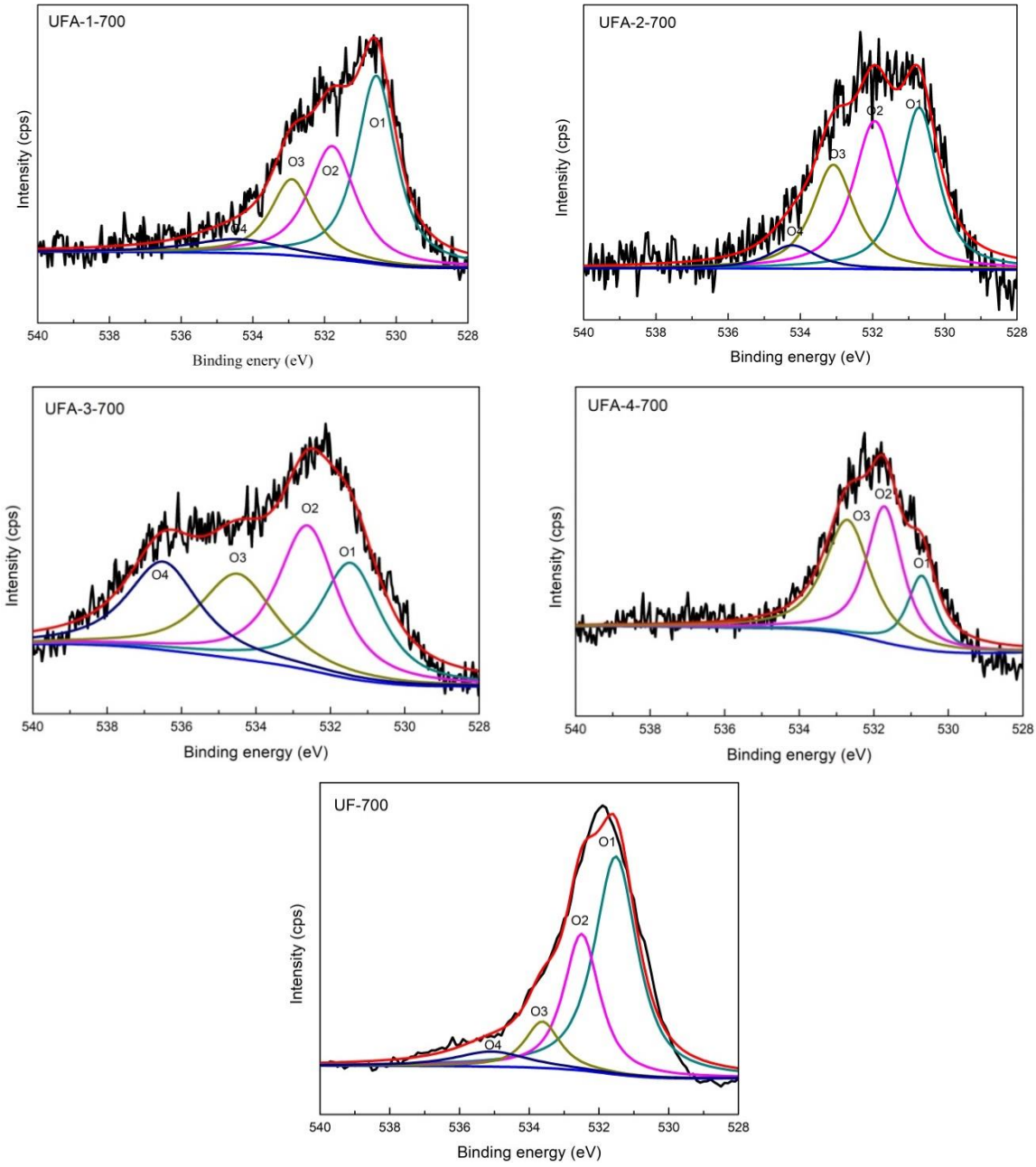

Fig. 7.13 Deconvoluted O1s XPS spectra of carbon adsorbents

The O1s spectra of samples (Fig. 7.13) are deconvoluted into four peaks. Here, carbonyl, ketone or lactone groups (O1) assigned at 531.52 eV; ether, alcohol (O2) at 532.5 eV; carboxyl group (O3) at 533.6 eV; and oxygen in water (O4) at 535.04 eV [132, 151]. Here, O1 & O2 are having higher contribution towards UFA-3-700 and O3 & O4 are higher towards UF-700 (Table 7.6). It has been reported in literature that O1 and O2 are responsible for basicity and O3 are responsible for acidity [1]. Thus, UFA-3-700 is more basic in nature than UF-700.

Table 7.6 XPS data of O1s core level spectra of adsorbents

Sample		O1	O2	O3	O4
UF-700	BE	531.52	532.50	533.64	535.08
	FWHM	1.46	1.21	1.19	2.46
	A %	24.95	28.77	22.40	22.17
UFA-1-700	BE	530.556	531.778	532.911	534.452
	FWHM	1.32	1.57	1.40	3.05
	A %	43.14	30.86	18.55	7.43
UFA-2-700	BE	530.715	531.943	533.08	534.23
	FWHM	1.25	1.42	1.38	1.57
	A %	34.13	35.41	24.27	6.16
UFA-3-700	BE	531.453	532.61	534.49	536.46
	FWHM	1.96	1.92	2.39	2.29
	A %	55.23	38.45	9.53	6.45
UFA-4-700	BE	530.72	532.72	533.71	-
	FWHM	0.92	1.16	1.47	-
	A %	17.21	39.99	42.79	-

7.2.9 Raman spectroscopy

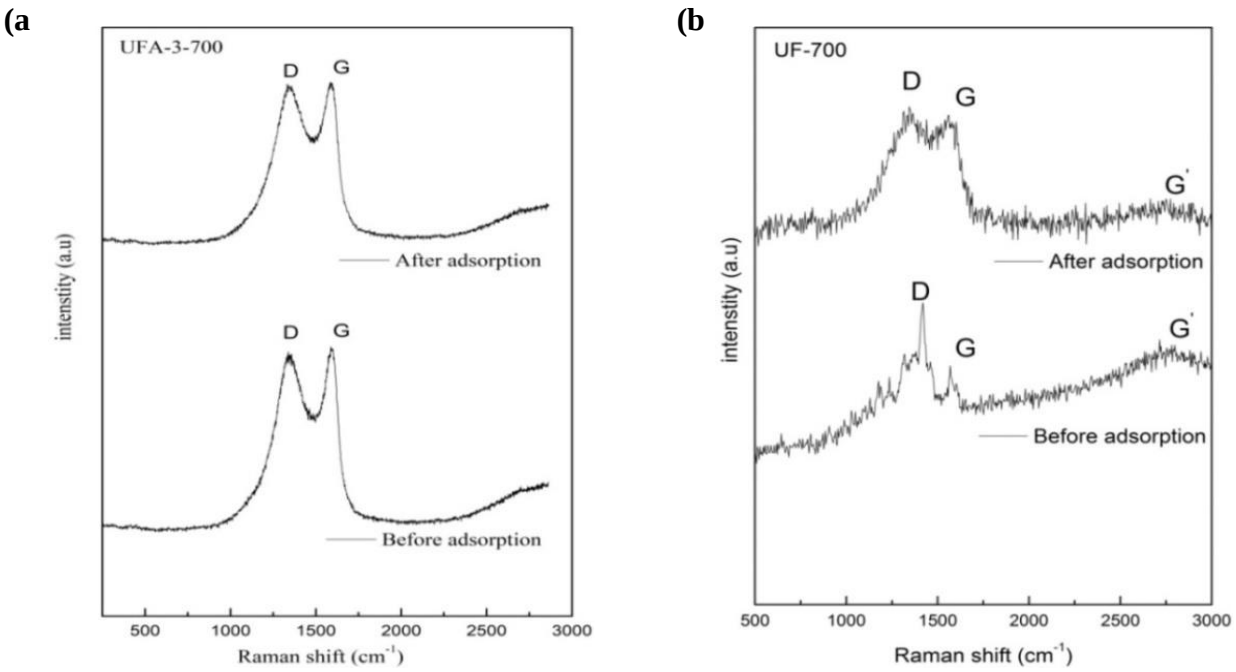

Fig. 7.14 Raman spectra of carbon adsorbents before and after CO_2 adsorption (a) UFA-3-700 and (b) UF-700

Fig. 7.14 shows Raman spectra of carbon adsorbents before and after CO_2 adsorption. Two bands in the range of 1300-1430 cm^{-1} and 1530-1582 cm^{-1} are seen. These are D and G bands, also called Raman bands [169]. G-band is due to in-plane bond-stretching motion of pair of sp^2 atom and D-band is due to breathing mode of six-fold rings, appeared due to breakage of graphite layer into smaller units. D-band also indicates degree of disordered carbon. It also corresponds to sp^3 carbon atoms. The intensity ratio I_D/I_G shows carbon structure, degree of graphitic carbon materials, number of defect sites in carbon and disorganized carbon content having direct effect on adsorption capacity and pore structure [171]. This was also seen in a study by Haghseresht *et al.* [172], in which the authors showed a relationship between micropore volume, mesopore volumes, total BET surface area and other parameters. They showed that as I_D/I_G ratio increases, adsorption capacity increases. They also showed that if the disorganized carbon is higher, higher will be the amount of aromatic compounds in comparison with aliphatic carbon and lesser space between the aromatic compounds. In our study, I_D/I_G ratio for UFA-3-700 is 0.98 which is higher as compared to UF-700 i.e., 0.89. Therefore, it is having higher defective nature and reduced degree of graphitization, signifying higher porous nature and disordered structure of the UFA-3-700, which is consistent with N_2 adsorption-desorption results and SEM. Although, intensity ratio

of UF-700 is 0.89 but the adsorption capacity is lower. This is because of acidic nature as confirmed from XPS results. Shifting of bands is seen in Fig. 7.14, showing adsorption of CO_2 molecules in the adsorbent pores. Shifting of peak position is because of intermolecular interaction between CO_2 molecules and adsorbent, which alters the intermolecular potential of gas molecules due to displacement of vibrational modes [173].

7.3 CO_2 adsorption performance

7.3.1 Influence of activation parameters on CO_2 adsorption capacity

To find the optimum conditions for the preparation of carbon materials, three parameters, which have a significant effect on the adsorption capacity of the adsorbent, were optimized. Parameters are KOH: UF ratio, activation temperature and activation time.

7.3.1.1 Activation time

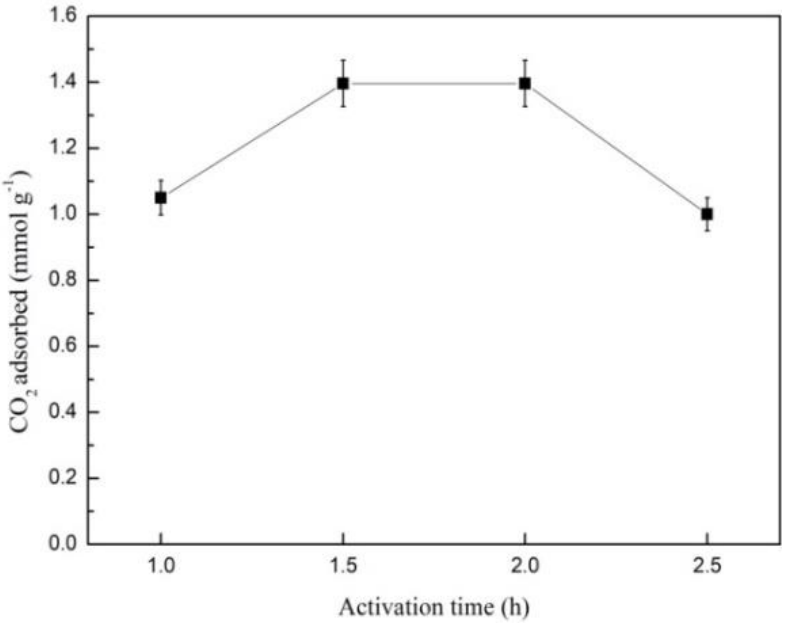

Fig. 7.15 Effect of activation time on CO_2 adsorption capacity of prepared adsorbents at 12.5% CO_2 and 30 °C

It is seen from Fig. 7.15 that CO_2 uptake obtained at different activation time's shows different CO_2 adsorption capacities. The CO_2 uptake was performed at 12.5% CO_2 concentration and at 30 °C adsorption temperature. Activation performed up to 1.5 h shows increase in CO_2 uptake capacity but further increase up to 2 h, it shows relatively constant

value. However, on further increase in time, decrease in CO_2 uptake capacity is seen. Therefore, optimum activation time of 2 h is chosen for this study.

7.3.1.2 KOH: UF mass ratio

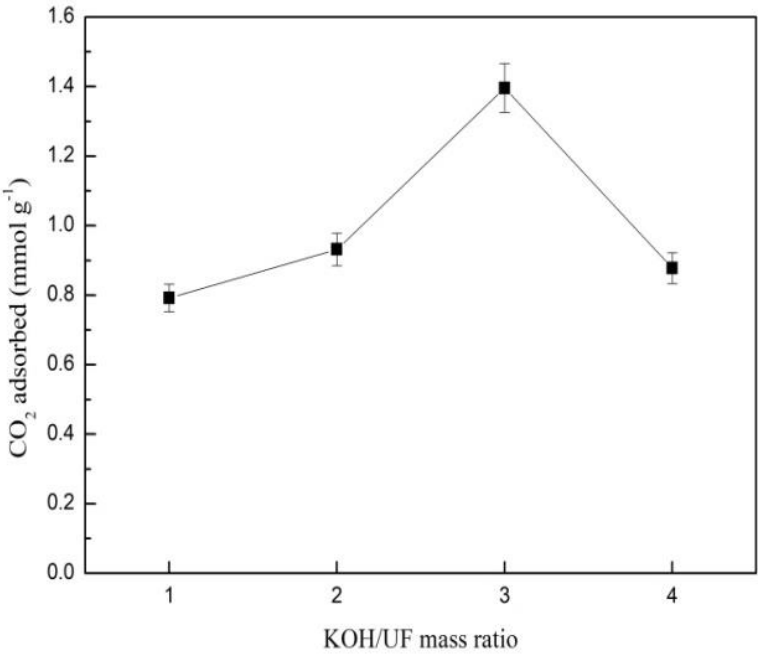

Fig. 7.16 Effect of KOH/UF mass ratio on CO_2 adsorption capacity of prepared adsorbents (700˚C and 2 h activation time) at 12.5% CO_2 and 30 °C

From Fig. 7.16, at fixed temperature and activation time (700 °C and 2 h), it is seen that increase in KOH:UF ratio up to 3, causes increase in the adsorption capacity while further increase in the ratio results in drastic decrease in adsorption capacity due to decrease in textural properties, blockage of pores due to higher KOH:UF mass ratio and higher acidic nature as confirmed from XPS. Thus, KOH: UF mass ratio of 3 is found to be optimum. Hu *et al.* [186] prepared activated carbons by varying KOH:C ratio from 3 to 6, and pointed out that the sample prepared at 5-6 ratio was not favorable for CO_2 adsorption. Therefore, we have not considered this ratio beyond 4.

7.3.1.3 Activation temperature

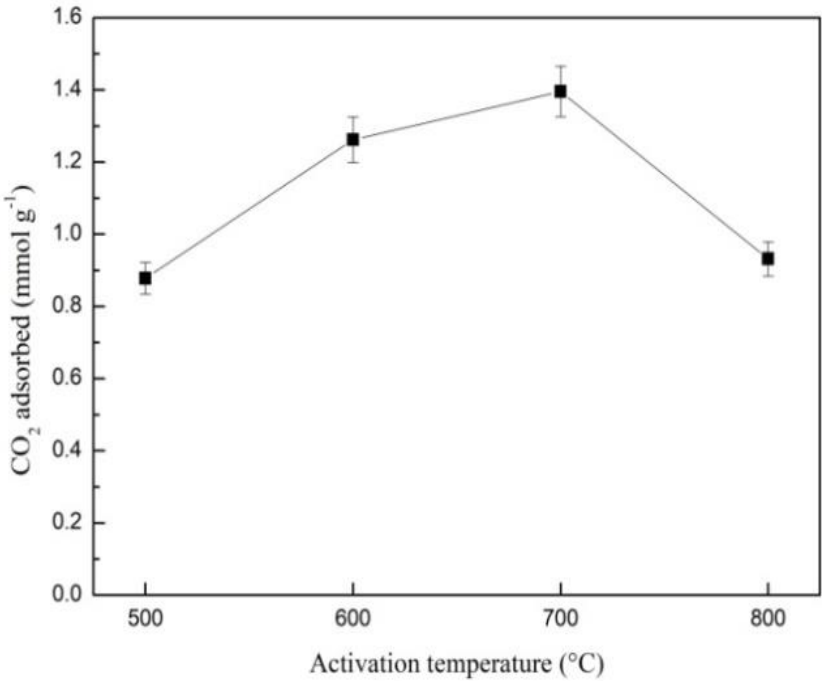

Fig. 7.17 Effect of activation temperature on CO_2 adsorption capacity at 12.5% CO_2 and 30 °C

Effect of activation temperature was also studied from 500 to 800 ˚C at fixed KOH:UF ratio of 3 and activation time of 2 h (Fig. 7.17). It was observed that the CO_2 uptake increased up to 700 ˚C. The CO_2 uptake at lower activation temperature shows lower value because at lower activation temperature, only a small amount of carbon atoms reacts with KOH, causing a small amount of formation of micropores whereas at higher temperature, more carbon atoms react that cause a large amount of formation of micro and mesopores. Similar results with increase in activation temperature were seen in N_2 adsorption-desorption section, because alkali metal atoms are getting removed resulting in generation of pores and increase in surface area and total pore volume. It is also observed from the Fig. 7.17 that further increase in activation temperature upto 800 ˚C, the CO_2 uptake decreased as micro- and meso-pores are burned off and matrix of carbon collapsed causing blockage of pores. Hence, the values of both the parameters decreased. Therefore, further studies were carried out with the optimized sample UFA-3-700.

7.3.2 Dynamic CO_2 adsorption performance

7.3.2.1 Effect of KOH:UF mass ratio

(a)

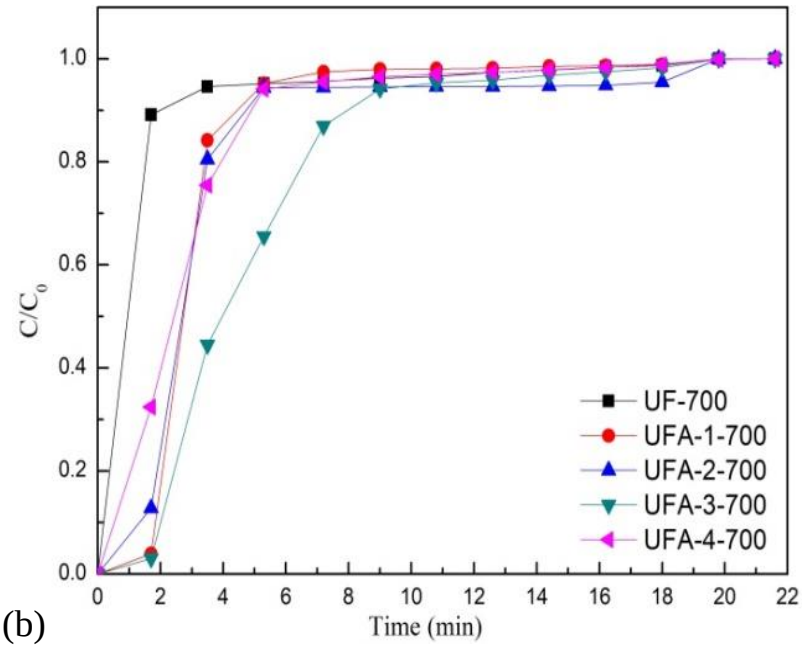

(b)

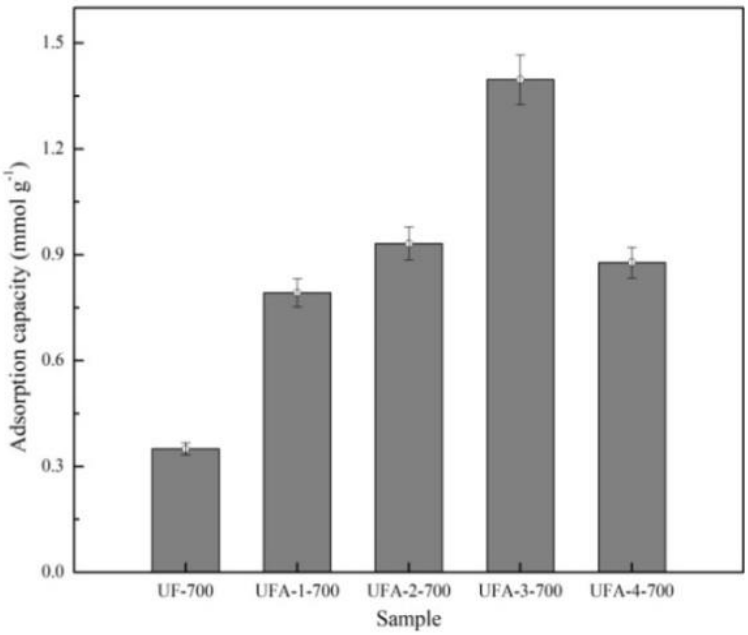

Fig. 7.18(a) CO_2 breakthrough curves, and (b) CO_2 adsorption capacity of carbons at 12.5% CO_2 and 30 °C

Fig. 7.18 shows CO_2 breakthrough curves and the equilibrium uptake capacity of the adsorbents under 12.5% CO_2 at 30 °C. It is seen that initially CO_2 was not detected in the bed outlet showing complete adsorption. After 1 min, CO_2 starts appearing in the effluent stream and mass transfer zone reaches bed outlet. Here, the sample UF-700 shows the steepest breakthrough curve and UFA-3-700 shows the broadest breakthrough curve. It is seen that increase in KOH:UF mass ratio up to 3 leads to increase in adsorption capacity but further increase in KOH:UF mass ratio causes decrease in CO_2 adsorption capacity.

Highest adsorption capacity for UFA-3-700 is seen because of increase in surface area, pore volume and higher basicity due to N1 and N2 as shown by XPS. UF-700 shows the lowest adsorption capacity amongst all because of poor textural property and acidic nature. CO_2 uptake capacity depends on both surface chemistry and textural properties [120]. Both adsorption capacity and breakpoint time (t_b) follow same order: UFZ-3-700>UFA-2-700>UFA-4-700>UFA-1-700>UF-700.

7.3.2.2 Effect of adsorption temperature and CO_2 feed concentration

7.3.2.2.1 Effect of adsorption temperature

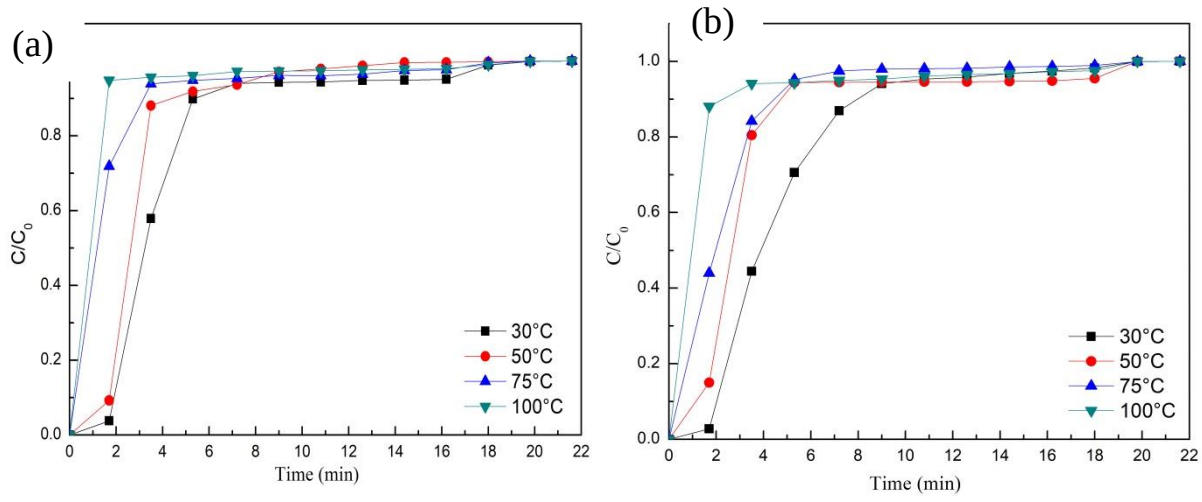

Fig. 7.19 CO_2 breakthrough curves at different temperatures for (a) 7.5% CO_2 and (b) 12.5% CO_2

Fig. 7.19 shows breakthrough curves at two CO_2 concentrations and different adsorption temperatures. It is seen that initially CO_2 molecules gets adsorbed completely in the pore sites and surface. At higher temperature, early saturation is achieved due to high energy. This is confirmed by shifting of breakpoint towards lower times as adsorption temperature

increases. Increase in adsorption temperature shows decrease in CO_2 adsorption capacity due to physiosorption nature. Similar observations was reported by Pevida *et al.* [187].

7.3.2.2.2 Effect of feed concentration

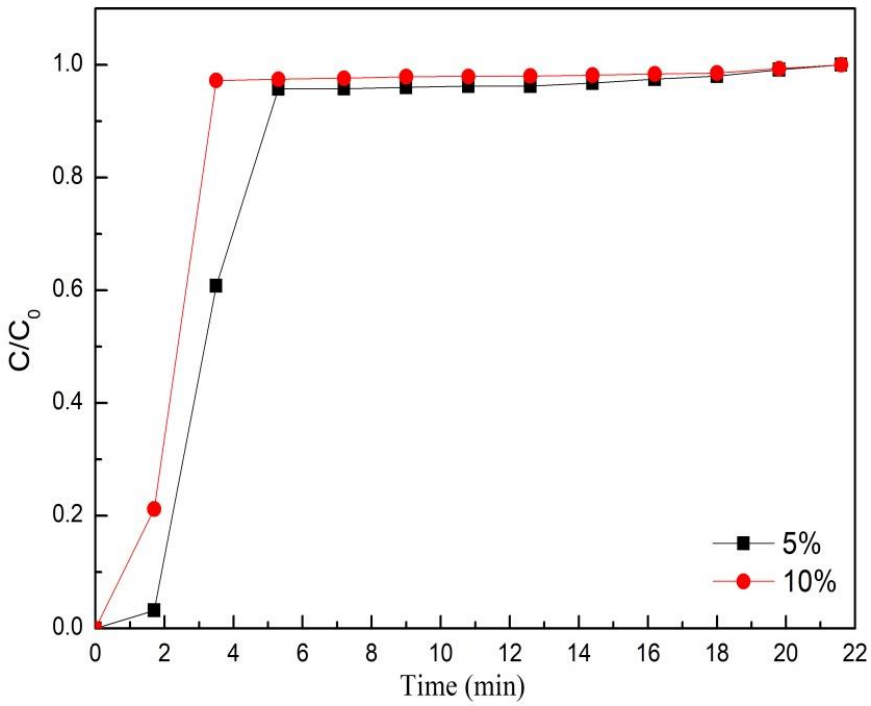

Fig. 7.20 CO_2 breakthrough curves for 5% and 10% CO_2 at 30 °C

Fig. 20 shows effect of CO_2 concentrations (5-10%) at fixed adsorption temperature (30 °C). With the increase in concentration from 5% to 10%, breakpoint appears earlier causing the bed to get saturated faster. This is seen that at 5%, breakpoint appears at 1.40 min, and at 10% it appears at 0.37 min. Similar observation was seen by Goel *et al.* [151]

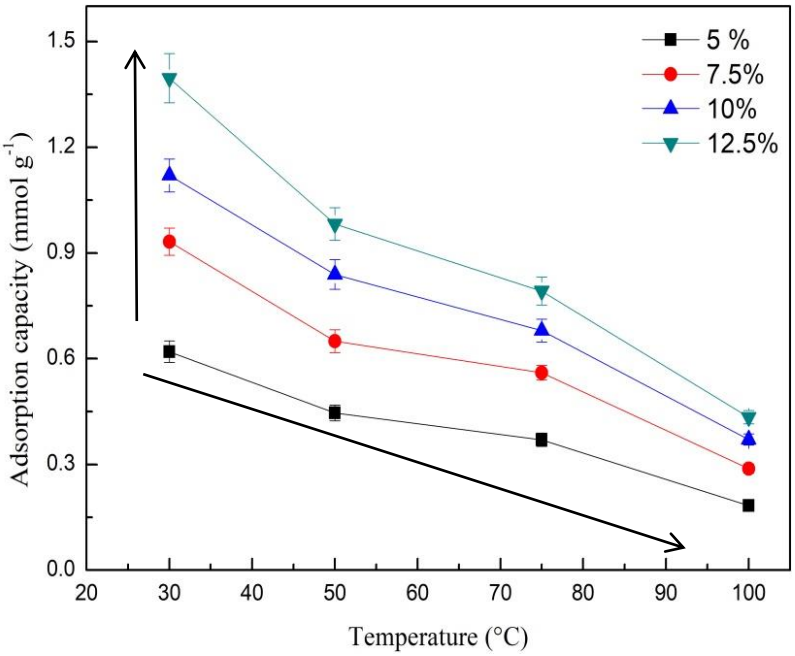

Fig. 7.21 CO_2 uptake capacity of adsorbent (UFA-3-700) at different temperatures and CO_2 concentrations

The above two effects are clearly seen in Fig. 7.21. Large number of active sites are taking part at high CO_2 concentration (12.5%), as seen from higher CO_2 uptake (1.40 mmol g^{-1}) while at lower CO_2 concentration (5%), adsorption capacity is 0.62 mmol g^{-1} due to lesser active sites taking part. On the other hand, with the increase in adsorption temperature from 30 to 100 °C at different CO_2 concentrations decrease in CO_2 uptake capacity is observed.

7.3.3 Adsorbent selectivity and regenerability

7.3.3.1 CO_2 selectivity

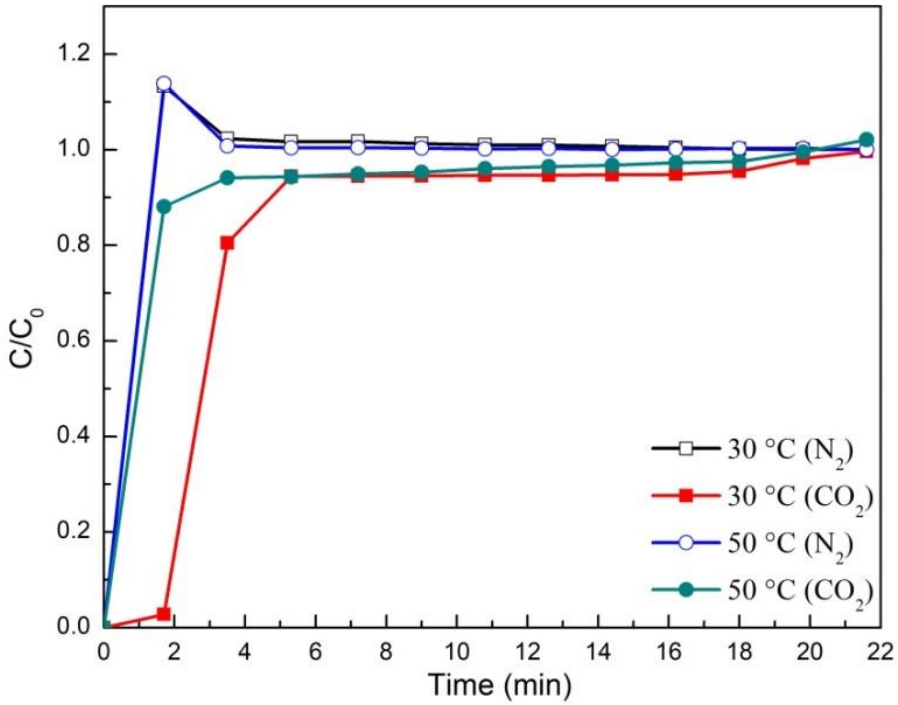

Fig. 7.23 CO_2/N_2 selectivity for 12.5% CO_2 (rest N_2) on UFA-3-700

Breakthrough curves of CO_2/N_2 at two different temperatures under 12.5% CO_2 (rest N_2) are shown in Fig. 7.23. It is seen that N_2 is detected immediately in comparison to CO_2. This indicates that N_2 adsorption capacity is very low as compared to CO_2. It is also seen that initial (C/C_0) value for N_2 is greater than 1 indicating that N_2 occupies more sites initially but as time progresses N_2 is replaced by CO_2 showing higher affinity of CO_2 in comparison to N_2. Similar pattern was reported by Goel *et al.* [138] also.

7.3.3.2 Cyclic adsorption/desorption study

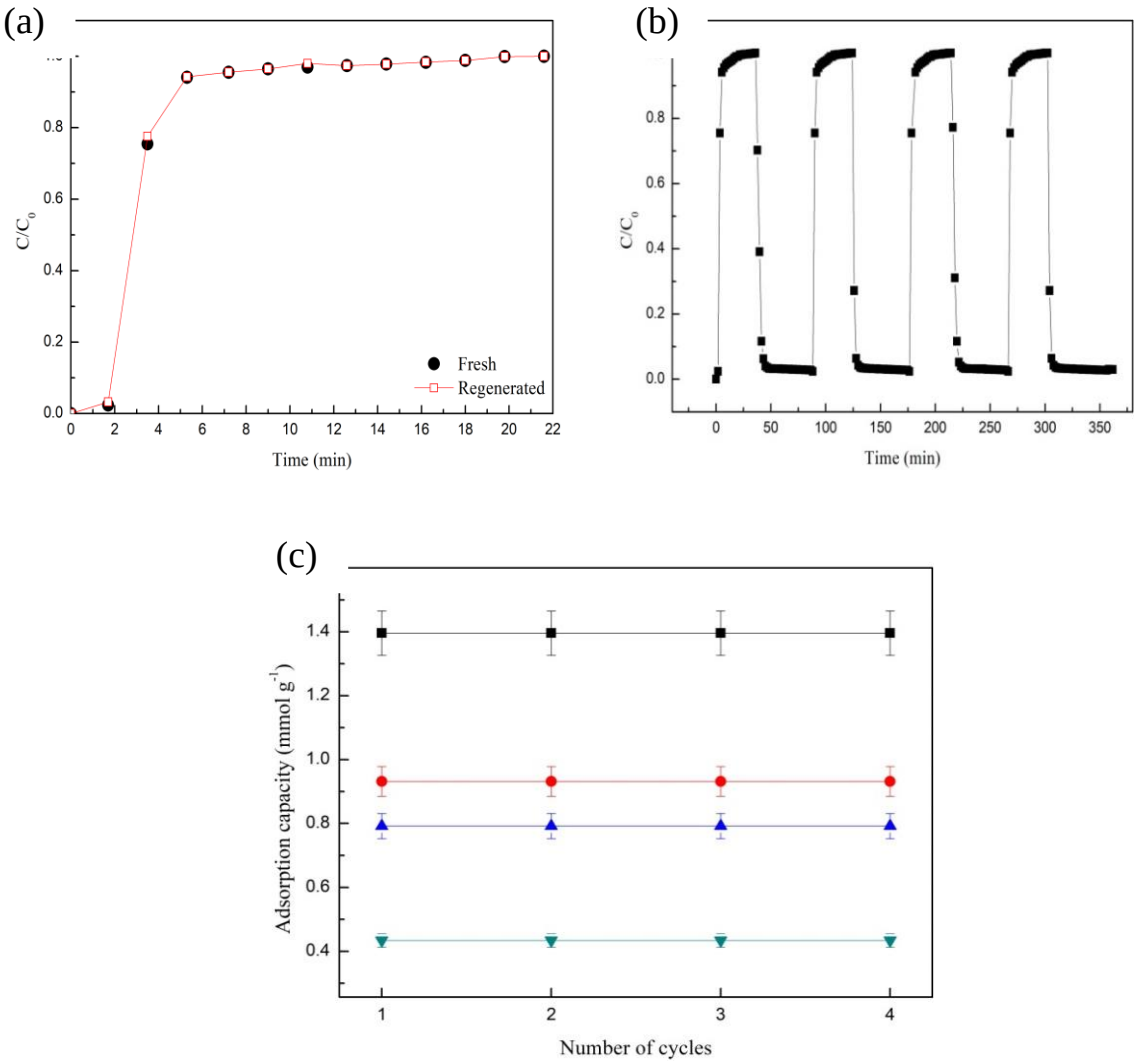

Fig. 7.22 (a) Breakthrough curves of fresh and regenerated adsorbents (b) multiple cycles of adsorption-desorption for UFA-3-700 at 30 °C and 12.5% CO_2 (c) multiple cycle CO_2 adsorption capacity at different temperatures

Regenerability, which is one of the important parameters of the adsorbents, is carried out after performing adsorption and by increasing temperature to 200 °C under N_2 atmosphere (50 ml min^{-1}). Similar breakthrough curve is seen in Fig. 7.23(a) of the fresh and regenerated adsorbent. This shows same adsorption capacity. Also, it is seen that CO_2 gets easily desorbed as shown in Fig. 7.23(b) from the sudden drop in CO_2 concentration to zero. Stability over four adsorption-desorption cycles is clearly seen in Fig. 7.23 (c).

7.4 Temperature programed desorption

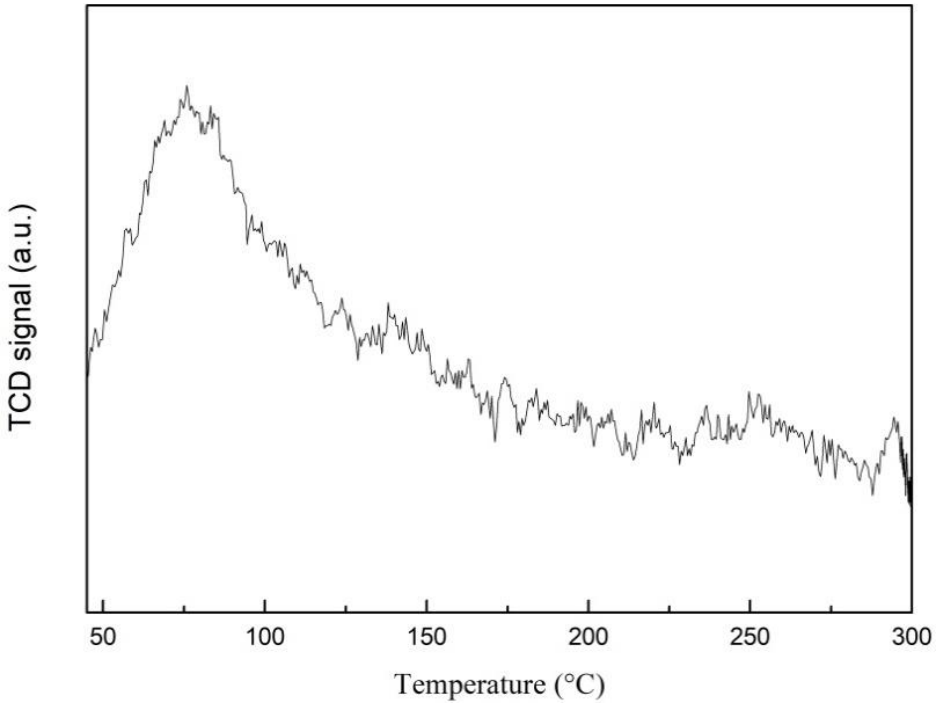

Fig. 7.24 Temperature programed desorption profile of CO_2 from UFA-3-700

Fig. 7.24 shows the TPD profile of UFA-3-700. Broad peak in the range of 70-110 °C is observed from TPD, with maximum of 80 °C. This may be because of removal of physically adsorbed CO_2 molecules from the adsorbent surface. Smaller contribution of chemisorption behavior is also seen from CO_2 signal which got smaller with a tail extending beyond 200 °C suggesting multiple type of adsorption sites with different binding strengths in this adsorbent. This also shows smaller contribution of chemisorption behavior. Similar kind of observation was also seen by Chen *et al.* [145] and Mane *et al.* [146] . Overall, it can be concluded that the adsorbent shows predominantly physisorption behavior.

Table 7.7 Chemically activated carbon adsorbents for CO_2 capture at atmospheric pressure (published during 2011-2017)

Precursor	Carbonization and activation conditions							**Max.** surface area (m^2 g^{-1})		Adsorption capacity (mmol g^{-1})				Reference
	Temp. (°C)	Time (h)	Activator	Impregnation ratio	Temp. (°C)	Time (h)	Flow rate (ml min^{-1})		CO_2 concn	0° C	25°C	50° C	75°C	100 °C	
Fly ash	-	-	KOH	5:1	700	2	-	161	100	-	0.6				[188]
Rice husk	-	-	$ZnCl_2$	1:1	500	1	100	927	100	-	1.3	-	0.5	-	[189]
Anthracite			steam			2		540	100		1.5				[190]
N-containing resin			K_2CO_3	1:1	700	1	11	1283	8		1.9				[110]
Carpet			KOH	1:1	800	1	100	1910.17	15		1.9				[191]
Urea*	**700**	**2**	**KOH**	**3:1**	**700**	**2**	**60**	**4547**		**-**	**1.40***	**0.93**	**0.79**	**0.43**	**Present work**
Bagasse	-	-	$ZnCl_2$	1:1	500	1	80	924	100	2.7	-	-	-	-	[189]
Polyfurfuryl Alcohol			KOH	4:1	800	1		2660	100		3.2				[192]
Urea	600	-	KOH	2:1	600	-	50	3581	100	-	3.21	-	1.27	-	[114]
Peanut shell	500	1.5	KOH	1:1	700	1.5	120	956	100	5.2	4.0	-	-	-	[193]
Bamboo	500	1.5	KOH	3:1	600	1.5	-	1846	100	7.0	4.5	-	-	-	[194]
Sawdust	230-250	2	KOH	2:1	600	1	-	1260	100	6.1	4.8	3.6		-	[195]
Sawdust	-	-	KOH	4:1	700	1	-	1643	100	8.0	4.8	-	-	-	[196]

**under dynamic conditions (all others in static conditions)*

Comparisons of surface area and adsorption capacity obtained in this work are done with the reported literature at different adsorption temperatures and CO_2 concentrations in Table 7.7. KOH seems to be the best activation agent by comparing the literature with our study which shows improvement in better surface area and adsorption capacity. It is also seen that our study reported the best surface area for any carbon adsorbents by optimizing proper activation conditions. Adsorption capacity reported in literature (few cases) is higher but CO_2 evaluation was not carried out by dynamic method which is more relevant for the flue gas point application. The other study by Martin *et al.* [191] using carpet under dynamic condition shows lower CO_2 uptake capacity in comparison to our study. Therefore, carbon material synthesized in this study seems to be a new promising carbon material for CO_2 capture from power plant flue gas and other relevant applications.

7.5 Kinetic study

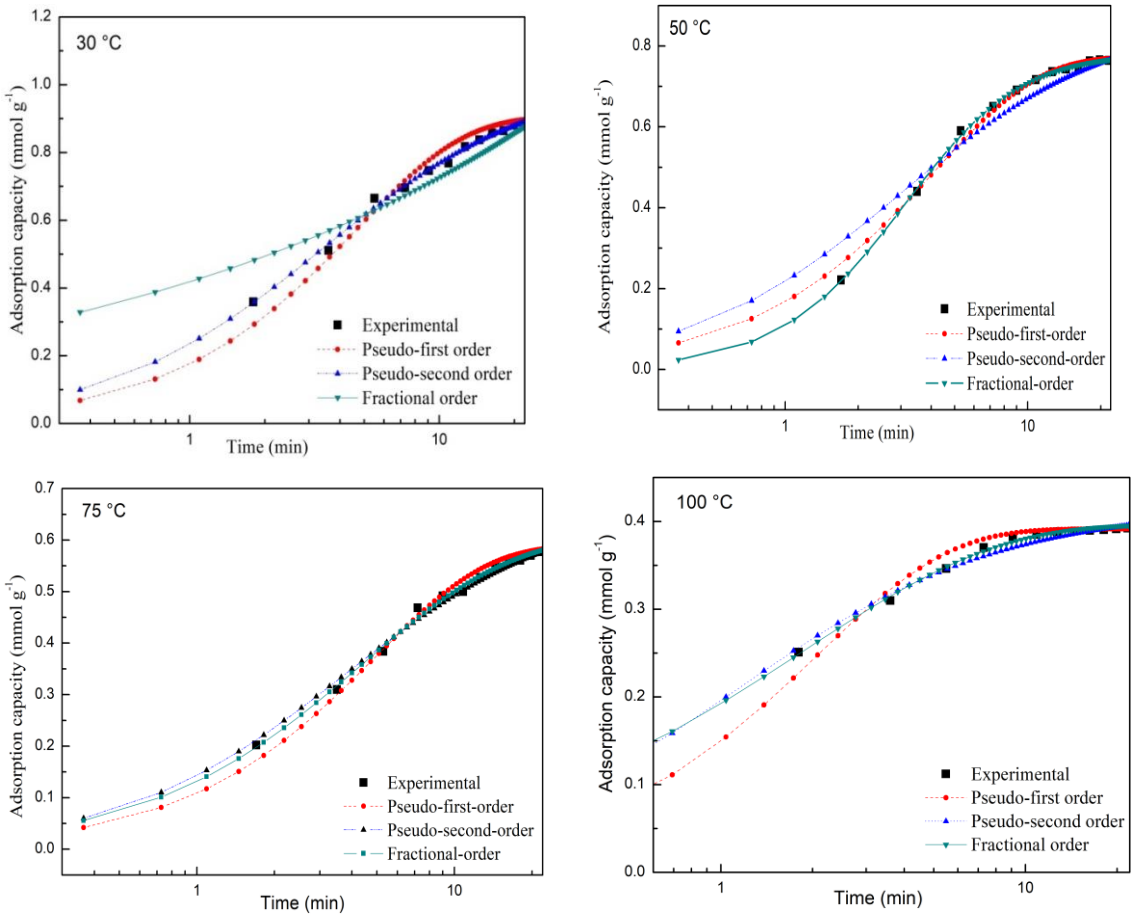

Fig. 7.25 Experimental and model predicted CO_2 uptake at 10% CO_2 and different temperatures

Table 7.8 Kinetic parameters of CO_2 adsorption on UFA-3-700

Model	Parameters	Temperature (°C)			
		30	50	75	100
Pseudo-first –order	k_1	0.21	0.18	0.11	0.24
	q_e	0.90	0.85	0.65	0.30
	R^2	0.98	0.90	0.97	0.85
	Error %	2.80	1.73	2.89	3.55
Pseudo-second –order	k_2	0.29	0.20	0.12	1.04
	q_e	1.02	1.01	0.84	0.33
	R^2	0.998	0.87	0.95	0.93
	Error %	7.83	4.71	1.36	2.48
Fractional –order	k_n	0.43	0.39	0.28	0.07
	q_e	0.94	0.84	0.86	0.34
	n	7.31	3.13	1.65	1.42
	m	7.28	5.88	1.38	0.30
	R^2	0.998	0.992	0.992	0.983
	Error %	1.30	1.45	1.6	0.95

Fig. 7.25 shows experimental and model predicted CO_2 uptake of samples as a function of time and their values of estimated parameters are shown in Table 7.8. It is seen that within 10 minutes, adsorption happened at a very high rate and further it gets slowed down until it reached equilibrium. This is because of decrease in unoccupied active sites and increase in diffusion resistance. Low R^2 and higher error% value and overestimated or underestimated at different regions confirmed that both pseudo-first and pseudo-second order not fitted properly. Fractional order kinetic model better predicted the kinetics of adsorption as compared to other models. This is further confirmed by lower value of error% and higher value of R^2 value, i.e., >0.99. Exothermic nature was confirmed with decrease in rate constant k_n, with rise in

temperature. Higher driving force was confirmed from higher value of *n* at 30 °C. Similar kind of observation was also seen by Liu *et al.* [180].

7.6 Isotherm study

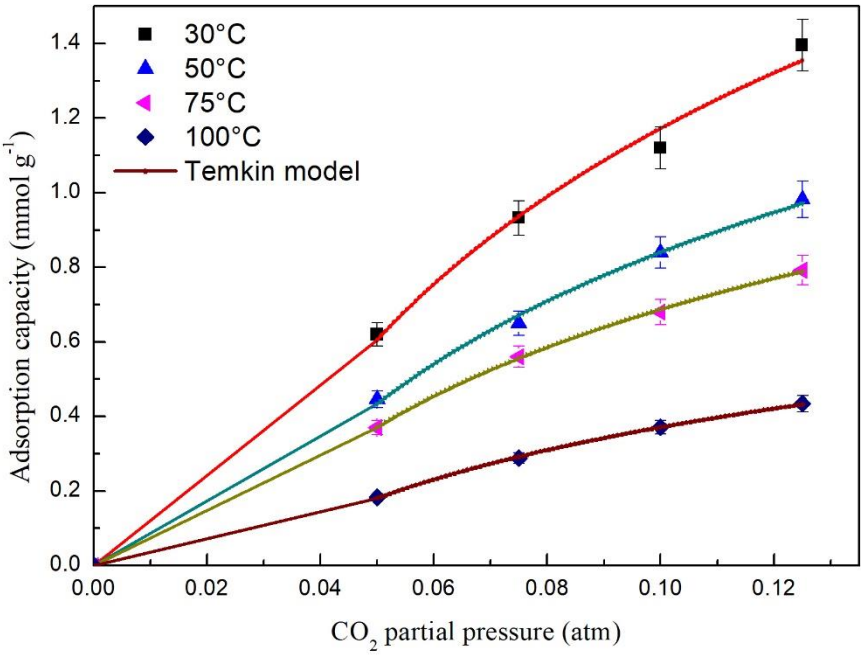

Fig. 7.26 Experimental and model predicted CO_2 uptake isotherm on UFA-3-700 values

Experimental and model predicted adsorption data for sample UFA-3-700 at different adsorption temperatures are shown in Fig. 7.26. Its corresponding parameter values are reported in Table 7.9. It is seen that among all the isotherms, Temkin isotherm fitted well indicating energetically heterogeneous nature of the adsorbent surface [55]. Physical adsorption process was confirmed by lower Temkin model constant *b* value i.e., <20 kJ mol^{-1}. Favorable adsorption at lower temperature and exothermic nature was confirmed from Freundlich parameter K_F and decrease in K_F and q_m values with rise of temperature. Higher value of n>1, indicates favorable adsorption condition [181].

Table 7.9 Adsorption isotherm of CO_2 adsorption onto UFA-3-700

Langmuir			
T (°C)	K_L (atm $^{-1}$)	q_m (mmol g^{-1})	R^2
30	3.29	6.94	0.98
50	2.16	4.64	0.997
75	1.99	2.73	0.983
100	1.45	2.37	0.98
Freundlich			
	K_F (mmol g^{-1} atm $^{-1/n}$)	n	R^2
30	8.20	1.17	0.989
50	5.78	1.98	0.995
75	4.12	1.27	0.990
100	2.88	1.11	0.985
Temkin			
	K_T (atm^{-1})	b (kJ mol^{-1})	R^2
30	41.87	3.11	0.98
50	45.24	4.63	0.993
75	38.87	6.42	0.998
100	35.78	11.48	0.998

7.7 Thermodynamic study

7.7.1 Thermodynamic parameters

Thermodynamic parameter values for CO_2 adsorption on UFA-3-700 at different adsorption temperatures, is reported in Table 7.10. As expected, exothermic nature is confirmed from the negative value of $\Delta H°$. $\Delta G°$ value was found to be negative at all temperatures showing spontaneity and feasibility of the adsorption process.

Table 7.10 Adsorption thermodynamic constants for CO_2 adsorption on UFA-3-700

Temperature (°C)	$\Delta G°$ (kJ mol^{-1})	$\Delta H°$ (kJ mol^{-1})	$\Delta S°$ (kJ $mol^{-1}K^{-1}$)
30	-9.30	-1.991	0.03
50	-10.24		
75	-10.59		
100	-11.09		

Isosteric heat of adsorption (Q_{st}) calculated from the Clausius-Clapeyron equation at a selected adsorbed amount of CO_2 [136] is shown in Fig. 7.27 and the corresponding values are reported in Table 7.11. The Q_{st} ranged from -14.71 to -16.99 kJ mol^{-1}, which are typical for physical adsorption [197]. Average value of Q_{st} (-16.15 kJ mol^{-1}) is found to be lower than for CO_2 adsorption on activated carbon (-20.3 kJ mol^{-1})[148]. Heterogeneous nature of adsorbent surface is seen by random trend obtained by Q_{st} value. This also indicates that molecules are attached by weak van der Waals forces to the surface which get easily desorbed.

Table 7.**11** Isosteric heat of adsorption at different q_e values

q_e (mmol g^{-1})	Q_{st} (kJ mol^{-1})
0.1	-14.81
0.15	-15.23
0.2	-16.73
0.25	-17.22
3	-16.89
Average	-16.17

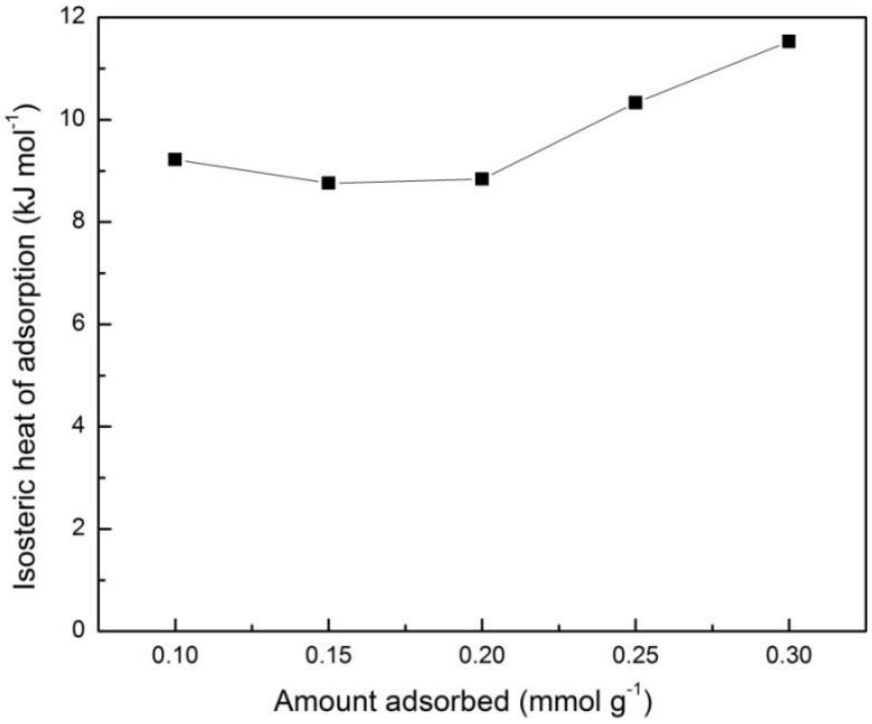

Fig. 7.27 Isosteric heat of adsorption of CO_2 on UFZ-700

7.7.2 Energy duty for desorption of CO_2

C_p for UFA-3-700 = 1.215 J g^{-1} K^{-1} (Calculated from DSC data)

Adsorption conditions: 30 °C, 12.5% CO_2 in N_2

Desorption conditions: 200 °C, 100% N_2

$\Delta T = (200 - 30)\,℃ = 170\,℃$

UFA-3-700 adsorption capacity

$$= 1.42 \text{ mmol } CO_2 \text{ per g adsorbent}$$
$$= 0.06248 \text{ kg } CO_2 \text{ per kg adsorbent}$$

$$\text{Hence, sensible heat} = \frac{1.2 \times 170}{1.42 \times 10^{-3}} \text{ J per mole CO2} = 143.66 \text{ kJ per mole } CO_2$$

Net sensible heat $= 35.91$ kJ per mole CO_2 (for 75% recovery of sensible heat [149])

Isosteric heat of adsorption, Q_{st} = 16.17 kJ per mole CO_2

Thermal energy input $= (16.17 + 35.91) = 52.08$ kJ per mole CO_2
$= 1.18$ MJ per kg CO_2

Therefore, desorption of 1.40 mmol g^{-1} of CO_2 which is equal to 0.06248 kg CO_2 per kg adsorbent**,** Energy required = 1.18×0.06248

= 0.073 MJ

Thus, CO_2 generated to produce 0.073 MJ of energy for desorption = 0.0884×0.073 kg CO_2

$= 6.51 \times 10^{-3}$ kg CO_2

= 0.00651 kg CO_2

7.8 Conclusions

An effective high surface area and high adsorption capacity adsorbent has been developed from urea-formaldehyde resin using optimized KOH activation conditions. XPS confirms the nitrogen functional groups' existence. Adsorbent capacity follows the order of UFA-3-700>UFA-2-700>UFA-4-700>UFA-1-700>UF-700. The highest adsorption capacity of 1.42 mmol g^{-1} for UFA-3-700 is obtained. Furthermore, it shows complete regenerability, stability, exothermic nature and better selectivity for CO_2 over N_2. Fractional order kinetic model provided best fit amongst all kinetic models tested. Heterogeneity of the adsorbent surface was confirmed from Temkin adsorption isotherm model fit and isosteric heat of adsorption values. Negative values of $\Delta G°$ and $\Delta H°$ confirm spontaneous, feasible and exothermic nature of adsorption process.

Chapter 8 - Conclusions and Recommendations for Future Work

8.1 Conclusions

High nitrogen containing MF resin as precursor and mesoporous zeolite MCM-41 as template using nanocasting technique results in development of nitrogen enriched nanostructured carbon adsorbents. Synthesized carbons show dependency on carbonization-activation temperature for their textural, surface and chemical properties. Carbon adsorbent shows highest surface area of 193 $m^2 g^{-1}$, pore volume of 0.32 $cm^3 g^{-1}$, nitrogen content of 22.27% and dynamic CO_2 uptake capacity of 0.64 mmol g^{-1}. The CO_2 capture capacity depends on both textural properties and nitrogen moieties.

High oxygen content epoxy resin as precursor using a nanocasting technique and template zeolite results in development of oxygen enriched nanostructured carbon adsorbents with high oxygen content (53.98 %), highest surface area (S_{BET} = 686 $m^2 g^{-1}$), pore volume (0.60 $cm^3 g^{-1}$) and highest CO_2 uptake of 0.65 mmol g^{-1}. The CO_2 capture capacity in addition to textural properties depends more on oxygen moieties.

High nitrogen containing UF resin as precursor and mesoporous zeolite MCM-41 as template using nanocasting technique results in development of nanostructured carbon having high surface area (337 $m^2 g^{-1}$) and mesopores (0.644 $cm^3 g^{-1}$). The CO_2 capture capacity depends more on the nitrogen functionalities in addition to textural properties and nitrogen content as UFZ-700 shows highest CO_2 adsorption of 0.84 mmol g^{-1}.

High nitrogen containing UF resin using a standard chemical activation with KOH results in development of high surface area carbon adsorbents till now with maximum surface area of 4547 $m^2 g^{-1}$. The CO_2 capture capacity depends on both the nitrogen functionalities and textural properties with maximum CO_2 uptake of 1.40 mmol g^{-1} for UFA-3-700.

XRD and TEM results confirmed nanostructure development. SEM results show better textural properties as compared to direct carbonized samples. Elemental analysis and XPS show

presence of nitrogen and oxygen content. For carbonization above 800 °C, the pore structure collapses partially leading to changes in textural properties, basicity imparted from both oxygen and nitrogen moieties and reduction in CO_2 uptake. CO_2 capture under dynamic conditions is highest at 700 °C for all the adsorbents. Decrease in CO_2 uptake capacity with increase in adsorption temperature shows exothermic adsorption process for all the adsorbents. Adsorbents show complete regenerability over multiple adsorption-desorption cycles. Among three kinetic models, fractional-order-model shows the best description for all the developed adsorbents at various temperatures with negative temperature dependence of rate constant. Heterogeneity of the adsorbent surface was confirmed from adsorption isotherm model fitting and isosteric heat of adsorption values. Adsorbent shows predominantly physisorption behavior with smaller contribution of chemisorption. Gibbs free energy change show feasibility and spontaneity of the adsorption process while enthalpy change indicated adsorption process to be exothermic in nature.

Urea based nitrogen enriched adsorbent obtained from physical activation with CO_2 and having highest CO_2 adsorption capacity of 0.84 mmol g^{-1} is best among the nanocasted adsorbent. While Urea based high surface area nitrogen enriched adsorbent obtained from chemical activation with KOH and having highest CO_2 adsorption capacity of 1.4 mmol g^{-1} is best among the without nanocasted adsorbent.

On direct carbonizing the polymeric resin, the carbon adsorbent exhibited poor surface area, pore volume, nitrogen content, surface basicity and least CO_2 uptake capacity, confirming advantage of nanocasting technique for developing carbon adsorbents with better properties and CO_2 uptake capacity which is a requirement in field of CO_2 capture.

Nature of the starting material i.e. polymeric precursor has a great effect on the kind of functional groups present on the carbon surface which affect the CO_2 adsorption capacity. Presence of nitrogen and oxygen moieties greatly affects the basic character of carbons thereby affecting the CO_2 adsorption.

The present work is a comprehensive study of development, characterization and performance evaluation, under dynamic conditions, of carbons adsorbents from nanocasting technique, direct carbonization followed by chemical activation and also for kinetics, isotherm and thermodynamic studies of CO_2 adsorption.

8.2 Recommendations for future work

- Synthesis of different carbon adsorbents can be carried out by using other template materials like silica (MCM-48 and SBA-15) and can be investigated for CO_2 capture.
- Effect of chemical activation, carbonization-activation conditions, like heating rate, and carbonization time, on the properties of the nanocasted carbons should be investigated that will further affect the CO_2 adsorption capacity.
- Further adsorption study of these developed carbons should be undertaken at high pressure conditions for other applications.
- Effect of various impurities like, SO_x and NO_x on CO_2 adsorption performance of these carbons can be evaluated in order to have complete overview of the capture process.

References

[1] M.K. Mondal, H.K. Balsora, P. Varshney, Progress and trends in CO_2 capture/separation technologies: A review, *Energy* 46 (2012) 431-441.

[2] S. Suresh, V. Srivastava, I. Mishra, Isotherm, thermodynamics, desorption, and disposal study for the adsorption of catechol and resorcinol onto granular activated carbon, *Journal of Chemical & Engineering Data* 56 (2010) 811-818.

[3] IPCC, 2014: Climate Change 2014: Mitigation of Climate Change. Contribution of working group III to the fifth assessment report of the Intergovernmental panel on climate change, in: O. Edenhofer, R. Pichs-Madruga, Y. Sokona, E. Farahani, S. Kadner, K. Seyboth, A. Adler, I. Baum, S. Brunner, P. Eickemeier, B. Kriemann, J. Savolainen, S. Schlömer, C. von Stechow, T. Zwickel, J.C. Minx (Eds.) Cambridge, United Kingdom and New York, NY, USA, 2014.

[4] IEA, Energy Technology Perspectives 2012: Pathways to a Clean Energy System, OECD Publishing, Paris, 2012.

[5] K.M.K. Yu, I. Curcic, J. Gabriel, S.C.E. Tsang, Recent advances in CO_2 capture and utilization, *ChemSusChem* 1 (2008) 893-899.

[6] R. Pietrzak, P. Nowicki, J. Kaźmierczak, I. Kuszyńska, J. Goscianska, J. Przepiórski, Comparison of the effects of different chemical activation methods on properties of carbonaceous adsorbents obtained from cherry stones, *Chemical Engineering Research and Design* 92 (2014) 1187-1191.

[7] S.I. Plasynski, J.T. Litynski, H.G. McIlvried, R.D. Srivastava, Progress and new developments in carbon capture and storage, *Critical Reviews in Plant Sciences* 28 (2009) 123-138.

[8] R. Lal, Sequestering atmospheric carbon dioxide, *Critical Reviews in Plant Sciences* 28 (2009) 90-96.

[9] U.S.E.P. Agency, *Climate change indicators in the United States*, 2014.

[10] P. Markewitz, W. Kuckshinrichs, W. Leitner, J. Linssen, P. Zapp, R. Bongartz, A. Schreiber, T.E. Muller, Worldwide innovations in the development of carbon capture technologies and the utilization of CO_2, *Energy & Environmental Science* 5 (2012) 7281-7305.

[11] M. Sharma, R.K. Vyas, K. Singh, A review on reactive adsorption for potential environmental applications, *Adsorption* 19 (2013) 161-188.

[12] H. Yang, Z. Xu, M. Fan, R. Gupta, R.B. Slimane, A.E. Bland, I. Wright, Progress in carbon dioxide separation and capture: A review, *Journal of Environmental Sciences* 20 (2008) 14-27.

[13] R. Steeneveldt, B. Berger, T.A. Torp, CO_2 capture and storage: Closing the knowing–doing gap, *Chemical Engineering Research and Design* 84 (2006) 739-763.

[14] S.-Y. Lee, S.-J. Park, A review on solid adsorbents for carbon dioxide capture, *Journal of Industrial and Engineering Chemistry* 23 (2015) 1-11.

[15] S. Sengupta, Studies on CO_2 capture using adsorption from simulated refinery flue gas, *Ph. D. Thesis,* Department of Chemical Engineering, Thapar University, Patiala, 2015.

[16] T. Wall, R. Stanger, Y. Liu, Gas cleaning challenges for coal-fired oxy-fuel technology with carbon capture and storage, *Fuel* 108 (2013) 85-90.

[17] B.J.P. Buhre, L.K. Elliott, C.D. Sheng, R.P. Gupta, T.F. Wall, Oxy-fuel combustion technology for coal-fired power generation, *Progress in Energy and Combustion Science* 31 (2005) 283-307.

[18] E.S. Rubin, H. Mantripragada, A. Marks, P. Versteeg, J. Kitchin, The outlook for improved carbon capture technology, *Progress in Energy and Combustion Science* 38 (2012) 630-671.

[19] K. Goto, K. Yogo, T. Higashii, A review of efficiency penalty in a coal-fired power plant with post-combustion CO_2 capture, *Applied Energy* 111 (2013) 710-720.

[20] J.D. Figueroa, T. Fout, S. Plasynski, H. McIlvried, R.D. Srivastava, Advances in CO_2 capture technology—The U.S. Department of Energy's Carbon Sequestration Program, *International Journal of Greenhouse Gas Control* 2 (2008) 9-20.

[21] C.W. Jones, CO_2 capture from dilute gases as a component of modern global carbon management, *Annual Review of Chemical and Biomolecular Engineering* 2 (2011) 31-52.

[22] R. Dong, H. Lu, Y. Yu, Z. Zhang, A feasible process for simultaneous removal of CO_2, SO_2 and NO_x in the cement industry by NH_3 scrubbing, *Applied Energy* 97 (2012) 185-191.

[23] Y. Lv, X. Yu, J. Jia, S.-T. Tu, J. Yan, E. Dahlquist, Fabrication and characterization of superhydrophobic polypropylene hollow fiber membranes for carbon dioxide absorption, *Applied Energy* 90 (2012) 167-174.

[24] Y. Lv, X. Yu, S.-T. Tu, J. Yan, E. Dahlquist, Experimental studies on simultaneous removal of CO_2 and SO_2 in a polypropylene hollow fiber membrane contactor, *Applied Energy* 97 (2012) 283-288.

[25] C.F. Song, Y. Kitamura, S.H. Li, Evaluation of Stirling cooler system for cryogenic CO_2 capture, *Applied Energy* 98 (2012) 491-501.

[26] R. Van Benthum, H. Van Kemenade, J. Brouwers, M. Golombok, Condensed rotational separation of CO_2, *Applied Energy* 93 (2012) 457-465.

[27] M. Zhang, Y. Guo, Rate based modeling of absorption and regeneration for CO_2 capture by aqueous ammonia solution, *Applied Energy* 111 (2013) 142-152.

[28] R. Idem, T. Supap, H. Shi, D. Gelowitz, M. Ball, C. Campbell, P. Tontiwachwuthikul, Practical experience in post-combustion CO_2 capture using reactive solvents in large pilot and demonstration plants, *International Journal of Greenhouse Gas Control* 40 (2015) 6-25.

[29] R. Muraleedharan, A. Mondal, B. Mandal, Absorption of carbon dioxide into aqueous blends of 2-amino-2-hydroxymethyl-1, 3-propanediol and monoethanolamine, *Separation and Purification Technology* 94 (2012) 92-96.

[30] A. Veawab, A. Aroonwilas, P. Tontiwachwuthikul, CO_2 absorption performance of aqueous alkanolamines in packed columns, *Fuel Chemistry Division Preprints* 47 (2002) 49-50.

[31] D. Aaron, C. Tsouris, Separation of CO_2 from flue gas: a review, *Separation Science and Technology* 40 (2005) 321-348.

[32] B.E. Gurkan, J.C. de la Fuente, E.M. Mindrup, L.E. Ficke, B.F. Goodrich, E.A. Price, W.F. Schneider, J.F. Brennecke, Equimolar CO_2 absorption by anion-functionalized ionic liquids, *Journal of the American Chemical Society* 132 (2010) 2116-2117.

[33] F. Bougie, M.C. Iliuta, CO_2 absorption in aqueous piperazine solutions: experimental study and modeling, *Journal of Chemical & Engineering Data* 56 (2011) 1547-1554.

[34] R. Ben-Mansour, M. Habib, O. Bamidele, M. Basha, N. Qasem, A. Peedikakkal, T. Laoui, M. Ali, Carbon capture by physical adsorption: Materials, experimental investigations and numerical modeling and simulations–A review, *Applied Energy* 161 (2016) 225-255.

[35] S.A. Rackley, Carbon capture and storage, Gulf Professional Publishing 2009.

[36] C. Goel, Preparation of adsorbent(s) using nano-casting technique for carbon dioxide capture from flue gases, *M.Tech. Thesis* Thapar University, Patiala, India 2011.

[37] S.-H. Ho, C.-Y. Chen, D.-J. Lee, J.-S. Chang, Perspectives on microalgal CO_2-emission mitigation systems—a review, *Biotechnology Advances* 29 (2011) 189-198.

[38] N Hedin, L Andersson, L Bergström, J Yan. Adsorbents for the post-combustion capture of CO_2 using rapid temperature swing or vacuum swing adsorption. *Applied Energy*. 104 (2013) 418-33.

[39] H. Deng, H. Yi, X. Tang, Q. Yu, P. Ning, L. Yang, Adsorption equilibrium for sulfur dioxide, nitric oxide, carbon dioxide, nitrogen on 13X and 5A zeolites, *Chemical Engineering Journal* 188 (2012) 77-85.

[40] X. Hu, E. Mangano, D. Friedrich, H. Ahn, S. Brandani, Diffusion mechanism of CO_2 in 13X zeolite beads, *Adsorption* 20 (2014) 121-135.

[41] S.G. Cavenati, C. A. and Rodrigues, A. E., , Adsorption equilibrium of methane, carbon dioxide and nitrogen on zeolite 13X at high pressures, *Journal of Chemical & Engineering Data* 49 (2004) 1095-1101.

[42] H.-M. Yoo, S.-Y. Lee, S.-J. Park, Ordered nanoporous carbon for increasing CO_2 capture, *Journal of Solid State Chemistry* 197 (2013) 361-365.

[43] D. Wang, X. Ma, C. Sentorun-Shalaby, C. Song, Development of carbon-based "Molecular Basket" sorbent for CO_2 capture, *Industrial & Engineering Chemistry Research* 51 (2012) 3048-3057.

[44] K. Sumida, D.L. Rogow, J.A. Mason, T.M. McDonald, E.D. Bloch, Z.R. Herm, T.H. Bae, J.R. Long, Carbon dioxide capture in metal-organic frameworks, *Chemical Reviews* 112 (2012) 724-781.

[45] L. Bastin, P.S. Barcia, E.J. Hurtado, J.A.C. Silva, A.E. Rodrigues, B. Chen, A microporous metal−organic framework for separation of CO_2/N_2 and CO_2/CH_4 by fixed-bed adsorption, *The Journal of Physical Chemistry C* 112 (2008) 1575-1581.

[46] X. Xu, X. Zhao, L. Sun, X. Liu, Adsorption separation of carbon dioxide, methane and nitrogen on monoethanol amine modified β-zeolite, *Journal of Natural Gas Chemistry* 18 (2009) 167-172.

[47] M.R. Melloa, D. Phanon, G.Q. Silveira, P.L. Llewellyn, C.M. Ronconi, Amine-modified MCM-41 mesoporous silica for carbon dioxide capture, *Microporous and Mesoporous Materials* 143 (2011) 174-179.

[48] M.D. Hornbostel, J. Bao, G. Krishnan, A. Nagar, I. Jayaweera, T. Kobayashi, A. Sanjurjo, J. Sweeney, D. Carruthers, M.A. Petruska, Characteristics of an advanced carbon sorbent for CO_2 capture, *Carbon* 56 (2013) 77-85.

[49] Z. Liu, C.A. Grande, P. Li, J. Yu, A.E. Rodrigues, Multi-bed vacuum pressure swing adsorption for carbon dioxide capture from flue gas, *Separation and Purification Technology* 81 (2011) 307-317.

[50] R.P.P.L. Ribeiro, C.A. Grande, A.E. Rodrigues, Adsorption of water vapor on carbon molecular sieve: thermal and electrothermal regeneration study, *Industrial & Engineering Chemistry Research* 50 (2011) 2144-2156.

[51] J.C.M. Pires, F.G. Martins, M.C.M. Alvim-Ferraz, M. Simões, Recent developments on carbon capture and storage: An overview, *Chemical Engineering Research and Design* 89 (2011) 1446-1460.

[52] L Wang, Y Yang, W Shen, X Kong, P Li, J Yu, A. Rodrigues. CO_2 capture from flue gas in an existing coal-fired power plant by two successive pilot-scale VPSA units. *Industrial & Engineering Chemistry Research*. 52 (2013) 7947-55.

[53] J. Merel, M. Clausse, F. Meunier, Experimental investigation on CO_2 post-combustion capture by indirect thermal swing adsorption using 13X and 5A zeolites, *Industrial & Engineering Chemistry Research* 47 (2008) 209-215.

[54] R.V. Siriwardane, M.-S. Shen, E.P. Fisher, Adsorption of CO_2 on zeolites at moderate temperatures, *Energy & Fuels* 19 (2005) 1153-1159.

[55] R.T. Yang, Adsorbents: Fundamentals And Applications, John Wiley & Sons, Inc.2003.

[56] M. Sharma, R.K. Vyas, K. Singh, A review on reactive adsorption for potential environmental applications, *Adsorption* 19 (2012) 161-188.

[57] C.S. Xiaochun Xu, John M. Andresen, Bruce G. Miller, and Alan W. Scaroni, Novel polyethylenimine-modified mesoporous molecular sieve of MCM-41 type as high-capacity adsorbent for CO_2 capture, *Energy & Fuels* 16 (2002) 1463-1469.

[58] X. Xu, C. Song, B.G. Miller, A.W. Scaroni, Adsorption separation of carbon dioxide from flue gas of natural gas-fired boiler by a novel nanoporous “molecular basket” adsorbent, *Fuel Processing Technology* 86 (2005) 1457-1472.

[59] X. Xu, C. Song, B.G. Miller, A.W. Scaroni, Influence of moisture on CO_2 separation from gas mixture by a nanoporous adsorbent based on polyethylenimine-modified molecular sieve MCM-41, *Industrial & Engineering Chemistry Research* 44 (2005) 8113-8119.

[60] X. Xu, C. Song, J.M. Andresen, B.G. Miller, A.W. Scaroni, Adsorption separation of CO_2 from simulated flue gas mixtures by novel CO_2 "molecular basket" adsorbents, *International Journal of Environmental Technology and Management* 4 (2004) 32-52.

[61] X. Xu, C. Song, J.M. Andrésen, B.G. Miller, A.W. Scaroni, Preparation and characterization of novel CO_2 “molecular basket” adsorbents based on polymer-modified mesoporous molecular sieve MCM-41, *Microporous and Mesoporous Materials* 62 (2003) 29-45.

[62] R.S. Franchi, P.J.E. Harlick, A. Sayari, Applications of pore-expanded mesoporous silica. development of a high-capacity, water-tolerant adsorbent for CO_2, *Industrial & Engineering Chemistry Research* 44 (2005) 8007-8013.

[63] Y. Belmabkhout, R. Serna-Guerrero, A. Sayari, Adsorption of from dry gases on MCM-41 silica at ambient temperature and high pressure. 1: Pure adsorption, *Chemical Engineering Science* 64 (2009) 3721-3728.

[64] Y. Belmabkhout, R. Serna-Guerrero, A. Sayari, Adsorption of CO_2-containing gas mixtures over amine-bearing pore-expanded MCM-41 silica: Application for gas purification, *Industrial & Engineering Chemistry Research* 49 (2010) 359-365.

[65] R. Serna-Guerrero, Y. Belmabkhout, A. Sayari, Triamine-grafted pore-expanded mesoporous silica for CO_2 capture: Effect of moisture and adsorbent regeneration strategies, *Adsorption* 16 (2010) 567-575.

[66] C. Chen, S.T. Yang, W.S. Ahn, R. Ryoo, Amine-impregnated silica monolith with a hierarchical pore structure: enhancement of CO_2 capture capacity, *Chemical Communications* (2009) 3627-3629.

[67] W.-J. Son, J.-S. Choi, W.-S. Ahn, Adsorptive removal of carbon dioxide using polyethyleneimine-loaded mesoporous silica materials, *Microporous and Mesoporous Materials* 113 (2008) 31-40.

[68] M.R. Mello, D. Phanon, G.Q. Silveira, P.L. Llewellyn, C.M. Ronconi, Amine-modified MCM-41 mesoporous silica for carbon dioxide capture, *Microporous and Mesoporous Materials* 143 (2011) 174-179.

[69] J. Zhang, R. Singh, P.A. Webley, Alkali and alkaline-earth cation exchanged chabazite zeolites for adsorption based CO_2 capture, *Microporous and Mesoporous Materials* 111 (2008) 478-487.

[70] S. Choi, J.H. Drese, C.W. Jones, Adsorbent materials for carbon dioxide capture from large anthropogenic point sources, *ChemSusChem* 2 (2009) 796-854.

[71] G. Li, P. Xiao, P. Webley, J. Zhang, R. Singh, M. Marshall, Capture of CO_2 from high humidity flue gas by vacuum swing adsorption with zeolite 13X, *Adsorption* 14 (2008) 415-422.

[72] S.U. Rege, R.T. Yang, A novel FTIR method for studying mixed gas adsorption at low concentrations: H_2O and CO_2 on NaX zeolite and γ-alumina, *Chemical Engineering Science* 56 (2001) 3781-3796.

[73] F. Brandani, D.M. Ruthven, The effect of water on the adsorption of CO_2 and C_3H_8 on type X zeolites, *Industrial & Engineering Chemistry Research* 43 (2004) 8339-8344.

[74] L. Bertsch, H. Habgood, An infrared spectroscopic study of the adsorption of water and carbon dioxide by Linde molecular sieve X1, *The Journal of Physical Chemistry* 67 (1963) 1621-1628.

[75] J. Ward, H. Habgood, The infrared spectra of carbon dioxide adsorbed on Zeolite X, *The Journal of Physical Chemistry* 70 (1966) 1178-1182.

[76] E. Gallei, G. Stumpf, Infrared spectroscopic studies of the adsorption of carbon dioxide and the coadsorption of carbon dioxide and water on CaY-and NiY-zeolites, *Journal of Colloid and Interface Science* 55 (1976) 415-420.

[77] D. Barthomeuf, Conjugate acid-base pairs in zeolites, *The Journal of Physical Chemistry* 88 (1984) 42-45.

[78] S. Cavenati, C.A. Grande, A.E. Rodrigues, Adsorption equilibrium of methane, carbon dioxide, and nitrogen on zeolite 13X at high pressures, *Journal of Chemical & Engineering Data* 49 (2004) 1095-1101.

[79] D. Saha, Z. Bao, F. Jia, S. Deng, Adsorption of CO_2, CH_4, N_2O, and N_2 on MOF-5, MOF-177, and Zeolite 5A, *Environmental Science & Technology* 44 (2010) 1820-1826.

[80] R.V. Siriwardane, M.-S. Shen, E.P. Fisher, J.A. Poston, Adsorption of CO_2 on molecular sieves and activated carbon, *Energy & Fuels* 15 (2001) 279-284.

[81] G. Domínguez, R. Hernández-Huesca, G. Aguilar-Armenta, Isosteric heats of adsorption of N_2O and NO on natural zeolites, *Journal of the Mexican Chemical Society* 54 (2010) 111-116.

[82] P.J. Harlick, F.H. Tezel, An experimental adsorbent screening study for CO_2 removal from N_2, *Microporous and Mesoporous Materials* 76 (2004) 71-79.

[83] R. Siriwardane, M. Shen, E. Fisher, J. Poston, A. Shamsi, Adsorption and desorption of CO_2 on solid sorbents, National Energy Technology Laboratory, and Morgantown, WV (United States), 2001.

[84] K.S. Walton, M.B. Abney, M.D. LeVan, CO_2 adsorption in Y and X zeolites modified by alkali metal cation exchange, *Microporous and Mesoporous Materials* 91 (2006) 78-84.

[85] P.D. Jadhav, R.V. Chatti, R.B. Biniwale, N.K. Labhsetwar, S. Devotta, S.S. Rayalu, Monoethanol amine modified zeolite 13X for CO_2 adsorption at different temperatures, *Energy & Fuels* 21 (2007) 3555-3559.

[86] R. Chatti, A.K. Bansiwal, J.A. Thote, V. Kumar, P. Jadhav, S.K. Lokhande, R.B. Biniwale, N.K. Labhsetwar, S.S. Rayalu, Amine loaded zeolites for carbon dioxide capture: Amine loading and adsorption studies, *Microporous and Mesoporous Materials* 121 (2009) 84-89.

[87] V. Jimenez, A. Ramirez-Lucas, J.A. Diaz, P. Sanchez, A. Romero, CO_2 capture in different carbon materials, *Environmental Science & Technology* 46 (2012) 7407-7414.

[88] A. Stein, Z. Wang, M.A. Fierke, Functionalization of porous carbon materials with designed pore architecture, *Advanced Materials* 21 (2009) 265-293.

[89] A. Wahby, J.M. Ramos-Fernández, M. Martínez-Escandell, A. Sepúlveda-Escribano, J. Silvestre-Albero, F. Rodríguez-Reinoso, High-surface-area carbon molecular sieves for selective CO_2 adsorption, *ChemSusChem* 3 (2010) 974-981.

[90] L. Zhou, X. Liu, J. Li, N. Wang, Z. Wang, Y. Zhou, Synthesis of ordered mesoporous carbon molecular sieve and its adsorption capacity for H_2, N_2, O_2, CH_4 and CO_2, *Chemical Physics Letters* 413 (2005) 6-9.

[91] M. Bikshapathi, A. Sharma, A. Sharma, N. Verma, Preparation of carbon molecular sieves from carbon micro and nanofibers for sequestration of CO_2, *Chemical Engineering Research and Design* 89 (2011) 1737-1746.

[92] M. Cinke, J. Li, C.W. Bauschlicher, A. Ricca, M. Meyyappan, CO_2 adsorption in single-walled carbon nanotubes, *Chemical Physics Letters* 376 (2003) 761-766.

[93] S. Sircar, T.C. Golden, M.B. Rao, Activated carbon for gas separation and storage, *Carbon* 34 (1996) 1-12.

[94] P. Davini, Flue gas treatment by activated carbon obtained from oil-fired fly ash, *Carbon* 40 (2002) 1973-1979.

[95] B.-K. Na, K.-K. Koo, H.-M. Eum, H. Lee, H. Song, CO_2 recovery from flue gas by PSA process using activated carbon, *Korean Journal of Chemical Engineering* 18 (2001) 220-227.

[96] S. Himeno, T. Komatsu, S. Fujita, High-pressure adsorption equilibria of methane and carbon dioxide on several activated carbons, *Journal of Chemical & Engineering Data* 50 (2005) 369-376.

[97] F. Rodriguez-Reinoso, M. Molina-Sabio, Activated carbons from lignocellulosic materials by chemical and/or physical activation: an overview, *Carbon* 30 (1992) 1111-1118.

[98] A. Ahmadpour, D. Do, The preparation of active carbons from coal by chemical and physical activation, *Carbon* 34 (1996) 471-479.

[99] J. Maciá-Agulló, B. Moore, D. Cazorla-Amorós, A. Linares-Solano, Activation of coal tar pitch carbon fibres: physical activation vs. chemical activation, *Carbon* 42 (2004) 1367-1370.

[100] R. Wang, P. Wang, X. Yan, J. Lang, C. Peng, Q. Xue, Promising porous carbon derived from celtuce leaves with outstanding supercapacitance and CO_2 capture performance, *ACS Applied Materials & Interfaces* 4 (2012) 5800-5806.

[101] A. Arenillas, K.M. Smith, T.C. Drage, C.E. Snape, CO_2 capture using some fly ash-derived carbon materials, *Fuel* 84 (2005) 2204-2210.

[102] M.M. Maroto-Valer, Z. Lu, Y. Zhang, Z. Tang, Sorbents for CO_2 capture from high carbon fly ashes, *Waste Management* 28 (2008) 2320-2328.

[103] M.G. Plaza, C. Pevida, B. Arias, J. Fermoso, M.D. Casal, C.F. Martín, F. Rubiera, J.J. Pis, Development of low-cost biomass-based adsorbents for postcombustion CO_2 capture, *Fuel* 88 (2009) 2442-2447.

[104] M.G. Plaza, C. Pevida, C.F. Martín, J. Fermoso, J.J. Pis, F. Rubiera, Developing almond shell-derived activated carbons as CO_2 adsorbents, *Separation and Purification Technology* 71 (2010) 102-106.

[105] J.A. Thote, K.S. Iyer, R. Chatti, N.K. Labhsetwar, R.B. Biniwale, S.S. Rayalu, In situ nitrogen enriched carbon for carbon dioxide capture, *Carbon* 48 (2010) 396-402.

[106] M. Olivares-Marín, S. García, C. Pevida, M.S. Wong, M. Maroto-Valer, The influence of the precursor and synthesis method on the CO_2 capture capacity of carpet waste-based sorbents, *Journal of Environmental Management* 92 (2011) 2810-2817.

[107] M. Sevilla, A.B. Fuertes, Sustainable porous carbons with a superior performance for CO_2 capture, *Energy & Environmental Science* 4 (2011) 1765-1771.

[108] T. Valdés-Solís, A.B. Fuertes, High-surface area inorganic compounds prepared by nanocasting techniques, *Materials Research Bulletin* 41 (2006) 2187-2197.

[109] P. Karandikar, K.R. Patil, A. Mitra, B. Kakade, A.J. Chandwadkar, Synthesis and characterization of mesoporous carbon through inexpensive mesoporous silica as template, *Microporous and Mesoporous Materials* 98 (2007) 189-199.

[110] T.C. Drage, A. Arenillas, K.M. Smith, C. Pevida, S. Piippo, C.E. Snape, Preparation of carbon dioxide adsorbents from the chemical activation of urea–formaldehyde and melamine–formaldehyde resins, *Fuel* 86 (2007) 22-31.

[111] G.P. Hao, W.C. Li, D. Qian, A.H. Lu, Rapid synthesis of nitrogen-doped porous carbon monolith for CO_2 capture, *Advanced Materials* 22 (2010) 853-857.

[112] M. Sevilla, P. Valle-Vigón, A.B. Fuertes, N-doped polypyrrole-based porous carbons for CO_2 capture, *Advanced Functional Materials* 21 (2011) 2781-2787.

[113] L.-Y. Meng, S.-J. Park, One-pot synthetic method to prepare highly N-doped nanoporous carbons for CO_2 adsorption, *Materials Chemistry and Physics* 143 (2014) 1158-1163.

[114] Z. Liu, Z. Du, H. Song, C. Wang, F. Subhan, W. Xing, Z. Yan, The fabrication of porous N-doped carbon from widely available urea formaldehyde resin for carbon dioxide adsorption, *Journal of Colloid and Interface Science* 416 (2014) 124-132.

[115] Z. Liu, Z. Du, W. Xing, Z. Yan, Facial synthesis of N-doped microporous carbon derived from urea furfural resin with high CO_2 capture capacity, *Materials Letters* 117 (2014) 273-275.

[116] M. Balsamo, T. Budinova, A. Erto, A. Lancia, B. Petrova, N. Petrov, B. Tsyntsarski, CO_2 adsorption onto synthetic activated carbon: Kinetic, thermodynamic and regeneration studies, *Separation and Purification Technology* 116 (2013) 214-221.

[117] R.-L. Tseng, F.-C. Wu, R.-S. Juang, Adsorption of CO_2 at atmospheric pressure on activated carbons prepared from melamine-modified phenol–formaldehyde resins, *Separation and Purification Technology* 140 (2015) 53-60.

[118] J. Lee, S. Han, T. Hyeon, Synthesis of new nanoporous carbon materials using nanostructured silica materials as templates, *Journal of Materials Chemistry* 14 (2004) 478-486.

[119] B. Xu, L. Peng, G. Wang, G. Cao, F. Wu, Easy synthesis of mesoporous carbon using nano-$CaCO_3$ as template, *Carbon* 48 (2010) 2377-2380.

[120] C. Pevida, T. Drage, C.E. Snape, Silica-templated melamine–formaldehyde resin derived adsorbents for CO_2 capture, *Carbon* 46 (2008) 1464-1474.

[121] M. Sevilla, A.B. Fuertes, CO_2 adsorption by activated templated carbons, *Journal of Colloid and Interface Science* 366 (2012) 147-154.

[122] Y. Zhao, L. Zhao, K.X. Yao, Y. Yang, Q. Zhang, Y. Han, Novel porous carbon materials with ultrahigh nitrogen contents for selective CO_2 capture, *Journal of Materials Chemistry* 22 (2012) 19726-19731.

[123] Q. Li, J. Yang, D. Feng, Z. Wu, Q. Wu, S. Park, C.-S. Ha, D. Zhao, Facile synthesis of porous carbon nitride spheres with hierarchical three-dimensional mesostructures for CO_2 capture, *Nano Research* 3 (2010) 632-642.

[124] C. Lu, H. Bai, B. Wu, F. Su, J.F. Hwang, Comparative study of CO_2 capture by carbon nanotubes, activated carbons, and zeolites, *Energy & Fuels* 22 (2008) 3050-3056.

[125] F. Su, C. Lu, H.S. Chen, Adsorption, desorption, and thermodynamic studies of CO_2 with high-amine-loaded multiwalled carbon nanotubes, *Langmuir* 27 (2011) 8090-8098.

[126] Q. Ye, J. Jiang, C. Wang, Y. Liu, H. Pan, Y. Shi, Adsorption of low-concentration carbon dioxide on amine-modified carbon nanotubes at ambient temperature, *Energy & Fuels* 26 (2012) 2497-2504.

[127] S. Lagergren, About the theory of so-called adsorption of soluble substances, *Kungliga Svenska Vetenskapsakademiens Handlingar 24* (1898) 139.

[128] Y.S. Ho, G. McKay, Pseudo-second order model for sorption processes, *Process Biochemistry* 34 (1999) 451-465.

[129] C. Shen, C.A. Grande, P. Li, J. Yu, A.E. Rodrigues, Adsorption equilibria and kinetics of CO_2 and N_2 on activated carbon beads, *Chemical Engineering Journal* 160 (2010) 398-407.

[130] A. Zhao, A. Samanta, P. Sarkar, R. Gupta, Carbon dioxide adsorption on amine-impregnated mesoporous SBA-15 sorbents: Experimental and kinetics study, *Industrial & Engineering Chemistry Research* 52 (2013) 6480-6491.

[131] A. Heydari-Gorji, A. Sayari, CO_2 capture on polyethylenimine-impregnated hydrophobic mesoporous silica: Experimental and kinetic modeling, *Chemical Engineering Journal* 173 (2011) 72-79.

[132] C. Goel, H. Bhunia, P.K. Bajpai, Resorcinol–formaldehyde based nanostructured carbons for CO_2 adsorption: kinetics, isotherm and thermodynamic studies, *RSC Advances* 5 (2015) 93563-93578.

[133] I. Langmuir, The constitution and fundamental properties of solids and liquids. Part I. Solids, *Journal of the American chemical society* 38 (1916) 2221-2295.

[134] H. Freundlich, Over the adsorption in solution, J. Phys. Chem 57 (1906) e470.

[135] M. Temkin, V. Pyzhev, Kinetics of ammonia synthesis on promoted iron catalysts, *Acta Physiochim*. URSS 12 (1940) 217-222.

[136] D. Fauth, M. Gray, H. Pennline, H. Krutka, S. Sjostrom, A. Ault, Investigation of porous silica supported mixed-amine sorbents for post-combustion CO_2 capture, *Energy & Fuels* 26 (2012) 2483-2496.

[137] C. Goel, H. Bhunia, P.K. Bajpai, Novel nitrogen enriched porous carbon adsorbents for CO_2 capture: Breakthrough adsorption study, *Journal of Environmental Chemical Engineering* 4 (2016) 346-356.

[138] C. Goel, H. Bhunia, P.K. Bajpai, Mesoporous carbon adsorbents from melamine–formaldehyde resin using nanocasting technique for CO_2 adsorption, *Journal of Environmental Sciences* 32 (2015) 238-248.

[139] S.M. Mahurin, J.S. Lee, X. Wang, S. Dai, Ammonia-activated mesoporous carbon membranes for gas separations, *Journal of Membrane Science* 368 (2011) 41-47.

[140] Laszlo K, Tombacz E, Josepovits K. Effect of activation on the surface chemistry of carbons from polymer precursors. *Carbon*. 39 (2001) 1217-1228.

[141] A. Contescu, M. Vass, C. Contescu, K. Putyera, J.A. Schwarz, Acid buffering capacity of basic carbons revealed by their continuous pK distribution, *Carbon* 36 (1998) 247-258.

[142] M. Olivares-Marín, S. García, C. Pevida, M. Wong, M. Maroto-Valer, The influence of the precursor and synthesis method on the CO_2 capture capacity of carpet waste-based sorbents, *Journal of Environmental Management* 92 (2011) 2810-2817.

[143] A. Arenillas, F. Rubiera, J. Parra, C. Ania, J. Pis, Surface modification of low cost carbons for their application in the environmental protection, *Applied Surface Science* 252 (2005) 619-624.

[144] Goel C. Development and characterization of nanostructured carbon adsorbents for carbon dioxide capture *Ph.D. Thesis* 2016, Thapar Univerity, Patiala, India.

[145] Chen H, Sun F, Wang J, Li W, Qiao W, Ling L. Nitrogen doping effects on the physical and chemical properties of mesoporous carbons. *The Journal of Physical Chemistry C*. 117 (2013) 8318-8328.

[146] Mane GP, Talapaneni SN, Anand C, Varghese S, Iwai H, Ji Q. Preparation of highly ordered nitrogen-containing mesoporous carbon from a gelatin biomolecule and its excellent sensing of acetic acid. *Advanced Functional Materials*. 22 (2012) 3596-3604.

[147] K.S. Lakhi, W.S. Cha, S. Joseph, B.J. Wood, S.S. Aldeyab, G. Lawrence, J.-H. Choy, A. Vinu, Cage type mesoporous carbon nitride with large mesopores for CO_2 capture, *Catalysis Today* 243 (2015) 209-217.

[148] I.A. Esteves, M.S. Lopes, P.M. Nunes, J.P. Mota, Adsorption of natural gas and biogas components on activated carbon, *Separation and Purification Technology* 62 (2008) 281-296.

[149] R. Veneman, H. Kamphuis, D. Brilman, Post-combustion CO_2 capture using supported amine sorbents: a process integration study, *Energy Procedia* 37 (2013) 2100-2108.

[150] B.D.H.a.E.R. Slatick, Carbon Dioxide Emission Factors for Coal, Energy Information Administration, Quarterly Coal ReportWashington, DC, 1994, pp. 1-8.

[151] C. Goel, H. Bhunia, P.K. Bajpai, Synthesis of nitrogen doped mesoporous carbons for carbon dioxide capture, *RSC Advances* 5 (2015) 46568-46582.

[152] A.C. Lua, T. Yang, Effect of activation temperature on the textural and chemical properties of potassium hydroxide activated carbon prepared from pistachio-nut shell, *Journal of Colloid and Interface Science* 274 (2004) 594-601.

[153] J.W. Zondlo, A. Saddawi, P. Stansberry, E. Kennel, Turbostratic Carbon Powder, (2004).

[154] J. Sreńscek-Nazzal, U. Narkiewicz, A. Morawski, R. Wróbel, A. Gęsikiewicz-Puchalska, B. Michalkiewicz, Modification of commercial activated carbons for CO_2 adsorption, *Acta Physica Polonica*, A. 129 (2016).

[155] Balsamo M, Budinova T, Erto A, Lancia A, Petrova B, Petrov N. CO_2 adsorption onto synthetic activated carbon: kinetic, thermodynamic and regeneration studies. *Separation and Purification Technology*. 116 (2013) 214-221.

[156] P. Kaur, A. Singh, A. Prince, J. Kushwaha, Optimization and evaluation of CBSOL LE red wool dye adsorption from aqueous solution onto commercial activated carbon, *International Journal of Environmental Science and Technology* 12 (2015) 3755-3766.

[157] B. Wang, T.P. Ang, A. Borgna, A rapid hard template method for the synthesis of N-doped mesoporous carbon replicated from TUD-1, *Microporous and Mesoporous Materials* 158 (2012) 99-107.

[158] A. Vinu, S. Anandan, C. Anand, P. Srinivasu, K. Ariga, T. Mori, Fabrication of partially graphitic three-dimensional nitrogen-doped mesoporous carbon using polyaniline nanocomposite through nanotemplating method, *Microporous and Mesoporous Materials* 109 (2008) 398-404.

[159] M. Ignat, E. Popovici, Synthesis of mesoporous carbon materials via nanocasting route–comparative study of glycerol and sucrose as carbon sources, *Rev. Roum. Chim* 56 (2011) 947-952.

[160] Z. Liu, Y. Yang, Z. Du, W. Xing, S. Komarneni, Z. Zhang, X. Gao, Z. Yan, Furfuralcohol co-polymerized urea formaldehyde resin-derived N-doped microporous carbon for CO_2 capture, *Nanoscale Research Letters* 10 (2015) 1.

[161] M.S. Shafeeyan, W.M.A.W. Daud, A. Houshmand, A. Arami-Niya, Ammonia modification of activated carbon to enhance carbon dioxide adsorption: effect of pre-oxidation, *Applied Surface Science* 257 (2011) 3936-3942.

[162] A. Vesel, I. Junkar, U. Cvelbar, J. Kovac, M. Mozetic, Surface modification of polyester by oxygen-and nitrogen-plasma treatment, *Surface and Interface Analysis* 40 (2008) 1444-1453.

[163] P. Burg, P. Fydrych, D. Cagniant, G. Nanse, J. Bimer, A. Jankowska, The characterization of nitrogen-enriched activated carbons by IR, XPS and LSER methods, *Carbon* 40 (2002) 1521-1531.

[164] H.F. Gorgulho, F. Gonçalves, M.F.R. Pereira, J.L. Figueiredo, Synthesis and characterization of nitrogen-doped carbon xerogels, *Carbon* 47 (2009) 2032-2039.

[165] Y. Wang, Y. Shao, D.W. Matson, J. Li, Y. Lin, Nitrogen-doped graphene and its application in electrochemical biosensing, *ACS Nano* 4 (2010) 1790-1798.

[166] M. Sevilla, J.B. Parra, A.B. Fuertes, Assessment of the role of micropore size and N-doping in CO_2 capture by porous carbons, *ACS Applied Materials & Interfaces* 5 (2013) 6360-6368.

[167] M. Sevilla, C. Falco, M.-M. Titirici, A.B. Fuertes, High-performance CO_2 sorbents from algae, *RSC Advances* 2 (2012) 12792-12797.

[168] J. Zhou, W. Li, Z. Zhang, W. Xing, S. Zhuo, Carbon dioxide adsorption performance of N-doped zeolite Y templated carbons, *RSC Advances* 2 (2012) 161-167.

[169] A. Ferrari, J. Meyer, V. Scardaci, C. Casiraghi, M. Lazzeri, F. Mauri, S. Piscanec, D. Jiang, K. Novoselov, S. Roth, Raman spectrum of graphene and graphene layers, *Physical Review Letters* 97 (2006) 187401.

[170] A.C. Ferrari, Raman spectroscopy of graphene and graphite: disorder, electron–phonon coupling, doping and nonadiabatic effects, *Solid State Communications* 143 (2007) 47-57.

[171] J. Wang, R. Krishna, J. Yang, K.P.R. Dandamudi, S. Deng, Nitrogen-doped porous carbons for highly selective CO_2 capture from flue gases and natural gas upgrading, *Materials Today Communications* 4 (2015) 156-165.

[172] F. Haghseresht, G. Lu, A. Whittaker, Carbon structure and porosity of carbonaceous adsorbents in relation to their adsorption properties, *Carbon* 37 (1999) 1491-1497.

[173] A. Centrone, D.Y. Siberio-Pérez, A.R. Millward, O.M. Yaghi, A.J. Matzger, G. Zerbi, Raman spectra of hydrogen and deuterium adsorbed on a metal–organic framework, *Chemical Physics Letters* 411 (2005) 516-519.

[174] D. Lázaro, C. Caldeira, M. Dantas, A. Franca, M. Mansur, Characterization of an absorbent based on Raphanus sativus (L. var.), a solid residue from biodiesel production, for the removal of methylene blue, *WIT Transactions on Ecology and the Environment* 135 (2010) 345-355.

[175] S.B. Hansen, R.W. Berg, E.H. Stenby, Raman spectroscopic studies of methane—ethane mixtures as a function of pressure, *Applied Spectroscopy* 55 (2001) 745-749.

[176] Y.a. Huang, F. Yang, Z. Xu, J. Shen, Nitrogen-containing mesoporous carbons prepared from melamine formaldehyde resins with $CaCl_2$ as a template, *Journal of Colloid and Interface Science* 363 (2011) 193-198.

[177] M. Plaza, S. García, F. Rubiera, J. Pis, C. Pevida, Evaluation of ammonia modified and conventionally activated biomass based carbons as CO_2 adsorbents in postcombustion conditions, *Separation and Purification Technology* 80 (2011) 96-104.

[178] M.M. Maroto-Valer, Z. Lu, Y. Zhang, Z. Tang, Sorbents for CO_2 capture from high carbon fly ashes, *Waste Management* 28 (2008) 2320-2328.

[179] A. Boonpoke, S. Chiarakorn, N. Laosiripojana, S. Towprayoon, A. Chidthaisong, Synthesis of activated carbon and MCM-41 from bagasse and rice husk and their carbon dioxide adsorption capacity, *Journal of Sustainable Energy & Environment* 2 (2011).

[180] Q. Liu, J. Shi, S. Zheng, M. Tao, Y. He, Y. Shi, Kinetics studies of CO_2 adsorption/desorption on amine-functionalized multiwalled carbon nanotubes, *Industrial & Engineering Chemistry Research* 53 (2014) 11677-11683.

[181] M.-S. Chiou, H.-Y. Li, Equilibrium and kinetic modeling of adsorption of reactive dye on cross-linked chitosan beads, *Journal of Hazardous Materials* 93 (2002) 233-248.

[182] S.-C. Hsu, C. Lu, F. Su, W. Zeng, W. Chen, Thermodynamics and regeneration studies of CO_2 adsorption on multiwalled carbon nanotubes, *Chemical Engineering Science* 65 (2010) 1354-1361.

[183] Y. Sun, J. Zhao, J. Wang, N. Tang, R. Zhao, D. Zhang, T. Guan, K. Li, Sulfur-Doped Millimeter-sized microporous activated carbon spheres derived from sulfonated poly (styrene-divinylbenzene) for CO_2 capture, *The Journal of Physical Chemistry* C (2017).

[184] J. Yu, M. Guo, F. Muhammad, A. Wang, G. Yu, H. Ma, G. Zhu, Simple fabrication of an ordered nitrogen-doped mesoporous carbon with resorcinol–melamine–formaldehyde resin, *Microporous and Mesoporous Materials* 190 (2014) 117-127.

[185] C. Chen, J. Kim, W.-S. Ahn, Efficient carbon dioxide capture over a nitrogen-rich carbon having a hierarchical micro-mesopore structure, *Fuel* 95 (2012) 360-364.

[186] X. Hu, M. Radosz, K.A. Cychosz, M. Thommes, CO_2-filling capacity and selectivity of carbon nanopores: synthesis, texture, and pore-size distribution from quenched-solid density functional theory (QSDFT), *Environmental Science & Technology* 45 (2011) 7068-7074.

[187] C. Pevida, M. Plaza, B. Arias, J. Fermoso, F. Rubiera, J. Pis, Surface modification of activated carbons for CO_2 capture, *Applied Surface Science* 254 (2008) 7165-7172.

[188] Y.A. Alhamed, S.U. Rather, A.H. El-Shazly, S.F. Zaman, M.A. Daous, A.A. Al-Zahrani, Preparation of activated carbon from fly ash and its application for CO_2 capture, *Korean Journal of Chemical Engineering* 32 (2015) 723-730.

[189] A. Boonpoke, S. Chiarakorn, N. Laosiripojana, S. Towprayoon, A. Chidthaisong, Synthesis of activated carbon and MCM-41 from bagasse and rice husk and their carbon dioxide adsorption capacity, *Journal of Sustainable Energy & Environment* 2 (2011) 77-81.

[190] M.M. Maroto-Valer, Z. Tang, Y. Zhang, CO_2 capture by activated and impregnated anthracites, *Fuel Processing Technology* 86 (2005) 1487-1502.

[191] M. Olivares-Marín, M. Maroto-Valer, Preparation of a highly microporous carbon from a carpet material and its application as CO_2 sorbent, *Fuel Processing Technology* 92 (2011) 322-329.

[192] M. Sevilla, A.B. Fuertes, CO_2 adsorption by activated templated carbons, *Journal of Colloid and Interface Science* 366 (2012) 147-154.

[193] S. Deng, B. Hu, T. Chen, B. Wang, J. Huang, Y. Wang, G. Yu, Activated carbons prepared from peanut shell and sunflower seed shell for high CO_2 adsorption, *Adsorption* 21 (2015) 125-133.

[194] H. Wei, S. Deng, B. Hu, Z. Chen, B. Wang, J. Huang, G. Yu, Granular bamboo-derived activated carbon for high CO_2 adsorption: The Dominant Role of Narrow Micropores, *ChemSusChem* 5 (2012) 2354-2360.

[195] X.-L. Zhu, P.-Y. Wang, C. Peng, J. Yang, X.-B. Yan, Activated carbon produced from paulownia sawdust for high-performance CO_2 sorbents, *Chinese Chemical Letters* 25 (2014) 929-932.

[196] M. Sevilla, A.B. Fuertes, Sustainable porous carbons with a superior performance for CO_2 capture, *Energy & Environmental Science* 4 (2011) 1765-1771.

[197] J. Szekely, Evans, and HY Sohn, Gas–Solid Reactions, Academic Press, New York, 1976.

LIST OF PUBLICATIONS

Publications

1. In Peer-Reviewed (SCI) Journals

1.1 Related to Ph. D. work

i. **Deepak Tiwari**, Chitrakshi Goel, Haripada Bhunia, and Pramod K. Bajpai, "Novel nanostructured carbons derived from epoxy resin and their adsorption characteristics for CO_2 capture", *RSC Advances*, 2016, *6*, 97728-97738. (Impact Factor: 2.936)

ii. **Deepak Tiwari**, Haripada Bhunia, and Pramod K. Bajpai, "Urea-formaldehyde derived porous carbons for adsorption of CO_2", *RSC Advances*, 2016, *6*, 111842-111855. (Impact Factor: 2.936)

iii. **Deepak Tiwari**, Chitrakshi Goel, Haripada Bhunia, and Pramod K. Bajpai, "Dynamic CO_2 capture by carbon adsorbents: kinetics, isotherm and thermodynamic studies", *Separation and Purification Technology*, 2017, *181*, 107-122. (Impact Factor: 3.927)

iv. **Deepak Tiwari**, Haripada Bhunia, and Pramod K. Bajpai, "Adsorption of CO_2 on KOH activated, N-enriched carbon derived from urea formaldehyde resin: kinetics, isotherm and thermodynamic studies", *Applied Surface Science*, 2018, 439C, 760-771. (Impact Factor: 4.439)

1.2 In related area

i. **Deepak Tiwari**, Chitrakshi Goel, Haripada Bhunia, and Pramod K. Bajpai, "Melamine formaldehyde derived porous carbons for adsorption of CO_2", *Journal of Environmental Management*, 2017, *197*, 415-427. (Impact Factor: 4.005)

ii. **Deepak Tiwari**, Haripada Bhunia, and Pramod K. Bajpai, "Epoxy based oxygen enriched porous carbons for CO_2 capture", *Applied Surface Science*, 2017, 414, 380-389. (Impact Factor: 4.439)

iii. **Deepak Tiwari**, Haripada Bhunia, and Pramod K. Bajpai, "Synthesis of nitrogen enriched porous carbons from urea formaldehyde resin and their carbon dioxide adsorption capacity", *Journal of CO_2 Utilization*, 2017, 21, 302-313. (Impact Factor: 5.503)

iv. **Deepak Tiwari**, Haripada Bhunia, and Pramod K. Bajpai, "Development of chemically activated N-enriched carbon adsorbents from urea-formaldehyde resin for CO_2

adsorption: Kinetics, isotherm, and thermodynamics", *Journal of Environmental Management*, 2018, 218, 579-592 (Impact Factor: 4.005).

2. In Conference

i. **Deepak Tiwari**, Haripada Bhunia, and Pramod K. Bajpai, "Synthesis of N-enriched porous carbons from urea formaldehyde resin and their CO_2 adsorption capacity", *National Conference on Sustainable Advanced Technological for Environmental Management,* Indian Institute of Engineering Science and Technology, Shibpur (W.B) India, June 28-30, 2017.

REPRINTS OF PUBLISHED ARTICLES

RSC Advances

PAPER

Cite this: *RSC Adv.*, 2016, **6**, 97728

Novel nanostructured carbons derived from epoxy resin and their adsorption characteristics for CO_2 capture†

Deepak Tiwari, Chitrakshi Goel, Haripada Bhunia* and Pramod K. Bajpai

In this work, a nanocasting technique has been used to synthesize oxygen enriched carbon adsorbents with epoxy resin as the precursor and mesoporous zeolite as a template. Carbonization and physical activation with CO_2 was carried out to prepare different carbon adsorbents. Characterization of the synthesized adsorbents was done using N_2 sorption, XRD, SEM, TEM, TGA, FTIR spectroscopy, CHN analysis, and XPS. The surface area and pore volume of the synthesized adsorbent prepared at 600 °C were found to be a maximum of 686.37 m^2 g^{-1} and 0.60 cm^3 g^{-1}, respectively, but showed a lower adsorption capacity due to lesser oxygen content as compared to the sample prepared at 700 °C. The sample prepared at 700 °C exhibited the highest CO_2 uptake, approximately 0.65 mmol g^{-1}, at 30 °C due to the high oxygen content, which was estimated to be about 53.98% determined using CHN analysis and also due to high surface basicity confirmed by XPS. The sample prepared by direct carbonization of the polymeric precursor shows a completely non-porous and highly acidic material having the least adsorption capacity. It was found that an increase in concentration of CO_2 increases adsorption capacity and an increase in adsorption temperature decreases adsorption capacity. CO_2 adsorption kinetics were performed by using three kinetic models and from the correlation coefficient, adsorption kinetics were found to obey fractional order with error% within the range of 4.24%. For checking the regenerability, four adsorption–desorption cycles were examined. It was found that the adsorbents exhibit easy regenerability, stable adsorption capacity and good selectivity for CO_2–N_2 separation. The experimental data are well fitted with the Freundlich isotherm, showing a heterogeneous adsorbent surface. The isosteric heat Q_{st} of CO_2 is 9.09 kJ mol^{-1}, which indicates the presence of the physisorption process. The negative value of Gibbs free energy suggests the spontaneous nature of the process. The values of $\Delta H°$ and $\Delta S°$ were found to be −2.562 kJ mol^{-1} and 0.033 kJ mol^{-1} K^{-1}, respectively. The negative value of $\Delta H°$ suggests the exothermic nature of the adsorption process.

Received 18th July 2016
Accepted 29th September 2016

DOI: 10.1039/c6ra18291g

www.rsc.org/advances

1. Introduction

CO_2, a major greenhouse gas, is the major contributor to climate change among all the gases. Approximately 30% of CO_2 in the atmosphere is due to the burning of fossil fuels.[1] Its concentration raised from 280 ppm to 401.8 ppm from the preindustrial age to the present day. It seems that its concentration continues to rise and it will reach a level of 550 ppm by 2100, because of the usage of fossil fuels as the major source of energy.[2] Therefore, to continue to enjoy the benefits of fossil fuels, low-cost technologies need to be developed to control the increasing CO_2 concentration. Carbon dioxide capture and sequestration (CCS) is an important strategy to reduce the concentration of CO_2.[3] The available CCS technologies that help in CO_2 capture are absorption, adsorption, membrane separation and cryogenic distillation. The conventional amine absorption technology for capture of CO_2 is efficient but presents a series of drawbacks like high energy requirements, equipment corrosion, and low efficiency.[4] Therefore, an available technology like adsorption seems to be viable due to high adsorption capacity, low energy requirements, and stability. However, the success of this technology depends on the development of easily regenerable and durable adsorbents.[5] Therefore, different adsorbents have been used for CO_2 capture including carbon-based adsorbents, activated carbon,[6] mesoporous silica materials, amine enriched sorbents,[7] carbonates and zeolites.[8] Adsorption by carbon-based adsorbents has advantages of high specific surface area, good mechanical stability, hydrophobicity and complete regeneration over multiple adsorption cycles. Different methods have been developed to synthesize carbon-based adsorbents such as sol–gel processes, direct carbonization of precursors and

Department of Chemical Engineering, Thapar University, Patiala-147004, Punjab, India. E-mail: Deepak.tiwari@thapar.edu; chitrakshigoel@yahoo.co.in; hbhunia@thapar.edu; pramod.iitk77@gmail.com; Fax: +91-175-2393005; Tel: +91-9316682355

† Electronic supplementary information (ESI) available. See DOI: 10.1039/c6ra18291g

RSC Advances

PAPER

Urea-formaldehyde derived porous carbons for adsorption of CO_2†

Deepak Tiwari, Haripada Bhunia* and Pramod K. Bajpai

Cite this: *RSC Adv.*, 2016, **6**, 111842

The aim of the research work is to develop high nitrogen content carbon adsorbents with high textural and surface properties using as a precursor urea-formaldehyde resin and as a template mesoporous-zeolite (MCM-41) through a nanocasting technique. The material undergoes carbonization followed by physical activation under a CO_2 atmosphere to generate different carbon structure adsorbents. Different characterization techniques such as XRD, SEM, TEM, FTIR, CHN, TKN, nitrogen sorption, TGA, TPD and XPS were used for thorough characterization of the samples. XRD and TEM reveal the development of nanostructured carbon adsorbents. CO_2 adsorption on adsorbents was investigated between temperatures of 30 and 100 °C and concentrations of 5 to 12.5% in a dynamic fixed bed column to overcome a gap in the literature. The carbon sample prepared at 700 °C through the nanocasting technique shows high basicity and exhibited a high CO_2 uptake of 0.84 mmol g^{-1} with a nitrogen content of 17.18%. It shows higher values at a high adsorption temperature (100 °C) as compared to the literature, which fulfills the objective of this study. An adsorbent prepared at 800 °C shows the highest surface area (337.07 m^2 g^{-1}), but shows a lower adsorption capacity as compared to one prepared at 700 °C whose surface area was slightly lower (297.68 m^2 g^{-1}). This shows that besides textural and nitrogen content, adsorption capacity depends on nitrogen functionalities. The adsorbents exhibit stability and easy regenerability over four adsorption–desorption cycles with better selectivity for CO_2. This was also confirmed from the lower value of Q_{st} (kJ mol^{-1}). The CO_2 adsorption kinetics follow a fractional order model with less than 5% error. The equilibrium adsorption data fitted the Freundlich isothermal model well, demonstrating the heterogeneous nature of the adsorbent surface. Thermodynamics suggests a spontaneous, feasible and exothermic process.

Received 3rd October 2016
Accepted 16th November 2016

DOI: 10.1039/c6ra24634f

www.rsc.org/advances

1. Introduction

The release of harmful greenhouse gases, including carbon dioxide (CO_2), methane (CH_4), chlorofluorocarbons (CFCs), and nitrous oxide (N_2O), is a major concern for world climate change and among these gases CO_2 is the major threat to the environment and is increasing tremendously with the utilization of non-renewable and carbon-emitting fuels such as coal, petroleum, and natural gas. According to the Intergovernmental Panel on Climate Change (IPCC), it is expected that carbon dioxide concentration will grow to 550 ppm in 2035, which will cause a rise of approximately 2 °C in the mean global temperature.[1]

In order to lower CO_2 emissions in the atmosphere, a carbon capture and storage strategy (CCS) has been introduced. This includes several approaches for CO_2 capture, *i.e.*, absorption, adsorption,[2] cryogenic processes,[3] and membrane separation *etc.* However, commercial technologies like absorption by alkanolamines such as mono-ethanolamine and di-ethanolamine are being used to the maximum, but they have several drawbacks such as equipment corrosion and environmental issues related to alkanolamines and high regeneration energy. Regeneration of alkanolamines needs a large amount of energy, which makes the process impractical for further applications.[4] Therefore, to overcome these techno-economical restrictions, the search for other technologies has been prompted. Adsorption by solid porous adsorbents is an attractive technology due to its high CO_2 adsorption capacities, simple process, low energy consumption *etc.*[5,6] Different adsorbents, such as activated carbon, zeolites, SBA-15, MCM-41,[7] and amine-enriched sorbents, are being studied. To improve CO_2 selectivity and the adsorption capacity of adsorbents, many research groups have modified the adsorbents by amine modification, but the modification caused the blocking of adsorbent pores and poor stability due to amine degradation. Alternatively, CO_2 capture by carbon-based adsorbents has advantages such as complete regeneration of adsorbents over multiple adsorption–desorption cycles, high surface area, good thermal/mechanical stability and hydrophobicity.[8] Moreover,

Department of Chemical Engineering, Thapar University, Patiala – 147004, Punjab, India. E-mail: hbhunia@thapar.edu; Deepak.tiwari@thapar.edu; pramod.iitk77@gmail.com; Fax: +91-175-2393005; Tel: +91-9316682355

† Electronic supplementary information (ESI) available. See DOI: 10.1039/c6ra24634f

Separation and Purification Technology 181 (2017) 107–122

Contents lists available at ScienceDirect

Separation and Purification Technology

journal homepage: www.elsevier.com/locate/seppur

Dynamic CO_2 capture by carbon adsorbents: Kinetics, isotherm and thermodynamic studies

Deepak Tiwari [a], Chitrakshi Goel [a,b], Haripada Bhunia [a,*], Pramod K. Bajpai [a]

[a] Department of Chemical Engineering, Thapar University, Patiala 147004, Punjab, India
[b] Ghent University – Laboratory for Chemical Technology, Technologiepark 914, B-9052 Ghent, Belgium

ARTICLE INFO

Article history:
Received 10 November 2016
Received in revised form 8 March 2017
Accepted 12 March 2017
Available online 14 March 2017

Keywords:
CO_2 capture
Nanocasting
Melamine formaldehyde
Adsorption kinetics
Isotherm

ABSTRACT

In this work, we report carbon adsorbents prepared using MCM-41 (mesoporous zeolite) template and high nitrogen content, melamine-formaldehyde resin as starting material by using nanocasting technique. The material was carbonized and physically activated with CO_2 at different temperatures to obtain different carbon adsorbents. Synthesized adsorbents were characterized using various techniques for their elemental, surface and textural properties. Effect of nanocasting technique was seen by the improvement in textural property e.g. the surface area and pore volume of the adsorbent prepared at 700 °C were found to be maximum, i.e. 193.28 $m^2 g^{-1}$ and 0.32 $cm^3 g^{-1}$, respectively. This was not seen for the sample prepared by direct carbonization (MF-700). Also, development of nanostructured carbon adsorbents was confirmed from XRD and TEM results. Adsorption of CO_2 on carbon adsorbents was evaluated at different temperatures (30–100 °C) and concentrations (5–12.5%) in a dynamic fixed bed column. Adsorbent prepared at 700 °C exhibited highest CO_2 uptake of 0.64 mmol g^{-1} due to high basicity as confirmed from X-ray photoelectron spectroscopy. Both surface and texture chemistry have a strong influence on the CO_2 adsorption performance. The CO_2 adsorption kinetic study was performed by using three kinetic models and was found that a fractional order fits well with the experimental data with maximum error% of 3.68%. Regeneration study of the adsorbent was carried out by using multiple adsorption-desorption cycles and found that the adsorbent exhibited easy regenerability and stability over multiple cycles. The Temkin isothermal model fitted best among three isotherm models indicating the heterogeneous surface of adsorbent surface. The isosteric heat of adsorption is found to be 15.05 kJ mol^{-1}, which indicates physiosorption process and also supports easy regenerability of the adsorbent. Thermodynamic parameters such as ΔH^0 and ΔS^0 were found to be −5.7 kJ mol^{-1} and 0.033 kJ mol^{-1} K^{-1}. The thermal energy estimated for CO_2 desorption is 2.15 MJ per kg CO_2.

1. Introduction

The major concerning issues among the global warming phenomenon are the greenhouse gases (GHG), including carbon dioxide (CO_2), methane (CH_4), chlorofluorocarbons (CFCs), and nitrous oxide (N_2O), and among these CO_2 is the major threat to the environment. Carbon emitting fuels such as coal, petroleum, natural gas and other non-renewable resources are the major source of CO_2 [1]. Fossil fueled power plants are ranked number one potential source of CO_2 emission and burning of fossil fuels contributes to about three-fourth increase in CO_2 [2]. According to the Intergovernmental Panel on Climate Change (IPCC), carbon dioxide concentration in the atmosphere has globally grown by around 100 ppm (36%) in the last 250 years: from 275 to 285 ppm in the pre-industrial age to around 407.46 ppm in 2017 and it may reach up to 570 ppm by 2100 causing a rise of approximately 1.9 °C in the mean global temperature, and an increase of 3.8 m in the mean sea level [3].

Different methods to reduce CO_2 emission in the atmosphere include (i) reduction in energy demand by improving the efficiency of energy conversion devices, (ii) by using renewable energy sources and increased usage of low carbon fuels including natural gas, hydrogen or nuclear power; (iii) applying geo-engineering approaches, e.g. afforestation and reforestation; and (iv) carbon dioxide capture and sequestration (CCS) system. The feasible way to mitigate this trend is to capture CO_2 from flue gas with adsorbents and then sequester it underground or make useful products [4].

The approaches to capture CO_2 include (i) pre-combustion capture, (ii) oxy-combustion and (iii) post-combustion capture. In the

* Corresponding author.
E-mail addresses: Deepak.tiwari@thapar.edu (D. Tiwari), chitrakshigoel@yahoo.co.in (C. Goel), hbhunia@thapar.edu (H. Bhunia), pramod.iitk77@gmail.com (P.K. Bajpai).

http://dx.doi.org/10.1016/j.seppur.2017.03.014
1383-5866/

Applied Surface Science 439 (2018) 760–771

Contents lists available at ScienceDirect

Applied Surface Science

journal homepage: www.elsevier.com/locate/apsusc

Full Length Article

Adsorption of CO_2 on KOH activated, N-enriched carbon derived from urea formaldehyde resin: kinetics, isotherm and thermodynamic studies

Deepak Tiwari, Haripada Bhunia *, Pramod K. Bajpai

Department of Chemical Engineering, Thapar Institute of Engineering and Technology, Patiala 147004, Punjab, India

ARTICLE INFO

Article history:
Received 2 November 2017
Revised 18 December 2017
Accepted 21 December 2017
Available online 09 January 2018

Keywords:
CO_2 adsorption
KOH activation
Kinetics
Isotherm
Thermodynamics

ABSTRACT

High surface area nitrogen enriched carbon adsorbents were prepared from a low cost and widely available urea-formaldehyde resin using a standard chemical activation with KOH and characterized using different characterization techniques for their porous structure and surface functional groups. Maximum surface area and total pore volume of 4547 $m^2\ g^{-1}$ and 4.50 $cm^3\ g^{-1}$ were found by controlling the activation conditions. Nitrogen content of this sample was found to be 5.62%. Adsorption of CO_2 uptake for the prepared carbon adsorbents was studied using a dynamic fixed bed adsorption system at different adsorption temperatures (30–100 °C) and at different CO_2 concentrations (5–12.5%), relevant from the flue gas point application. Maximum CO_2 uptake of 1.40 mmol g^{-1} for UFA-3-700 at 30 °C under 12.5% CO_2 flow was obtained. Complete regenerability of the adsorbents over multiple adsorption-desorption cycles was obtained. Fractional order kinetic model provided best description over all adsorption temperatures and CO_2 concentrations. Heterogeneity of the adsorbent surface was confirmed from Temkin adsorption isotherm model fit and isosteric heat of adsorption values. Negative value of $\Delta G°$ and $\Delta H°$ confirms spontaneous, feasible nature and exothermic nature of adsorption process. Overall, very high surface area of carbon adsorbent makes this adsorbent a new promising carbon material for CO_2 capture from power plant flue gas and for other relevant applications.

1. Introduction

Increase in the concentration of anthropogenic carbon dioxide (CO_2) in the environment is the major cause of global warming. Increased combustion of fossil fuels for world's energy requirements is the major reason for its increase in the atmosphere. From the current scenario, its concentration has increased almost up to 409 ppm [1,2] and seems to increase further causing rise of global temperature and rise of sea levels which will have a detrimental effect on the climate and on the marine life. Therefore, there is a great need to reduce the concentration of CO_2. Carbon capture and sequestration (CCS) is the key technology which will play an important role. It includes capture of carbon dioxide by using various methods like absorption, adsorption, membrane and cryogenic methods. CO_2 capture on a large scale by amine-based absorption is in use in industry but it has several disadvantages like, equipment corrosion, high energy consumption and environmental problems [3,4]. Alternatively, adsorption using solid adsorbents has received much attention because of reducing energy penalty. Also, some characteristics like high adsorption capacity, selectivity and fast kinetics coupled with good thermal and mechanical stability provide its use in near term. Potential adsorbent such as zeolites [5], activated carbons [6,7], metal-organic frameworks [8,9], amine supported mesoporous materials [10,11], etc. have been studied but among them, carbon based adsorbents have more potential. They are having better properties as compared to others, like well-developed porous structures, high adsorption capacities, fast kinetics, easy regenerabilty, high thermal and chemical stability. They can be prepared from a huge range of low cost sources by using various preparation techniques like sol-gel, carbonization of carbon containing precursors and nanocasting technique [4]. Their CO_2 uptake capacity can be increased by using heteroatoms like nitrogen, oxygen, etc. [4] in the carbon matrix which improve the surface property of the adsorbent towards CO_2. This also provides better selectivity of the adsorbents towards CO_2 which is one of the important characteristics needed for this application.

Hao et al. [4] synthesized nitrogen-doped porous carbon monoliths by pyrolysis of copolymer of resorcinol, formaldehyde and lysine which exhibited static CO_2 adsorption capacity of 3.13 mmol g^{-1} at 25 °C under pure CO_2 atmosphere. Nitrogen rich carbon material synthesized by Wang et al. [12,13] using chemical

* Corresponding author.
E-mail addresses: deepak.tiwari@thapar.edu (D. Tiwari), hbhunia@thapar.edu (H. Bhunia), pramod.iitk77@gmail.com (P.K. Bajpai).

https://doi.org/10.1016/j.apsusc.2017.12.203
0169-4332/

Journal of Environmental Management 197 (2017) 415–427

Contents lists available at ScienceDirect

Journal of Environmental Management

journal homepage: www.elsevier.com/locate/jenvman

Research article

Melamine-formaldehyde derived porous carbons for adsorption of CO_2 capture

Deepak Tiwari [a], Chitrakshi Goel [a, b], Haripada Bhunia [a, *], Pramod K. Bajpai [a]

[a] Department of Chemical Engineering, Thapar University, Patiala 147004, Punjab, India
[b] Ghent University – Laboratory for Chemical Technology, Technologie park 914, B-9052 Ghent, Belgium

ARTICLE INFO

Article history:
Received 4 September 2016
Received in revised form
22 February 2017
Accepted 5 April 2017

Keywords:
CO_2 capture
Nanocasting
Melamine formaldehyde
Adsorption kinetics
Isotherm

ABSTRACT

In this work, we report carbon adsorbents obtained from high nitrogen content melamine-formaldehyde resin as starting material and mesoporous zeolite MCM-41 as template through nanocasting technique. To synthesize different carbon structure adsorbents with improved textural and surface properties, the material undergo carbonization followed by physical activation under CO_2 atmosphere at different temperatures. Characterizations of the adsorbents using SEM, TEM, XPS, nitrogen sorption, CHN, TKN, and TPD have been carried out. Characterization results reveal the development of nanostructured carbon adsorbents with better texture and surface properties as compared to the sample prepared by direct carbonization. Sample prepared at carbonization-activation temperature of 700 °C shows highest basicity, surface area (193.28 $m^2\ g^{-1}$) and pore volume (0.32 $cm^3\ g^{-1}$). Performance evaluation of adsorbent was performed thermo gravimetrically at different temperatures and concentrations and was found that the adsorbent synthesized at 700 °C exhibit highest CO_2 uptake of 0.93 mmol g^{-1} with nitrogen content of 22.73%. It was found that both surface area and nitrogen functional group have a major impact on adsorption capacity. Physiosorption process was confirmed by a decrease in adsorption capacity with increase in temperature. Three kinetic models and isotherms were used in this study and found that fractional order kinetic model and Freundlich isotherm best fitted with the experimental data. Isotherm study depicts the heterogeneous nature of adsorbent surface. Adsorbent exhibited complete regenerability and was stable over four adsorption-desorption cycles. Low value of isosteric heat of adsorption of 15.75 kJ mol^{-1}, indicates physiosorption process. Negative value of ΔG^0 and ΔH^0 confirms spontaneous, feasible and exothermic nature of adsorption process.

1. Introduction

Global warming caused by increasing CO_2 concentration in the atmosphere is the major current challenging issue. The increase in CO_2 concentration is due to burning of fossil fuel such as coal, natural gas or petroleum etc. Its concentration has increased from 280 ppm to 406.67 ppm at present (2017) and it is expected to rise up to a level of 550 ppm by 2100 (Tiwari et al., 2016a, 2016b) as the fossil fuels will continue to be the major source of energy. Increase in concentration of CO_2 at this rate will harm the global environment and will create problem like drought, global surface temperature rise, and increase in acidity of sea level. Therefore, there is a need to reduce anthropogenic CO_2 emissions by capturing CO_2 with inexpensive adsorbents (Lu and Schüth, 2006).

Some of the adsorbents tested by different research groups are activated carbon (Siriwardane et al., 2005), zeolites (Wahby et al., 2010), mesoporous silica material SBA-15, MCM-41 (Sun et al., 2015), and amine-enriched sorbents (Himeno et al., 2005). But the problems like corrosion, high energy requirement for regeneration, lack of adsorption stability are still there. An ideal adsorbent should have the characteristics of high adsorption capacity, low energy requirement for regeneration, cost effective, stable over multiple cycles and high surface area (Hornbostel et al., 2013).

Recent studies show that carbon adsorbents fulfill the above criteria and can be easily prepared by various technologies like nanocasting, direct carbonization of precursor and sol-gel process (Hornbostel et al., 2013; Karandikar et al., 2007). Among these methods, adsorbent prepared by nanocasting technology is very

* Corresponding author.
E-mail addresses: Deepak.tiwari@thapar.edu (D. Tiwari), chitrakshigoel@yahoo.co.in (C. Goel), hbhunia@thapar.edu (H. Bhunia), pramod.iitk77@gmail.com (P.K. Bajpai).

http://dx.doi.org/10.1016/j.jenvman.2017.04.013
0301-4797/

Applied Surface Science 414 (2017) 380–389

Contents lists available at ScienceDirect

Applied Surface Science

journal homepage: www.elsevier.com/locate/apsusc

Full Length Article

Epoxy based oxygen enriched porous carbons for CO_2 capture

Deepak Tiwari, Haripada Bhunia*, Pramod K. Bajpai

Department of Chemical Engineering, Thapar University, Patiala, 147004, Punjab, India

ARTICLE INFO

Article history:
Received 25 February 2017
Received in revised form 5 April 2017
Accepted 17 April 2017
Available online 19 April 2017

Keywords:
Epoxy resin
Nanocasting
CO_2 capture
Regenerability
Adsorption kinetics
Isotherm

ABSTRACT

Oxygen enriched carbon adsorbents were successfully synthesized for the first time from template zeolite and epoxy resin as precursor using a nanocasting technique. Carbonization and CO_2 activation were performed at various temperatures (500–800 °C) to prepare different carbon structure adsorbents. Several characterization techniques were used to characterize the textural structure, oxygen content and surface functional groups of the adsorbents. The carbon adsorbents show high oxygen content (47.51%), highest surface area (S_{BET} = 686.37 $m^2 g^{-1}$) and pore volume (0.60 $cm^3 g^{-1}$), respectively. The materials were evaluated thermogravimetrically at different adsorption temperatures (30–100 °C) and CO_2 concentrations (6–100%). Adsorbent prepared at 700 °C exhibited highest CO_2 uptake of 0.91 mmol g^{-1} due to high surface basicity. Further, regeneration studies of adsorbent exhibited easy regenerability and stability over four multiple adsorptions-desorption cycles. Kinetic models for CO_2 adsorption at various CO_2 concentrations and temperatures were studied and it was found that the fractional order provided best fitting for the adsorption behavior with an error of less than 3%. The experimental data for CO_2 adsorption were analyzed using different isothermal models and found that the Freundlich isothermal model presented perfect fit among all isotherm models depicting heterogeneous adsorbent surface. The isosteric heat of adsorption was estimated to be 11.75 kJ mol^{-1}, indicating physiosorption process. Overall, the above results suggested that the synthesized adsorbent using nanocasting technique provides a feasible way for CO_2 capture from point source due to their environmentally benign nature, low cost and stable adsorption capacity.

1. Introduction

Recently, global warming has become major environmental problems due to increase in the concentration of carbon dioxide (CO_2) in the atmosphere. The increase in the concentration of CO_2 is due to the burning of fossil fuels such as coal, petroleum, and natural gas which are the major sources of energy. There are several technological options available which can cut down CO_2 emission in the atmosphere: (i) increase the efficiency of fossil fuels; (ii) increase the use of renewable energy; (iii) CO_2 capture from flue gas with an inexpensive adsorbent and then sequester it in underground (CCS). Among them, carbon dioxide capture and sequestration (CCS) strategy has a potential to inhibit the increase of CO_2 concentration [1–5]. A number of CCS technologies like absorption, adsorption, membrane separation and cryogenic distillation have been used for CO_2 capture [6,7]. Conventional amine absorption technology used in the industry for large scale CO_2 capture is effective, but it has intrinsic limitations like low efficiency, equipment corrosion, high energy requirement and solvent loss [8]. As a result, adsorption by porous carbons is found to be attractive because it reduces cost, requires less amount of energy for regeneration [9]. Currently, a large variety of porous solids has been tested by researchers like mesoporous silica, COFs [10], carbon-based adsorbents, metal-organic-frameworks, etc. [11]. But, CO_2 capture based on carbon-based adsorbents has attracted the most, as it fulfills the criteria of an ideal adsorbent like low cost, high availability, large surface area, easy to design the pore structure, etc. [12]. However, the synthesis of this type of adsorbents can be done by different ways like direct carbonization approach or nanocasting approach. Synthesis based on nanocasting is simple and effective to prepare adsorbents with controlled porous structure.

Incorporation of heteroatoms is beneficial to increase the adsorption capacity of the adsorbents, as compared to the case without heteroatoms. Wickramaratne et al. [13] reported CO_2 uptake of 4.6 mmol g^{-1} on phenolic resin based carbon at 23 °C and 1 atm pressure. De souza et al. [14] reported CO_2 uptake at 25 °C on adsorbents synthesized by phenolic resin by chemical activation under KOH. Resultant adsorbent exhibited a static adsorption capacity of 4.36 mmol g^{-1}. The current literature study shows that

* Corresponding author.
E-mail addresses: Deepak.tiwari@thapar.edu (D. Tiwari), hbhunia@thapar.edu (H. Bhunia), pramod.iitk77@gmail.com (P.K. Bajpai).

http://dx.doi.org/10.1016/j.apsusc.2017.04.128
0169-4332/

Journal of CO_2 Utilization 21 (2017) 302–313

Contents lists available at ScienceDirect

Journal of CO_2 Utilization

journal homepage: www.elsevier.com/locate/jcou

Synthesis of nitrogen enriched porous carbons from urea formaldehyde resin and their carbon dioxide adsorption capacity

Deepak Tiwari, Haripada Bhunia*, Pramod K. Bajpai

Department of Chemical Engineering, Thapar University, Patiala, 147004, Punjab, India

ARTICLE INFO

Keywords:
Carbon dioxide capture
Nanocasting
Urea-formaldehyde resin
Regeneration
Kinetics
Isotherm

ABSTRACT

Carbon dioxide capture needs development of cost effective CO_2 capture technologies. This paper describes nitrogen enriched porous carbons synthesized from nanocasting technique using mesoporous silica as template and urea-formaldehyde resin as precursor. These carbon materials were evaluated as sorbents for CO_2 capture by using a thermogravimetric analysis under dynamic conditions. Carbonization and physical activation with CO_2 at different temperatures (500–800 °C) were carried out that resulted in the generation of different carbon adsorbents containing nitrogen functional groups. The textural characterization result reveals effect of nanocasting technique, which is confirmed from the generation of mesopores (0.644 $cm^3 g^{-1}$), micropores (0.123 $cm^3 g^{-1}$) and high surface area (337.07 $m^2 g^{-1}$) of adsorbent. The CO_2 capture capacity depends more on the nitrogen functionalities in addition to textural properties and nitrogen content, as the sample synthesized at 700 °C shows highest uptake capacity of 1.3 mmol g^{-1}. Furthermore, it was found that adsorbent can be easily regenerated, which was also seen by the lower value of isosteric heat of adsorption. Ten adsorption-desorption cycles show established materials' excellent stability as an adsorbent. Different kinetic models were fitted for the adsorption data and on the basis of correlation coefficient (R^2), fractional order provided best fit with the experimental data. The heterogeneous nature of the adsorbent surface was seen by best fitting of Freundlich isotherm and from the pattern of isosteric heat of adsorption. Exothermic, spontaneous and feasible nature was suggested by thermodynamic parameters' values. The thermal energy needed for desorption of CO_2 from the adsorbent surface was around 1.28 MJ per kg CO_2.

1. Introduction

Nowadays, world is facing tremendous challenges due to increase in greenhouse gas emissions (mainly carbon dioxide), which causes a major global warming problem. Its release into the atmosphere is mainly due to burning of fossil fuels such as coal, petroleum and natural gas [1,2]. It is expected that its concentration will get doubled by 2050, if no major actions are taken [3]. Various methods are available to reduce CO_2 emission in the atmosphere such as geo-engineering approaches, afforestation and reforestation, carbon dioxide capture & sequestration (CCS) system and by using renewable energy sources and increased usage of low carbon fuels [4–7]. Its capture & sequestration (CCS) has drawn much global attention.

The available CCS technologies to capture CO_2 are absorption, adsorption [8], cryogenic processes [9], and membrane separation. In this respect, mature technologies like gas absorption by alkanomines solutions have been used maximum for CO_2 scrubbing on industrial scale. However, they have several shortcomings such as inherent regeneration cost and inefficiency [10]. Therefore, there is a need to find an alternative route. In contrast, it is widely recognized that adsorption by porous adsorbents is attractive because of its low energy consumption and higher adsorption capacity [11,12]. Current research activities are focused on carbon based adsorbents [13], zeolites [14,15], mesoporous silica material SBA-15 [16], and amine-enriched sorbents to separate CO_2 from fossil fueled power plants. Some of them also tried to improve uptake capacity and selectivity of adsorbents through amine modification, but they faced problems like poor stability and blocking of adsorbent pores. Therefore, carbon based adsorbents are found to be attractive among them due to its high surface area, lesser amount of energy for regeneration, good thermal/mechanical stability and hydrophobicity [17]. Three methods are available for the synthesis of carbon materials: (a) carbonization and activation of carbon containing precursor, (b) sol gel process and (c) nanocasting method [18–20]. By using first two methods (sol gel and carbonization followed by activation), mesoporous carbons with somewhat tunable properties can be developed. But it is not possible with this method to develop adsorbents

* Corresponding author.
E-mail addresses: Deepak.tiwari@thapar.edu (D. Tiwari), hbhunia@thapar.edu (H. Bhunia), pramod.iitk77@gmail.com (P.K. Bajpai).

http://dx.doi.org/10.1016/j.jcou.2017.08.002
Received 8 November 2016; Received in revised form 21 July 2017; Accepted 2 August 2017

Journal of Environmental Management 218 (2018) 579–592

Contents lists available at ScienceDirect

Journal of Environmental Management

journal homepage: www.elsevier.com/locate/jenvman

Research article

Development of chemically activated N-enriched carbon adsorbents from urea-formaldehyde resin for CO_2 adsorption: Kinetics, isotherm, and thermodynamics

Deepak Tiwari, Haripada Bhunia*, Pramod K. Bajpai

Department of Chemical Engineering, Thapar Institute of Engineering & Technology (Deemed to be University), Patiala 147004, Punjab, India

ARTICLE INFO

Article history:
Received 1 August 2017
Received in revised form
11 April 2018
Accepted 20 April 2018

Keywords:
Low cost carbon adsorbents
Chemical activation
CO_2 adsorption
Adsorption kinetics
Adsorption isotherm

ABSTRACT

Nitrogen enriched carbon adsorbents with high surface areas were successfully prepared by carbonizing the low-cost urea formaldehyde resin, followed by KOH activation. Different characterization techniques were used to determine the structure and surface functional groups. Maximum surface area and total pore volume of 4547 $m^2 g^{-1}$ and 4.50 $cm^3 g^{-1}$ were found by controlling activation conditions. The optimized sample denoted as UFA-3-973 possesses a remarkable surface area, which is found to be one of the best surface areas achieved so far. Nitrogen content of this sample was found to be 22.32%. Dynamic CO_2 uptake capacity of the carbon adsorbents were determined thermogravimetrically at different CO_2 concentrations (6–100%) and adsorption temperatures (303–373 K) which have a much more relevance for the flue gas application. Highest adsorption capacity of 2.43 mmol g^{-1} for this sample was obtained at 303 K under pure CO_2 flow. Complete regenerability of the adsorbent over four adsorption-desorption cycles was obtained. Fractional order kinetic model provided best description of adsorption over all adsorption temperatures and CO_2 concentrations. Heterogeneity of the adsorbent surface was confirmed from the Langmuir and Freundlich isotherms fits and isosteric heat of adsorption values. Exothermic, spontaneous and feasible nature of adsorption process was confirmed from thermodynamic parameter values. The combination of high surface area and large pore volume makes the adsorbent a new promising carbon material for CO_2 capture from power plant flue gas and for other relevant applications.

1. Introduction

Increasing concentration of anthropogenic carbon dioxide (CO_2) in the atmosphere due to combustion of fossil fuels is the major cause of global climate deterioration. Its concentration has reached to a level of 408.84 ppm (Earth's CO_2, 2018) according to current scenario and is expected to increase up to a level of 570 ppm by 2100 (Yu et al., 2008). Currently, carbon dioxide capture and storage from fixed point sources is the prevailing strategy to reduce carbon dioxide in the atmosphere (Tiwari et al., 2017a; b). In this respect, on a large scale, amine absorption technology using monoethanol amine and alkanolamine is well-tried technology (Chatti et al., 2009) but this technology suffers from several drawbacks e.g., equipment corrosion, high energy consumption and environmental problems. Therefore, there is a great need to develop alternative capture technology. Adsorption technology is another promising and cost effective route which offers several advantages over absorption technology such as mild operating conditions and low energy consumptions (Siriwardane et al., 2001). However, high adsorption capacity, outstanding cycling performance and high CO_2/N_2 selectivity are the key essentials for temperature and pressure swing adsorption technologies (Liu et al., 2014). Large variety of porous adsorbents have been tested like zeolites (Khelifa et al., 2004), porous carbons (Sevilla and Fuertes, 2011), amine modified materials (Chatti et al., 2009), covalent-organic-frameworks (COFs) (Abid et al., 2012) and metal-organic-frameworks (MOFs) (Patel et al., 2012) for CO_2 adsorption.

Compared with other materials, carbonaceous adsorbents possess unique superiority such as low-cost, high stability, high hydrophobicity, low energy requirement for regeneration and tunable pore structure (Liu et al., 2015). Recently, researchers have focused on enhancing adsorption capacity and selectivity of carbon materials using nitrogen, oxygen etc. as a heteroatoms and by

* Corresponding author.
E-mail addresses: deepak.tiwari@thapar.edu (D. Tiwari), hbhunia@thapar.edu (H. Bhunia), pramod.iitk77@gmail.com (P.K. Bajpai).

https://doi.org/10.1016/j.jenvman.2018.04.088
0301-4797/